AFRRI REPORTS
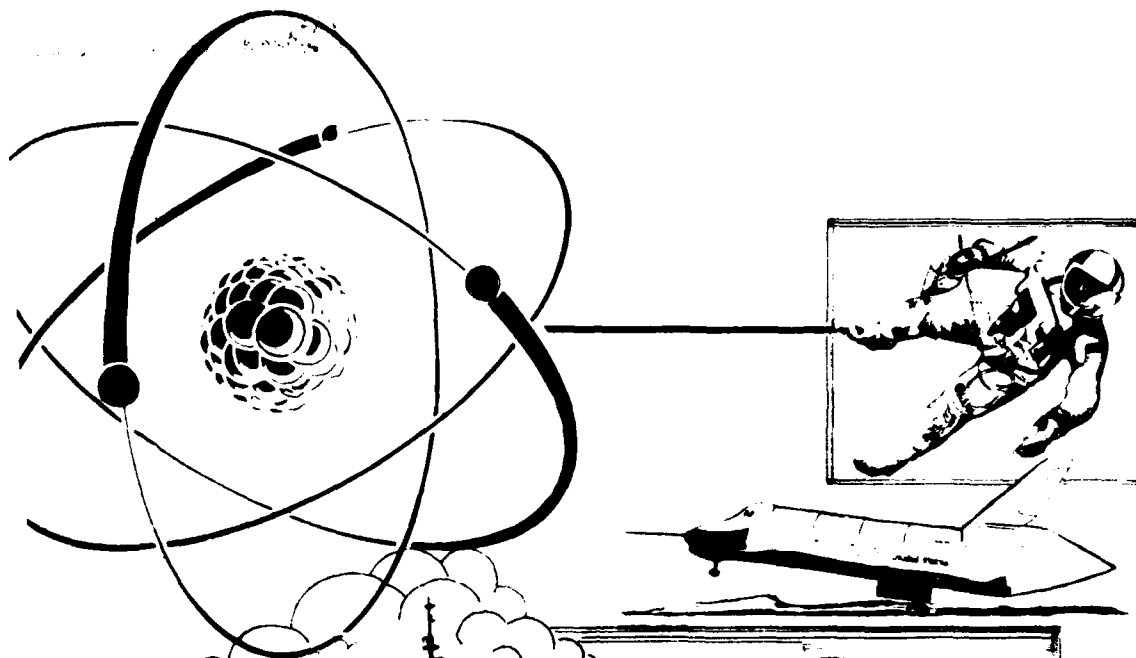
AD–A208 803

January
February
March
1989

89   6 09 039

Defense Nuclear Agency
Armed Forces Radiobiology Research Institute
Bethesda, Maryland 20814-5145

REPORT DOCUMENTATION PAGE

1a. REPORT SECURITY CLASSIFICATION	1b. RESTRICTIVE MARKINGS
UNCLASSIFIED	

2a. SECURITY CLASSIFICATION AUTHORITY	3. DISTRIBUTION / AVAILABILITY OF REPORT
	Approved for public release; distribution unlimited.
2b. DECLASSIFICATION / DOWNGRADING SCHEDULE	

4. PERFORMING ORGANIZATION REPORT NUMBER(S)	5. MONITORING ORGANIZATION REPORT NUMBER(S)
SR89-1 - SR89-14	

6a. NAME OF PERFORMING ORGANIZATION	6b. OFFICE SYMBOL (If applicable)	7a. NAME OF MONITORING ORGANIZATION
Armed Forces Radiobiology Research Institute	AFRRI	

6c. ADDRESS (City, State, and ZIP Code)	7b. ADDRESS (City, State, and ZIP Code)
Defense Nuclear Agency Bethesda, Maryland 20814-5145	

8a. NAME OF FUNDING / SPONSORING ORGANIZATION	8b. OFFICE SYMBOL (If applicable)	9. PROCUREMENT INSTRUMENT IDENTIFICATION NUMBER
Defense Nuclear Agency	DNA	

8c. ADDRESS (City, State, and ZIP Code)	10. SOURCE OF FUNDING NUMBERS			
	PROGRAM ELEMENT NO.	PROJECT NO	TASK NO.	WORK UNIT ACCESSION NO
Washington, DC 20305	NWED QAXM			

11. TITLE (Include Security Classification)
   AFRRI Reports, Jan-Mar 1989

12. PERSONAL AUTHOR(S)

13a. TYPE OF REPORT	13b. TIME COVERED		14. DATE OF REPORT (Year, Month, Day)	15. PAGE COUNT
Reprints/Technical	FROM _____	TO _____	1989 January	132

16. SUPPLEMENTARY NOTATION

17.	COSATI CODES		18. SUBJECT TERMS (Continue on reverse if necessary and identify by block number)
FIELD	GROUP	SUB-GROUP	

19. ABSTRACT (Continue on reverse if necessary and identify by block number)

   This volume contains AFRRI Scientific Reports SR89-1 through SR89-14 for Jan-Mar 1989.

20. DISTRIBUTION / AVAILABILITY OF ABSTRACT	21. ABSTRACT SECURITY CLASSIFICATION
☐ UNCLASSIFIED/UNLIMITED ☒ SAME AS RPT. ☐ DTIC USERS	UNCLASSIFIED

22a. NAME OF RESPONSIBLE INDIVIDUAL	22b. TELEPHONE (Include Area Code)	22c. OFFICE SYMBOL
Gloria Ruggiero	(301)295-3536	ISDP

DD FORM 1473, 84 MAR

83 APR edition may be used until exhausted
All other editions are obsolete

CONTENTS.

Scientific Reports

SR89-13: Walden, T. L., Jr., Buchner, J., Pizzitola, V., and Blakely, W. F. Thermospray liquid chromatography mass spectrometry of thiol radioprotective agents: Characteristic spectra.

SR89-14: Walden, T. L., Jr., and Kalinich, J. F. Radioprotection by leukotrienes: Is there a receptor mechanism?
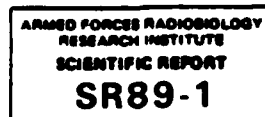
Technical Reports

AFRRI TR88-2: Schauer, D. A., Zeman, G. H., and Pellmar, T. C. A low-energy x-ray irradiator for electrophysiological studies.

Accession For		
NTIS GRA&I	☑	
DTIC TAB	☐	
Unannounced	☐	
Justification		
By		
Distribution/		
Availability Codes		
Dist	Avail and/or Special	
A-1		

EFFECTS OF ETHIOFOS (WR-2721) AND RADIATION ON MONKEY VISUAL DISCRIMINATION PERFORMANCE

V. Bogo*, C. G. Franz*, A. J. Jacobs†, J. F. Weiss† and R. W. Young‡

*Behavioral Sciences and † Radiation Biochemistry Departments, Armed Forces Radiobiology Research Institute, Bethesda, Maryland 20814-5145, U.S.A.
‡ Radiation Policy Division, Radiation Sciences Directorate, Defense Nuclear Agency, Washington, DC 20305-1000, U.S.A.

WR-2721 (ethiofos) is a promising protector against radiation-induced lethality and may be useful in cancer radiotherapy (Davidson *et al.*, 1980). However, ethiofos also produces nausea, vomiting, diarrhea, and hypotension, which implies severe behavioral consequences (Bogo *et al.*, 1985). We studied the effects of ethiofos on behavior in monkeys and its ability to mitigate early transient incapacitation (ETI). ETI is the abrupt cessation of performance (for at least 1 min) following rapidly delivered, high doses of radiation and usually occurs 5 – 10 min after irradiation and lasts for 1 – 15 min (Bogo, 1988a).

Male rhesus (*Macaca mulatta*) monkeys ($N = 24$) were obtained from the Joint Services Primate Breeding Colony, Naval Aerospace Medical Research Laboratory, Pensacola, Florida, and quarantined 60 d for evaluation, tuberculosis testing, and stabilization. Monkeys were maintained in conventional stainless steel, wall-mounted cages in rooms maintained at 72 ± 2°F, with 50% ± 10% relative humidity using 100% conditioned fresh air at 12 air changes per hr. They were provided commercial monkey chow and hyperchlorinated tap water *ad libitum*, and were kept on a 12 hr light/12 hr dark, full-spectrum light cycle with no twilight.

Monkeys seated in plastic chairs were exposed to a TRIGA reactor pulse (50 msec) of neutron/gamma radiation (ratio 0.4). The doses were 14, 16, 22, and 24 Gy. A 22 Gy pulse was used in the ethiofos/radiation condition because it was known to be 90% effective in producing ETI in monkeys performing the speed stress visual discrimination task (SSVDT) (Bogo *et al.*, 1987). Since the ETI dose was well above the LD $_{50/30}$ of 6 Gy for a monkey, ethiofos was not expected to offer any protection from lethality. Ethiofos was given i.v. (saphenous vein) at least 30 min before irradiation. The 200 mg/kg dose was diluted in 60 cc saline and injected with an infusion pump over 5 min.

Performance was assessed with either a visual discrimination task (VDT) or an SSVDT. In these shock avoidance tasks, trained monkeys discriminated between a circle and a square (always the correct choice) randomly presented every 10 s on backlit press-plates. Maximum response time in the VDT was 5.0 s, and 0.7 s or less in the SSVDT. Performance was assessed 15 min before and after ethiofos, during radiation exposure, and for 90 min after irradiation. The test measures were (a) ETI 90 min following radiation, (b) percent correct choice following ethiofos and/or radiation, (c) emesis after ethiofos and/or radiation, and (d) time to death.

In the repeat-measure study, the same six monkeys (mean weight 8.3 kg) were tested on the SSVDT as follows: (a) sham ethiofos (saline)/sham radiation (baseline control), (b) ethiofos/sham radiation, and (c) ethiofos/radiation. A three week interval was allowed between tests. At the time of the study the number of large, trained monkeys was limited, and no concurrent radiation-only control group existed to illustrate ETI. Radiation-only controls were obtained from the Armed Forces Radiobiology Research Institute's Primate Behavioral Data Base in smaller but similarly handled monkeys (weight 3.7 kg) (Franz *et al.*, 1981). The 14 and 16 Gy irradiated monkeys performed the SSVDT, and the 24 Gy irradiated monkeys performed the VDT. All monkeys were monitored before and after exposure to record incidence of emesis and were
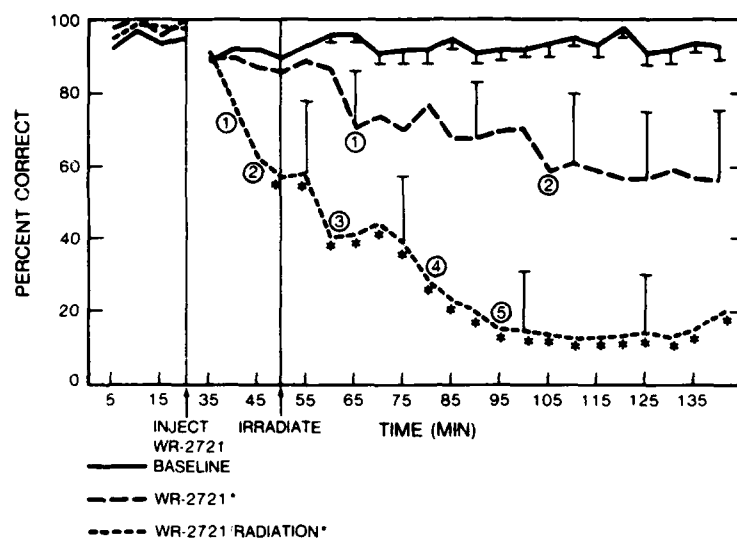
FIG. 1. Baseline, post-ethiofos, and post-ethiofos/radiation performance on the SSVDT. Circles show the number of subjects with ETI. Significant effects compared with controls are shown with asterisks $(p < 0.05)$. $N = 6$.
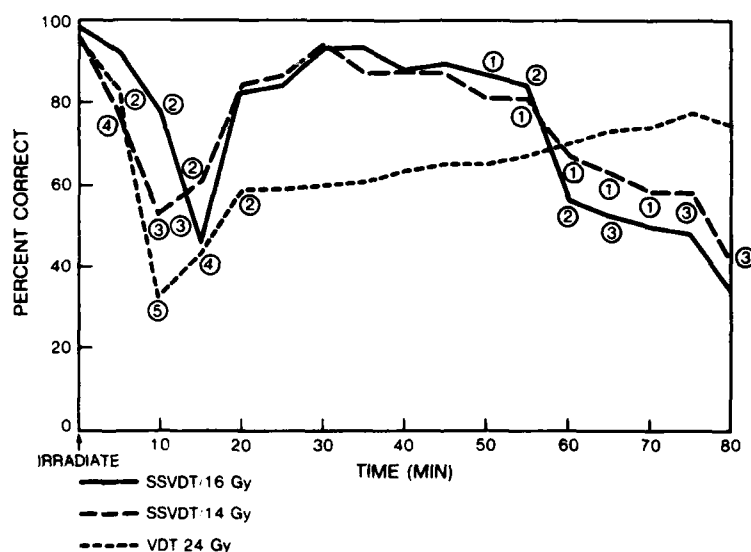
FIG. 2. Radiation control conditions for Fig. 1. Performance on the SSVDT after 14 and 16 Gy radiation, and performance on the VDT after 24 Gy radiation. Circles show the number of subjects with ETI. $N = 6$/group.

monitored until death. Percent correct performance was analyzed by two-way ANOVAs. Chi-square analysis was used to compare incidence of ETI and emesis.

In the repeat-measure conditions, performance during the post-ethiofos test period was significantly below the same-subject baseline, ranging from 25% to 30% below baseline at 45 and 85 min posttreatment, respectively (Fig. 1). Performance of the ethiofos/radiation condition was significantly below both the same-subject baseline and ethiofos conditions after treatment. The decrements ranged from 35% below baseline 10 min after irradiation to 80% below baseline 45 min after exposure. Both the ethiofos and ethiofos/radiation conditions were overall significantly below the same-subject baseline.

In the radiation-only conditions, performance dropped an average of 56%, 10–15 min postexposure (Fig. 2). Performance in the 14 and 16 Gy conditions recovered to 15% below control after 20 min postexposure, while recovery was more gradual in the 24 Gy condition, to 25% below control at 70 min. All radiation-only conditions in Fig. 2 were significantly below the baseline condition in Fig. 1.

The incidence of ETI was significantly greater in the ethiofos/radiation condition (83%) than ethiofos alone (33%). The incidence of emesis did not differ significantly between the combined and ethiofos-alone conditions (42%). The time until death did not differ significantly between the monkeys irradiated with 24 Gy alone and those treated with ethiofos and irradiated with 22 Gy, i.e. average time to death was 24 hr.

Ethiofos produced a decrement in the SSVDT and offered no protection against radiation-induced ETI; performance was worse in the combined condition than in either the ethiofos or radiation conditions alone. These findings are similar to those previously reported in rats performing a motor function task (Bogo et al., 1985). Since ethiofos is behaviorally toxic in two animal models, future work will focus on either reducing its behavioral toxicity or searching for other effective radioprotectors with less toxic effects on behavior (Bogo, 1988b).

REFERENCES

Bogo, V. (1988a) Early behavioral toxicity produced by acute ionizing radiation. *Comments on Toxicology* (in press).

Bogo, V. (1988b) Behavioral radioprotection. *Pharmac. Ther.* **39:** 73–78, this volume.

Bogo, V., Jacobs, A. J. and Weiss, J. F. (1985) Behavioral toxicity and efficacy of WR-2721 as a radioprotectant. *Radiat. Res.* **104:** 182–190.

Bogo, V., Franz, C. G. and Young, R. W. (1987) Effects of radiation on monkey visual discrimination performance. *Proceedings of the Eighth International Congress on Radiation Research*, p. 259, Fielden, E. M., Fowler, J. F., Hendry, J. H. and Scott, D. (eds) Taylor and Francis, London.

Davidson, D. E., Grenan, M. M. and Sweeney, T. R. (1980) Biological characteristics of improved radioprotectors. In: *Radiation Sensitizers. Their Use in the Clinical Management of Cancer*, pp. 309–320, Brady, L. W. (ed.) Masson Publishing, New York.

Franz, C. G., Young, R. W. and Mitchell, W. E. (1981) *Behavioral Studies Following Ionizing Radiation Exposures: A Data Base*. Technical Report TR81-4. Armed Forces Radiobiology Research Institute, Bethesda, Maryland.

GAMMA RADIOLYSIS OF RNA:

AN ESR AND SPIN-TRAPPING STUDY

Alasdair J. Carmichael, Carmen M. Arroyo, and
Thomas L. Walden

Radiation Biochemistry Department
Armed Forces Radiobiology Research Institute
Bethesda, Maryland 20814, U.S.A.

INTRODUCTION

It is well known that the radiolytic cleavage of water produces hydroxyl radicals ($\cdot$OH), hydrogen atoms ($\cdot$H) and hydrated electrons (e^-_{aq}).[1] Although these species react rapidly with the individual nucleic acid bases,[2-4] it is generally accepted that when nucleic acid (DNA, RNA) solutions are exposed to ionizing radiation, the principal reaction leading to nucleic acid damage is caused by $\cdot$OH. Besides direct formation, $\cdot$OH is formed from H_2O_2, also a product of the radiolysis of water, in the presence of trace amounts of divalent metal ions.[5] The study reported here deals with the reaction of RNA with $\cdot$OH, produced in aqueous solutions by gamma radiolysis. Of concern are the processes that occur following this reaction. For instance, are the precursors to the nucleic acid damage localized at specific base sites or do they occur indiscriminately throughout the nucleic acid molecule? Recently Kuwabara et al.[6] using HPLC, spin trapping and ESR identified the precursors of thymine damage in X-irradiated DNA solutions. For the present study, poly A, poly C, poly G and poly U were used as standards for RNA, and RNA was used as a model system for similar reactions that may occur in DNA. The nucleic acid free radical intermediates were detected and identified by ESR and spin trapping following hydrolysis of the spin-trapped nucleic acid molecules.

MATERIALS AND METHODS

To eliminate possible small-molecular-weight contaminants, solutions of RNA, poly A, poly C, poly G and poly U were dialyzed against several changes of doubly deionized distilled water and then lyophylized. The spin trap 2-methyl-2-nitrosopropane (MNP) was prepared by dissolving 20-30 mg of MNP in 10 ml of water and stirring in a water bath at 45°C for approximately 2 h. Solutions of RNA and of the various polynucleotides were prepared by dissolving the lyophylized powders (5×10^{-4} to 1×10^{-3} M) directly in the MNP solution and adjusting the pH to 8. These solutions were ^{60}Co gamma-irradiated at a dose rate of 45 Gy/min to a total dose of 700 Gy. ESR spectra of the spin-trapped RNA and polynucleotides were immediately recorded following irradiation. The spin-trapped RNA samples were hydrolyzed with base (NaOH, pH 12.6) or enzymatically (RNAase). The spin-trapped polynucleotides were hydrolyzed with base. ESR spectra were recorded at

437

various times during hydrolysis until the hydrolysis was complete as judged by the resolution of the ESR spectra. ESR spectra were recorded on a Varian E-109 X-band spectrometer at 100 KHz magnetic field modulation. The spectra were analyzed by comparison with computer-generated ESR spectra.

RESULTS AND DISCUSSION

The ESR spectrum obtained for the spin-trapped RNA is shown in Figure 1a. This spectrum consisting of three broad lines is characteristic of nitroxide groups bound to slowly tumbling large molecules in solution. Figure 1b shows the ESR spectrum obtained following base or enzymatic hydrolysis of the spin-trapped RNA. This spectrum consists of a triplet of sextets indicating that the unpaired nitroxide electron is interacting with the nuclei of a β nitrogen and β hydrogen. The hyperfine coupling constants for this spectrum are $a_N=1.48$ mT, $a_N^\beta = 0.25$ mT and $a_H^\beta = 0.15$ mT. Following base hydrolysis of the spin-trapped polynucleotides, only poly C (Figure 2a) and poly U (Figure 2B) yielded ESR spectra consisting of a triplet of sextets. The hyperfine coupling constants for the ESR spectrum corresponding to the hydrolyzed poly C are $a_N = 1.49$ mT, $a_N^\beta = 0.27$ mT and $a_H^\beta = 0.16$ mT. For the hydrolyzed poly U, $a_N = 1.48$ mT, $a_N^\beta = 0.25$ mT and $a_H^\beta = 0.15$ mT.
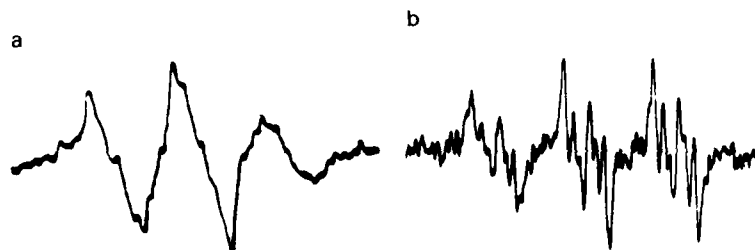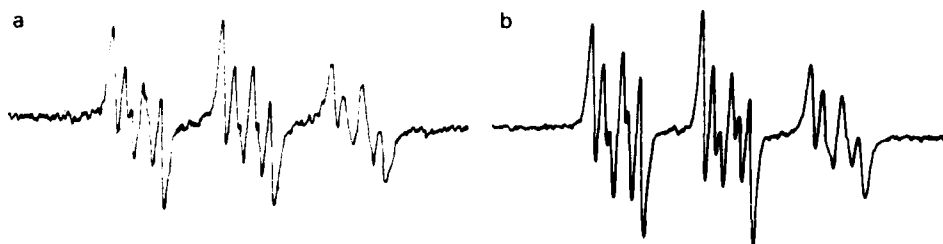
Figure 1.

Figure 2.

The results suggest that in RNA only uracil radicals were spin trapped. Furthermore, due to the β nitrogen and β hydrogen interaction with the unpaired nitroxide electron, the results indicate that MNP reacted with uracil-C6-carbon-centered radicals. Because hydroxyl radicals react with all bases at approximately the same rate,[2] two possible explanations for the

observed results are immediately obvious: 1) The spin-trapping efficiency is not equal for radicals formed on each base, and 2) the stability of the various spin adducts is not equal. Although still being investigated, the first possibility appears unlikely because [MNP]>[RNA]>[˙OH] which should permit MNP to react with any base radical formed in RNA. The second possibility is unlikely because the ESR spectra of the polynucleotide spin adducts and of their hydrolyzed products persist for 48 h or longer. Another explanation for the observed results is that the free radical spin density migrates via an intramolecular mechanism, still unclear at this time, to the uracil bases. Radiolysis of poly (A,U) and poly (C,U) in the presence of MNP support this explanation. The results of these experiments also show specific uracil spin trapping.

REFERENCES

1. I. G. Draganic and Z. D. Draganic, "The Radiation Chemistry of Water," Academic Press, New York (1971).
2. L. M. Dorfman and G. E. Adams, "Reactivity of the Hydroxyl Radical in Aqueous Solutions," (NSRDS 46.) U.S. Government Printing Office, Washington, D.C. (1973).
3. M. Anbar, Farhataziz, and A. B. Ross, "Selected Specific Rates of Reactions of Transients from Water in Aqueous Solutions. II . Hydrogen Atoms," (NSRDS-NBS 51.) U.S. Government Printing Office, Washington, D.C. (1975).
4. M. Anbar, M. Bambenek, and A. B. Ross, "Selected Specific Rates of Reactions of Transients from Water in Aqueous Solutions. I . Hydrated Electron," (NSRDS-NBS 43.) U.S. Government Printing Office, Washington, D.C. (1973).
5. W. Bors, M. Saran, and G. Czapski, "Biological and Clinical Aspects of Superoxide and Superoxide Dismutase," (W. Bannister and J. V. Bannister, Eds.) Elsevier, North Holland/New York (1980).
6. M. Kuwabara, O. Inanami, D. Endoh, and F. Sato, Spin Trapping of Precursors of Thymine Damage in X-Irradiated DNA, Biochemistry 26:2458 (1987).

Phospholipid Storage in the Secretory Granule of the Mast Cell*

Stephen P. Chock‡ and Elsa A. Schmauder-Chock

From the Department of Experimental Hematology, Armed Forces Radiobiology Research Institute, Bethesda, Maryland 20814-5145

A spontaneous membrane assembly process has been postulated to account for the rapid perigranular membrane enlargement which occurs during mast cell secretory granule activation. This process requires the presence of a phospholipid store in the quiescent granule. By using purified granules with intact membranes we have determined the total phospholipid content of the average quiescent granule. The results suggest that the average quiescent granule contains sufficient phospholipid to sustain at least a trebling of its perigranular membrane surface area during activation. As much as two-thirds of the total cellular phospholipid is found in the granules, and since a large portion of this phospholipid is extruded into the extracellular space along with the granule matrix during exocytosis, it is implied that this phospholipid can serve as the substrate for the formation of the lipid-derived mediators of inflammation.

Phospholipid is the primary building block of all biological membranes. It also provides the arachidonic acid required for the formation of the eicosanoids such as prostaglandins, leukotrienes, and thromboxanes, which are potent mediators of inflammation (1, 2). Since membrane receptor activation might be coupled to a rapid phospholipid turnover and phospholipid metabolites can mediate many cellular responses, the role of phospholipid in cellular metabolism has become increasingly important.

Membranous structures such as vesicles, myelin bodies, and membrane whorls have been observed within the secretory granules of many cells (3-6). More recently, a process of spontaneous membrane assembly has been observed in the secretory granule of the mast cell during histamine secretion (7-9). Since it is generally believed that membrane assembly is coupled to phospholipid biosynthesis at the endoplasmic reticulum (10), it follows that most, if not all, of the cellular phospholipid must exist in membrane form. Since no membrane or membrane vesicles are present within the matrix of the quiescent secretory granule prior to activation, a question is raised about the nature of the granule matrix components which are responsible for sustaining the *de novo* membrane assembly process during secretion. Therefore it is important to determine if phospholipid is indeed present in the secretory granules of the mast cell.

By determining the phospholipid content of the membrane-bound secretory granules and correcting for the amount of phospholipid attributed to the original perigranular membrane, we concluded that the average mast cell granule contains sufficient phospholipid to accomplish at least a trebling of its perigranular membrane surface area during exocytosis.

MATERIALS AND METHODS

The procedure used for mast cell granule purification is based on the modification of several established methods (3, 11-13). Briefly, mast cells were purified from male Sprague-Dawley rats. Immediately following death by carbon dioxide inhalation, the peritoneal cavity was washed by injecting 25 ml of calcium-free Hanks' balanced salt solution (HBS)[1] with 10 units/ml heparin and 0.2% bovine serum albumin and drained through an incision in the abdominal wall. The combined lavages were centrifuged at $30 \times g$ for 20 min. The pellet was resuspended in a small volume of lavage buffer and filtered through a Spectra/mesh nylon acetate filter (Spectrum Medical, Los Angeles, CA) to remove particulates. Following centrifugation at $30 \times g$ for 10 min. the pellet was resuspended in several milliliters of lavage buffer. Two-ml aliquots of cell suspension were layered over each 4 ml of isotonic 38% bovine serum albumin in 15-ml polystyrene centrifuge culture tubes. The 38% (w/v) bovine serum albumin solution was made by dissolving fatty acid-free bovine serum albumin (Sigma) in calcium-free HBS and sterilizing by ultrafiltration. Following a 15-min $573 \times g$ centrifugation, the contaminant cells at the interface were first carefully removed by aspiration with a plastic pipette. The final purity of the mast cell preparation depends heavily on this step. Following removal of the remaining top aqueous phase, cells adhering to the wall above the albumin were removed by repeat rinsing with buffer without disturbing the albumin phase. The combined albumin phases were diluted to about 3 times their volume with calcium-free HBS and centrifuged at $446 \times g$ for 10 min. The pellet was washed twice by suspension in 15 ml of calcium-free HBS and centrifuged for 10 min at $32 \times g$. The pellet which contained pure mast cells was resuspended in 2.5 ml of calcium-free HBS in a 15-ml plastic centrifuge tube and sonicated using a Branson model W350 sonifier equipped with a microprobe for five pulses at an output setting of 2.5 and 25% duty cycle operating at the "puise" mode. Following vigorous vortexing the mixture was centrifuged at $50 \times g$ for 5 min. The supernatant containing the granules was transferred using a pipette without disturbing the cell pellet. The pellet which contained unbroken mast cells was resuspended in 2.5 ml of buffer. This same procedure of sonication followed by a 5-min $50 \times g$ centrifugation to remove the granule-containing supernatant was repeated for the 10-, the 15-, and the 20-pulse sonications, respectively. The combined supernatants (about 10 ml) were centrifuged at $72 \times g$ for 10 min to remove aggregates. The supernatant was centrifuged at $960 \times g$ for 15 min to pellet the granules. The purified granules were carefully resuspended in a desired volume of buffer and used immediately.

Routine electron microscopy of mast cells and mast cell granules was carried out according to established procedure (14). The average diameter of the quiescent granule was determined by two separate procedures. In the first procedure, the average granule diameter was obtained by measuring the diameters of the granule images on the electron micrographs of nine different unstimulated mast cells. Although most granules are spherical, to avoid unfair contribution from

[1] The abbreviations used are: HBS, Hanks' balanced salt solution; TNBS, trinitrobenzenesulfonate.

nonspherical granules, x-y coordinates were arbitrarily assigned to the enlarged image of each mast cell. Two diameters, parallel to the x and y axes, respectively, and which best divide each granule into four equal quadrants, were measured. The results were tallied and the granule diameter distribution plotted. An average diameter was calculated using a routine statistical program written for the IBM microcomputer.

In the second procedure, the average quiescent granule diameter was obtained from ultrastructural images of serial thin sections of each cell. The x and y coordinate diameter measurements of each granule were done as described for the first procedure. Since the diameter of the granule profile becomes smaller as it is sectioned away from the center of the granule, at least five diameter measurements were taken from serial sections of each granule. Only granules with their diameters going through a maximum within the series were chosen. The maximum x and the maximum y coordinate measurements of the same granule were averaged. This averaged value is taken as the true diameter of the granule. Data from 50 different granule series were compiled, and their mean diameter was calculated.

To determine the phospholipid content the number of granules in each preparation was first counted using a Cellozone particle counter (Particle Data, Inc., Elmhurst, IL) equipped with a 30-μm orifice tube and a 50-μl metering section. The equipment was standardized with 2.02-μm diameter latex beads, and the counting procedure was similar to that established for the study of platelets (15). After adding 0.1 ml of acetic acid to each ml of granule suspension, the phospholipid was immediately extracted by adding 3 ml of chloroform:methanol (2:1) to each milliliter of granule suspension with repeated vigorous vortexing. After removing the bottom organic phase which contained the phospholipid, the remaining aqueous phase was further extracted two more times with an addition of 3 ml of the extracting solvent each time. Phospholipid extraction using the procedure of Bligh and Dyer (16) has also been compared, and the result was similar. The combined chloroform phase, which contained the phospholipid, was carefully evaporated to dryness using a stream of nitrogen.

The phospholipid content of the samples was determined according to the recommended procedure of Vaskovsky *et al.* (17) with minor modifications. Briefly, dried sample was digested by the addition of 0.1 ml of 62% perchloric acid and then heated in an aluminum block to 200 °C for 25 min. (Caution is necessary since excessive heating of concentrated perchlorate can cause an explosion.) To monitor the completeness of the digestion step, parallel digestions of phosphatidylcholine and phosphatidylethanolamine standards (Supelco, Inc., Bellefonte, PA) were routinely carried out along with the unknown samples. After cooling, 0.9 ml of working reagent was added, mixed, heated in a boiling water bath for 15 min, cooled, and the adsorbance was read at 800 nm in a spectrophotometer. The working reagent was made by adding 34.25 ml of water to a mixture of 13 ml of 1 N sulfuric acid and 2.75 ml of stock reagent. The stock reagent was made as follows. Solution A (200 mg of hydrazinium chloride in 7 ml of 4 N HCl) was added to solution B (5 g of sodium molybdate in 30 ml of 4 N HCl) and heated in a boiling water bath for 20 min. After the mixture had cooled, 7 ml of concentrated sulfuric acid was slowly added with mixing and cooling. The volume was adjusted to 50 ml with water and stored in a dark bottle at room temperature. This solution is stable for weeks. The standard curve was constructed from potassium orthophosphate (99.3% pure, Fisher high pressure liquid chromatography grade), and the phosphorous content of the phospholipid standards, phosphatidylcholine and phosphatidylethanolamine, was checked against the standard curve.

The simultaneous determination of granule phospholipid and cholesterol content was also carried out on a single granule preparation. The granule lipid was extracted according to the phospholipid extraction procedure described above except that the extraction was only repeated once. The combined organic phase was dried under a stream of nitrogen and dissolved in 0.5 ml of chloroform. The separation of cholesterol from the phospholipid fraction was achieved using a silicic acid column as described by Dittmer and Wells (18). The chloroform eluate which contained the cholesterol was dried under a stream of nitrogen and immediately analyzed for total cholesterol using the procedure of Courchaine *et al.* (69) and Zlatkis *et al.* (70) as described by Kates (19). The methanol eluate which contained the phospholipid was also dried and analyzed for phospholipid according to the procedure described above.

Protein determination was done using the micro-trinitrobenzenesulfonate (TNBS) procedure with one modification, *i.e.* the stock 35 mg/ml TNBS reagent was made up in water instead of in the 0.25 M borate buffer as misstated in the original paper (20). The remaining

aqueous phase from the phospholipid extraction was warmed and a stream of nitrogen bubbled through to evaporate dissolved methanol and chloroform. The remaining solution was made to contain 7% trichloroacetic acid. After vigorous agitation, the sample was equilibrated at room temperature for 20 min. The protein precipitate was sedimented at 1000 × g for 20 min. The pellet was dissolved in 0.5 ml of a solution containing 0.1 M Na$_2$CO$_3$ and 0.5% lithium dodecyl sulfate (Sigma). Occasionally, the protein results from the TNBS method were also compared with the results obtained using the Lowry method as modified by Markwell *et al.* (21).

RESULTS

By using a mild sonication procedure we have been able to obtain membrane-bound secretory granules from rat peritoneal mast cells. The degree of homogeneity of such a preparation can be seen in Fig. 1. Aside from some "altered granules" (*arrow*) which have dispersed matrices and have lost their perigranular membranes, most of the granules still have intact membranes and have condensed matrices similar to those found in quiescent mast cells.

Fig. 2 shows the size distribution of the quiescent granule diameters in unstimulated mast cells. This figure represents the compilation of 2106 diameter measurements of 1053 granule profiles from nine randomly selected unstimulated mast cells. The average granule diameter calculated for each of the individual cells is summarized in Table I. From these data, the mean diameter ± S.D. of the quiescent granule can be calculated to be 0.62 ± 0.04 μm. In thin sections of granules such as those used to produce an electron micrograph the frequency of granule profiles reflecting the true granule diameter decreases as granules are sectioned away from their
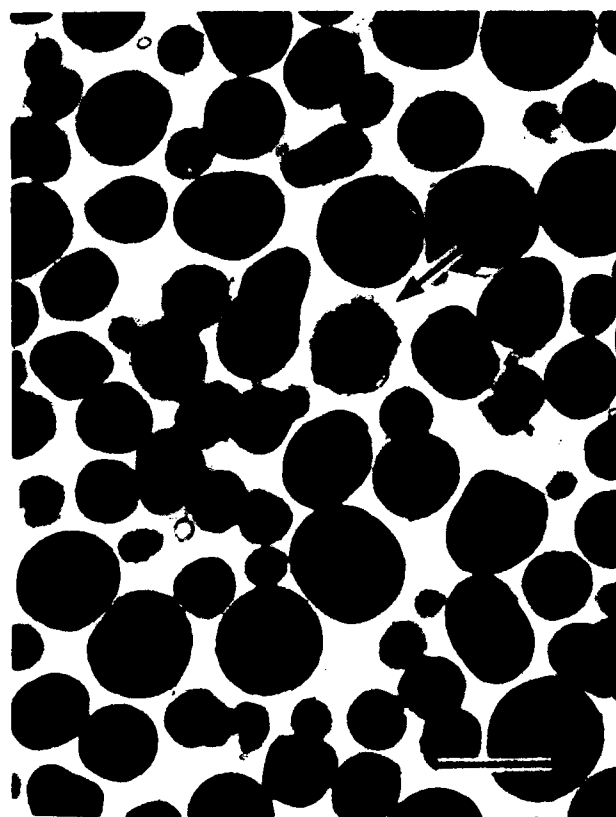

FIG. 1. **Purified granules with intact perigranular membranes.** An electron micrograph of purified granules shows the typical electron-dense, osmophilic, and amorphous matrix associated with quiescent granules of unstimulated mast cells. The presence of "altered granules" (*arrow*) with unraveled matrix and devoid of perigranular membrane can also be seen. The *bar* represents 1 μm.
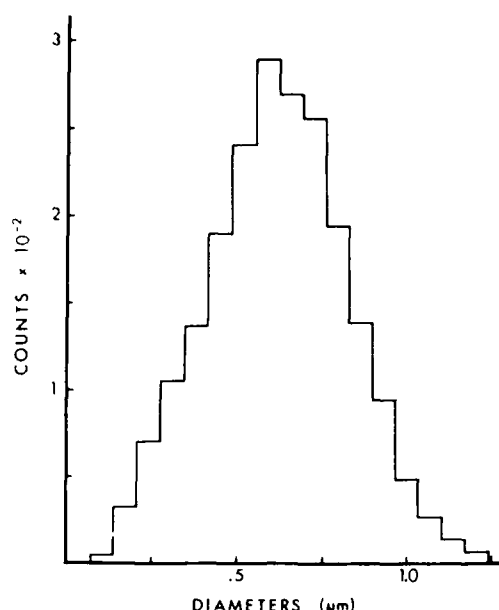
Fig. 2. **Size distribution of quiescent granules from unstimulated mast cells.** The results from 2106 granule diameter measurements from nine different unstimulated mast cells have been plotted. The mean diameter ± S.D. calculated from these data yields a value of 0.624 ± 0.037 μm for the average quiescent granule.

TABLE I

Determination of the average diameter for the quiescent mast cell granule

Data are for a total of 2106 measurements. The mean diameter ± S.D. was 0.62 ± 0.037 μm.

Cell	Average diameter
	μm
1	0.543
2	0.604
3	0.647
4	0.593
5	0.637
6	0.656
7	0.650
8	0.638
9	0.645

centers. This stereological artifact can be corrected by applying the equation of Elias and Hyde (22)

$$R = (4/\pi)r = 1.27r \tag{1}$$

where R is the true radius and r is the mean profile radius. This calculation yields a mean diameter of 0.79 μm for the average quiescent granule. Examination of the granule profile frequency distribution curve (Fig. 2) according to the visual procedure of Hennig and Elias (23) also suggests that the mean diameter of the quiescent granules has a value near 0.63 μm if the maximum granule diameter from Fig. 2 is 1.25 μm. This corrected value of 0.79 μm for the mean diameter of the quiescent granule is in good agreement with the values of 0.6 μm reported by Uvnas (24) and 0.777 μm reported by Helander and Bloom (25) calculated from pooled size distribution of granule profiles and corrected using the method of Bach (26).

An accurate estimation of the diameter of a spherical granule can also be achieved by determining its true diameter from serial sections. This method eliminates the uncertainty due to the artifact introduced when a granule is sectioned away from its equator. By using this procedure we have determined the diameters of 50 different granules and calcu-

lated their mean diameter ± S.D. to be 0.77 ± 0.01 μm. This value is in good agreement with the corrected value of 0.79 μm obtained above.

If we assume the granule to be spherical, the mean surface area of the quiescent granules can be determined for the granules represented by the frequency distribution curve in Fig. 2. The equations used for calculating the mean square radius (R^2), the standard deviation (S.D.), and the mean granule surface area (A) are

$$R^2 = \sum_i^n (r'_i)^2/n \tag{2}$$

$$S.D. = \left(\sum_i^n ((r'_i)^2 - R^2)^2/(n-1) \right)^{\frac{1}{2}} \tag{3}$$

$$A = 4\pi R^2 \tag{4}$$

where $r'_i = 1.27r$, according to Equation 1 and $n = 2106$. This calculation yields a mean square radius ± S.D. of 0.145 ± 0.089 μm². After multiplying by 4π according to Equation 4, a corrected mean surface area of 1.82 μm² is obtained for the mean quiescent granule. This value is similar to the surface area of 1.96 μm² calculated for a sphere with a diameter of 0.79 μm.

The mean phospholipid content of the quiescent granule was determined using the microtechnique of Vaskovsky et al. (17). This method yields a sensitive linear standard curve as seen in Fig. 3. Since the unit for the inorganic phosphate plotted on the x axis is in nanomoles, one can easily estimate the molecular weight of an unknown with a given adsorbance if its amount in micrograms present in the sample is known. From a series of phospholipid standards, phosphatidylcholine and phosphatidylethanolamine, we have estimated their average molecular weight in Fig. 3 to be 800. A mean molecular weight for a phospholipid mixture can also be calculated if the phospholipid class composition and the molecular weight of each phospholipid class are known. The mast cell phospholipid is composed of 29.6% phosphatidylcholine, 26.7% phosphatidylethanolamine, 16.1% phosphatidylserine and phosphatidylinositol, 19.8% sphingomyelin, and 7.7% undetermined phospholipid (27). The fatty acid composition of each phospholipid class has also been determined. Based on this information, a mean molecular weight of 790 can be calculated for the mast cell phospholipid. Since this calculated value is not so different from the 800 generally assumed for the
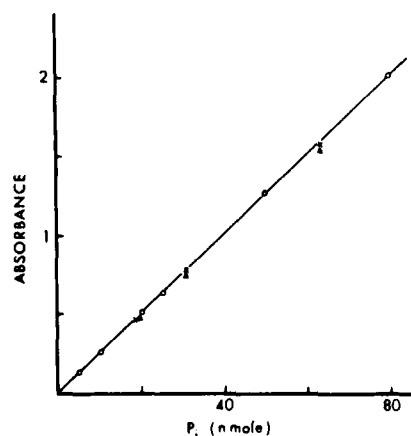

Fig. 3. **Phospholipid determination using the procedure of Vaskovsky et al. (17).** The linear standard curve is constructed from standard inorganic phosphate (O). The 800-nm adsorbance for a series of phospholipid standards, phosphatidylcholine (×) and phosphatidylethanolamine (△) of known concentration is also plotted.

average molecular weight of phospholipid, we have used this same value for our calculations.

The results of phospholipid determination on 10 separate granule preparations are shown in Table II. From these data the average phospholipid content of an average granule can be calculated to be $33.08 \pm 9.24 \times 10^{-18}$ mol. This, based on an average molecular weight of 800, would yield a value of 0.027 pg of phospholipid for the average quiescent granule. In terms of the number of phospholipid molecules, this value corresponds to 19.9×10^6 for an average granule.

Since the average surface area of a phospholipid molecule in a bilayer is known (28), we can estimate the bilayer surface area attainable by the granule phospholipid content. A mean surface area of 66 Å^2 has been determined for phospholipid in a mixed phospholipid liposome (without cholesterol) in the presence of 0.16 M NaCl (29). Based on this value, the corresponding bilayer that can be covered by 19.9×10^6 phospholipid molecules (33.08×10^{-18} mol) is equal to 6.57 μm^2. Since the surface area of an average quiescent granule equals 1.82 μm^2, this amount corresponds to 3.6 times the area of the original perigranular membrane. Therefore we can safely conclude that the average granule contains enough phospholipid alone to sustain at least a 3-fold expansion of its perigranular membrane during activation.

Since cholesterol is an important component of membrane, we have carried out a simultaneous determination of total granule cholesterol and phospholipid content in a granule preparation after the lipid fractions were first separated using a silicic acid column. The results showed that the granule contained about 0.008 pg (or 2.07×10^{-17} mol) of cholesterol and 0.039 pg (or 4.86×10^{-17} mol) of phospholipid. This suggests a phospholipid:cholesterol ratio of about 2.5:1 for the quiescent granule. The 4.86×10^{-17} mol of phospholipid obtained here can cover up to 9.67 μm^2 of bilayer. This, when compared to the 1.82 μm^2 for the mean granule surface area, would represent a 5.3-fold expansion.

The protein content of the quiescent granules was also determined using the TNBS procedure. The results of six different granule preparations are listed in Table III. From these results the average protein content of the quiescent granule can be calculated to equal 0.38 ± 0.07 pg. This, compared with the phospholipid result of 0.027 pg, gives a protein:phospholipid ratio of about 14:1 for the quiescent granule.

DISCUSSION

By using membrane-bound granules we have minimized the loss of matrix-bound components during the purification procedure. The loss of perigranular membrane by hypo-osmotic shock and/or the presence of a large population of altered

TABLE II

Determination of the phospholipid content of the mast cell granule

The mean content $\pm$ S.D. was $33.08 \pm 9.24 \times 10^{-18}$ mol of phospholipid/granule.

Experiment	Granule $\times 10^{-4}$	P. content	Phospholipid/granule
		nmol	*mol $\times 10^{18}$*
1	2.86	95	33.2
2	4.26	128	30.1
3	2.02	88	43.6
4	4.05	100	24.7
5	5.10	130	25.5
6	2.10	70	33.3
7	4.00	159	39.8
8	1.77	33	18.6
9	1.84	60	32.6
10	3.16	156	49.4

TABLE III

Determination of the granule protein content

The average granule protein content $\pm$ S.D. was 0.38 ± 0.07 pg.

Experiment	Protein content
	pg
1	0.34
2	0.35
3	0.5
4	0.36
5	0.3
6	0.44

granules in granule preparations might have contributed to the low granule phospholipid content reported earlier (30, 31). By using a sensitive phospholipid determination technique we have estimated the phospholipid content of the average secretory granule of the quiescent mast cell. The results suggest that the average quiescent granule contains sufficient phospholipid in its matrix to sustain at least a 3-fold expansion of its perigranular membrane during activation. This sequestration and coalescence of this matrix-stored phospholipid into membrane vesicles and their rapid fusion into the perigranular membrane are the basis of the trebling of the perigranular membrane surface area reported previously for the activated granule (14).

The 3-fold membrane generation potential reported here should be considered as the lower limit for the following reasons. 1) In our phospholipid determination we have assumed that all of the granules analyzed contained intact perigranular membranes and have not lost their granule contents. In fact, all of our granule preparations contained some altered granules which were devoid of perigranular membranes. Their presence might be the result of accidental activation during the purification procedure. The normal basal level of mast cell secretory activity could also contribute to the formation of altered granules. The presence of altered granules could conceivably have lowered our phospholipid measurement. 2) We have overestimated the phospholipid contribution attributed to the original perigranular membrane by assuming that the original perigranular membrane was composed of pure phospholipid. If other membrane components such as cholesterol, glycolipid, and membrane protein are assumed to be present in the original perigranular membrane, the actual amount of phospholipid present in the original granule membrane would have been less than what we have assumed in our calculation. 3) We have not included the contributions of granule glycolipid and cholesterol in our calculation of the granule membrane generation potential. Although we did not verify the presence of glycolipid, we have estimated the amount of cholesterol in the granule. When compared with the concentration of phospholipid, our results suggest that there can be as much as 1 mol of cholesterol for every 2.5 mol of phospholipid present in the granule. Given the fact that the presence of just 10% cholesterol in a bilayer can increase the membrane surface area by as much as 30% (29, 32), the potential contribution of the granule cholesterol to the granule membrane generation potential would be substantial.

It should be pointed out that the amount of phospholipid determined here only represents the mean of a wide population of granules. It does not preclude the possibility of a granule-phospholipid concentration difference related to the chronological age and/or the location of the granule in the cell. The purpose of the large phospholipid store is to bring about the process of *de novo* membrane generation which enables the activated granule to approach contact with the

plasma membrane and/or with other granule membranes in order for fusion and pore formation to occur. Once pore formation has occurred the remaining unspent phospholipid is exteriorized along with other granule matrix contents. It should also be pointed out that the process of spontaneous membrane assembly can also result in the formation of membrane vesicles with matrix contents in them (see Fig. 2 in Ref. 8 and Fig. 1 in Ref. 9). The fusion of such vesicles with the perigranular membrane would result in the extrusion of some granule matrix contents, including phospholipid, into the cytoplasm according to the model in Fig. 4.

From our phospholipid data we can estimate the distribution of the cellular phospholipid in the average quiescent mast cell. Since the average mast cell contains about 1020 secretory granules (25), the total amount of phospholipid present in the granules would equal approximately 27 pg; and since the average mast cell contains 41.4 pg of phospholipid (27), the portion of phospholipid found in the secretory granules would account for 65.2% or about two-thirds of the total cellular phospholipid. Such a tremendous amount of phospholipid, which is stored in the secretory granules in nonbilayer form, poses an interesting problem in the mechanism of cellular phospholipid synthesis and trafficking. The current dogma of linking phospholipid synthesis to membrane assembly at the endoplasmic reticulum (10, 33) requires that most, if not all, of the cellular phospholipid exist in bilayer form. With this in mind, the possibility of an alternative mechanism which permits packaging or transport of phospholipid to secretory granules must be considered.

The average granule protein content of 0.38 pg, determined using the TNBS procedure, agrees reasonably well with the published result of Parekh and Glick (34). When calculated for the average mast cell, our value would equal 389 pg, which is higher than the 330 pg reported by them for the total cellular protein. However, our result becomes too high when compared with the value of 209 pg reported by Diamant and Lowry (35). We cannot explain this discrepancy other than pointing out that our TNBS method which measures the content of primary amine might have reflected the unusually high amount of lysine-containing basic protein in the granules (24, 36). However, this does not explain why the modified

Lowry procedure (21) consistently yielded an answer about 20% higher than the TNBS procedure when parallel samples were tested using both methods. Since at least 15% of the granule protein is an active chymotrypsin-like protease (36, 37), its presence might have complicated the protein results. However, in our analyses the protease should have been inactivated during the acidic phospholipid extraction procedure which takes place immediately following granule purification.

The presence of a high concentration of phospholipid in the secretory granule raises the question about the nature of its interaction with other granule components such as histamine, which can amount to 15–30 pg for the rat peritoneal mast cell (3, 24). The matrix of the quiescent mast cell granule appears very electron-dense and amorphous, but following activation the matrix becomes dispersed and unraveled (14, 38, 39). Detergent extraction of the granule revealed a ribbon-like "proteo-heparin" backbone material suggesting the existence of a basic matrix structure (11). Filamentous matrix proteins have also been seen adhering to the surface of the de novo generated vesicles (8), but the nature of their interaction is not well understood. Since membrane bilayer owes its existence to the presence of water (the hydrophobic effect (40)), the absence of bilayer in the quiescent granule must imply that the granule contains little or no water. This suggests that the phospholipid could conceivably either be bound to the hydrophobic matrix protein or aggregate in a liquid crystalline form throughout the granule. Since the granule is also known to contain a millimolar concentration of calcium (41) and has an acidic environment (42), the precipitation of phospholipid and matrix proteins may occur. The binding and precipitation of granule components might be a design to maintain isotonicity between the densely packed quiescent granule and the cytoplasm. The disruption of this osmotic equilibrium during granule activation might contribute to the driving force for the influx of cellular water into the granule, causing the sequestration and coalescence of the granule phospholipid into vesicles (7, 8).

A specific interaction between histamine and phospholipid under acidic conditions has been studied using NMR (43). The interaction between phosphatidylserine and histamine is
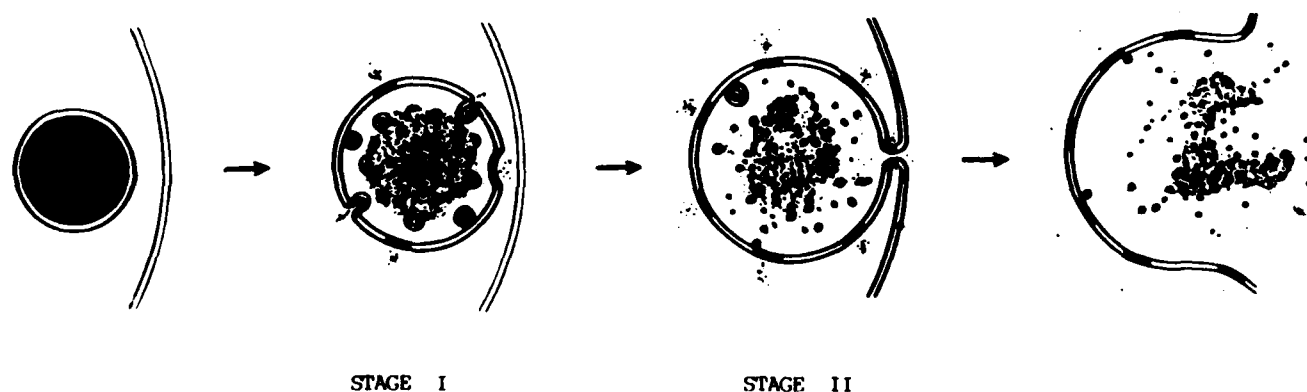
STAGE I   STAGE II

FIG. 4. **A working model for secretory granule exocytosis.** The views from *left* to *right* depict the main stages which a condensed quiescent secretory granule in the cytoplasm can undergo following activation to secrete. *Stage I* represents the step in which the process of spontaneous membrane assembly occurs. This process results in the formation of membrane vesicles of various sizes, some of which may contain matrix components. The rapid fusion between the newly assembled membrane vesicles and the perigranular membrane results in the release of some granule matrix contents into the cytoplasm and the rapid enlargement of the perigranular membrane. *Shaded bilayer*, reinsertion of newly assembled membrane. *Stage II* depicts the fusion of the expanding perigranular membrane with the plasma membrane which results in pore formation. Following pore formation the granule matrix becomes exposed to the extracellular fluid. With the aid of an ion-exchange mechanism and diffusion, the granule matrix unravels and disperses.

mediated via the imidazole proton of the histamine. The addition of histamine to phosphatidylethanolamine results in precipitation under acidic pH. The interaction of noradrenaline, a major component of the chromaffin granule, with phosphatidylserine has also been studied (44). This interaction is pH-dependent, and their binding follows the Langmuir isotherm.

Historically, phospholipid has been found to be a major component of many secretory granules. As early as 1928, Ling *et al.* (45) reported that the secretion of pepsin was accompanied by phospholipid secretion. In 1943 Claude (46, 47) concluded that the secretory granules of the pancreas and the liver from both guinea pigs and rats contained about 20% phospholipid. The presence of phospholipid has also been reported in the chromaffin granules (48–50), the platelet granules (6, 51), the parotid acinar cell (52), the thymus gland cells (53), the prostate gland cells (54), and the poison gland cells of the centipede (55). The significance of these reports might have been overlooked due to the inability to comprehend the purpose of phospholipid storage in secretory granules and the preconceived notion that cellular phospholipid exists only in bilayer form.

Hokin and Hokin (56) found a rapid incorporation of ^{32}P into the phospholipid fraction of stimulated pancreatic slices. Since the 7-fold increase in the specific activity of phospholipid after a 2-h incubation with acetylcholine or carbamylcholine occurred under aerobic conditions, they attributed their results to an increase in phospholipid synthesis subsequent to the loss of granule phospholipid during amylase secretion. More recently, a rapid phospholipid turnover has also been found in many receptor-mediated exocytoses including the mast cell (57–60). In conjunction with the phospholipid turnover, a rapid generation of prostaglandins, leukotrienes, thromboxanes, and other eicosanoids has also been detected during secretion (61–64). Many of these lipid-derived factors are potent mediators of inflammation. Other lipid-derived chemotactic factors such as platelet-activating factor, acetyl-glyceryl-ether-phosphorylcholine, have also been detected during mast cell secretion (65). About 16.1% of the mast cell phospholipid is composed of phosphatidylinositol and phosphatidylserine, and about 18.2% of the phospholipid fatty acid is composed of arachidonic acid (27). Since about two-thirds of the phospholipid resides in the secretory granules, it can be assumed that a portion of this arachidonic acid would be extruded with the matrix into the extracellular space and become available as the substrate for eicosanoid synthesis. This may be the basis for the formation of the "slowly reacting substances" and the mechanism of delayed inflammatory response. Furthermore, the spontaneous membrane assembly process which takes place during granule activation can also result in the extrusion of some granule phospholipid including phosphatidylinositol into the cytoplasm of the stimulated mast cell according to the model in Fig. 4. Since a high concentration of phospholipase C is localized in the cytosol (66–68), the presentation of phosphatidylinositol would provoke a rapid phospholipid hydrolysis. This might account for some of the phosphatidylinositol turnover elucidated in the stimulated mast cell.

REFERENCES

1. Malmsten, C. L. (1984) *CRC Crit. Rev. Immunol.* **4**, 307–334
2. Bomalaski, J. S., Williamson, P. K., and Zurier, R. B. (1983) *Clin. Lab. Med.* **3**, 695–717
3. Kruger, P. G., Lagunoff, D., and Wan, H. (1980) *Exp. Cell Res.* **129**, 83–93
4. Lawson, D., Raff, M. C., Gomperts, B., Fewtrell, C., and Gilula, N. B. (1977) *J. Cell Biol.* **72**, 242–259
5. Henderson, W. R., and Chi, E. Y. (1985) *J. Cell Sci.* **73**, 33–48
6. White, J. G., and Krivit, W. (1966) *Blood* **27**, 167–186
7. Chock, S. P., and Chock, E. S. (1985) *Fed. Proc.* **44**, 1324 (Abstr. 5341)
8. Chock, S. P., and Schmauder-Chock, E. A. (1985) *Biochem. Biophys. Res. Commun.* **132**, 134–139
9. Schmauder-Chock, E. A., and Chock, S. P. (1987) in *Proceedings of the 45th Annual Meeting of the Electron Microscopy Society of America* (Bailey, G. W., ed) pp. 782–783, San Francisco Press, San Francisco
10. Alberts, B., Bray, D., Lewis, J., Raff, M., Roberts, K., and Watson, J. D. (1983) *Molecular Biology of the Cell*, p. 350, Garland Publishing Inc., New York
11. Chock, S. P., and Schmauder-Chock, E. (1987) in *Prostaglandins and Lipid Metabolism in Radiation Injury* (Walden, T. L., and Hughes, H. N., eds) pp. 127–132, Plenum Publishing Corp., New York
12. Amende, L. M., and Donlon, M. A. (1985) *Biochim. Biophys. Acta* **812**, 713–720
13. Sullivan, T. J., Parker, K. L., Stenson, W., and Parker, C. W. (1975) *J. Immunol.* **114**, 1473–1478
14. Schmauder-Chock, E. A., and Chock, S. P. (1987) *Histochem. J.* **19**, 413–418
15. Corash, L., Tan, H., and Gralnick, H. R. (1977) *Blood* **49**, 71–87
16. Bligh, E. G., and Dyer, W. J. (1959) *Can. J. Biochem. Physiol.* **37**, 911–917
17. Vaskovsky, V. E., Kostetsky, E. Y., and Vasendin, I. M. (1975) *J. Chromatogr.* **114**, 129–141
18. Dittmer, J. C., and Wells, M. A. (1969) *Methods Enzymol.* **14**, 482–530
19. Kates, M. (1986) *Techniques of Lipidology: Isolation, Analysis and Identification of Lipids*, pp. 360–361, North-Holland Publishing Co., Amsterdam
20. Hazra, A. K., Chock, S. P., and Albers, R. W. (1984) *Anal. Biochem.* **137**, 437–443
21. Markwell, M. A. K., Haas, S. M., Bieber, L. L., and Tolbert, N. E. (1978) *Anal. Biochem.* **87**, 206–210
22. Elias, H., and Hyde, D. M. (1983) *A Guide to Practical Stereology*, Vol. 1, pp. 57–126, Karger Continuing Education Series, Karger Basel, Basel, Switzerland
23. Hennig, A., and Elias, H. (1970) *J. Microsc.* **93**, 101–107
24. Uvnas, B. (1982) in *The Secretory Granules* (Poisner, A. M., and Trifaro, J. M., eds) pp. 357–384, Elsevier Science Publishing Co., Amsterdam
25. Helander, H. F., and Bloom, G. D. (1974) *J. Microsc.* **100**, 315–321
26. Bach, G. (1967) in *Quantitative Methods in Morphology* (Weibel, E. R., and Elias, H., eds) pp. 23–45, Springer-Verlag, Heidelberg, West Germany
27. Strandberg, K., and Westerberg, S. (1976) *Mol. Cell. Biochem.* **11**, 103–107
28. Small, D. M. (1967) *J. Lipid Res.* **8**, 551–557
29. Johnson, S. M. (1973) *Biochim. Biophys. Acta* **307**, 27–41
30. Lagunoff, D., Phillips, M. T., Iseri, O. A., and Benditt, E. P. (1964) *Lab. Invest.* **13**, 1331–1344
31. Bergqvist, U., Samuelsson, G., and Uvnas, B. (1971) *Acta Physiol. Scand.* **83**, 362–372
32. Bourges, M., Small, D. M., and Dervichian, D. G. (1967) *Biochim. Biophys. Acta* **137**, 157–167
33. Bishop, W. R., and Bell, R. M. (1985) *Cell* **42**, 51–60
34. Parekh, A. C., and Glick, D. (1962) *J. Biol. Chem.* **237**, 280–286
35. Diamant, B., and Lowry, O. H. (1966) *J. Histochem. Cytochem.* **14**, 519–524
36. Lagunoff, D., and Pritzl, P. (1976) *Arch. Biochem. Biophys.* **173**, 554–563
37. Yurt, R. W., and Austen, K. F. (1977) *J. Exp. Med.* **146**, 1405–1419
38. Bloom, G. D., Fredholm, B., and Haegermark, O. (1967) *Acta Physiol. Scand.* **71**, 270–282
39. Rohlich, P., Anderson, P., and Uvnas, B. (1971) *J. Cell Biol.* **51**, 465–483
40. Tanford, C. (1980) *The Hydrophobic Effect: Formation of Micelles and Biological Membranes*, 2nd Ed., John Wiley & Sons, New York

41. Chock, E. S., Donlon, M. A., Fiori, C. E., and Catravas, G. N. (1982) *J. Cell Biol.* **95**, 409a (Abstr. 20087)
42. Lagunoff, D., and Rickard, A. (1983) *Exp. Cell Res.* **144**, 353–360
43. Abernethy, D., Fitzgerald, T. J., and Walaszek, E. J. (1974) *Biochem. Biophys. Res. Commun.* **59**, 535–541
44. Formby, B. (1967) *Mol. Pharmacol.* **3**, 284–289
45. Ling, S. M., Liu, A. C., and Lim, R. K. S. (1928) *Chin. J. Physiol.* **2**, 305–328
46. Claude, A. (1943) *Science* **87**, 451–456
47. Claude, A. (1943) in *Biological Symposia* (Cattell, J., ed.) Vol. 10 pp. 111–129, Jaques Cattell Press, Lancaster, PA
48. Blaschko, H., Firemark, H., Smith, A. D., and Winkler, H. (1967) *Biochem. J.* **104**, 545–549
49. Helle, K. B. (1973) *Biochim. Biophys. Acta* **318**, 167–180
50. Mylroie, R., and Koenig, H. (1971) *FEBS Lett.* **12**, 121–124
51. Marcus, A. J., Ullman, H. L., and Safier, L. B. (1969) *J. Lipid Res.* **10**, 108–114
52. Simson, J. A. V., Hall, B. J., and Spicer, S. S. (1973) *Histochem. J.* **5**, 239–254
53. Curtis, S. K., Cowden, R. R., and Nagel, J. W. (1979) *J. Morphol.* **160**, 241–274
54. Kanwar, U., and Kansal, M. (1980) *J. Helminthol.* **54**, 263–266
55. Nagpal, N., and Kanwar, U. (1981) *Toxicon* **19**, 898–901
56. Hokin, M. R., and Hokin, L. E. (1953) *J. Biol. Chem.* **203**, 967–977
57. Berridge, M. J., and Irvine, R. F. (1984) *Nature* **312**, 315–321
58. Cockcroft, S. (1982) *Cell Calcium* **3**, 337–349
59. Ishizuka, Y., Imai, A., Nakashima, S., and Nozawa, Y. (1983) *Biochem. Biophys. Res. Commun.* **111**, 581–587
60. Kennerly, D. A., Sullivan, T. J., and Parker, C. W. (1979) *J. Immunol.* **122**, 152–159
61. Ishizaka, T., and Ishizaka, K. (1984) *Prog. Allergy* **34**, 188–235
62. Garcia-Gil, M., and Siraganian, R. P. (1986) *J. Immunol.* **136**, 3825–3828
63. Roberts, L. J., II, Lewis, R. A., Oates, J. A., and Austen, K. F. (1979) *Biochim. Biophys. Acta* **575**, 185–192
64. Reichman, M., Nen, W., and Hokin, L. E. (1987) *Biochem. Biophys. Res. Commun.* **146**, 1256–1261
65. Demopoulos, C. H., Pinckard, R. N., and Hanahan, D. J. (1979) *J. Biol. Chem.* **254**, 9355–9358
66. Hofmann, S. L., and Majerus, P. W. (1982) *J. Biol. Chem.* **257**, 6461–6469
67. Kennerly, D. A., Sullivan, T. J., Sylvester, P., and Parker, C. W. (1979) *J. Exp. Med.* **150**, 1039–1044
68. Ryu, S. H., Suh, P. G., Cho, K. S., Lee, K. Y., and Rhee, S. G. (1987) *Proc. Natl. Acad. Sci. U. S. A.* **84**, 6649–6653
69. Courchaine, A. J., Miller, W. H., and Stein Jr., D. B. (1959) *Clin. Chem.* **5**, 609–614
70. Zlatkis, A., Zak, B., and Boyle, A. J. (1953) *J. Lab. Clin. Med.* **41**, 486–492

Physiological localization of an agonist-sensitive pool of Ca^{2+} in parotid acinar cells

[stimulus-secretion coupling/fura-2/salivary epithelial cells/intracellular Ca^{2+} stores/bis(2-aminophenoxy)ethane-N,N,N',N'-tetraacetate]

J. Kevin Foskett[*†], Pamela J. Gunter-Smith[*], James E. Melvin[‡], and R. James Turner[‡]

*Physiology Department, Armed Forces Radiobiology Research Institute, Bethesda, MD 20814; and ‡Clinical Investigations and Patient Care Branch, National Institute of Dental Research, National Institutes of Health, Bethesda, MD 20892

ABSTRACT   Muscarinic stimulation of fluid secretion by mammalian salivary acinar cells is associated with a rise in the level of intracellular free calcium ($[Ca^{2+}]_i$) and activation of a calcium-sensitive potassium (K^+) conductance in the basolateral membrane. To test in the intact cell whether the rise of $[Ca^{2+}]_i$ precedes activation of the K^+ conductance (as expected if Ca^{2+} is the intracellular messenger mediating this response), $[Ca^{2+}]_i$ and membrane voltage were measured simultaneously in carbachol-stimulated rat parotid acinar cells by using fura-2 and an intracellular microelectrode. Unexpectedly, the cells hyperpolarize (indicating activation of the K^+ conductance) before fura-2 detectable $[Ca^{2+}]_i$ begins to rise. This occurs even in Ca^{2+}-depleted medium where intracellular stores are the only source of mobilized Ca^{2+}. Nevertheless, when the increase in $[Ca^{2+}]_i$ was eliminated by loading cells with the Ca^{2+} chelator bis(2-amino-5-methylphenoxy)ethane-N,N,N',N'-tetraacetate (Me_2BAPTA) and stimulating in Ca^{2+}-depleted medium, membrane hyperpolarization was also eliminated, indicating that a rise of $[Ca^{2+}]$ is required for the agonist-induced voltage response. Stimulation of Me_2BAPTA-loaded cells in Ca^{2+}-containing medium dramatically accentuates the temporal dissociation between the activation of the K^+ conductance and the rise of $[Ca^{2+}]_i$. The data are consistent with the hypothesis that muscarinic stimulation results in a rapid localized increase in $[Ca^{2+}]_i$ at the acinar basolateral membrane followed by a somewhat delayed increase in total $[Ca^{2+}]_i$. The localized increase cannot be detected by fura-2 but is sufficient to open the Ca^{2+}-sensitive K^+ channels located in the basolateral membrane. We concluded that a receptor-mobilized intracellular store of Ca^{2+} is localized at or near the basolateral membrane.

Fluid secretion by mammalian exocrine cells, including salivary acinar cells, is regulated by alterations in plasma membrane ion permeabilities (1). Among the earliest events associated with agonist-induced stimulation of fluid secretion are a rapid plasma membrane hyperpolarization (1–4) and a dramatic loss of cellular K^+ (5). Patch-clamp studies have identified Ca^{2+}- and voltage-sensitive K^+ channels in salivary and pancreatic acinar basolateral membranes whose activation by secretagogues is believed to underlie these effects (6). Another early event associated with agonist stimulation is a rapid rise in the level of intracellular free calcium ($[Ca^{2+}]_i$) (7–11). As in a wide variety of other cell types, $[Ca^{2+}]_i$ is thought to rise as a result of inositol trisphosphate mobilization of intracellular stores (9, 12, 13), as well as enhanced Ca^{2+} influx across the plasma membrane (7, 14–17). A large body of evidence indicates that the rise of $[Ca^{2+}]_i$ is directly responsible for activating the K^+ channels in the acinar basolateral membranes. Specifically, it has been shown that (i) the Ca^{2+}

sensitivity of the K^+ channels is within the appropriate physiological (agonist-induced) range of $[Ca^{2+}]_i$ (6, 18–21), (ii) the cellular K^+ loss is abolished in Ca^{2+}-depleted cells stimulated in Ca^{2+}-free medium (22, 23), (iii) the application of Ca^{2+} ionophores to acinar cells activates K^+ channels and causes a loss of cellular K^+ similar to that caused by agonists (23–26), (iv) the intracellular perfusion of a Ca^{2+} chelator blocks the agonist-stimulated increase in K^+ conductance (18, 26, 27), and (v) the intracellular perfusion of inositol trisphosphate activates the K^+ conductance (28).

One aspect that has not yet been explored, however, is the temporal relationship between the agonist-induced rise of $[Ca^{2+}]_i$ and the activation of the basolateral membrane K^+ conductance. If Ca^{2+} is indeed the relevant intracellular messenger, one would expect the rise in Ca^{2+} to precede the response that it signals. Recently, a new generation of Ca^{2+} indicator dyes has made it possible to measure agonist-induced changes in $[Ca^{2+}]_i$ with high temporal resolution in single cells (29). In the present study, we examine the relationship between the agonist-induced rise of $[Ca^{2+}]_i$ (measured with the Ca^{2+}-sensitive fluorescent dye fura-2) and membrane K^+ conductance (measured simultaneously with an intracellular microelectrode) in rat parotid acinar cells. The data indicate that a receptor-mobilized store of Ca^{2+} is localized at or near the basolateral membrane.

MATERIALS AND METHODS

Parotid Acinar Cell Preparation. Parotid acini from Wistar strain rats (euthanized by exsanguination while under general anesthesia) were isolated by collagenase/hyaluronidase digestion (30). A light fraction consisting of the pooled supernates from three 30-sec centrifugations (400 × g) of this preparation was used in the present studies. This fraction consisted of single cells, doublets, triplets, single acini, and small clumps of acini, as well as fragments of ducts. This material was suspended in albumin-free medium and plated onto glass coverslips.

Fura-2 and BAPTA Loading. Cells and aggregates adhering within 90 sec following plating were loaded with fura-2 (Molecular Probes) by incubation in 1.5 μM fura-2 acetoxymethyl ester at 37°C for 30 min in 5 ml of normal Ca^{2+} medium (see below). The volume associated with cells that adhered to a single coverslip was negligible compared to this volume of bathing medium. Based on previous work (7, 8), this incubation resulted in an intracellular fura-2 concentration of 10–20 μM. Bis(2-aminophenoxy)ethane-N,N,N',N'-tetraacetate

---

Abbreviations: BAPTA, bis(2-aminophenoxy)ethane-N,N,N',N'-tetraacetate; Me_2BAPTA, 5,5'-dimethyl-BAPTA; DIC, differential interference contrast.
†To whom reprint requests should be sent at present address: Division of Cell Biology, Hospital for Sick Children, 555 University Avenue, Toronto, ON M5G1X8, Canada.

(BAPTA) loading was accomplished by first loading the cells with fura-2 as described, then incubating the cells for an additional 90 min in 15 μM of the permeant acetoxymethyl ester of 5,5'-dimethyl-BAPTA (Me₂BAPTA; Molecular Probes) under identical conditions. The rationale for this procedure was based on two observations. First, cells loaded with fura-2 and examined 2 hr later were only slightly dimmer than cells examined immediately after loading (J.K.F., unpublished observations), indicating slow dye leakage. Second, the $[Ca^{2+}]_i$ responses of these cells were indistinguishable from freshly loaded cells, indicating that most of the dye remained in the cytoplasm as the Ca^{2+}-sensitive free acid. Fura-2 was not loaded simultaneously with BAPTA to avoid competition for cellular esterases by BAPTA, which was at a much higher concentration than the fura-2.

Microscopy and Fluorescence and Electrophysiological Measurements. The coverslip was mounted in a chamber and perfused continuously (bath volume = 50 μl; flow rate ≈ 4 ml/min) with a medium containing 110 mM NaCl, 5.4 mM KCl, 25 mM NaHCO₃, 0.8 mM MgCl₂, 0.4 mM KH₂PO₄, 0.33 mM NaH₂PO₄, 20 mM Hepes, 1.2 mM CaCl₂, 11 mM glucose, 2 mM glutamine, and 0.01% bovine albumin (pH 7.4) at 37°C in 95% O₂/5% CO₂ on the stage of an inverted microscope (Zeiss IM35). EGTA (1 mM) replaced the CaCl₂ in zero-Ca^{2+} medium. Membrane voltage was measured with respect to bath-ground with a glass microelectrode (100–200 MΩ, filled with 0.5 M KCl/10 mM potassium citrate in HPLC-grade water) coupled to an amplifier (750, World Precision Instruments, New Haven, CT). Voltage was recorded on a chart recorder and displayed on the screen of an oscilloscope. The microelectrode was positioned and impalements were performed with a stepper motor-driven micromanipulator while viewing the cell in differential interference contrast (DIC) optics by using a ×63 oil-immersion 1.25 numerical aperture objective lens. The microscope is designed to allow simultaneous DIC imaging and low-light level fluorescence measurements without the light losses normally associated with DIC (31). A video camera viewed the image in DIC optics and relayed its signal to a monitor and to a video mixer. Fluorescence excitation was accomplished by placing interference filters (350 and 380 nm; ±10 nm bandwidth) between each of two xenon arc lamps coupled to a rotating chopper wheel mounted on a separate table to prevent vibration transmission to the microelectrode. A shutter between the chopper wheel and the microscope limited the duration of fluorescence excitation to minimize probe photobleaching and photodynamic damage to the cells. The chopper alternately exposed the cells to 350 nm and 380 nm excitation at 60 Hz. Fluorescence emission (500 ± 40 nm) was detected by a photomultiplier tube coupled to a current-to-voltage converter whose output was displayed on the oscilloscope screen. Stray light was minimized by conducting all experiments in red room light. In most experiments, an aperture was placed in an intermediate image plane to collect fluorescence emission only from the cell impaled with the electrode. The oscilloscope was line triggered; thus, the photomultiplier tube output appeared as two stationary peaks on the oscilloscope screen: the peaks are a measure of fluorescence emission at 350 and 380 nm excitation, respectively. A second video camera (newvicon; response time = 20 msec) viewed the oscilloscope screen and relayed its signal to the video mixer. The DIC image of the cell was inserted into the image of the oscilloscope screen allowing the simultaneously determined photomultiplier tube and microelectrode outputs and the image of the cell to be viewed side-by-side as one video output on a television monitor. This video signal was recorded at 15 Hz on a video disk recorder. This frequency represents the temporal resolution of these experiments since the response time of the electrode amplifier, photomultiplier tube, and oscilloscope are all much faster than this. Also, the

response time of the newvicon tube is sufficiently fast (50 Hz) to avoid significant lag in the measured response. With regard to this latter point, any lag associated with the newvicon tube will affect the amplifier and photomultiplier tube outputs equally, since both are imaged by the newvicon. In many instances, the rapidity of the voltage and $[Ca^{2+}]_i$ changes observed in response to stimulation caused dual traces of each output to appear in the captured video frame, representing the temporal difference (16 msec) in acquisition of each video field. In these cases, the video field displaying the first detectable change was used for analyses. In most experiments, the transmitted light was shuttered off during fluorescence measurement to ensure against spectral contamination of the fura-2 signal. The data were analyzed by transfer of images from the video disk recorder to an image processing system (31). Fluorescence ratios (350/380 nm) were determined by division of background-subtracted peaks of emission at each excitation wavelength determined by using interactive software.

When fura-2 fluorescence was monitored during microelectrode penetrations in Ca^{2+} medium, most impalements resulted in some increase in the 350 nm/380 nm ratio, indicating that $[Ca^{2+}]_i$ had risen. This was not observed in cells in zero-Ca^{2+} medium, indicating that the rise in $[Ca^{2+}]_i$ was the result of Ca^{2+} leaking into the cell around the edge of the microelectrode. Successful impalements were less likely in single cells and doublets compared to cells in single acini or acinar clumps, as has been observed by others (18). In several cells, it was possible to achieve an impalement in Ca^{2+} medium with no or little evidence of a rise in $[Ca^{2+}]_i$. In these cells, the early responses of $[Ca^{2+}]_i$ and membrane voltage to stimulation by carbachol were indistinguishable from cells stimulated in zero-Ca^{2+} medium.

Fura-2 Calibration. Fluorescence ratios were converted to $[Ca^{2+}]_i$ by calibration of a separate group of cells. After determination of the control (resting) ratio R, the cells were perfused with 1.5 μM ionomycin in a solution containing 140 mM KCl, 20 mM Hepes, 0.1 mM carbachol, and 5 mM EGTA (pH 7.3) at 37°C. When the limiting ratio for the unbound form of fura-2 was determined (R_{min}), the perfusate was switched to a similar one in which 2.4 mM CaCl₂ replaced the EGTA, and the limiting ratio of the bound form (R_{max}) was determined. $[Ca^{2+}]_i$ was calculated by using the equation $[Ca^{2+}]_i = \beta \cdot K_d[(R - R_{min})/(R_{max} - R)]$, where K_d (the dissociation constant of the dye) was assumed to be 220 nM and β is the ratio of fluorescence at 380 nm excitation for fura-2 (unbound)/fura-2 (bound) (29). For $n = 6$ cells, $\beta = 7.1$ and $R_{max}/R_{min} = 10$. Calculated resting $[Ca^{2+}]_i = 46 \pm 4$ nM. For the purposes of calibrating the cells used in experiments, resting $[Ca^{2+}]_i$ was assumed to equal this value, and this value with the derived β and R_{max}/R_{min} values was used to calculate $[Ca^{2+}]_i$ during stimulation. For Me₂BAPTA-loaded cells, the 350 nm/380 nm ratio was converted to $[Ca^{2+}]_i$ based on similar calibrations of a separate group of Me₂BAPTA-loaded cells. Average resting $[Ca^{2+}]_i$ in Me₂BAPTA-loaded cells was 41 nM. For both groups of cells, the length of time between loading and calibration was comparable to that between loading and experimentation.

RESULTS

The muscarinic agonist carbachol typically caused a rapid ($t_{1/2} \approx 600$ msec) hyperpolarization (by 10–50 mV) of rat parotid acinar cells in both Ca^{2+} and zero-Ca^{2+} (0 mM Ca^{2+}/1 mM EGTA) medium (Fig. 1A). Membrane hyperpolarization by muscarinic agonists has been previously observed (2–4) and, as already mentioned, is thought to be mediated by activation of large-conductance K⁺ channels (6). Simultaneous determinations of $[Ca^{2+}]_i$ and membrane potential in rat parotid acinar cells (Fig. 1B) demonstrated that the rapid
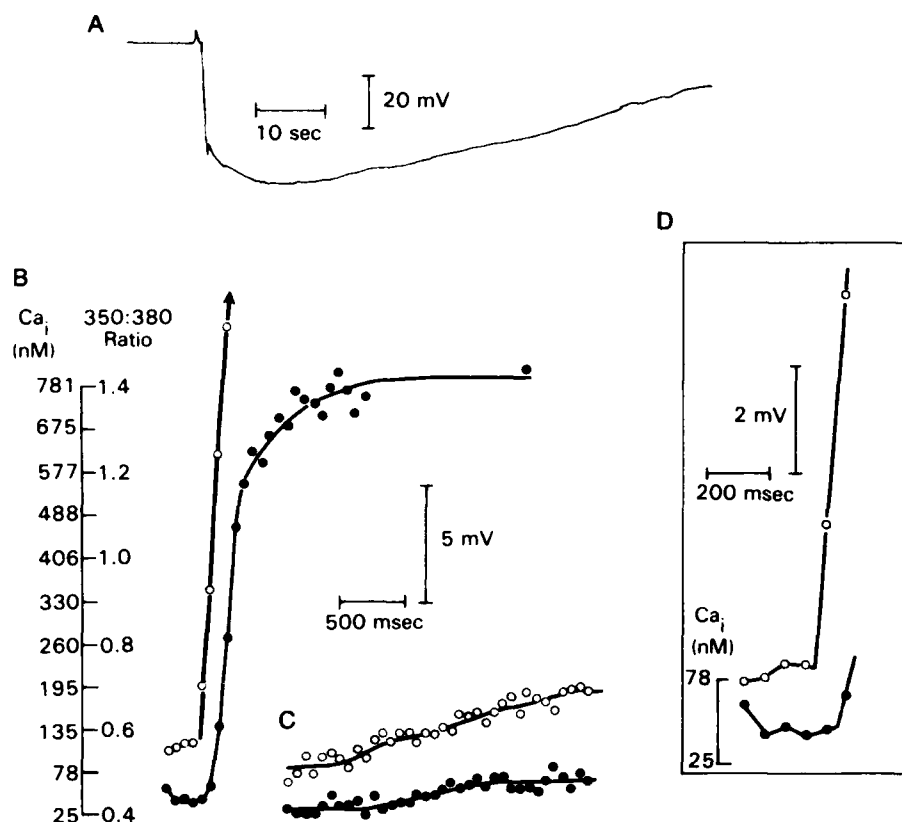
FIG. 1. Responses of $[Ca^{2+}]_i$ and membrane voltage in a rat parotid acinar during muscarinic stimulation. (*A*) Response of membrane voltage to rapid exposure to 1 mM carbachol in zero-Ca^{2+} medium. Downward deflection indicates membrane hyperpolarization. Cells stimulated in Ca^{2+} medium exhibited similar rapid hyperpolarizations but not the subsequent relaxation toward baseline voltage. Resting membrane potential = -28 mV; peak voltage = -78 mV. (*B*) Same data as in *A* at greater temporal resolution (15 Hz), along with simultaneously determined $[Ca^{2+}]_i$ measured with fura-2. Fura-2 350 nm/380 nm excitation ratios have been converted to $[Ca^{2+}]_i$ (in nM) according to calibration procedures described in *Materials and Methods*. Hyperpolarization is shown as an upward deflection to facilitate comparison with the fura-2 signal. (*C*) Same cell as in *A* and *B* showing responses of membrane voltage and $[Ca^{2+}]_i$ to a second application of 1 mM carbachol ≈ 2 min following removal of carbachol from the first exposure. (*D*) Same data as in *B* with expanded scales. ●, $[Ca^{2+}]_i$; ○, membrane voltage.

agonist-induced membrane hyperpolarization is paralleled by an equally rapid rise in $[Ca^{2+}]_i$ from ≈ 50 nM to ≈ 700 nM ($t_{1/2} < 500$ msec). Removal and subsequent reapplication of the agonist a few minutes later elicited comparable responses in cells in Ca^{2+} medium (data not shown), but cells stimulated a second time in zero-Ca^{2+} medium exhibited a weak membrane hyperpolarization and only a small associated rise in $[Ca^{2+}]_i$ (Fig. 1*C*). Thus, the agonist-induced elevation of $[Ca^{2+}]_i$ and membrane hyperpolarization parallel each other both temporally and quantitatively. This suggests that the magnitude and kinetics of $[Ca^{2+}]_i$ determine the magnitude and kinetics of the membrane voltage responses, as expected if $[Ca^{2+}]_i$ is the intracellular activator of the K^+ channels. However, close examination of the temporal relationship between $[Ca^{2+}]_i$ and membrane voltage (Fig. 1*D*) in cells stimulated in either Ca^{2+} or zero-Ca^{2+} media revealed that the earliest detectable change in membrane potential typically preceded the earliest detectable increase in $[Ca^{2+}]_i$ by at least 67 msec (range, 0–200 msec; mean ± SEM = 80 ± 12 msec; $n = 23$), the resolution of our apparatus (see *Materials and Methods*). This result is unexpected since a rise of $[Ca^{2+}]_i$ should precede the hyperpolarization if indeed $[Ca^{2+}]_i$ is the intracellular messenger activating the basolateral K^+ conductance.

One possible explanation for the above result is that Ca^{2+} is not the relevant intracellular messenger. To confirm that a rise of $[Ca^{2+}]_i$ is necessary to elicit the agonist-induced hyperpolarization, cells were loaded with the Ca^{2+} chelator Me_2BAPTA ($K_d = 40$ nM) (32) and stimulated in zero-Ca^{2+} medium. Under these conditions, the only source of Ca^{2+} that can be mobilized by carbachol will be intracellular stores. Provided the cells have been loaded with sufficient Me_2BAPTA, stimulation should result in a diminished Ca^{2+} response. In 8 of 10 Me_2BAPTA-loaded cells tested, the agonist-induced increase of $[Ca^{2+}]_i$ and membrane hyperpolarization were both abolished (data not shown). In the 2 other cells, carbachol elicited slow hyperpolarizations from 2 to 5 mV (Fig. 2*A*), associated with elevation of $[Ca^{2+}]_i$ by only ≈ 30 nM over several seconds to a minute (data not shown).

Taken together with previous data (6, 18–28), these results indicate that a rise in $[Ca^{2+}]_i$ is in fact necessary to activate basolateral membrane K^+ conductance. The blunted response of Me_2BAPTA-loaded cells (Fig. 2*A*) is not due to nonspecific toxic effects of Me_2BAPTA itself (33, 34) since, when Me_2BAPTA-loaded cells in zero-Ca^{2+} medium were exposed for a brief period to Ca^{2+} medium (3 min) following stimulation (Fig. 2*B*), a second application of carbachol in zero-Ca^{2+} medium elicited a normal rapid hyperpolarization
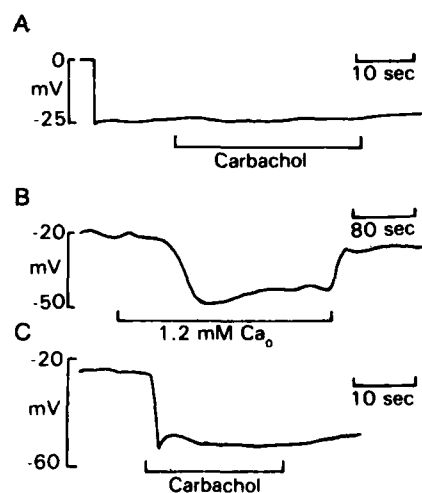
FIG. 2. Voltage responses of Me_2BAPTA-loaded cell stimulated in zero-Ca^{2+} medium. A Me_2BAPTA-loaded cell was impaled (rapid deflection at beginning of trace) in zero-Ca^{2+} medium. The cell was exposed to 1 mM carbachol (*A* and *C*) or 1.2 mM Ca^{2+} (*B*) as indicated. The traces in *A–C* are a continuous record. As observed by others (4), exposure to Ca^{2+} medium in the absence of carbachol (*B*) caused the membrane to hyperpolarize; the ionic basis for this effect is unknown. It was not associated with a fura-2-detectable rise in $[Ca^{2+}]_i$ (data not shown).

(Fig. 2C), demonstrating that Me₂BAPTA-loaded cells possess intact signal transduction processes.

An explanation that reconciles the seemingly contradictory observations that activation of the K⁺ permeability requires a rise of $[Ca^{2+}]_i$ and yet precedes that rise is that, during the earliest times of stimulation, the plasma membrane senses a region of locally elevated $[Ca^{2+}]$, which precedes the increase in whole cell $[Ca^{2+}]_i$ measured by fura-2. To explore this possibility, we measured the responses of Me₂BAPTA-loaded cells stimulated in Ca^{2+} medium. Under these conditions, in addition to the finite amount of Ca^{2+} that can be mobilized from intracellular stores, the cytoplasm will have access to an essentially infinite extracellular pool of Ca^{2+} as a result of the agonist-induced increase in plasma membrane Ca^{2+} permeability (7, 8, 14–17). If this Ca^{2+} influx is great enough, one would expect the eventual saturation of intracellular Me₂BAPTA and a consequent rise in $[Ca^{2+}]_i$. Since Ca^{2+} influx is at the basolateral membrane, the Me₂BAPTA near the basolateral membrane might be expected to saturate before the Me₂BAPTA in the bulk cytoplasm does. As a result, one would predict that $[Ca^{2+}]_i$ would rise first at the membrane, followed by a rise in the rest of the cytoplasm, which would be slowed by the presence of the chelator. Since the membrane hyperpolarization presumably depends on a rise of $[Ca^{2+}]_i$ adjacent to the inner surface of the basolateral membrane, under appropriate Me₂BAPTA loading conditions, the cell should hyperpolarize significantly earlier than the fura-2-detected rise of $[Ca^{2+}]_i$. This is in fact exactly what is observed. Stimulation of Me₂BAPTA-loaded cells in Ca^{2+} medium resulted in a large membrane hyperpolarization (Fig. 3) ($\Delta V = 26 \pm 4$ mV; $n = 9$ cells). Particularly striking, however, was the significant delay between the onset of the hyperpolarization and the earliest rise in $[Ca^{2+}]_i$. Generally, the earliest detectable increase in $[Ca^{2+}]_i$ occurred after the membrane completely hyperpolarized (Fig. 3A). In some cells (3 out of 9), $[Ca^{2+}]_i$ began to rise ≈300–1500 msec after the initial hyperpolarization, although the rate and magnitude of this increase were considerably diminished compared to unloaded cells (Fig. 3A). In other cells (4 out of 9), $[Ca^{2+}]_i$ remained unchanged during the first several seconds following the initial membrane hyperpolarization (Fig. 3B). In one of these cells for which a longer time course was followed, $[Ca^{2+}]_i$ eventually rose to higher levels (≈300 nM) by 75 sec. In two remaining cells, the responses of membrane potential and $[Ca^{2+}]_i$ were similar to those in unloaded cells.

DISCUSSION

Two possible explanations were given for the observation that the earliest detectable membrane hyperpolarization following carbachol stimulation of rat parotid acinar cells precedes the earliest detectable rise in $[Ca^{2+}]_i$. The first, that $[Ca^{2+}]_i$ is not the relevant intracellular messenger, appears highly unlikely. This is supported by (*i*) the parallel diminutions of the rise of $[Ca^{2+}]_i$ and membrane hyperpolarization during repeat stimulation of normal cells in zero-Ca^{2+} medium (Fig. 1), (*ii*) the elimination of both responses in Me₂BAPTA-loaded cells stimulated in zero-Ca^{2+} medium (Fig. 2A) in contrast to the ability of Me₂BAPTA-loaded cells to hyperpolarize in Ca^{2+} medium (Fig. 3), and (*iii*) the ability of the Ca^{2+} ionophore ionomycin to cause a rapid membrane hyperpolarization similar to that observed with carbachol (data not shown). Taken together with results from patch-clamp studies that indicate that Ca^{2+}-activated K⁺ channels underlie the membrane hyperpolarization observed in response to carbachol (1), these data provide strong evidence that a rise of $[Ca^{2+}]_i$ is directly responsible for the activation of these channels and the associated membrane hyperpolarization.

The second explanation for the temporal relationship between the hyperpolarization and the rise of $[Ca^{2+}]_i$ is that
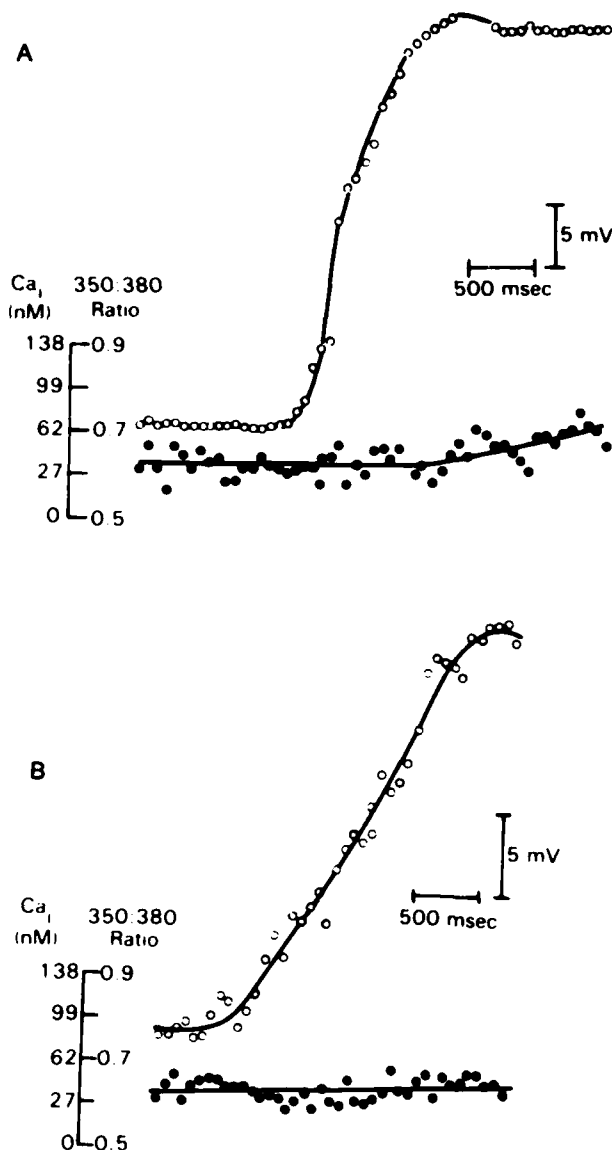
Fig. 3. Responses of $[Ca^{2+}]_i$ and membrane voltage in single Me₂BAPTA-loaded cells stimulated with 1 mM carbachol in Ca^{2+} medium. (A) In some cells, $[Ca^{2+}]_i$ began to rise ≈300–1500 msec after the initial hyperpolarization. (B) In other cells, $[Ca^{2+}]_i$ remained unchanged during the first several seconds following the initial hyperpolarization. ○, Membrane voltage; ●, $[Ca^{2+}]_i$.

$[Ca^{2+}]$ rises at the membrane before it rises in the bulk cytoplasm. Implicit in this explanation is the conclusion that fura-2 is unable to detect a highly localized, fast change of $[Ca^{2+}]$ at the basolateral membrane in the vicinity of the Ca^{2+}-activated K⁺ channels. This conclusion is supported by experiments in which Me₂BAPTA-loaded cells were stimulated in Ca^{2+} medium. These experiments were expressly designed to produce a transient, local rise of Ca^{2+} at the plasma membrane followed by a more gradual increase in $[Ca^{2+}]_i$ in the cytoplasm as Ca^{2+} influx from the extracellular solution saturated intracellular Me₂BAPTA. In these studies, carbachol produced a hyperpolarization that considerably preceded any fura-2 detectable increase of $[Ca^{2+}]_i$. The magnitude of the hyperpolarization was equivalent to that observed in unloaded cells, indicating that $[Ca^{2+}]$ at the inner surface of the basolateral membrane rose sufficiently to activate the K⁺ channels to the extent observed in control cells. However, in most cells the rate of hyperpolarization was considerably slowed (compare Fig. 3 A and B with Fig. 1A), which is as expected since Ca^{2+} entering

Cell Biology: Foskett *et al.*

Proc. Natl. Acad. Sci. USA 86 (1989) 171

the cell by way of the basolateral membrane must first interact with a large pool of Ca^{2+} chelator (Me_2BAPTA) at the inner surface of the membrane. The observed slow kinetics of cytosolic $[Ca^{2+}]_i$ measured with fura-2 are likewise consistent with Ca^{2+} interacting with a large Ca^{2+}-buffer pool throughout the cytoplasm. Cell-to-cell variability in the Me_2BAPTA-loading efficiency, as well as in the magnitude of the agonist-induced Ca^{2+} influx, would be expected to generate variability in the kinetics of hyperpolarization and $[Ca^{2+}]_i$ among these cells, as observed.

These experiments clearly demonstrate that, when $[Ca^{2+}]$ is expected to rise first at the plasma membrane, the membrane can indeed sense that Ca^{2+} before it can be detected in the cytoplasm. Taken together with previous results (6, 18–28), the data presented here indicate that the magnitude and kinetics of the voltage response to carbachol provide an independent measure of $[Ca^{2+}]$ at the inner surface of the basolateral membrane. Thus, the most likely explanation for the observation that the rise of fura-2-detected $[Ca^{2+}]_i$ does not precede the membrane hyperpolarization in normal cells stimulated in zero-Ca^{2+} medium (Fig. 1D) is that the earliest rise of $[Ca^{2+}]_i$ is localized near the plasma membrane. Since the only source of mobilized Ca^{2+} in zero-Ca^{2+} medium is intracellular stores, those stores must be localized at or near the basolateral membrane. By a similar argument, Ca^{2+} from the extracellular medium must also enter the cytoplasm at or close to the basolateral membrane.

The experiments shown in Fig. 2 provide further evidence that the agonist-sensitive intracellular pool of Ca^{2+} is localized near the basolateral membrane. Although Me_2BAPTA-loaded cells stimulated in zero-Ca^{2+} medium fail to hyperpolarize or show a rise of $[Ca^{2+}]_i$, after these cells were exposed for a brief (3 min) period to Ca^{2+} medium following a stimulation in zero-Ca^{2+} medium (Fig. 2B), a repeat stimulation in zero-Ca^{2+} medium elicited a normal, rapid hyperpolarization (Fig. 2C), which was not associated with a fura-2-detectable increase of $[Ca^{2+}]_i$ (data not shown). The most plausible explanation for these data is that Me_2BAPTA depletes the agonist-sensitive intracellular stores of Ca^{2+} and that exposure to extracellular Ca^{2+} following stimulation replenishes them. Subsequent stimulation causes a release of Ca^{2+} from these stores, which is sensed by the basolateral membrane, causing it to hyperpolarize (as for non-BAPTA-loaded cells). Since this released Ca^{2+} is not detected by fura-2, the Ca^{2+} released from the stores must be localized in the immediate vicinity of the basolateral membrane. The amount of Ca^{2+} released is sufficient to saturate the Me_2BAPTA adjacent to the membrane but insufficient to overcome the buffering in the cytoplasm, which allows $[Ca^{2+}]$ to rise only at the basolateral membrane and cause a normal hyperpolarization.

In rat parotid acinar cells (9, 12, 13), as in many other cell types (35), Ca^{2+} is mobilized from intracellular stores by inositol trisphosphate. Inositol trisphosphate is formed at the basolateral membrane by receptor–ligand activation of phospholipase C hydrolysis of phosphatidylinositol 4,5-bisphosphate (9, 12, 36–40). In many cell types (41), including the parotid acinar cell (13, 42), inositol trisphosphate-induced Ca^{2+} release is associated with a microsomal fraction enriched in endoplasmic reticulum markers. Whether the entire endoplasmic reticulum, only a specialized fraction of it (35, 42–47), or another organelle (48) represents the Ca^{2+} pool is unresolved. Although the endoplasmic reticulum is distributed throughout the cytoplasm of the parotid acinar cell, as in most cells, the results of the present study demonstrate that a receptor-mobilized pool of Ca^{2+} must be localized at or near the basolateral membrane. Other studies are now required to define the physical basis of this pool. A recent model by Putney (49) also proposes a close physical association between the plasma membrane and the agonist-

sensitive intracellular pool of Ca^{2+} in order to explain refilling of that pool following stimulation. Subcellular localization of Ca^{2+} pools may represent a general mechanism employed by cells to promote agonist-induced increases in $[Ca^{2+}]$ at spatially discrete intracellular sites.

1. Petersen, O. H. (1987) in *Physiology of the Gastrointestinal Tract*, ed. Johnson, L. R. (Raven, New York), pp. 745–771.
2. Roberts, M. L. & Petersen, O. H. (1978) *J. Membr. Biol.* **39**, 297–312.
3. Gallacher, D. V. & Petersen, O. H. (1980) *J. Physiol. (London)* **305**, 43–57.
4. Petersen, O. H. & Pedersen, G. L. (1974) *J. Membr. Biol.* **16**, 353–362.
5. Poulsen, J. H. & Oakely, B., II (1979) *Proc. R. Soc. London Ser. B* **204**, 99–104.
6. Maruyama, Y., Gallacher, D. V. & Petersen, O. H. (1983) *Nature (London)* **302**, 827–829.
7. Nauntofte, B. & Dissing, S. (1987) *Am. J. Physiol.* **253**, G290–G297.
8. Merritt, J. E. & Rink, T. J. (1987) *J. Biol. Chem.* **262**, 4958–4960.
9. Aub, D. L. & Putney, J. W., Jr. (1987) *J. Dent. Res.* **66**, 547–551.
10. O'Doherty, J., Stark, R. J., Crane, S. J. & Brugge, K. L. (1983) *Pflügers Arch.* **398**, 241–246.
11. Takemura, H. (1985) *Biochem. Biophys. Res. Commun.* **131**, 1048–1055.
12. Putney, J. W., Jr., Aub, D. L., Taylor, C. W. & Meritt, J. E. (1986) *Fed. Proc. Fed. Am. Soc. Exp. Biol.* **45**, 2634–2638.
13. Bonis, D., Giraud, D. & Rossignol, B. (1986) *Biol. Cell* **57**, 271–274.
14. Poggioli, J. & Putney, J. W., Jr. (1982) *Pflügers Arch.* **392**, 239–242.
15. Koelz, H. R., Kondo, S., Blum, A. L. & Schulz, I. (1977) *Pflügers Arch.* **370**, 37–44.
16. Miller, B. E. & Nelson, D. L. (1977) *J. Biol. Chem.* **252**, 3629–3636.
17. Poggioli, J., Weiss, S. J., McKinney, J. S. & Putney, J. W., Jr. (1983) *Mol. Pharmacol.* **23**, 71–77.
18. Findlay, I. (1984) *J. Physiol. (London)* **350**, 179–195.
19. Maruyama, Y., Petersen, O. H., Flanagan, P. & Pearson, G. T. (1983) *Nature (London)* **305**, 228–232.
20. Findlay, I., Dunne, M. J. & Peterson, O. H. (1985) *J. Membr. Biol.* **83**, 169–175.
21. Gallacher, D. V. & Morris, A. P. (1986) *J. Physiol. (London)* **373**, 379–395.
22. Putney, J. W., Jr. (1977) *J. Physiol. (London)* **268**, 139–149.
23. Parod, R. J. & Putney, J. W., Jr. (1978) *J. Physiol. (London)* **281**, 371–381.
24. Iwatsuki, N., Maruyama, J., Matsumoto, O. & Nishiyama, A. (1985) *Jpn. J. Physiol.* **35**, 933–944.
25. Poggioli, J., Leslie, B. A., McKinney, J. S., Weiss, S. J. & Putney, J. W., Jr. (1982) *J. Pharmacol. Exp. Ther.* **221**, 247–253.
26. Marty, A., Tan, Y. P. & Trautmann, A. (1984) *J. Physiol. (London)* **357**, 293–325.
27. Findlay, I. & Petersen, O. H. (1985) *Pflügers Arch.* **403**, 328–330.
28. Evans, M. G. & Marty, A. (1986) *Proc. Natl. Acad. Sci. USA* **83**, 4099–4103.
29. Grynkiewicz, G., Poenie, M. & Tsien, R. Y. (1985) *J. Biol. Chem.* **260**, 3440–3450.
30. Melvin, J. E., Kawaguchi, M., Baum, B. J. & Turner, R. J. (1987) *Biochem. Biophys. Res. Commun.* **145**, 754–759.
31. Foskett, J. K. (1988) *Am. J. Physiol.* **255**, C566–C571.
32. Tsien, R. Y. (1980) *Biochemistry* **19**, 2396–2404.
33. Tiffert, T., Garcia-Sancho, J. & Lew, V. L. (1984) *Biochim. Biophys. Acta* **773**, 143–156.
34. Garcia-Sancho, J. (1985) *Biochim. Biophys. Acta* **813**, 148–150.
35. Berridge, M. J. & Irvine, R. F. (1984) *Nature (London)* **312**, 315–321.
36. Merritt, J. E. & Rink, T. J. (1987) *J. Biol. Chem.* **262**, 14912–14916.
37. Berridge, M. J., Dawson, R. M. C., Downes, C. P., Heslop, J. P. & Irvine, R. F. (1983) *Biochem. J.* **212**, 478–482.
38. Downes, C. P. & Wusteman, M. M. (1983) *Biochem. J.* **216**, 633–640.
39. Irvine, R. F., Letcher, A. J., Lander, D. J. & Downes, C. P. (1984) *Biochem. J.* **223**, 237–243.
40. Irvine, R. F., Anggard, E. E., Letcher, A. J. & Downes, C. P. (1985) *Biochem. J.* **229**, 505–511.
41. Berridge, M. J. (1986) *J. Exp. Biol.* **124**, 323–335.
42. Henne, V., Puper, A. & Soling, H.-D. (1987) *FEBS Lett.* **218**, 153–158.
43. Taylor, C. W. & Putney, J. W., Jr. (1985) *Biochem. J.* **232**, 435–438.
44. Muallem, S., Schoeffield, M., Pandol, S. & Sachs, G. (1985) *Proc. Natl. Acad. Sci. USA* **82**, 4433–4437.
45. Jean, T. & Klee, C. B. (1986) *J. Biol. Chem.* **261**, 16414–16420.
46. Payne, R. & Fein, A. (1987) *J. Cell Biol.* **104**, 933–937.
47. Biden, T. J., Wollheim, C. B. & Schlegel, W. J. (1986) *J. Biol. Chem.* **261**, 7223–7229.
48. Volpe, P., Krause, K.-H., Hashimoto, S., Zorzato, F., Pozzan, T., Meldolesi, J. & Lew, P. D. (1988) *Proc. Natl. Acad. Sci. USA* **85**, 1091–1095.
49. Putney, J. W., Jr. (1986) *Cell Calcium* **7**, 1–12.

CHANGES IN CANINE NEUTROPHIL FUNCTION(S) FOLLOWING CELLULAR ISOLATION BY PERCOLL GRADIENT CENTRIFUGATION OR ISOTONIC LYSIS[1,2]

Dale F. Gruber* and Michele M. D'Alesandro
Experimental Hematology Department
Armed Forces Radiobiology Research Institute
Bethesda MD 20814-5145

ABSTRACT

Analysis of cellular effector function(s) often requires their isolation from other cellular types. Cell separatory techniques could mask, or select out, clinically important functional lesions. We examined differences in canine peripheral blood neutrophil functions, i.e. migration and H_2O_2 production, following two commonly used cell separation techniques: isotonic lysis or density gradient (Percoll) centrifugation. Separation methodology was observed to have a significant impact on both metabolic and mobility functions. In comparison to isotonic lysis, Percoll separation caused near 100% increases in random migration, near 40% decreases in chemotaxis and 70% increases in H_2O_2 production.

INTRODUCTION

Many functional and biochemical studies require large numbers of purified cells. Investigators have long sought to develop in vitro minimally manipulative methodologies allowing suitable cellular separation and recovery. Numerous new techniques have evolved some of which have included; cell sorting, electrophoresis and various affinity methods. Investigators have also attempted to make use of cellular density differences. The application of density separating techniques has resulted in three general approaches; (i) neutral density sedimentation, (ii) discontinuous-gradient, and (iii) isopycnic-gradient separations. Two of the more

537

frequently used separation mediums are Ficoll/Hypaque (a
copolymer of sucrose and epichlorohydrin) and Percoll
(colloidal silica coated with polyvinyl pyrrolidone).
For many investigators Percoll has become the separation
medium of choice because of it's lower viscosity (1),
greater cell yields (2), noncytotoxic character (3,4),
and because it is not actively phagocytized (3). Since
Percoll's inception, many papers making use of its
separation qualities have been published. In this
report, we demonstrate differences in canine neutrophil
effector functions after separation by whole-blood
isotonic lysis or Percoll density gradient methods.

MATERIALS AND METHODS

Dogs: Male and female littermates (<2 years old, 10-12
kg Hra beagles) were used. Dogs were quarantined on
arrival and screened for evidence of disease before
being released to experiments. Animals were kenneled in
an AAALAC-accredited facility in runs, and provided
commercial dog chow and tap water ad libitum.

Cell Separation and Isolation: Peripheral blood samples
in preservative-free heparin (10 U/ml) were drawn from
the lateral saphenous vein, centrifuged (400 x g, 10
minutes) to remove plasma, diluted 2-fold in saline
and divided into two aliquots. One aliquot was
isotonically lysed with 0.83% NH4Cl (4°C, 5 minutes),
washed in saline and resuspended in saline supplemented
with 0.2% heat-inactivated fetal bovine serum (56°C, 30
minutes). The second aliquot was layered unto a 60%
(p=1.077)/70% (p=1.080) discontinuous Percoll gradient
and centrifuged (700 x g, 30 minutes, room temperature).
Neutrophils sedimented to the 60%/70% interface whereas
mononuclear cells (i.e., monocytes, lymphocytes)
remained on top of the 60% Percoll. The neutrophil layer
was aspirated from the gradient and washed to remove
adherent Percoll. Contaminating red blood cells in the
Percoll isolate were isotonically lysed as described
above, washed and resuspended in supplemented saline.
On the basis of vital dye exclusion cellular viabilities
were routinely >95%.

Cellular Migration: Neutrophil migration was evaluated
by quantitating cells that migrated through a 10 um-
thick polycarbonate membrane. A 48-well micro-chemotaxis
chamber assembly (Neuro Probe Inc., Bethesda, MD) was
used as previously described (5). Lower wells contained
a 1:100 dilution of chemoattractant (zymosam activated
plasma (6)) or buffer. Upper wells contained 50 ul of

cellular suspension which had been corrected to 2x10e6 neutrophils/ml. Chambers were incubated at 37°C in a humidified environment and gassed with 5% CO_2 and air for 1 hour. Membranes were fixed in 100% methanol for 1 minute before being stained with Dif-Quick differential stain (Fisher Scientific, Silver Spring, MD). Seven high power (100X) microscopic fields across the diameter of the well were examined and the mean cellular migration/ field/hour was determined.

Quantitation of Intracellular H2O2 Production: Neutrophil H2O2 production was assayed as described by Bass et al (7). Neutrophils (1x10e6 cells/ml) were incubated with 5 uM dichlorofluorescein diacetate (DCFH-DA) for 10 minutes at 37°C. DCFH-DA traverses the cell membrane and is converted by cellular esterases into intracellularly trapped nonfluorescent DCFH. Cytosolic H2O2 endogenously present in resting cells or produced following activation, oxidizes DCFH to DCF, a fluorescent analogue. The relative fluorescence intensity of the cell is, therefore, an indirect measure of cellular H2O2 production. Cells were analyzed on a FACS analyzer (Becton Dickinson, Mountain View, CA). Green fluorescence was monitored between 515 and 545 nm after excitation with a mercury arc lamp using a 485/22 nm excitation filter. Cells were stimulated with phorbol myristate acetate (100 ng/ml, 15 minutes, 37°C) and analyzed. Neutrophils were distinguished from other cellular types on the basis of coulter volumes(s) and right angle light scatter properties.

RESULTS

The leukocyte population isolated from peripheral blood by isotonic lysis was >85% neutrophils based on differential analysis. The neutrophil population at the 60%/70% Percoll interface was >95% neutrophils. Less than 5% of the total neutrophil population remained with the mononuclear cells above the 60% Percoll layer.

No differences due to sex were apparent within the parameters examined in this report. Male: compared to separation by isotonic lysis, random migration of Percoll separated neutrophils was increased >100% (Figure 1), H2O2 production was increased by 79% (Figure 2), and chemotactic migration decreased by 37% (Figure 3). Female: Random migration of Percoll separated neutrophils increased by 95% (Figure 1), H2O2 production increased by 66% (Figure 2), and chemotactic migration (Figure 3) decreased by 43% compared with cells isolated by whole blood lysis.
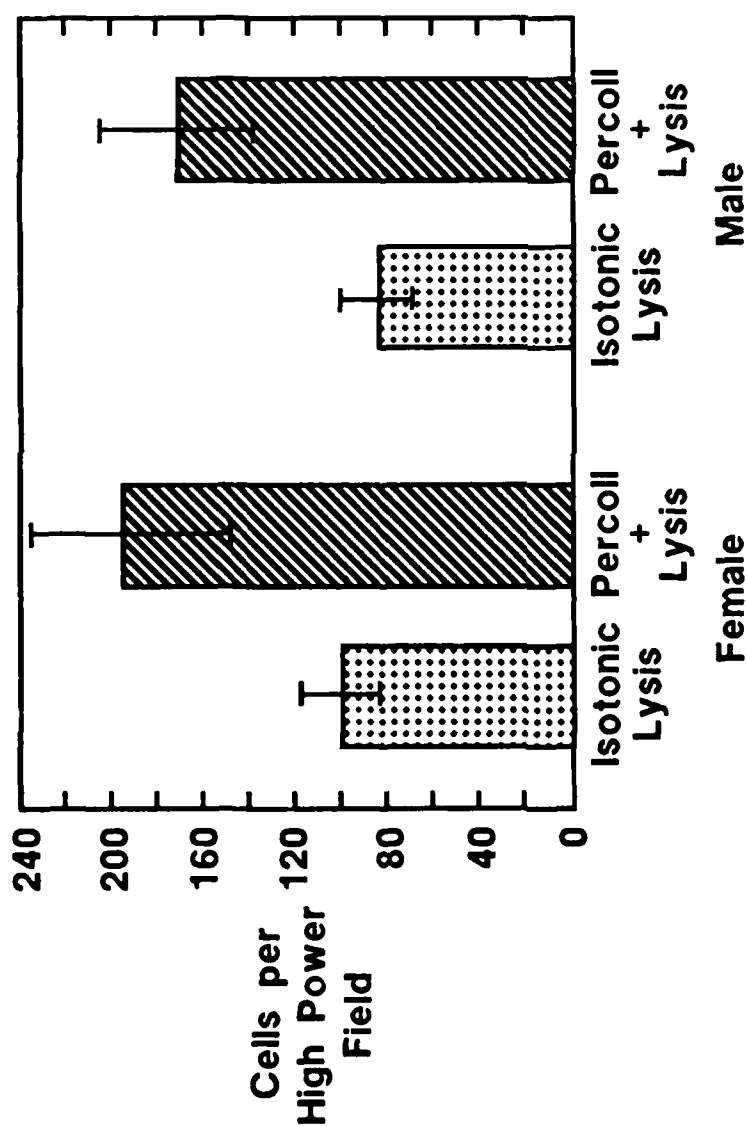
GRUBER AND D'ALESANDRO

Figure 1. Random migration of canine neutrophils isolated by isotonic lysis alone or Percoll gradient separation followed by isotonic lysis. Each data point represents the mean +/- SEM number of migrating cells per high-power field from a minimum of six animals.
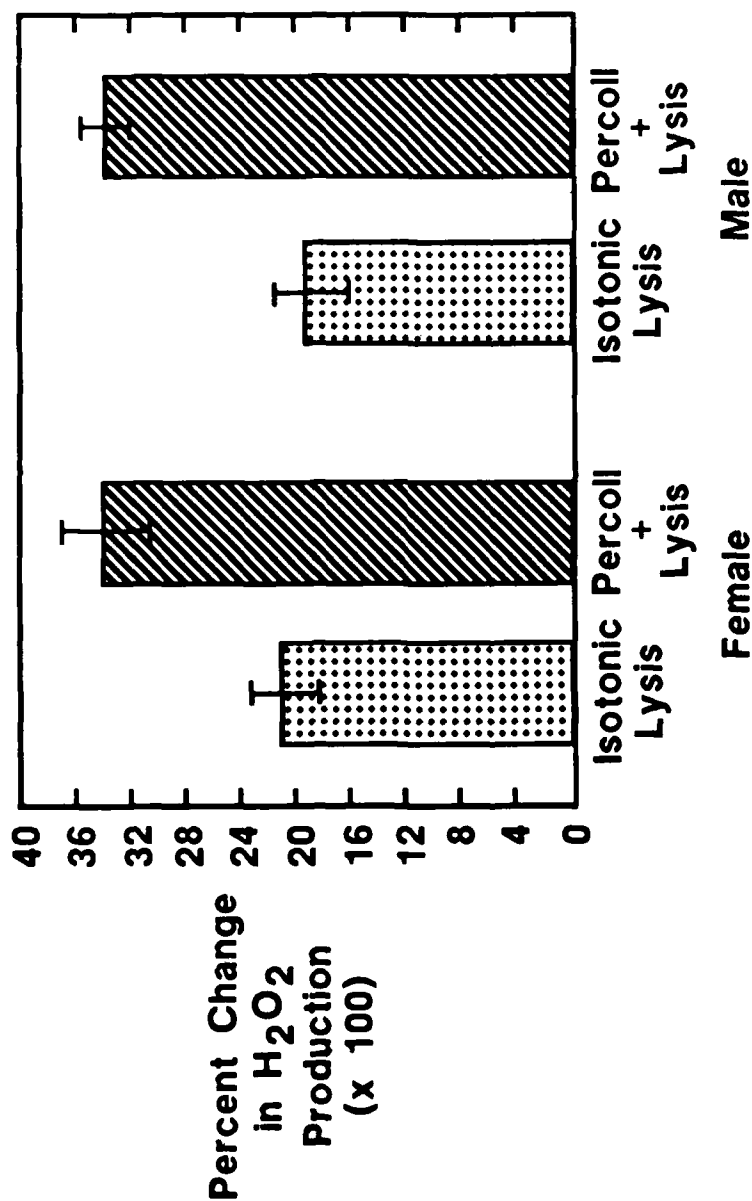
Figure 2. H2O2 production following isotonic lysis alone or Percoll gradient separation followed by isotonic lysis. Each data point represents the mean +/- SEM percent change in production (x100) following PMA stimulation from a minimum of six animals.
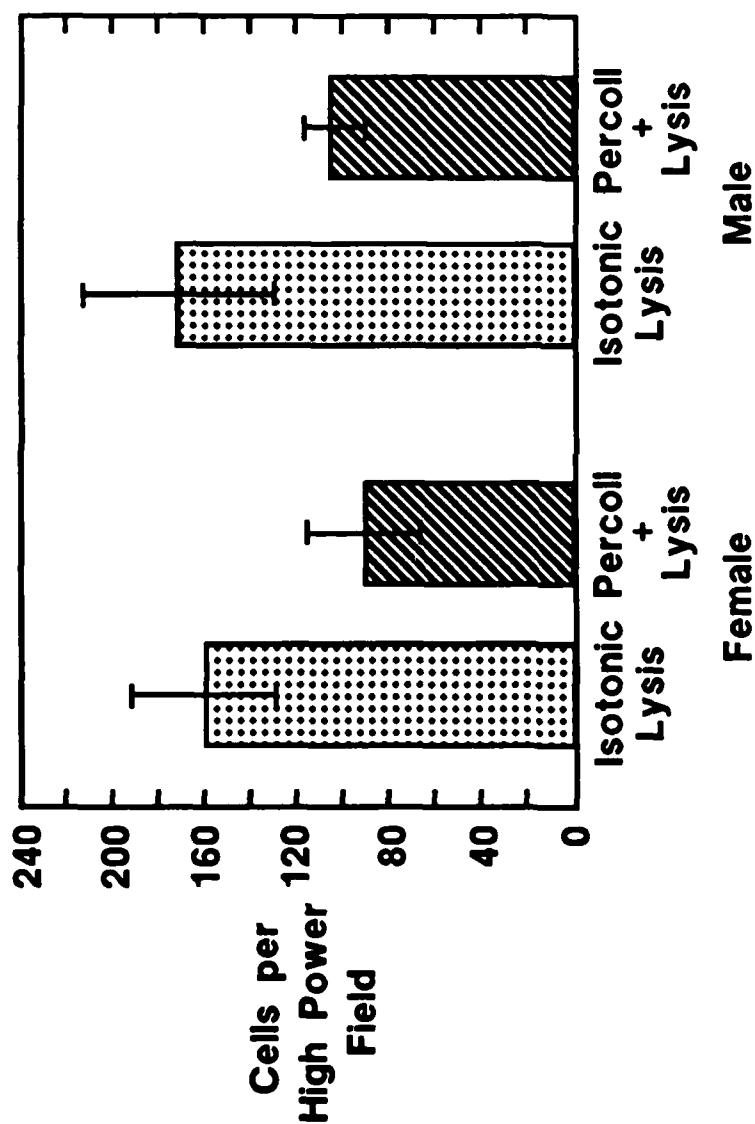
Figure 3. Chemotaxis of canine neutrophils to zymosan-activated normal dog plasma (10e-2 M) following isotonic lysis alone or Percoll gradient separation followed by isotonic lysis. Each data point represents the mean +/- SEM number of migrating cells per high-power field from a minimum of six animals.

DISCUSSION

Clinically relevant immunological dysfunction(s) may be the result of subtle cellular alterations. Unfortunately studies of specific cellular effector function(s) often require the isolation of the cell(s) of interest from other contaminating elements, cellular and otherwise. We demonstrate here that the isolation method significantly affects the metabolic and motility effector function(s) of canine neutrophils. Previous studies have reported that isolation through Ficoll-metrizoate density gradients altered membrane events so as to produce an oxidative burst (8). Based on the data presented here, separation-induced anomalies can be extended to include metabolic and motility functions as well. Percoll separation followed by isotonic lysis, in comparison to lysis alone, increased the basal motility of neutrophils evidenced by significant increases in levels of random migration. Previous reports (9,10), in conjunction with the functional differences reported here, suggest that cellular anomalies may be inherent to the manner of separation and must be considered before making judgements on apparent effector cell dysfunction(s).

FOOTNOTES

1. Supported by the Armed Forces Radiobiology Research Institute, Defense Nuclear Agency, under research work unit 00130. Views presented in this paper are those of the authors; no endorsement by the Defense Nuclear Agency has been given or should be inferred.

2. Research was conducted according to the principles enunciated in the 'Guide for the Care and Use of Laboratory Animals' prepared by the Institute of Laboratory Research, National Research Council.

REFERENCES

1. Kurnick, J.T, Ostberg, L., Stegagno, M., Kimura, A.K., Orn, A., and Sjoberg, O., A rapid method for the separation of functional lymphoid cell populations of human and animal origin on PVP-silica (Percoll) density gradients, Scand. J. Immunol., 10:563, 1979.

2. Dettman, G.L., and Wilber, S.M., Colloidal silica-aluminum modified-PVP density gradient centrifugation: centrifuge tube wall, cell

adherence, aggregation, separation properties and comparison to BSA and Ficoll, J. Immunol. Methods, 27:205, 1979.

3. Pertoft, H., Laurent, T.C., Laas, T., and Kagedal, L., Density gradients prepared from colloidal silica particles coated with polyvinylpyrrolidone (Percoll), Anal. Biochem., 88:271, 1978.

4. Gmelig-Meyling, F., and Waldmann, T.A., Separation of human blood monocytes and lymphocytes on a continuous Percoll gradient. J. Immunol. Methods, 33:1, 1980.

5. Harvath, L., Falk, W. and Leonard, E.J., Rapid quantitation of neutrophil chemotaxis: use of a polyvinylpyrrolidone-free polycarbonate membrane in a multiwell assembly. J. Immunol. Methods, 37:39, 1980.

6. Redl, H., Flynn, P., Lamche, H., Schiesser, A., Schlag, G., and Hammerschmidt, D.E., Aggregation, chemotaxis and chemiluminescence of canine granulocytes. Studies utilizing improved cell preparation techniques, Inflammation 7:67, 1983.

7. Bass, D.L., Parce, J.W., Dechatelet, L.R., Szejda, P., Seeds, M.C., and Thomas, M., Flow cytometric studies of oxidative product formation by neutrophils: a graded response to membrane stimulation, J. Immunol., 130:1910, 1983.

8. Berkow, R.L., Tzeng, D.Y., Williams, L.V., and Baehner, R.L., The comparative responses of human polymorphonuclear leukocytes obtained by counterflow centrifugal elutriation and Ficoll-Hypaque density centrifugation. I. Resting volume, stimulus-induced superoxide production, and primary and secondary granule release, J. Lab. Clin. Med., 102:811, 1984.

9. Seeds, M.C., Parce, J.W., Szejda, P. and Bass, D.A., Independant stimulation of membrane potential changes and the oxidative metabolic burst in polymorphonuclear leukocytes, Blood, 65:233, 1985.

10.Poston, L., Jones, R.B and Hilton, P.F., Sodium transport on polymorphonuclear leukocytes: effect of isolation by the Ficoll/Triosil method, Clin. Sci., 62:563, 1982.

IMPAIRED REPAIR OF UVC-INDUCED DNA DAMAGE IN L5178Y-R CELLS: SEDIMENTATION STUDIES WITH THE USE OF 5'-BROMODEOXYURIDINE PHOTOLYSIS

Michael P. Hagan [1], Daniel P. Dodgen[1] and Janusz Z. Beer[2]

[1]Cellular Radiobiology Division, AFRRI-DNA, Bethesda, MD 20814 and [2]Center for Devices and Radiological Health, Food and Drug Administration, Rockville, MD 20857, USA

Abstract—Relative to their L5178Y-S counterparts, L5178Y-R cells have an impaired capacity to form patches in DNA after exposure to UVC radiation. The photolysis of 5'-bromodeoxyuridine (BrdUrd) incorporated into DNA was used to estimate the number of 'repair patches' formed in response to a 254 nm UV (UVC) exposure. L5178Y-S cells, typical of rodent cell lines, formed a small number of patches in exposed DNA (1-2 patches per 1 × 10⁸ dalton during a 6 h recovery after an exposure of 20 J m⁻²). In contrast, DNA extracted from L5178Y-R cells exposed to UVC and subsequently incubated with BrdUrd for 6 h showed no evidence of BrdUrd incorporation indicating no capacity to form sites of repair (fewer than 0.5 sites of BrdUrd incorporation per 1 × 10⁸ dalton). Moreover, in L5178Y-R cells high fluences of UVC caused an extensive DNA degradation. Such degradation was not observed in L5178Y-S cells during the 24-h post-exposure period. These results are consistent with the notion that L5178Y-R cells have a reduced capacity to repair DNA damage induced by UVC radiation.

INTRODUCTION

Mutant mammalian cell lines, selected on the basis of their sensitivities to physical and chemical damaging agents are cultured and examined in the hopes of identifying those molecular mechanisms associated with cell mutagenesis and cell survival. Two such cell strains derived from L5178Y mouse lymphoma cells originally were designated L5178Y-R (resistant) and L5178Y-S (sensitive) to reflect their sensitivity to X-rays (Alexander and Mikulski, 1961; Beer *et al.*, 1963). L5178Y-R (LY-R) and L5178Y-S (LY-S) cells have since been shown to be inversely cross-sensitive to X-rays and to UVC radiation (Beer *et al.*, 1973; Beer *et al.*, 1984; Walicka *et al.*, 1976).

In addition to their disparate sensitivities to UVC radiation and X-rays, these two cell lines possess a wide array of characteristics related to DNA repair. For UVC radiation, the mean lethal fluence (D_0) values are 3-fold higher for LY-S cells than for LY-R cells when the cells are exposed in medium (Szumiel, 1979) and 8-fold higher when the cells are exposed in phosphate-buffered saline (Walicka and Beer, 1979; Jacobson *et al.*, 1984). Additionally, UVC radiation produces considerably more mutants in LY-R cells than in LY-S cells (Jacobson *et al.*, 1984; Evans *et al.*, 1986a,b). LY-R cells are also more sensitive than LY-S cells to a *cis*-platinum complex (Szumiel, 1979). Interestingly, LY-R cells cannot be sensitized to UVC or the *cis*-platinum complex by caffeine (Szumiel and Wlodek, 1978; Walicka *et al.*, 1978), and LY-R cells suffer a more prolonged interruption in DNA synthesis after exposure to UVC (Szumiel *et al.*, the companion paper). In the companion paper, Szumiel *et al.* show that, when incubated with ara-C, LY-R cells do not accumulate single-strand breaks in response to UVC irradiation.

Several of these observations are consistent with a probable defect in excision repair in the LY-R cells. The experiments described below examine this possibility. Although the excision repair efficiency of rodent cells has been shown to be extensive for antigenic sites induced by UVC radiation, measurements involving the removal of pyrimidine dimers or the formation of 'patches' containing BrdUrd[+] have shown only a modest repair capacity (Clarkson *et al.*, 1983; Trosko and Kasschau, 1967; Meyn *et al.*, 1974; Setlow and Regan, 1981; Szumiel *et al.*, the companion paper). For this reason we expected that our study would require both the detection of few sites of repair and the use of prolonged repair periods.

Recently, Rosenstein *et al.* (1980, 1985) have improved the sensitivity of the BrdUrd photolysis assay for some forms of DNA damage. The modified assay has been applied in a unique fashion by Xi-Chang *et al.* (1986) to the study of the UVC damage. As the experiments described below involved high fluences of UVC and were aimed at identifying qualitative differences between LY-R and LY-S cells, we chose to modify the BrdUrd-photolysis technique after the suggestions of Setlow and Regan (1981), including the use of cysteamine after Beattie (1972). These modifications have been

*Correspondence should be addressed to: Dr. Michael Hagan. Baylor College of Medicine, One Baylor Plaza, Houston, TX 77030, USA

†*Abbreviations*: BrdUrd, 5'-bromodeoxyuridine; dThd, thymidine; HU, hydroxyurea; Cys, cysteamine; ssb, single-strand break.

shown to permit the observation of one repair site per 1×10^9 daltons, which was an adequate precision of measurement for the comparison of the two cell lines in question. Using the modified assay, we found that relative to LY-S cells, LY-R cells exhibit a profound deficiency in the formation of repair patches following exposure to UVC radiation. Our results indicate that LY-R cells may be completely unable to form such patches.

MATERIALS AND METHODS

Cell culture. LY-R and LY-S cells were cultured in Fischer's medium supplemented with 10% donor horse serum (Flow Laboratories, Springfield, Virginia) and 1 g/l Pluronic F68. Cells grown in a humidified atmosphere of 5% CO₂ and 95% air were routinely diluted to maintain exponential growth. Cell lines were examined weekly for the morphological changes associated with conversion of the LY-R phenotype into the LY-S phenotype (Beer et al., 1983) and they were periodically tested for sensitivity to UVC radiation. Bromodeoxyuridine, $1 \times 10^{-4} M$, was routinely administered in complete medium in the presence of $1 \times 10^{-6} M$ 5-fluorodeoxyuridine. Under these conditions, LY-R and LY-S cells incorporated identical amounts of BrdUrd; this was determined by acid precipitable radioactivity measurements performed after exposure of the cells to [¹⁴C]BrdUrd.

DNA extraction. DNA was extracted by following a modified Marmur (1961) procedure. Cells, washed with phosphate buffered saline were resuspended in buffer containing 0.1 M NaCl and 0.1 M Tris (pH 8.0). Cells were then lysed for 10 min in 2% Sarkosyl and 0.5% Brij 58 detergents (Sigma Chemical Co., St. Louis, MO). The lysate was digested at 37°C for 30 min in 50 µg/ml RNAase (preheated for 20 min at 80°C) and then digested for 60 min in Pronase (0.1 mg/ml, self-digested). The final salt concentration was then increased to 1.0 M NaCl and the DNA extracted with isoamyl alcohol-chloroform (1 : 24) for 30 min at room temperature. The mixture was centrifuged at 2000 g to separate phases. The extraction was repeated until no material was visible at the interface.

UVC (254 nm) irradiation. Cells suspended in phosphate-buffered saline and distributed in plastic culture dishes were exposed directly to two 15 W germicidal lamps (General Electric Company) at a flux of 0.89 J/m² as determined with an Eppley thermopile (Eppley, Stamford, Connecticut) and a Keithley (Cleveland, Ohio) microammeter.

UVB (313 nm) irradiation. DNA (75 µg/ml) dissolved in TEN buffer [15 mM Tris-HCl (pH 8.0), 11.5 mM Na₂EDTA, and 25 mM NaCl] was irradiated with monochromatic 313 nm light (10 nm band width) at a fluence rate of 40 W/m². The radiation source consisted of a 1 kW Hg-Xe lamp (Oriel Corp., Stamford, Connecticut) filtered through 80 mm column of $1.0 \times 10^{-3} M$ 2'-deoxyadenosine and focused onto a monochromator (Kratos, Inc., Ramsey, New Jersey). Once again, the flux was determined with an Eppley thermopile and Keithley microammeter.

Reagents. Radiolabeled BrdUrd (5,6-¹⁴C) and thymidine (6-methyl-³H or 5,6-¹⁴C) were purchased from the New England Nuclear Company (Boston, MA). Cysteamine was purchased from the Sigma Chemical Company (St. Louis, MO) and hydroxyurea from the Aldrich Chemical Company (Milwaukee, WI).

Alkaline sucrose gradient sedimentation. The technique of alkaline sucrose gradient sedimentation was detailed previously (Hagan et al., 1982). In brief, 50 µl samples of cell suspensions at 2×10^6 cell/ml in phosphate-buffered saline or 50 µl of DNA suspended in TEN buffer were layered onto a discontinuous gradient with the upper layer containing 0.01 M Na₂EDTA, 0.55 M NaCl, 0.45 M

NaOH, and 0.1% Brij 58 detergent. The upper layer had previously been layered onto a linear alkaline sucrose gradient (5 ml) prepared from solutions containing 0.7 M NaCl, 0.3 N NaOH, 0.01 M Na₂EDTA, and 5–20% sucrose. Centrifugation was performed at 0°C in SW 50.1 rotors (L5-50 Beckman ultracentrifuge). Distribution of radioactivity through the gradient was measured by the paper-strip technique of Carrier and Setlow (1971).

Calculation of single-strand breaks. The method for determining the number averaged molecular weight and single-strand breaking of the DNA sample has been detailed elsewhere (Hagan et al., 1982). Briefly, the weight averaged molecular weight was determined from the distribution of radioactivity on each gradient, and the number of single-strand breaks calculated from the expression below. The number averaged weight was estimated as $\frac{1}{2}M_w$.

$$N = 1 \times 10^8 \left[\frac{2}{M_{w,t}} - \frac{2}{M_{w,c}} \right] \qquad \text{where}$$

N = number of single-strand breaks per 10^8 Da, $M_{w,t}$ = weight averaged molecular weight of the treated sample, $M_{w,c}$ = weight averaged molecular weight of the control sample.

The UVB fluence response for single-strand breaking was determined over the range 0–240 kJ m². For these experiments the fluence response approached saturation at 120 kJ m² with further increase in single-strand breaking being less than the error of measurement.

RESULTS

Modification of the BrdUrd-photolysis assay

The photolysis assay for repaired regions in DNA involves the UVB irradiation of DNA containing BrdUrd both in repaired regions and in regions which have undergone semi-conservative synthesis during the time allowed for repair. The photolysis of BrdUrd in repaired regions provides an estimate of the number of sites of repair (Regan et al., 1971). As has been observed previously (Setlow and Regan, 1981), however, photolysis of BrdUrd incorporated through semi-conservative synthesis can confound the assay of repair sites. This can be a very significant problem in experiments involving lengthy repair periods. In such experiments, BrdUrd is not only incorporated in sites of repair but also is likely to be incorporated in the strand opposite to that being repaired. The extensive photolysis of that now heavily labeled opposing strand induces breaks in the strand of interest [approximately one opposite strand break for every 100 breaks in the heavily labeled strand (Hutchinson, 1973)]. Further, if the UVB photolysis involves chromatin, and either high fluence of UVB or a prior exposure to UVC, extensive BrdUrd to protein crosslinking results (Smith, 1976; present data). These two processes result in an extensive breakdown and reduced extractability of the control DNA, such as is seen in Fig. 1A. In this figure, radiolabeled but otherwise untreated cells were incubated in $1.0 \times 10^{-4} M$ BrdUrd and photolysed with UVB prior to direct lysis upon alkaline sucrose gradients. A major fraction of the sample, sediment-
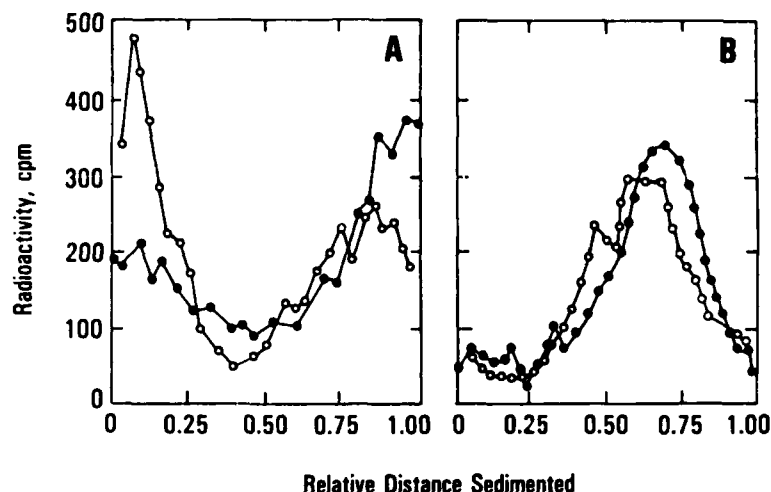
Relative Distance Sedimented

Figure 1. Alkaline sucrose gradient analysis of whole cell lysates vs extracted DNA. Panel A: LY-R cells labeled overnight with [^{14}C]dThd were exposed for 6 h to BrdUrd (●) and then exposed to 60 kJ m^2 of UVB radiation (○). Panel B: DNA extracted from cells treated as in panel A was either sedimented directly (●) or exposed in solution to 60 kJ/m^2 of UVB radiation (○). All sedimentations were performed at 1.5 × 10^{11} rad^2 s^{-1}.

ing near the top of the gradient, could only be released to sediment after extensive proteinase treatment. As is shown in Fig. 1B, however, this situation was improved by extracting the DNA prior to UVB photolysis. Here, although the control DNA was reduced in molecular weight, exposure to UVB radiation did not reduce the extractability. Unavoidably, the extraction process caused some breaking of the DNA, limiting the precision of the assay. Gentle extraction techniques, however, routinely produced DNA greater than $8 × 10^7$ Da MW (weight averaged) resulting in a precision of measurement of approximately 0.5 alkali-labile lesions per $1 × 10^8$ Da (determined with the use of viral DNAs of known molecular weight). With these conditions of DNA extraction, and in the absence of BrdUrd, UVB exposure of 120 kJ/m^2 resulted in no detectable alkali-labile lesions in the control DNA preparations. Determined empirically, the same exposure induced approximately $1.2 × 10^3$ alkali-labile lesions per $1.0 × 10^8$ Da in DNA heavily substituted with BrdUrd.

DNA strand breaking induced by BrdUrd photolysis of the opposite strand was also controlled in our experiments. This phenomenon, believed to be caused by radicals generated during the photolytic event, normally can be neglected due to its low probability (Hutchison, 1973; Setlow and Regan, 1981). In the experiments reported below, however, the long periods allowed for repair and high fluences of UVB radiation caused these breaks, if uncontrolled, to be equivalent to or greater in number than the repair sites expected. To reduce this confounding effect cysteamine (Cys) was incorporated in the photolysis step (Beattie, 1972).

To examine the efficacy of the addition of Cys and the sensitivity of these procedures, the amount

of semi-conservative synthesis was increased beyond that which would be associated with the repair assay. This was accomplished by uniform labeling of cells (overnight incubation in [^{14}C]dThd, 0.1 μCi/mℓ, $1 × 10^{-5}$ M) and subsequent exposure of the cells to BrdUrd ($1 × 10^{-4}$ M, 6 h). As shown in Fig. 2, when no Cys was added and no attempt was made to block semiconservative DNA replication during the BrdUrd treatment, an exposure to 60 kJ/m^2 of UVB radiation induced considerable damage (approximately 2.7 ssb per $1 × 10^8$ Da in the radiolabeled material). Further, as expected, when semiconservative DNA synthesis was inhibited by exposure to hydroxyurea (2 mM), breaking was reduced. Likewise, breaking was reduced to fewer than 1.0 ssb per $1 × 10^8$ Da after 60 kJ/m^2 when the material that had replicated in the presence of BrdUrd was exposed to UVB radiation in the presence of Cys (40 mM).

In subsequent experiments Cys was added before the photolysis of the repair assay samples. In the experiments to follow, DNA was labeled during a brief (30 min) exposure of cells to [^{3}H]dThd (5 μCi/mℓ; $1 × 10^{-5}$ M) followed by incubation in the presence of $1 × 10^{-4}$ M BrdUrd for either 6 or 24 h.

Repair of UVC damage in LY-R and LY-S cells

Using the above described technique, a comparison was made of the capacities of LY-R and LY-S cells to repair DNA damage resulting from an expsure to UVC radiation. LY-S cells, more resistant to the lethal effects of UVC radiation than their LY-R counterparts, were exposed to UVC radiation. Irradiation was followed by a 6 h exposure to BrdUrd, DNA extraction, and UVB
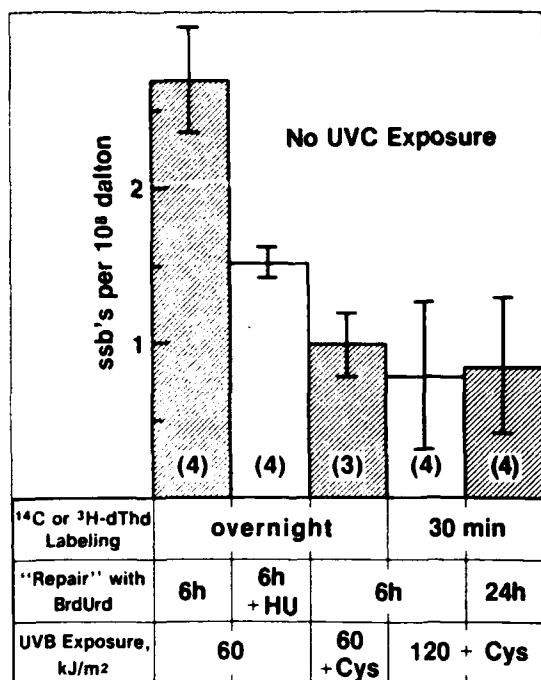
Figure 2. UVB-photolytic breakage of radiolabeled LY-R DNA: the effects of labeling the opposite strand with BrdUrd; the effects of HU presence during repair or Cys during photolysis. The mean number of ssb's was calculated as described in Materials and Methods; the number of experiments performed is shown in parentheses. As indicated in the figure, cells were radiolabeled either for thirty minutes or overnight. LY-R and LY-S cells behaved identically under these conditions.

Table 1. Single-strand breaks induced by UVB photolysis in BrdUrd-labeled DNA, determined after different recovery periods

Cell strain	Fluence (J m⁻²)	Number of single-strand breaks per 1 × 10⁹ Da — Recovery period (h)	
		6	24
LY-R	0	0.8 ± 0.5 (8)	0.8 ± 0.4 (6)
	20	0.5 ± 0.5 (6)	ND*
	40	0.6 ± 0.4 (8)	ND
LY-S	0	0.5 ± 0.2 (4)	
	20	1.3 ± 0.6† (6)	
	40	1.9 ± 0.5† (6)	0.7 ± 0.3† (6)

*Single-strand breaks, although apparent, were not estimated due to the large amount of low molecular weight DNA observed.
†Significantly different from control values at the 95% confidence level.

photolysis. Each condition of exposure, detailed in Table 1, was repeated from four to eight times; typical results are presented in Fig. 3. For the more UV-resistant LY-S cells, it could be calculated from these data that fluences of 20 J m⁻² (Fig. 3A) and
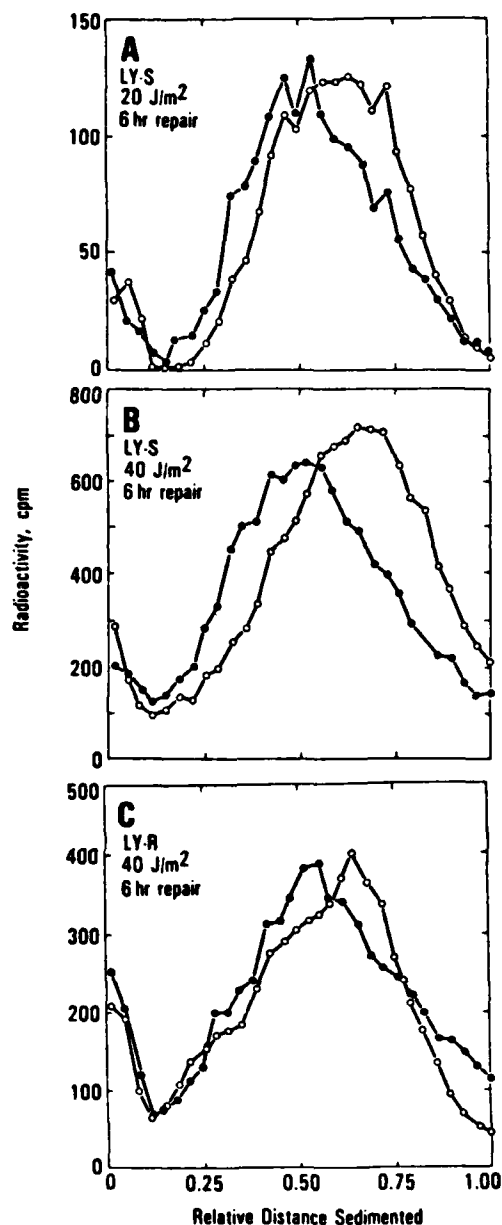

Figure 3. Examples of sedimentation patterns for DNA isolated from LY-R and LY-S cells following their exposure to UVC radiation (fluences indicated in the panels). Cells treated as indicated in the text were allowed 6 h for repair in the presence of BrdUrd, and then extracted and exposed to 0 (○) or 120 kJ m⁻² (●) of UVB radiation.

40 J m⁻² (Fig. 3B) of UVC radiation produced, respectively, 1.3 ± 0.6 and 1.9 ± 0.5 sites of BrdUrd photolysis per 1 × 10⁹ Da. In contrast, the more UV-sensitive LY-R cells showed no measureable capacity to form sites of repair at any fluence of UVC radiation tested (5–40 J m⁻², only the sedimentation data at 40 J m⁻² are shown, Fig. 3C).

More striking, however, was the comparison after a 24-h repair period. From the data shown in Fig. 4A one notes that in LY-R cells only 30% of the
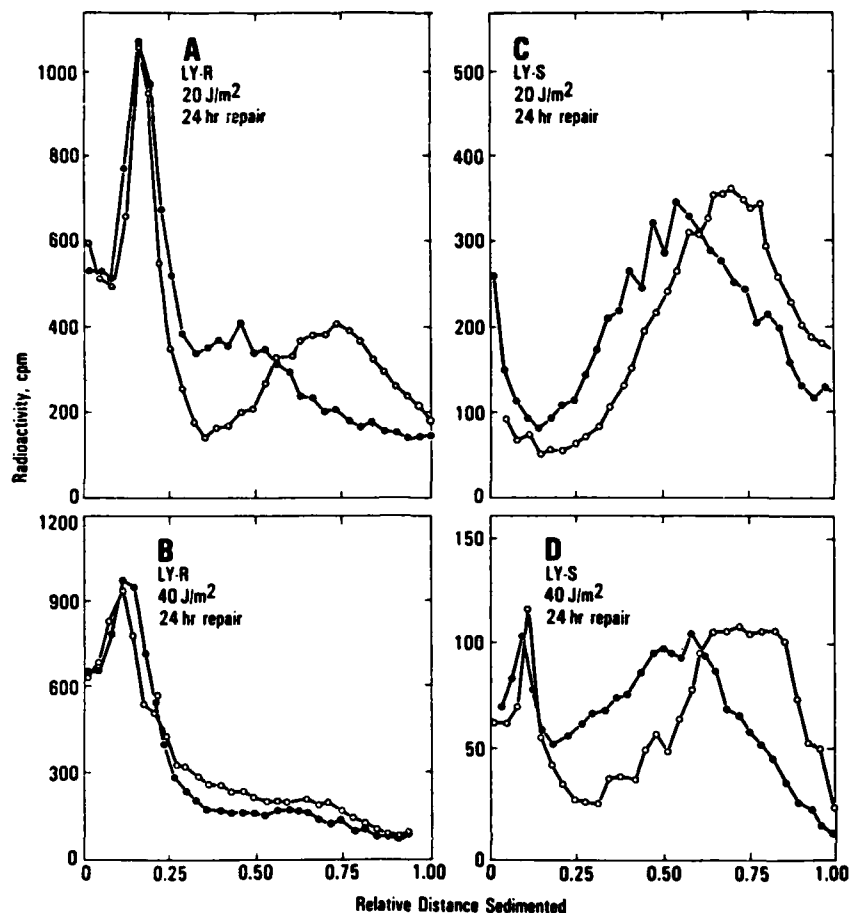
Figure 4. Examples of sedimentation patterns for DNA isolated from LY-R and LY-S cells following their exposure to UVC radiation (fluences indicated in the panels). Cells treated as described in the text were allowed 24 h to recover in the presence of BrdUrd. (○) no UVB radiation; (●) 120 kJ/m² of UVB radiation.

labeled material remained at high molecular weight and could be photolysed with UVB radiation. Although the DNA at high molecular weight could be photolysed, the majority of the sample was degraded to small molecular weight [(1.26 ± 0.39) × 10⁶ Da]. By contrast, after 24 h of repair following an identical exposure to UVC radiation, more than 80% of the labeled DNA from LY-S cells remained at high molecular weight. The exposure of this DNA to UVB radiation revealed an additional 1.6 ± 0.2 ssb per 1 × 10⁸ Da. At an exposure of 40 J/m² of UVC radiation again 80% of the DNA from LY-S cells remained at high molecular weight and showed an additional 3.1 ± 0.3 ssb per 1 × 10⁸ Da after 24 h of repair.

DISCUSSION

The results presented above indicate that different responses of LY-R and LY-S cells to UVC radiation may be explained by different efficiencies of DNA repair in the two cell lines. More specifically, our experiments indicate that UVC-irradiated

LY-S cells are capable of forming 'repair patches' in DNA. In LY-R cells, however, this capacity is either considerably reduced or completely absent. The high fluence of UVC employed prevent any detailed estimate of repair capacities but serve well to illustrate the differences between the two cell lines.

For the purpose of this study we modified the BrdUrd-photolysis assay for excision repair (Regan et al., 1971; Setlow and Regan, 1981; Ley, 1981). Extraction of DNA prior to sedimentation and addition of Cys to the UVB photolysed mixture allowed us to measure ssb's as a reflection of the repair process, with a standard error of measurement of approximately 0.5 ssb per 1 × 10⁸ Da. These measurements indicated induction of at most 0.5 ssb per 1 × 10⁸ Da in LY-R cells incubated in the presence of BrdUrd for 6 h after exposure to any dose from 5 to 40 kJ/m² of UVC radiation. As such, these data most likely reflect the precision ('noise') of the assay (e.g. Fig. 3C). We consider this result as an indication that LY-R cells have very low capacity to excise UVC-modified fragments of

DNA molecules during the first 6 h of recovery. Under identical conditions (Fig. 3B), as well as after lower UVC fluences (Fig. 3A), and during longer 'repair periods' (Fig. 4, C and D) LY-S cells underwent measurable photolytic degradation indicating their ability to form 'repair patches' in UVC-modified DNA.

The only photolytic indication of 'repair patch' formation in LY-R cells was observed after 24 h of recovery and was associated with extensive DNA degradation (Figs. 4, A and B). This conveys the clearest disparity between the two cell lines with respect to recovery from UVC-induced damage. Examination of the sedimentation data after 24 h of recovery, as in Fig. 4A, shows that the DNA remaining at high molecular weight was easily photolysed, indicating a repair activity following UVC exposure. This repair activity, however, obviously did not lead to reconstitution of fully functional DNA.

More striking, however, was the appearance of low molecular weight DNA in these samples. After either 20 or 40 J/m² of UVC radiation most of the labeled DNA in LY-R cells was reduced to a size approximately equivalent to the interdimer distance. In sharp contrast, in LY-S cells 80–90% of the DNA remained at high molecular weight. This behavior is consistent with the notion that in LY-R cells either the incision step or a conversion to an apyrimidinic site occurs, but a later step in the repair process is faulty and the cells fail to generate high molecular weight DNA.

LY-S cells are a product of spontaneous conversion occurring during in vitro cultivation of LY-R cells (Beer et al., 1983). Several observations indicate that this conversion involves loss of repair capacity for damage induced by ionizing radiation (Beer et al., 1973; Korner et al., 1977; Evans et al., 1985, 1986a,b). It is interesting that this loss of repair capacity for ionizing radiation-induced damage coincides with an apparent gain of both a repair capacity for and increased cell survival after UVC-induced damage.

From these results and those described by Szumiel et al. in the companion paper, it appears that LY-R cells have an impaired ability to form the initial nucleolytic breaks in UVC-damaged DNA molecules. Inability to form such breaks impairs repair whose completion may be important for the recovery of the normal reproductive capacity of the cells. From the time course of the repair process and the recovery of the cells. From the time course of the repair process and the recovery of DNA synthesis, it appears as though these two phenomena could be coupled. These observations when combined with others previously cited, indicate that the LY-R/LY-S system is extremely useful for the comparison of cellular and subcellular mechanisms responsible for mammalian cell killing and mutagenesis.

REFERENCES

Alexander, P. and Z. B. Mikulski (1961) Mouse lymphoma cells with different radiosensitivities. Nature (London) 192, 572–573.

Beattie, K. L. (1972) Breakage of parental DNA strands in Haemophilus influenzae by 313 nm radiation after replication in the presence of 5-bromodeoxyuridine. Biophys. J. 12, 1573–1582.

Beer, J. Z., E. Budzicka, E. Niepokojczycka, O. Rosiek, I. Szumiel and M. Walicka (1983) Loss of tumorigenicity with simultaneous changes in radiosensitivity and photosensitivity during in vitro growth of L5178Y murine lymphoma cells. Cancer Res. 43, 4736–4742.

Beer, J. Z., E. D. Jacobson, H. H. Evans and I. Szumiel (1984) X-ray and UV mutagenesis in two L5178Y cell strains differing in tumorigenicity, radiosensitivity, and DNA repair. Br. J. Cancer 49, Suppl. VI, 107–111.

Beer, J. Z., J. T. Lett and P. Alexander (1963) Influence of temperature and medium on the X-ray sensitivities of leukaemia cells in vitro. Nature 199, 193–194.

Beer, J. Z., I. Szumiel and M. Walicka (1973) Cross-sensitivities to UV-light and X-rays of two strains of murine lymphoma L 5178Y cells in vitro. Studia Biophysica (Berlin) 36/37, 175–182.

Carrier, W. L. and R. B. Setlow (1971) Paper strip method for assaying gradient fractions containing radioactive macromolecules. Anal. Biochem. 43, 427–432.

Clarkson, J. M., D. L. Mitchell and G. M. Adair (1983) The use of an immunological probe to measure the kinetics of DNA repair in normal and UV-sensitive mammalian cell lines. Mutation Res. 112, 287–299.

Evans, H. H., M. F. Horng and J. Z. Beer (1986a) Lethal and mutagenic effects of radiation and alkylating agents on two strains of mouse L5178Y cells. Mutation Res. 161, 91–97.

Evans, H. H., M. F. Horng, J. Mencl, K. G. Glazier and J. Z. Beer (1985) The influence of dose rate on the lethal and mutagenic effects of X-rays in proliferating L5178Y cells differing in radiation sensitivity. Int. J. Radiat. Biol. 47, 553–562.

Evans, H. H., J. Mencl, M. F. Horng, M. Ricanati, C. Sanchez and J. Hozier (1986b) Locus specificity in the mutability of L5178Y mouse lymphoma cells: The role of multilocus lesions. Proc. Natl. Acad. Sci. USA, 83, 4379–4383.

Hagan, M. P., R. Matsushita, R. Bonura and A. Shotola (1982) Alkali-labile lesion and uracil-DNA-glycosylase-sensitive site removal after BrdUrd and UVB treatment of Chinese hamster cells. Photochem. Photobiol. 35, 371–377.

Hutchinson, F. (1973) The lesions produced by ultraviolet light in DNA containing 5-bromouracil. Q. Rev. Biophys. 6, 201–246.

Jacobson, E. D., K. Krell, Z. Olempska-Beer and J. Z. Beer (1984) UV-induced mutagenesis at the hypoxanthine-guanine phosphoribosyl transferase locus in two L5178Y mouse lymphoma cell strains with different UV sensitivities. Mutat. Res. 129, 259–267.

Korner, I., M. Walicka, W. Malz and J. Z. Beer (1977) DNA repair in two L5178Y cell lines with different X-ray sensitivities. Studia Biophysica (Berlin) 61, 141–149.

Ley, R. D. (1981) Measurement of gap filling by bromouracil photolysis. In DNA Repair. A Laboratory Manual of Research Procedures (Edited by B. E. Friedberg and P. Hanawalt), pp. 493–498. Dekker, New York.

Marmur, J. and D. Lane (1960) Strand separation and

specific recombination in nucleic acids: biological studies *Proc. Natl. Acad. Sci. USA* **46**, 453–461.

Meyn, R. E., D. L. Vizard, R. R. Hewitt and R. M. Humphrey (1974) The fate of pyrimidine dimers in the DNA of ultraviolet-irradiated Chinese hamster cells. *Photochem. Photobiol.* **20**, 221–226.

Regan, J. D., R. B. Setlow and R. D. Ley (1971) Normal and defective repair of damaged DNA in human cells: a sensitive assay utilizing the photolysis of bromodeoxyuridine. *Proc. Natl. Acad. Sci. USA* **68**, 708–711.

Rosenstein, B. S., J. T. Murphy and J. M. Ducore (1985) Use of a highly sensitive assay to analyze the excision repair of dimer and nondimer DNA damages induced in human skin fibroblasts by 254 nm and solar ultraviolet radiation. *Cancer Res.* **45**, 5526–5531.

Rosenstein, B. S., R. B. Setlow and F. E. Ahmed (1980) Use of the dye Hoechst 33258 in a modification of the bromodeoxyuridine photolysis technique for the analysis of DNA repair. *Photochem. Photobiol.* **31**, 215–222.

Setlow, R. B. and J. D. Regan (1981) Measurement of repair synthesis by photolysis of bromouracil. In *DNA Repair: A Laboratory Manual of Research Procedures* (Edited by E. C. Friedberg and P. C. Hanawalt), pp. 307–318. Dekker, New York.

Smith, K. C. (1976) The radiation induced addition of proteins and other molecules to nucleic acids. In *Photochemistry and Photobiology of Nucleic Acids, Vol. II* (Edited by S. Y. Wang), p. 195. Academic Press, New York.

Szumiel, I. (1979) Response of two strains of L5178Y cells to *cis*-dichlorobis-(cyclopentylamine) platinum (II). I. Cross-sensitivity to *cis*-PAD and UV light. *Chem.*

Biol. Interact. **24**, 51–72.

Szumiel, I. and D. Wlodek (1978) Effect of caffeine on DNA synthesis in L5178 cells treated with an antitumor platinum complex or UV-light. *Nukleonika* **23**, 865–871.

Szumiel, I., D. Wlodek and K.-J. Johanson (1988) Impaired repair of UVC-induced DNA damage in L5178Y-R cells: alkaline unwinding strands with the use of A-B-O.

Trosko, J. E., E. H. Y. Chu and W. L. Carrier (1965) The induction of thymidine dimers in ultraviolet-irradiated mammalian cells. *Radiat. Res.* **24**, 667–672.

Trosko, J. E. and M. R. Kasschau (1967) Study of pyrimidine dimers in mammalian cells surviving low doses of ultraviolet radiation. *Photochem. Photobiol.* **6**, 215–219.

Walicka, M. and J. Z. Beer (1979) UV-light sensitivity and split-dose effects in two strains or murine leukemia L5178Y cells. *Fortschritte der Onkologie* **4**, 73–84.

Walicka, M., I. Korner, W. Malz and J. Z. Beer (1978) The effect of caffeine on post-replication repair and survival in two L5178Y cell lines with different sensitivities to UV irradiation. *Mutat. Res.* **52**, 265–272.

Walicka, M., I. Szumiel and J. Z. Beer (1976) L5178Y cell strains cross-sensitive to X-rays and UV-light: similarities and differences in recovery at the cellular level. In *Radiation and Cellular Control Processes* (Edited by J. Kiefer), pp. 196–204. Springer, Berlin.

Xi-Chang, G., W. F. Morgan and J. E. Cleaver (1986) Hoechst 33258 dye generates DNA-protein cross-links during ultraviolet light-induced photolysis of bromodeoxyuridine in replicated and repaired DNA. *Photochem. Photobiol.* **44**, 131–136.

COMPARATIVE BEHAVIORAL TOXICITY OF FOUR SULFHYDRYL RADIOPROTECTIVE COMPOUNDS IN MICE: WR-2721, CYSTEAMINE, DIETHYLDITHIOCARBAMATE, AND N-ACETYLCYSTEINE

MICHAEL R. LANDAUER,* HIRSCH D. DAVIS,* JASON A. DOMINITZ*
and JOSEPH F. WEISS†

*Behavioral Sciences and †Radiation Biochemistry Departments, Armed Forces Radiobiology Research Institute,
Bethesda, MD 20814-5145, U.S.A.

A number of sulfhydryl compounds have been shown to protect against ionizing radiation. One of the most effective radioprotectors is S-2(3-aminopropylamino)ethylphosphorothioic acid, also known as ethiofos, gammaphos, or WR-2721 (Davidson, 1980; Giambarresi and Jacobs, 1987). This drug is currently under clinical investigation for its potential in protecting normal tissue during radiation treatment and chemotherapy (Blumberg *et al.*, 1982; Glover *et al.*, 1988; Yuhas *et al.*, 1980). β-Mercaptoethylamine (MEA, cysteamine) was for years the standard against which the effectiveness of other radioprotectors was judged, but is more toxic than WR-2721 (Giambarresi and Jacobs, 1987). Diethyldithiocarbamate (DDC) and N-acetylcysteine (NAC) are other compounds shown to have radioprotective properties (Milas *et al.*, 1988; Weiss *et al.*, 1984).

Studies in a variety of animal species have shown significant behavioral toxicity after administration of WR-2721 (Bogo *et al.*, 1985; Bogo, 1988; Landauer *et al.*, 1987b, 1988). Side effects that can be considered detrimental to performance have also been observed during the clinical evaluation of this drug (Blumberg *et al.*, 1982; Glover *et al.*, 1988). The purpose of the present study was to compare the behavioral toxicity and radioprotective qualities of WR-2721 to three other sulfhydryl compounds.

Adult male (BALB/c × DBA/2)F1 mice, also known as CD2F1 mice (Charles River, Wilmington, MA), weighing 25–36 g served as subjects. They were individually housed in polycarbonate isolator cages on a 12-hr light–dark cycle with lights on at 0700. Temperature was maintained at 21 ± 1°C with 50 ± 10% relative humidity. Food and acidified (pH 2.5 using HCl) water were freely available.

The sulfhydryl compounds evaluated were WR-2721, MEA, DDC, and NAC. Dose–response determinations were made for each drug: WR-2721 (25–400 mg/kg) MEA (12.5–200 mg/kg), DDC (12.5–800 mg/kg), and NAC (125–1000 mg/kg). The doses selected were based on the maximum tolerated dose (MTD), defined as the LD_{10}. MTD has previously been used as a basis for comparing radioprotective compounds (Brown *et al.*, 1982). The highest dose tested was equivalent to one-half the MTD. There were 8–16 animals tested at each dose for each drug. All compounds were administered i.p. in physiological saline (pH 6–8). They were injected in a volume equivalent to 1% of body weight (10 ml/kg) immediately before behavioral evaluation.

Locomotor activity was measured using a computerized Digiscan animal activity monitor (Omnitech Electronics, Columbus, OH), which recorded horizontal activity (ambulation) and the number of vertical movements (rearing) by means of infrared photodetectors. The horizontal and vertical detectors were positioned 1.3 and 6.3 cm, respectively, above the floor of the arena. Animals were habituated to the testing apparatus for 1 hr on the day before testing. Locomotor

98

M. R. LANDAUER et al.

TABLE 1 Comparison of Toxicity, Radioprotective and Behavioral Effects of Sulfhydryl Compounds

	WR-2721	MEA	DDC	NAC
1 2 LD$_{10}$ (mg kg)^a	400	200	800	1000
% 30-day survival^b	100	62	62	25
ED$_{50}$ (mg kg)^c horizontal activity	271	103	224	>1000
BTI^d	3.0	3.9	7.1	<2.0
ED$_{50}$ (mg kg) vertical activity	105	57	129	667
BTI	7.6	7.0	12.4	3.0

^{a}Radioprotection and behavioral effects were evaluated at doses up to one-half the LD$_{10}$ (maximum tolerated dose).

^{b}Radioprotection was determined by exposing mice to an equitoxic dose (one-half LD$_{10}$) at 13 Gy and observing them for 30 days

^{c}The ED$_{50}$ is defined as the dose of the compound that resulted in a 50% reduction in the behavioral response when compared to the saline control group.

^{d}BTI = Behavioral Toxicity Index = LD$_{10}$ divided by ED$_{50}$. The higher the ratio, the more toxic the compound and the less desirable for use as a radioprotector.

LOCOMOTOR ACTIVITY

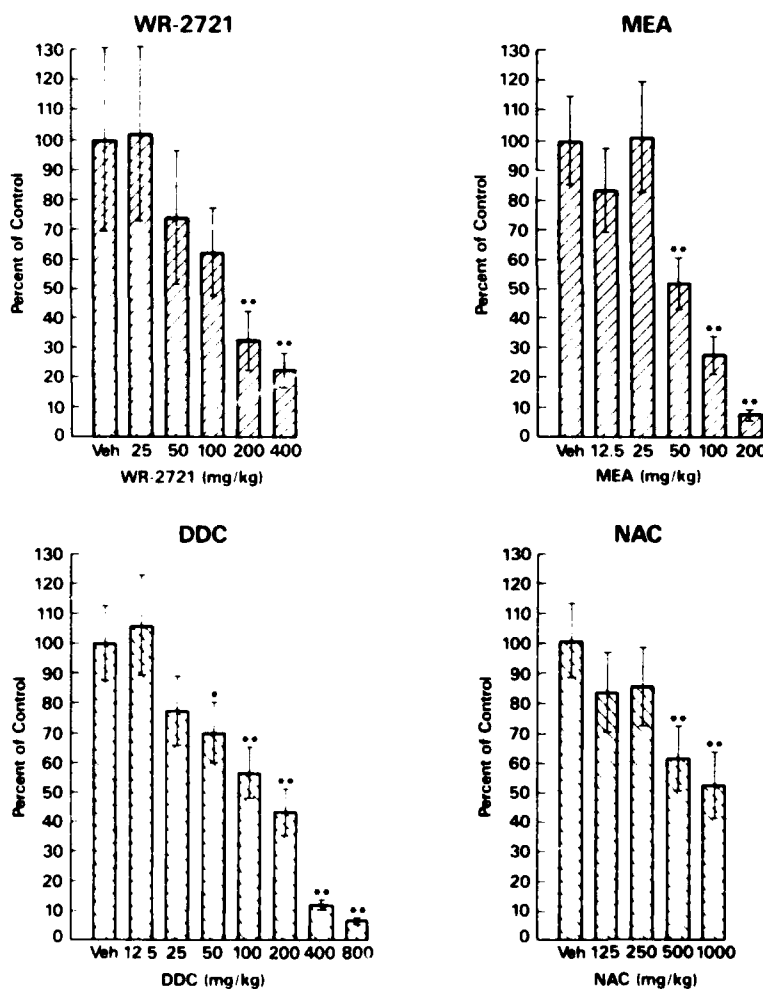
FIG. 1 Dose response determinations for effects of four sulfhydryl compounds on locomotor activity WR-2721, S-2-(3-aminopropylaminoethylphosphorothioic acid; MEA, β-mercaptoethylamine; DDC, diethyldithiocarbamate; NAC, N-acetylcysteine. Illustrations are of vertical activity (number of vertical movements) during each 60-min test (N = 8-16 dose). Animals were tested only once. Data are expressed as percent of vehicle (veh) control group. A one-way ANOVA was performed on each compound. Post hoc comparisons were made using Dunnett's test. Vertical bars represent ± S E M. *p < 0.05, **p < 0.01 from control group

activity was recorded for 1 hr immediately following drug administration. The effective dose of each compound that disrupted horizontal and vertical activity by 50% from vehicle control levels (ED_{50}) at 1 hr postinjection was calculated by linear regression.

The radioprotective effects of these drugs at an equitoxic dose were also determined. Mice were administered a dose of the compound equivalent to one-half the LD_{10}, 30 min before irradiation with 13 Gy cobalt-60 (1 Gy/min). Irradiation was accomplished with bilateral, whole-body exposure to gamma-ray photons from a cobalt-60 source. All mice were placed into ventilated Plexiglas restraint devices for approximately 13 min during radiation exposure. For each drug (N = 8) the percent of animals surviving at 30 days was determined.

A comparison of the behavioral effects, radioprotective efficacy, and comparative toxicity is presented in Table 1. Vertical activity (Fig. 1) and horizontal activity (data not shown) exhibited similar dose-dependent patterns of decreases in locomotor activity. The figure is shown as percent of the control group in order that drugs can be readily compared. [The WR-2721 data are modified from Landauer *et al.* (1987b) and presented here for purposes of comparison.] When tested at one-half the LD_{10} dose, WR-2721 was the most effective radioprotector, with 100% of the animals surviving a 13-Gy exposure. WR-2721 was followed by MEA and DDC and finally NAC (see Table 1). When the ED_{50} for horizontal activity decrements was compared to the LD_{10}, DDC was the most toxic compound, followed by MEA, WR-2721, and NAC. For vertical activity a similar pattern was exhibited: however, WR-2721 was slightly more toxic than MEA.

The assessment of locomotor activity proved to be a sensitive test in the evaluation of behavioral toxicity of sulfhydryl compounds. All four compounds tested exhibited dose-dependent decreases in activity. The ED_{50} for vertical activity was consistently lower than that for horizontal activity, indicating that vertical activity is a more sensitive measure of locomotor behavioral disruption for these compounds. When the ED_{50}s for activity were compared to the LD_{10}, DDC was demonstrated to be the most toxic compound and NAC the least. WR-2721 and MEA showed similar patterns of relative toxicity as well as radioprotection. At equitoxic doses, WR-2721 was the most effective sulfhydryl radioprotector examined and NAC the least. Thus, although NAC was the least behaviorally toxic compound, it also offered the least radioprotection.

Previous research has demonstrated that for a given compound, radioprotective efficacy and behavioral toxicity are well correlated. Thus doses of WR-2721 that resulted in the greatest behavioral decrements are doses that have yielded the best radioprotection. In our laboratory, the dose modifying factors for doses of 100, 200, and 400 mg/kg WR-2721 in CD2F1 mice are approximately 1.2, 1.6, and 2.2, respectively. Only the lowest dose did not significantly affect locomotor activity. A similar relationship between the degree of radioprotection and the degree of locomotor deficit has been reported for 16,16-dimethyl prostaglandin E_2 (Landauer *et al.*, 1987d)

The present study examined the behavioral toxicity of four radioprotective compounds when administered alone. Both gamma (Landauer *et al.*, 1987a) and neutron (Landauer *et al.*, 1987c) irradiation of mice result in locomotor decrements, and the combination of radiation and radioprotective compounds (WR-2721) has been shown to result in greater behavioral toxicity than either treatment alone (Bogo *et al.*, 1985; Bogo, 1988; Landauer *et al.*, 1988). Studies are in progress to examine compounds that may mitigate the toxic effects of radiation and/or radioprotective compounds.

REFERENCES

BOGO V., NOLD D. F., GREWSON M., GOOKER D., GURE J. H., YOUNG J. M. and KOGERMAN M. M. 1985. Combined trials of WR-2721 with radiation therapy. *Int. J. Radiat. Oncol. Biol. Phys.* **8:** 561–563.
BOGO V. 1988. Behavioral radioprotection. *Pharmac. Ther.* **39:** 73–78, this volume.

BOGO,V., JACOBS, A. J. and WEISS, J. (1985) Behavioral toxicity and efficacy of WR-2721 as a radioprotectant. Radiat. Res. 104: 182–190.

BROWN, D. Q., PITTOCK, J. W. III and RUBINSTEIN, J. S. (1982) Early results of the screening program for radioprotectors. Int. J. Radiat. Oncol. Biol. Phys. 8: 565–570.

DAVIDSON, D. E., GRENAN, M. M. and SWEENEY, T. R. (1980) Biological characteristics of some improved radioprotectors. In: Radiation Sensitizers: Their Use in the Clinical Management of Cancer, pp. 309–320. BRADY, L. W. (ed.). Masson, New York.

GIAMBARRESI, L. and JACOBS, A. J. (1987) Radioprotectants. In: Military Radiobiology, pp. 265–301, CONKLIN, J. J. and WALKER, R. I. (eds). Academic Press, New York.

GLOVER, D., FOX, K. R., WEILER, C., KLIGERMAN, M. M., TURRISI, A. and GLICK, J. H. (1988) Clinical trials of WR-2721 prior to alkylating agent chemotherapy and radiotherapy. Pharmac. Ther. 39: 3–7, this volume.

LANDAUER, M. R., DAVIS, H. D., DOMINITZ, J. A. and PIERCE, S. J. (1987a) Effects of acute gamma radiation exposure on locomotor activity in Swiss–Webster mice. Toxicologist 7: 253.

LANDAUER, M. R., DAVIS, H. D., DOMINITZ, J. A. and WEISS, J. F. (1987b) Dose and time relationships of the radioprotector WR-2721 on locomotor activity in mice. Pharmac. Biochem. Behav. 27: 573–576.

LANDAUER, M. R., LEDNEY, G. D. and DAVIS, H. D. (1987c) Locomotor behavior in mice following exposure to fission neutron irradiation and trauma. Aviat. Space Environ. Med. 58: 1205–1210.

LANDAUER, M. R., WALDEN, T. L., DAVIS, H. D. and DOMINITZ, J. A. (1987d) Alterations in locomotor activity induced by radioprotective doses of 16,16-dimethyl prostaglandin E_2. In: Prostaglandin and Lipid Metabolism in Radiation Injury, pp. 245–251, WALDEN, T. L. and HUGHES, H. N. (eds). Plenum Press, New York.

LANDAUER, M. R., DAVIS, H. D., DOMINITZ, J. A. and WEISS, J. F. (1988) Long-term effects of radioprotector WR-2721 on locomotor activity and body weight of mice following exposure to ionizing radiation. Toxicology (in press).

MILAS, L., MURRAY, D., BROCK, W. A. and MEYN, R. E. (1988) Radioprotectors in tumor radiotherapy: factors and settings determining therapeutic ratio. Pharmac. Ther. 39: 179–187, this volume.

WEISS, J. F., SRINIVASAN, V., JACOBS, A. J. and RANKIN, W. A. (1984) Effect of sulfur compounds on radiation-induced suppression of delayed-type hypersensitivity to oxazolone in mice. Proc. Am. Assoc. Cancer Res. 25: 235.

YUHAS, J. M., SPELLMAN, J. M. and CULO, F. (1980) The role of WR-2721 in radiotherapy and/or chemotherapy. In: Radiation Sensitizers: Their Use in the Clinical Management of Cancer, pp. 303–308, BRADY, L. W. (ed.). Masson, New York.
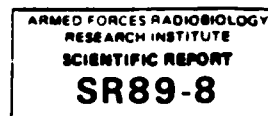
MEASUREMENT OF THE RADIOSENSITIVITY OF RAT MARROW BY FLOW CYTOMETRY

K. F. McCarthy and M. L. Hale

Radiation Biochemistry Department, Armed Forces Radiobiology Research Institute, Bethesda, Maryland 20814-5145, U.S.A.

1. INTRODUCTION

Monoclonal antibodies directed against the three major glycoproteins of rat thymocytes were found to be useful for identifying hematopoietic stem cells by flow cytometry (McCarthy *et al.*, 1985, 1987). These antibodies and their specificities are OX-7, which recognizes a determinant expressed on the Thy 1.1 membrane glycoprotein; OX-22, which recognizes the high molecular weight form of the leukocyte common antigen; and W3/13, which identifies some leukocyte sialoglycoproteins. In previous studies (McCarthy *et al.*, 1985, 1987; Hale *et al.*, 1987) it was determined that the rat hematopoietic stem cell (HSC), colony-forming unit-spleen (CFU-S), and prothymocyte had the phenotype of OX-7 upper 20% positive (OX-7up20%) and OX-22$^-$. The number of cells in the marrow with this phenotype was found to be 0.34% of the total marrow population. This subpopulation could be further divided by three-parameter immunofluorescent analysis into two further subpopulations, a W3/13 dim and a W3/13 positive population, each representing approximately 0.17% of the total marrow cell population. Ongoing research indicates that the HSC is W3/13 dim (K. F. McCarthy, unpublished). For comparison, a value of 0.14% for marrow HSC concentration was calculated using the CFU-S assay and a 24 hr seeding efficiency of 3.2%.

The agreement between the clonogenic CFU-S and phenotypic flow cytometry assays for determining the size of the HSC compartment led us to attempt to measure the radiosensitivity of the HSC by flow cytometry. The results of these experiments are compared with the radiation survival curve generated using the classical CFU-S clonogenic assay for HSCs, which is generally used when estimating the protective effects of drugs against hematopoietic damage.

2. METHODS

Male, 6–8 week old Lewis rats (Charles River Laboratories, Kingston, New York) were quarantined on arrival and screened for evidence of disease before being released from quarantine. They were maintained in an AALAC-accredited facility in plastic microisolator cages on hardwood-chip contact bedding, and provided commercial rodent chow, and acidified tap water *ad libitum*. The rats were on a 12 hr light/dark full spectrum lighting cycle with no twilight. Total-body radiation of 0.5 to 6 Gy at 1 Gy/min absorbed dose was delivered with an opposing ^{60}Co radiation source. Irradiated rats were given 1.0 mg/ml tetracycline in their drinking water. The CFU-S assay and the detection and enumeration of HSCs by flow cytometry were performed as previously described (McCarthy *et al.*, 1987). Rats were euthanized with methoxyfurane and were cared for according to the principles enunciated in the *Guide for the Care and Use of Laboratory Animals* (Institute of Laboratory Animal Resources, National Research Council).
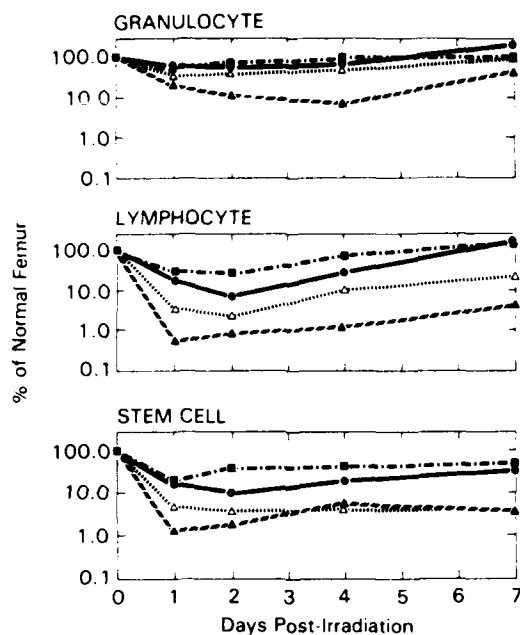
FIG. 1. Recovery of marrow granulocytes, lymphocytes, and HSCs as a function of time postirradiation. TBR ■——■, 0.5 Gy, ●—●, 1.5 Gy; , 3.0 Gy; and ▲——▲, 6.0 Gy. One hundred thousand cells were measured by flow cytometry per point.
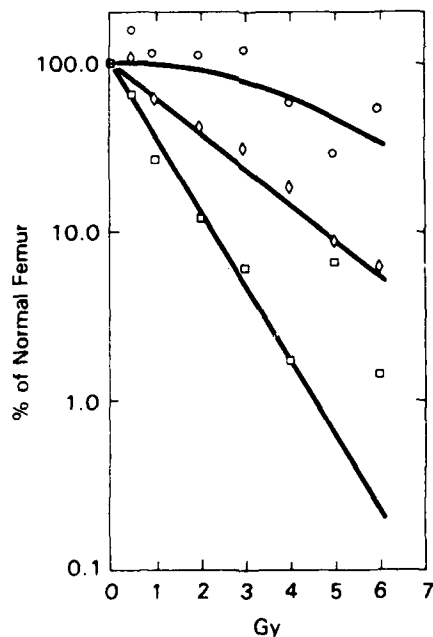

FIG. 2. Dose-response curve measured 2 d postirradiation. ——, marrow granulocytes; ◊—◊, marrow HSCs. ——, marrow lymphocytes. One hundred thousand cells were measured by flow cytometry per point.

3. RESULTS

Figure 1 shows the relationship between radiation dose, survival, and regeneration of marrow granulocytes (OX-7, OX-22⁻, W3/13⁺), lymphocytes (OX-7⁺, OX-22⁺, W3/13⁻), and HSCs (OX-7up20%, OX-22⁻, W3/13 dim) as determined by flow cytometry. All three populations
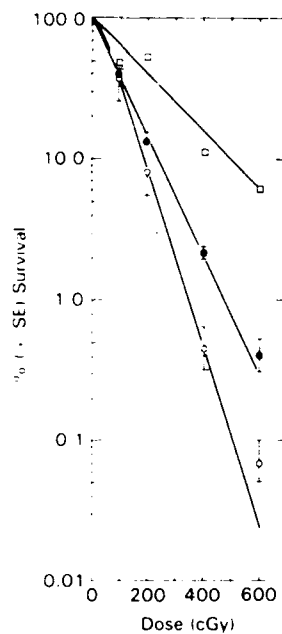
FIG. 3 Dose response curves for CFU-S. ●—●, CFU-S$_{0d}$ measured immediately postirradiation; · · ·, CFU-S$_{2d}$ measured 2 d postirradiation; — , HSCs measured by flow cytometry 2 d postirradiation. One hundred thousand cells were measured by flow cytometry per point.
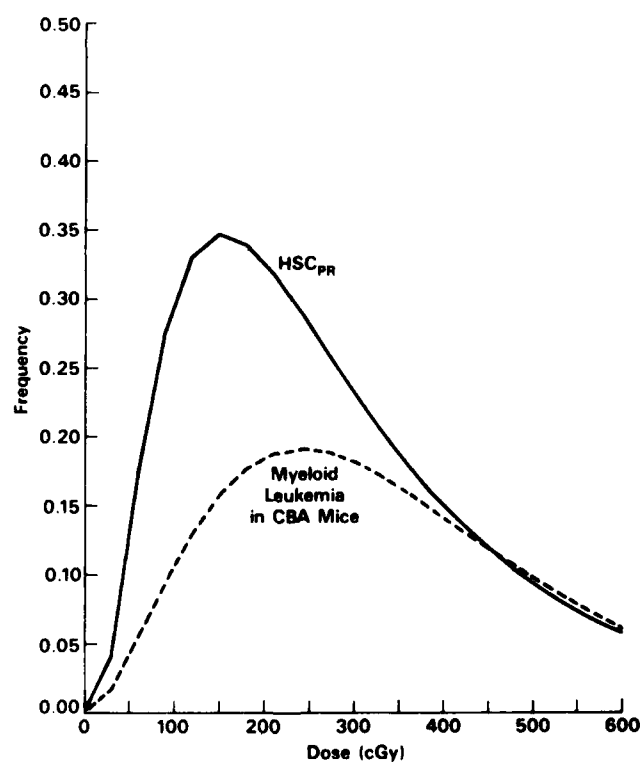
FIG. 4 Relative marrow concentration of HSC$_{PR}$ plotted as a function of dose 2 d postirradiation. — , curve generated by the equation $(1-e^{-D/0.6\,Gy})^{1.93}_{CFU-S} - (1-e^{-D/2.2\,Gy})^{1.03}_{FACS}$ (see text for explanation) ·-·, curve generated by the equation $2.4 \times 10^{-5}\, D^2 e^{-8.25 \times 10^{-3}\,D}$, which predicts the frequency of myeloid leukemia as a function of dose in postirradiated CBA male mice. The D$_0$ and n values for CFU-S$_{0d}$ were determined to be 0.95 Gy and 1.02.

decreased in number to a minimum value between days 1 and 2 postirradiation and then began slowly increasing in number between days 2 through 7. Figure 2 shows dose–response curves plotting the log% survival as a function of dose for marrow granulocytes, lymphocytes, and HSCs 2 d postirradiation. Data indicate that marrow granulocytes are radioresistant. The dose required to reduce the irradiated femur granulocyte population to 37% of control values was ~6.50 Gy, marrow lymphocytes were extremely radiosensitive (D_{37} = 0.90 Gy), and HSCs were, in terms of radiosensitivity, intermediate between these two populations (D_{37} = 2.30 Gy).

The CFU-S survival curves determined immediately following irradiation and 2 d postirradiation are plotted in Fig. 3. Interestingly, fewer CFU-S were detected in the marrow 2 d postirradiation than immediately following irradiation. Hendry (1973) noted a similar phenomenon in irradiated mice, and this observation was not pursued further. Also shown in Fig. 3, for comparison, is the survival curve for HSCs as determined by flow cytometry 2 d postirradiation. Major differences in the radiation survival curves of HSCs as measured by flow cytometry and the CFU-S assay exist and are plotted as a function of dose in Fig. 4, based on the survival curve $f = [1 - (1 - e^{-D/D_0})^n]$ and therefore

$$\Delta f_{2day} = (1 - e^{-D/D_0})^n_{CFU-S} - (1 - e^{-D/D_0})^n_{FACS}$$

The values for D_0s and ns are given in the legend to Fig. 4. These values were derived from the curves in Fig. 3.

4. DISCUSSION

We studied the effect of ionizing radiation on three marrow subpopulations by a phenotypic assay based on fluorochrome-conjugated monoclonal antibodies and flow cytometry. The three marrow subpopulations were bone marrow lymphocytes that are in a state of proliferation in young rats, bone marrow granulocytes that are nearly terminally differentiated cells and hence nonproliferating cells, and HSCs that, although in a G_0 or nonproliferating state in a normal healthy rat, must undergo extensive proliferation to express their hematopoietic potential in clonogenic assays such as the CFU-S assay.

The interaction of ionizing radiation with the marrow lymphocytes or granulocytes was predictable. The proliferating lymphocytes were, as expected, extremely sensitive to radiation, while the terminally differentiated granulocytes appeared to be radioresistant. In a sense, these two populations served as controls for measurements of the HSC compartment because, depending on whether the phenotypic (monoclonal antibody/flow cytometry) assay or the clonogenic (CFU-S) assay was used, the HSCs could be classified as somewhat radioresistant or extremely radiosensitive. Possible explanations for this discrepancy are as follows:

(1) In the postirradiated state, nonspecific staining of dying and dead marrow cells may lead to the detection of cells other than HSCs in OX-7up20%⁺, OX-22⁻, and W3 13 dim cell population. At the present time we cannot gate out dead cells with the vital stains propidium iodide or fluorescein diacetate because the fluorescence emission spectrum of these two compounds overlaps those of phycoerythrin B and fluorescein isothiocyanate, respectively. Further development of flow cytometric techniques will be necessary to solve this problem.

(2) Another explanation might be that as long as HSCs remain in a nonproliferative or G_0 state following irradiation, the radiation-induced lethal lesion is not expressed. Only when these damaged HSCs leave G_0 and enter cell cycle is this lesion expressed, ultimately leading to cell death. Blackett (1973) referred to this population of cells as 'doomed' HSCs and questioned what influence they might have on the triggering of HSCs into cell cycle and the subsequent regeneration of the postirradiated marrow.

(3) A third possibility is that radiation may alter HSCs in such a fashion that although they remain viable, they are proliferatively restricted, and as such, they are detected by the phenotypic fluorescence activated cell sorter (FACS) assay but are not detected by the clonogenic CFU-S assay.

By subtracting the fraction survival of clonogenic CFU-S from the fraction survival of HSCs as determined by the flow cytometry assay, we can arrive at a rough estimate of the generation of HSCs in the postirradiated rat that are undetectable by the CFU-S clonogenic assay. We will refer to this population of cells as HSC_{PR} and note that it is probably a heterogeneous population of doomed or dying HSCs, proliferatively restricted HSCs, and possibly other dead cells that have been mislabeled. Nevertheless, the dose – response relationship is highly curvilinear, with optimum numbers of HSC_{PR} being generated by a gamma-ray dose of approximately 1 – 2 Gy. A threefold increase in dose decreased the frequency of HSC_{PR} by nearly an order of magnitude and it may not be coincidental that this HSC_{PR} frequency curve bears a resemblance to those describing the lifetime occurrence of myeloid leukemia in male CBA mice following whole-body X-ray exposure (Mole et al., 1983 and Fig. 4).

In summary, there is some evidence that not all radiation-damaged HSCs are rapidly sloughed off in the immediate postirradiated state. Whether these cells can remain in the marrow long after irradiation is not known. Their influence on seeding to the marrow of transplanted HSCs, their effect on marrow regeneration, and their contributions to myeloid leukemia, if any, are currently being investigated.

REFERENCES

BLACKETT, R. M. (1973) Cell population kinetics of erythropoietic cells in response to radiation. In: *Advances in Radiation Research: Biology and Medicine*, Vol. 2, DAPLAN, J. F. and CHAPIRO, A. (eds) Gordon and Breach, New York.

HALE, M. L., GRIENER, D. L. and McCARTHY, K. F. (1987) Characterization of rat prothymocyte with monoclonal antibodies recognizing rat lymphocyte membrane antigenic determinants. *Cell Immunol.* **107**: 188 – 200.

HENDRY, J. H. (1972) Differential split-dose radiation response of resting and regenerating hematopoietic stem cells. *Int. J. Radiat. Biol.* **24**: 469 – 473.

McCARTHY, K. F., HALE, M. L. and FEHNEL, P. L. (1985) Rat colony-forming unit spleen is OX-7 positive, W3/13 positive, OX-1 positive and OX-22 negative. *Exp. Hematol.* **13**: 847 – 854.

McCARTHY, K. F., HALE, M. L. and FEHNEL, P. L. (1987) Purification and analysis of rat hematopoietic stem cells by flow cytometry. *Cytometry* **8**: 296 – 305.

MOLE, R. H., PAPWORTH, D. G. and CORP, M. J. (1983) The dose – response for X-ray induction of myeloid leukaemia in male CBA H mice. *Br. J. Cancer* **47**: 285 – 291.
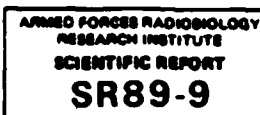
RADIOPROTECTION BY BIOLOGICAL RESPONSE MODIFIERS ALONE AND IN COMBINATION WITH WR-2721

MYRA L. PATCHEN, MICHELE M. D'ALESANDRO. MICHAEL A. CHIRIGOS* AND
JOSEPH F. WEISS

*Armed Forces Radiobiology Research Institute, Besthesda, MD 20814. U.S.A. and *United States Army Medical Research
Institute of Infectious Diseases, Fort Detrick, Maryland 21701. U.S.A.*

1. INTRODUCTION

Currently, protection against radiation exposure depends primarily on physical means such as shielding and avoidance. However, for individuals who might be required to engage in activities such as decontamination of fallout areas, clean-up of radiation accidents, or polar spaceflights, protection of physical means may be inadequate and/or impractical. In these situations, the availability of agents capable of providing protection against radiation injury would be of benefit. In addition, agents capable of protecting normal tissues from radiation injury and/or capable of enhancing the recovery of normal tissues postirradiation would assist patients undergoing aggressive radiotherapy.

Physiologically, the effects of radiation can be categorized into three syndromes (Walker, 1988). The hemopoietic syndrome occurs following the lowest radiation doses and results from irreversible damage to bone marrow hemopoietic stem cells. Under normal circumstances, these stem cells continually proliferate and differentiate to replace mature hematologic and immunologic cells being constantly lost through attrition. Following the loss of hemopoietic stem cells, hematologic and immunologic depletion rapidly occurs, and within a few weeks death ensues as a result of infection, hemorrhage and anemia (Talmage, 1955; Patt and Moloney, 1963; Taliaferro *et al.*, 1964).

Some substances, when administered prior to irradiation, have been recognized as being radioprotective specifically in the radiation dose range causing the hemopoietic syndrome. The best known of these substances is endotoxin (Mefferd *et al.*, 1953; Ainsworth, 1988), but impressive radioprotection also has been observed with *Bacillus Calmette Guerin* (BCG) and *Corynebacterium parvum*. All of these agents have been demonstrated to be potent nonspecific hemopoietic and immunologic stimuli. Optimal radioprotective effects usually have been observed with these agents administered 20-24 hr prior to irradiation. Because of this, the radioprotective mechanisms of these agents are thought to be different from those of traditional 'free-radical scavenging' sulfhydryl radioprotectors, which are most effective when administered within minutes of exposure. It has been suggested that the former agents mediate their radioprotective effects by mechanisms such as increasing the size of the preirradiation stem cell pools, synchronizing hemopoietic stem cells into less radiosensitive phases of the cell cycle, and/or by accelerating hemopoietic and immune repopulation from surviving stem cells postirradiation.

Ironically, substances found to be radioprotective specifically in the hemopoietic syndrome radiation dose range were never designed as radioprotectors (Torrence, 1985). The primary scientific interest in such agents, commonly referred to as immunomodulators or biological response modifiers (BRMs), was because of their potential therapeutic application in stimulating the immune system to fight cancer. Unfortunately, these BRMs also produced a variety of undesirable side effects, which precluded their use in man (Mansell and Klementz, 1973; Scott, 1974; Ribi, 1984). Over the past several decades (for reasons related to cancer therapy rather
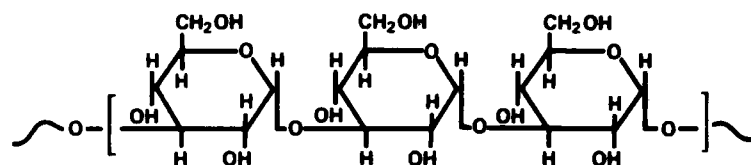
Fig. 1. Chemical structure of glucan, a polyglycan consisting of β-1,3-glucoside linkages.

than radioprotection), a great deal of time, energy and money has been dedicated to the discovery and/or development of new BRMs that are less toxic yet maintain potent immunomodulatory activity.

We have evaluated a variety of recently developed BRMs for the ability to enhance hemopoiesis and survival in irradiated animals (Patchen et al., 1987a). This paper discusses the radioprotective effects of the BRM glucan, its modes of action, and the possibility of using glucan in combination with other agents to further protect and/or enhance recovery from radiation injury.

2. GLUCAN: BACKGROUND AND GENERAL IMMUNOLOGIC AND HEMOPOIETIC EFFECTS

Glucan (Fig. 1) is a beta-1,3-polyglucose isolated from the inner cell wall of the yeast *Saccharomyces cerevisiae* (Hassid et al., 1941; DiLuzio et al., 1979). Upon injection, glucan appears to be specifically taken up by macrophages (Gilbert et al., 1977). Monocytes and macrophages recently have been demonstrated to possess glucan receptors (Czop and Austin, 1985; Abel et al., 1987); hence, glucan's effects may be receptor-mediated. It has been recognized for many years that glucan is a potent macrophage activator (Wooles and DiLuzio, 1963, 1964; DiLuzio et al., 1970). In addition, both primary and secondary immune responses and a variety of cell-mediated immune responses have been shown to be enhanced following glucan administration (Wooles and DiLuzio, 1963; DiLuzio, 1967; Cook et al., 1978). These later effects are suspected of resulting via cytokine-mediated cascades initiated following macrophage activation. In addition to these immunological effects, glucan also has been shown to dramatically enhance hemopoiesis at the pluripotent stem cell and committed progenitor cell levels (Patchen and Lotzova, 1980); Patchen and MacVittie, 1983).

Original glucan preparations were particulate in nature and because of this, glucan's clinical potential was limited. In recent years, however, soluble glucan preparations have been developed and have been demonstrated to induce immunologic and hemopoietic effects similar to those observed with the original participate glucan preparations (Patchen and MacVittie, 1986a,b).

3. GLUCAN-MEDIATED RADIOPROTECTION

Based on the ability to enhance survival in otherwise lethally irradiated mice, both participate and soluble glucan have been shown to be radioprotective (Patchen, 1983; Patchen and MacVittie, 1986b; Patchen et al., 1986, 1987b). This effect is dependent on the route of glucan injection, the glucan dose and the time elapsed between glucan injection and irradiation. Optimal radioprotection is generally observed with glucan injected intravenously approximately 20 prior to irradiation (Fig. 2).

In sublethally irradiated mice, it has been demonstrated that glucan accelerates the repopulation of both pluripotent hemopoietic stem cells (CFU-s) and committed granulocyte-macrophage (GM-CFC), pure macrophage (M-CFC), and erythroid (CFU-e, BFU-e) hemopoietic progenitor cells (Patchen and MacVittie, 1982; Pospisil et al., 1982; Patchen, 1983; Patchen et al., 1984a,b). This has been shown to occur with glucan administered either 1 day before, 1 hr before, or even 1 hr after irradiation. However −1 day glucan injection was generally more effective than −1 hr injection, and −1 hr injection generally more effective than +1 hr injection.
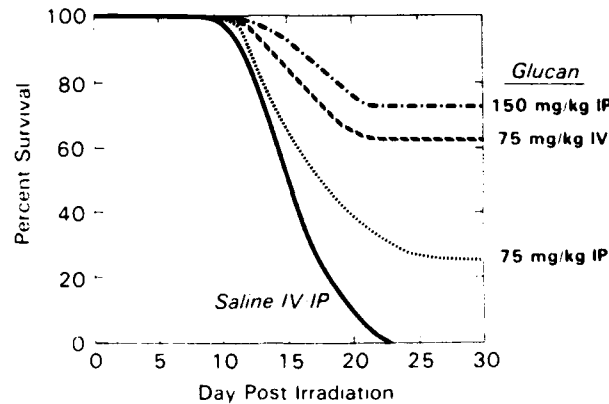
Fig. 2. Survival-enhancing effects of glucan. C3H/HeN mice were injected with saline, glucose (75 mg kg), or glucan (75 or 150 mg/kg) ~20 hr prior to receiving 9.0 Gy ^{60}Co radiation. Data represent cumulative survival data obtained from 45–61 mice in each treatment group.

TABLE 1. *Effect of Glucan on Survival and on Pluripotent Hemopoietic Stem Cell Recovery in Irradiated Mice* [*]

Day post irradiation	Percent survival		CFU-s/femur [+] (percent control)		CFU-s/spleen [‡] (percent control)	
	Saline	Glucan	Saline	Glucan	Saline	Glucan
11	96	99	0	0	0	0
13	80	95§	0	0	0	0.51 ± 0.08§
15	49	86§	0	0.15 ± 0.09§	0.02 ± 0.02	0.68 ± 0.12^4
18	18	75§	− ¶	0.96 ± 0.16	− ¶	12.94 ± 0.96
21	0	72§	− ¶	2.56 ± 0.31	− ¶	20.58 ± 2.06

[*]C3H HeN mice were injected i.v. with either saline or particulate glucan (75 mg/kg) ~20 hr prior to receiving 9.0 Gy ^{60}Co radiation.

[+]The number of CFU-s per femur in normal control mice was 1655 ± 55.

[‡]The number of CFU-s per spleen in normal control mice was 3315 ± 97.

§Compared to saline control values, $p < 0.05$.

¶Too few surviving mice to adequately evaluate at these time points.

In otherwise lethally irradiated mice, glucan also accelerates CFU-s and GM-CFC recovery (Patchen et al., 1987a,b; Table 1). However, at day 21 postirradiation (when all radiation control mice have died, and after which no glucan-treated mice die), the bone marrow and splenic CFU-s contents of surviving glucan-treated mice contain only 2.56% and 20.58%, respectively, of the CFU-s contents observed in normal control mice. Furthermore, no hemopoietic recover is detected until day 13 postirradiation. This, coupled with the fact that as early as 9 days postirradiation opportunistic bacterial infections occur less frequently in glucan-treated mice than in radiation control mice (Patchen et al., 1986, 1987a,b; Table 2), suggests that glucan-mediated radioprotection involves mechanisms other than those solely related to hemopoietic regeneration.

Macrophages, which have been shown to be activated following glucan administration, have also been shown to be some of the most radioresistant of all hemopoietic and immunologic cells (Gallin and Green, 1987). In addition, these cells play a major role in host defense against microbial invasion and synthesize and release cytokines capable of stimulating hemopoietic proliferation and differentiation (Griffin, 1982; Reichard and Filkens, 1984). In light of this, we suspected that glucan's initial survival-enhancing effects may be macrophage-mediated. Experiments in which 5'-nucleotidase activity (an ectoenzyme whose activity decreases with macrophage activation) was used as an indicator of macrophage activation revealed that although macrophages from both saline-treated and glucan-treated mice become activated within 1 hr after irradiation, macrophages from saline-treated mice soon revert to an unactivated state, while those in glucan-treated mice remain activated for several weeks (Patchen et al., 1987b; Fig. 3).

TABLE 2. Effect of Glucan on Survival and on Splenic Bacterial Translocation in Irradiated Mice*

Day post-irradiation	Percent survival		Percent of surviving mice exhibiting splenic bacterial translocation[†]	
	Saline	Glucan	Saline	Glucan
7	100	100	12.2 ± 0.9	10.0 ± 0.7
9	100	100	32.2 ± 1.4	15.8 ± 0.9 ‡
11	96	99	41.0 ± 1.8	22.4 ± 1.1 ‡
13	80	95 ‡	57.2 ± 3.1	10.1 ± 0.8 ‡
15	49	86 ‡	80.1 ± 4.9	6.9 ± 0.4 ‡
18	18	75 ‡	—§	5.7 ± 0.4
21	0	72 ‡	—§	4.1 ± 0.3

*C3H/HeN mice were injected i.v. with either saline or particulate glucan (75 mg/kg) ~20 hr prior to receiving 9.0 Gy ^{60}Co radiation.

[†] Organisms detected were Proteus mirabilis, Escherichia coli and Staphylococcus aureus.

‡Compared to saline control values, $p < 0.05$.

§Too few surviving mice to adequately evaluate at these time points.
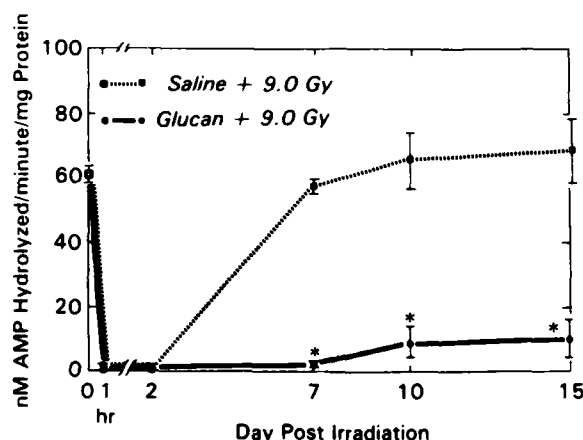
FIG. 3. 5'-Nucleotidase activity in peritoneal macrophages obtained from C3H/HeN mice injected i.p. with either saline or particulate glucan (75 mg/kg) ~20 hr prior to 9.0 Gy ^{60}Co radiation. Each data point represents the mean ± standard error of values obtained from 3–4 experiments, each performed with cells pooled from 8–10 mice. Statistical differences were determined by Student's t-test; * represents $p < 0.05$ with respect to control mice.

The role of macrophages in mediating BRM-induced radioprotection is also suggested by hemopoietic and survival data obtained with a variety of other BRMs. In a comparison of 17 BRMs, agents whose primary target cells included macrophages generally were more capable of enhancing hemopoiesis in irradiated mice than BRMs whose primary target cells did not include macrophages (Patchen et al., 1987a). Furthermore, only BRMs whose primary target cells included macrophages were capable of enhancing survival in otherwise lethally irradiated mice (Patchen et al., 1987a; Chirigos and Patchen, 1988).

4. RADIOPROTECTIVE COMBINATIONS

We have recently suggested that safer and more effective radioprotection may be achieved by combining nontoxic doses of several radioprotectors that function via different mechanisms. Examples of several such combinations are described below.
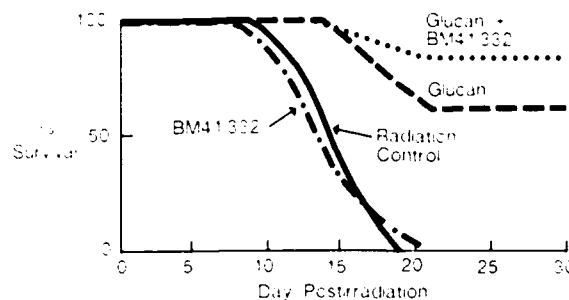
Fig. 4 Effects of combined BM41.332 and glucan administration on survival of irradiated C3H/HeN mice Approximately 20 hr prior to 9.0 Gy ⁶⁰Co radiation, mice were injected i.v. with particulate glucan (75 mg kg), BM41.332 (10 mg/kg), or both substances. Data represent cumulative survival data obtained from 47–77 mice in each treatment group.
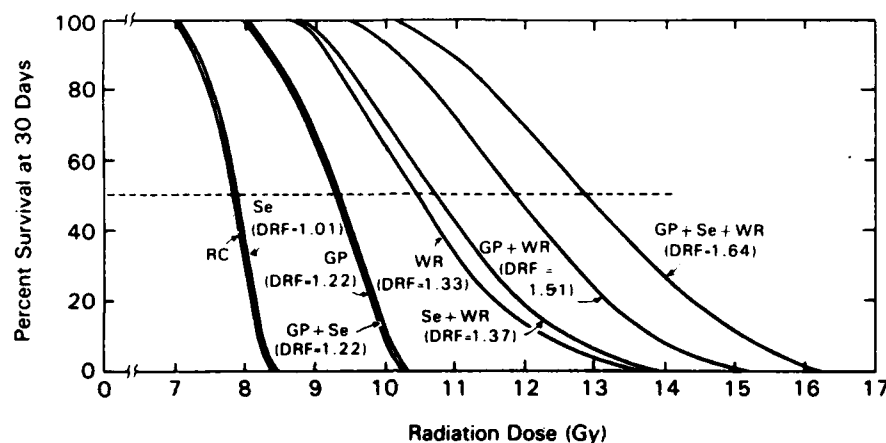

Fig. 5. Effects of combined glucan, selenium and WR-2721 administration on survival in irradiated C3H/HeN mice. Particulate glucan (GP, 75 mg/kg, i.v.), and selenium (Se, 0.8 mg/kg as sodium selenite, i.p.) were administered ~20 hr prior to irradiation. WR-2721 (WR, 200 mg/kg, i.p.) was administered ~30 min prior to irradiation. RC = saline-injected, irradiated mice. Data represent cumulative survival data obtained from 51–673 mice in each treatment group.

4.1. BRM–BRM Combinations

Radioprotective BRM combinations have been created using BRMs that are targeted at different cell populations. One such example is the use of glucan in combination with 2-cyano-1-[(2-methoxy-6-methyl-pyridin-3yl)-methyl]-aziridine (BM41.332). BM41.332 is not at all radioprotective when administered alone. However, when combined with a radioprotective dose of glucan, a synergistic survival enhancement approximately 20% greater than that obtained with glucan alone is observed (Fig. 4). Synergistic or additive radioprotective effects also have been obtained recently using combinations of immunomodulating cytokines (Neta et al., 1987). However, in spite of the fact that BRM–BRM combinations have enhanced survival beyond that observed with single-agent BRM treatments, the dose reduction factors (DRFs) obtained with such combinations still have been limited to ~1.2–1.3. This suggests that BRMs protect primarily cells comprising the hemopoietic and immune systems.

4.2. BRM–Aminothiol Combinations

In an attempt to obtain DRFs greater than 1.2–1.3, BRMs have been combined with other more generalized radioprotectors. The aminothiol WR-2721 (ethiofos) has been demonstrated to be one of the most potent radioprotectors available (Brown et al., 1988). When administered
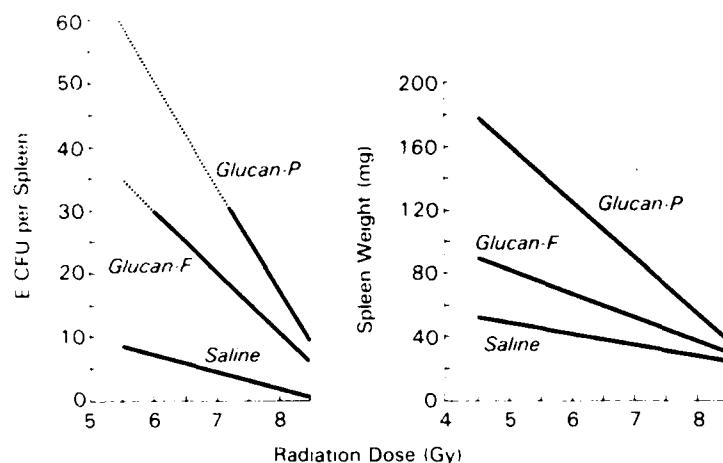
FIG. 6 Effect of postirradiation glucan administration on endogenous spleen colony formation (E-CFU) and spleen weight. C3H/HeN mice were exposed to the indicated doses of ⁶⁰Co radiation and 1 hr later intravenously injected with saline, particulate glucan (Glucan-P, 75 mg/kg), or soluble glucan (Glucan-F, 250 mg/kg). Twelve days later, the spleens were removed, fixed in Bouin's solution, weighed, and the number of E-CFU counted. Data were plotted and computer-generated extrapolation lines drawn through the data points. Dotted portions of lines indicate radiation doses at which confluent E-CFU formation was observed.
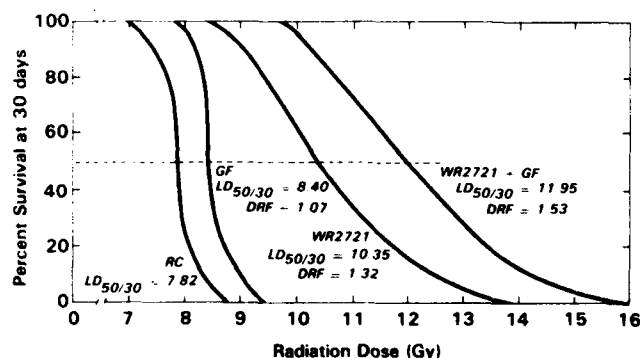
FIG. 7 Survival-enhancing effects of postirradiation glucan administration combined with preirradiation WR-2721 administration. C3H/HeN mice were injected i.p. with WR-2721 (200 mg/kg) ~30 min prior to irradiation and injected i.v. with soluble glucan (GF, 250 mg/kg) ~1 hr after irradiation. Data represent cumulative survival data obtained from 75–623 mice in each treatment group.

shortly before irradiation, WR-2721 protects a variety of tissues from radiation injury; however, the best effects have been observed in hemopoietic tissues. Unfortunately, the radioprotective effects of WR-2721 are directly dose-dependent, and WR-2721 doses that produce the best radioprotection also induce nausea, vomiting and other potentially more dangerous side effects (Cairnie, 1983; Kligerman et al., 1984). We have attempted to reduce side effects and yet maintain good radioprotection by administering nontoxic doses of WR-2721 in combination with BRMs. Figure 5 illustrates the results of survival studies in which glucan and a low dose of WR-2721 were used. The DRF of 1.51 obtained with the combination of these two agents is additive between that obtained with glucan (DRF 1.22) and that obtained with low-dose WR-2721 (DRF 1.33). If selenium, which has been shown to reduce the endogenous toxicity of WR-2721 (Weiss et al., 1987), is also administered ~20 hr prior to irradiation, a DRF of 1.64 is observed (Fig. 5). These studies demonstrate the feasibility of using nontoxic doses of several agents to additively and/or synergistically produce DRFs greater than 1.2.–1.3.

Another approach to the use of glucan in combination with WR-2721 has been its administration postirradiation. This approach is based on our observation that, even when administered postirradiation, glucan can significantly increase hemopoietic stem cell numbers (Fig. 6). Thus,

TABLE 3. Effect of WR-2721 and Glucan on Endogenous Hemopoietic Spleen Colony Formation (E-CFU) and on Spleen Weight*

	10 Gy		11 Gy		12 Gy	
	E-CFU	SPL WT‡	E-CFU	SPL WT‡	E-CFU‡	SPL WT‡
Radiation control	0.04	14.5	0.00	13.0	0.00	12.9
WR-2721	7.05	25.8	2.00	19.5	0.74	16.5
Glucan	0.20	16.5	0.01	16.3	0.00	16.0
WR-2721 + Glucan	24.47	59.5	13.42	39.5	4.65	23.2

*C3H HeN mice were injected i.p. with saline or WR-2721 (200 mg/kg) ~ 30 min prior to irradiation and injected i.v. with saline or soluble glucan (250 mg/kg) ~ 1 hr after irradiation
‡E-CFU were counted 12 days after irradiation
Weight in mg

if low-dose WR-2721 treatment prevents the destruction of even a very few hemopoietic stem cells, postirradiation glucan therapy should be capable of stimulating the proliferation of these cells and result in accelerated hemopoietic recovery and increased survival. Results supporting this hypothesis and demonstrating synergistic hemopoiesis- and survival-enhancing effects of preirradiation low-dose WR-2721 treatment combined with postirradiation glucan treatment are illustrated in Fig. 7 and Table 3. Interestingly, multiple postirradiation glucan injections did not enhance survival beyond that observed with a single glucan injection given 1 hr after exposure (Patchen, unpublished results).

5. GENERAL COMMENTS AND CONCLUSIONS

It is clear that even when used alone glucan can function protectively and/or therapeutically in radiation-injured host. When used in this manner, 'radioprotective' potential appears to be limited to DRFs of 1.2–1.3. However, when used in combination with even low doses of traditional aminothiol radioprotectors such as WR-2721, glucan can additively or synergistically increase DRFs to 1.5–1.6. Such results suggest that not only better radioprotection but also reduced toxicity may be obtained by using low-to-modest doses of several radioprotective agents that act via different mechanisms. Furthermore, based on measurements of motor performance in mice, glucan even appears to reduce the behavioral toxicity of WR-2721 (Landauer and Patchen, manuscript in preparation).

Glucan is only one of several macrophage-activating BRMs that have been demonstrated to be both hemopoietic stimulants and radioprotectors (Patchen et al., 1987a). Numerous other BRMs remain to be evaluated for these effects, and they may prove to be as good as or better than glucan as radioprotectors. As more data accumulate, it appears that these agents (alone or in combination with other agents) are establishing their usefulness in the treatment and/or prevention of acute radiation injury.

REFERENCES

ABEL, G., DORA, C., NAGY, S., SZOLLOSI, J., PATCHEN, M., CHIHARA, G. and FACHET, J. (1987) Stimulation of endocytotic activity of murine macrophages via specific receptors by different types of glucans. Proc. Eighth European Immunology Meeting. Abstract (in press).
AINSWORTH, E. J. (1988) From endotoxins to newer immunomodulators: Survival promoting effects of microbiol polysaccharide complexes in irradiated animals. Pharmac. Ther. 39: 223–241, this volume.

Brown, D. Q., Graham, W. J., MacKenzie, L. J., Pittock, J. W. and Shaw, L. M. (1988) Can WR-2721 be improved upon? Pharmac. Ther. 39: 157–168, this volume.

Cairnie, A. B. (1983) Adverse effects of the radioprotector WR-2721. Radiat. Res. 94: 221–226.

Chirigos, M. A. and Patchen, M. L. (1988) Survey of newer biologic response modifiers for possible use in radioprotection. Pharmac. Ther. 39: 243–246, this volume.

Cook, J. A., Taylor, D., Cohen, C., Rodrigue, J., Malshet, U. and DiLuzio, N. R. (1978) Comparative evaluation of the role of macrophages and lymphocytes in mediating the antitumor action of glucan. In: Immune Modulation and Control of Neoplasia by Adjuvant Therapy, pp. 183–194. Chirigos, M. A. (ed.) Raven Press, New York.

Czop, J. K. and Austin, K. F. (1985) A beta-glucan inhibitable receptor on human monocytes. Its identity with the phagocytic receptor for particulate activators of the alternate complement pathway. J. Immunol. 134: 2588–2593.

DiLuzio, R. (1967) Evaluation by the graft-vs-host reaction of the immune competence of lymphoid cells of mice with altered reticuloendothelial function. J. Reticuloendothel. Soc. 4: 459–475.

DiLuzio, N. R., Pisano, J. C. and Saba, T. M. (1970) Evaluation of the mechanism of glucan-induced stimulation of the reticuloendothelial system. J. Reticuloendothel. Soc. 7: 731–742.

DiLuzio, N. R., Williams, D. L., McNamee, R. B., Edwards, B. F. and Kitahama, A. (1979) Comparative tumor inhibitory and antibacterial activity of soluble and particulate glucan. Int. J. Cancer 24: 773–779.

Gallin, E. K. and Green, S. W. (1987) Exposure to γ-irradiation increases phorbol myristate acetate-induced H_2O_2 production in human macrophages. Blood 70: 694–701.

Gilbert, K., Chu, F., Jones, E. and DiLuzio, N. R. (1977) Fate of ^{14}C-glucan in normal and acute myelogenous leukemic rats. J. Reticuloendothel. Soc. 22: 319–327.

Griffin, F. M. (1982) Mononuclear cell phagocyte mechanisms and host defense. Adv. Host Def. Mech. 1: 31–55.

Hassid, W. Z., Joslyn, M. A. and McCready, R. M. (1941) The molecular constitution of an insoluble polysaccharide from the yeast Saccharomyces cerevisiae. J. Am. Chem. Soc. 63: 295–298.

Klingerman, M. M., Glover, D. J., Turrisi, A. T., Norfleet, A. L., Yuhas, J. M., Coia, L. R., Simone, C., Glick, J. H. and Goodman, R. L. (1984) Toxicity of WR-2721 administered in single and multiple doses. Int. J. Radiat. Oncol. Biol. Phys. 10: 1773–1776.

Mansfield, P. and Klementz, E. (1973) Reaction to BCG. JAMA 226: 1570–1571.

Mefferd, R. B., Henkel, D. T. and Loeffer, J. B. (1953) Effect of piromen on survival in irradiated mice. Proc. Soc. Exp. Biol. Med. 83: 54–56.

Neta, R., Vogel, S. N., Sipe, J. D., Oppenheim, J. J., Gilcas, P. C. and Douches, S. D. (1987) Comparison of in vivo effects of rIL-1 and rTNF in radioprotection, induction of CSF and of acute phase reactants. Fed. Proc. 46: 1200. Abstract.

Patchen, M. L. (1983) Immunomodulators and hemopoiesis. Surv. Immunol. Res. 2: 237–242.

Patchen, M. L. and Lotzova, E. (1980) Modulation of murine hemopoiesis by glucan. Exp. Hematol. 8: 409–422.

Patchen, M. L. and MacVittie, T. J. (1982) Use of glucan to enhance hemopoietic recovery after exposure to cobalt-60 irradiation. Adv. Exp. Med. Biol. 155: 267–272.

Patchen, M. L. and MacVittie, T. J. (1983) Dose-dependent responses of murine pluripotent stem cells and myeloid and erythroid progenitor cells following administration of the immunomodulating agent. Immunopharmacology 5: 303–313.

Patchen, M. L. and MacVittie, T. J. (1986a) Comparative effects of soluble and particulate glucan on survival in irradiated mice. J. Biol. Response Mod. 5: 45–60.

Patchen, M. L. and MacVittie, T. J. (1986b) Hemopoietic effects of intravenous soluble glucan administration. J. Immunopharmacol. 8: 407–425.

Patchen, M. L., DiLuzio, N. R., Jacques, P. and MacVittie, T. J. (1984a) Soluble polyglycans enhance recovery from cobalt-60 induced hemopoietic injury. J. Biol. Response Mod. 3: 627–633.

Patchen, M. L., MacVittie, T. J. and Wathen, L. M. (1984b) Effect of pre- and postirradiation glucan treatment on pluripotent stem cells, granulocyte, macrophage, and erythroid progenitor cells, and hemopoietic stromal cells. Experientia 4: 1240–1244.

Patchen, M. L., MacVittie, T. J. and Brook, I. (1986) Glucan-induced hemopoietic and immune stimulation: Therapeutic effects in sublethally and lethally irradiated mice. Methods Find. Exp. Clin. Pharmacol. 8: 151–155.

Patchen, M. L., Chirigos, M. A. and Brook, I. (1987a) Use of glucan and sixteen other immunopharmaceutical agents in prevention of acute radiation injury. Comments Toxicol. (in press).

Patchen, M. L., D'Alesandro, M. M., Brook, I., Blakely, W. F. and MacVittie, T. J. (1987b) Glucan: Mechanisms involved in its "radioprotective" effect. J. Leukocyte Biol. (in press).

Patt, H. M. and Moloney, M. (1963) A comparison of radiation-induced granulocytopenia in several mammalian species. Radiat. Res. 18: 213–235.

Pospisil, M., Jary, J., Netikova, J. and Marek, M. (1982) Glucan-induced enhancement of hemopoietic recovery in gamma-irradiated mice. Experientia 38: 1232–1234.

Reichard, S. M. and Filkins, J. P. (1984) The Reticuloendothelial System: Physiology. Plenum Press, New York.

Ribi, E. (1984) Beneficial modification of the endotoxin molecule. J. Biol. Response Mod. 3: 1–9.

Scott, M. (1974) Corynebacterium parvum as a therapeutic antitumor agent in mice. I. Systemic effects of intravenous injection. J. Natn. Cancer Inst. 53: 855–860.

Taliaferro, W. H., Taliaferro, L. G. and Jaroslow, B. N. (1964) Radiation and Immune Mechanisms. Academic Press, New York.

Talmage, D. W. (1955) Effect of ionizing radiation on resistance to infection. Ann. Rev. Microbiol. 9: 335–346.

Torrence, P. (1985) Biological Response Modifiers. Academic Press, New York.

Walker, R. I. (1988) Acute radiation injuries. Pharmac. Ther. 39: 9–12, this volume.

Weiss, J. F., Hoover, R. L. and Kumar, K. S. (1987) Selenium pretreatment enhances the radioprotective effect and reduces the lethal toxicity of WR-2721. Free Rad. Res. Commun. 3: 33–38.

Wooles, W. R. and DiLuzio, N. R. (1963) Reticuloendothelial function and the immune response. Science 142: 1078–1080.

Wooles, W. R. and DiLuzio, N. R. (1964) The phagocytic and proliferative response of the RES following glucan administration. J. Reticuloendothel. Soc. 1: 160–169.

Postirradiation Glucan Administration Enhances the Radioprotective Effects of WR-2721

M. L. PATCHEN, T. J. MACVITTIE, AND W. E. JACKSON

*Departments of Experimental Hematology and Computers and Electronics, Armed Forces
Radiobiology Research Institute, Bethesda, Maryland 20814-5145*

PATCHEN, M. L., MACVITTIE, T. J., AND JACKSON, W. E. Postirradiation Glucan Administration Enhances the Radioprotective Effects of WR-2721. *Radiat. Res.* 117, 59–69 (1989).

Based on murine survival studies, endogenous hemopoietic spleen colony formation (E-CFU), and recovery of bone marrow and splenic granulocyte–macrophage colony-forming cells (GM-CFC), it was demonstrated that the postirradiation administration of glucan, an immunomodulator and hemopoietic stimulant, enhances the radioprotective effects of WR-2721. $LD_{50/30}$ dose reduction factors for mice treated with WR-2721 (200 mg/kg ~30 min before irradiation), glucan (250 mg/kg ~1 h after irradiation), or both agents were 1.37, 1.08, and 1.52, respectively. Enhanced survival in mice treated with both agents appeared to be due in part to glucan's ability to accelerate hemopoietic regeneration from stem cells initially protected from radiation-induced lethality by WR-2721. Following a 10-Gy radiation exposure, E-CFU numbers in mice treated with saline, WR-2721, glucan, or both WR-2721 and glucan were 0.05 ± 0.03, 6.70 ± 1.05, 0.95 ± 0.24, and 33.90 ± 2.96, respectively. Similarly, bone marrow and splenic GM-CFC numbers were greater in mice treated with both WR-2721 and glucan than in mice treated with either agent alone. These results demonstrated at least additive radioprotective effects when mice were given WR-2721 prior to irradiation and glucan following irradiation. These effects appeared to depend on the sequential cell protection mediated by WR-2721 and hemopoietic repopulation mediated by glucan. © 1989 Academic Press, Inc.

INTRODUCTION

The thiol compound WR-2721 [ethiofos, S-2-(3-aminopropylamino) ethylphosphorothioic acid] is one of the most effective exogenous radioprotectors available (*1–3*). Free radical scavenging, hydrogen atom donation, and induction of hypoxia have been suggested as mechanisms through which WR-2721 protects cells from radiation-induced lethality (*4, 5*). As a survival enhancer, WR-2721 is most effective when relatively high doses are administered 30 min to 3 h prior to radiation exposure (*6*). However, because high doses of WR-2721 cause undesirable and/or toxic side effects (*7, 8*), doses that yield large radiation dose reduction factors (DRFs) are also the most toxic.

Immunomodulators are another class of radioprotectors that can enhance survival in irradiated animals (*3, 9*). These agents are also most effective when administered prior to irradiation. However, the maximum DRFs obtainable with immunomodulators are generally lower than those of thiol compounds. Glucan, a β-1,3 polyglucose isolated from the inner cell wall of the yeast *Saccharomyces cerevisiae*, is one such radioprotective immunomodulator (*10–12*). Although free-radical scavenging may

59

play a role in glucan's radioprotective effect (13, 14), glucan mediates its protection primarily by (1) enhancing host resistance to life-threatening postirradiation opportunistic infections, and (2) accelerating hemopoietic regeneration (13, 15, 16). Presumably because of these same mechanisms, one form of glucan (glucan-F) also enhances survival even when administered after radiation exposure (12).

Because WR-2721 mediates its radioprotective effect by preventing cell death, whereas glucan mediates its effect by enhancing the reconstitution and/or function of hemopoietic cell populations, we hypothesized that these two agents might produce additive or synergistic radioprotective effects. For this particular study, we hypothesized that, by protecting a small population of hemopoietic cells using a low (nontoxic) dose of WR-2721, it should be possible to use glucan after irradiation to stimulate hemopoietic regeneration and/or function, thus producing better survival than with either agent alone. This paper discusses hemopoietic and survival data obtained from studies in which mice were given WR-2721 prior to irradiation and glucan after irradiation.

MATERIALS AND METHODS

Mice

Mice used were VAF/Plus C3H/HeN females (~20 g) purchased from Charles River Laboratories (Raleigh, NC). They were housed 10 per cage in plastic microisolator cages, tested for *Pseudomonas* contamination, and quarantined until the test results were obtained. Only healthy mice were used in the experiments. They were maintained in an AAALAC-accredited facility in microisolator cages on hardwood chip, contact bedding, and were provided commercial rodent chow and acidified tap water (pH 2.5) *ad libitum*. Animal holding rooms were maintained at 70 ± 2°F with 50 ± 10% relative humidity using at least 10 air changes per hour of 100% conditioned fresh air. Mice were also routinely exposed to full-spectrum light from 6:00 AM to 6:00 PM, but with no twilight.

WR-2721 and Glucan

Stock WR-2721 was obtained from Dr. David Davidson (Walter Reed Army Institute of Research, Washington, DC) and kept frozen at −20°C until use. Immediately before each use, WR-2721 was dissolved in sterile pyrogen-free saline. Exposure of the material to light was minimized. Approximately 30 min prior to irradiation, mice were intraperitoneally (ip) injected with 200 mg/kg WR-2721 in a volume of 0.5 ml. This dose has minimal toxic effects in mice (7, 8). WR-2721 control mice received 0.5 ml saline ip. The glucan used in these studies was a soluble endotoxin-free preparation obtained from Dr. N. R. DiLuzio (Tulane University School of Medicine, New Orleans, LA). The preparation of this glucan (sometimes referred to as glucan-F) has been described by DiLuzio *et al.* (17). Approximately 1 h after irradiation, mice were injected with 250 mg/kg glucan into the lateral tail veins in a volume of 0.5 ml. Glucan control mice received 0.5 ml saline. Controls for mice receiving both WR-2721 and glucan received both ip and iv saline injections. However, because no significant differences were observed in the responses of mice receiving ip, iv, or both ip and iv saline injections, data from all saline-treated mice were pooled.

Irradiation

Mice were placed in ventilated Plexiglas containers and exposed to bilateral total-body γ rays at a dose rate of 0.4 Gy/min. The AFRRI ⁶⁰Co source was used for all irradiations. Dosimetry was determined by ionization chambers as previously described (18). Radiation doses ranged from 7 to 16 Gy.

Survival Assays

Irradiated mice were returned to the animal facility and treated routinely; survival was monitored daily for 30 days. Each treatment group within each experiment consisted of 10–20 mice. Experiments were

repeated 4-6 times to obtain an "n" of at least 40 animals for each treatment group at each radiation dose. The percentage of mice surviving each radiation dose at 30 days postexposure was used to construct a probit plot survival curve for each treatment group. Probit analyses were performed according to Finney (19) to obtain LD$_{5/30}$, LD$_{50/30}$, and LD$_{95/30}$ values. These values were used to determine DRFs (20).

Endogenous Spleen Colony-Forming Unit Assay

Endogenous spleen colony-forming units (E-CFU) were evaluated using the method of Till and McCulloch (21). Mice from the various treatment groups were exposed to 8, 9, 10, 11, or 12 Gy of total-body radiation to partially oblate endogenous hemopoietic stem cells. Twelve days after irradiation, mice were euthanized by cervical dislocation. Their spleens were removed, fixed in Bouin's solution, and weighed, and grossly visible spleen colonies were counted. Each treatment group within each experiment consisted of 5-10 mice. Experiments were repeated 4-5 times to obtain an "n" of at least 20 animals for each treatment group at each radiation dose. Student's t test was used to determine statistical differences in E-CFU and spleen weight data.

Granulocyte-Macrophage Colony-Forming Cell Assay

Hemopoietic progenitor cells committed to granulocyte and/or macrophage development were assayed by MacVittie's modification (22) of the *in vitro* granulocyte-macrophage colony-forming cell (GM-CFC) assay originally described by Bradley and Metcalf (23) and Pluznik and Sachs (24). Colonies (>50 cells) were counted after 10 days incubation in a 37°C humidified environment containing 5% CO_2. The cell suspensions used for these assays represented the pool of tissues from 3-12 normal, irradiated, or treated and irradiated mice at each time. Cells were flushed from femurs with 3 ml McCoy's 5A medium containing 5% heat-inactivated fetal bovine serum. Spleens were pressed through a stainless-steel mesh screen, and the cells were washed from the screen with 6 ml medium. The total number of nucleated cells in each suspension was determined by counting the cells on a hemocytometer. Data represent mean values obtained from three separate experiments and were analyzed using Student's t test.

RESULTS

Effects of WR-2721, Glucan, or Both Agents on Survival of Irradiated Mice

The LD$_{5/30}$, LD$_{50/30}$, and LD$_{95/30}$ values for saline-treated mice were 7.21 [7.02, 7.34] Gy, 7.82 [7.74, 7.89] Gy, and 8.49 [8.38, 8.64] Gy, respectively (Fig. 1). As anticipated, preirradiation administration of even the relatively low dose of WR-2721 used in these experiments significantly increased survival compared to saline. The LD$_{5/30}$, LD$_{50/30}$, and LD$_{95/30}$ values for WR-2721-treated mice were 8.65 [8.36, 8.90] Gy, 10.73 [10.57, 10.89] Gy, and 13.30 [12.96, 13.73] Gy. In addition, WR-2721 treatment significantly altered the slope of the survival curve ($P < 0.001$). This slope shift reflected the fact that WR-2721 enhanced survival more effectively at high radiation doses than at low radiation doses. Compared to saline, WR-2721 produced DRFs of 1.20, 1.37, and 1.57 at the respective LD$_{5/30}$, LD$_{50/30}$, and LD$_{95/30}$ values. Administration of glucan alone at 1 h after irradiation also significantly enhanced survival, but to a much lesser degree than did treatment with WR-2721 prior to irradiation. In this instance, the LD$_{5/30}$, LD$_{50/30}$, and LD$_{95/30}$ values were 7.97 [7.76, 8.10] Gy, 8.45 [8.36, 8.53] Gy, and 8.96 [8.84, 9.15] Gy, respectively. Compared to saline controls, the DRF obtained with glucan treatment at the LD$_{50/30}$ value was 1.08. Because glucan treatment did not alter the slope of the survival curve, this DRF was observed at all LD values. Combined WR-2721 and glucan treatment yielded a survival curve parallel to that obtained with WR-2721 treatment. However, as hypothe-
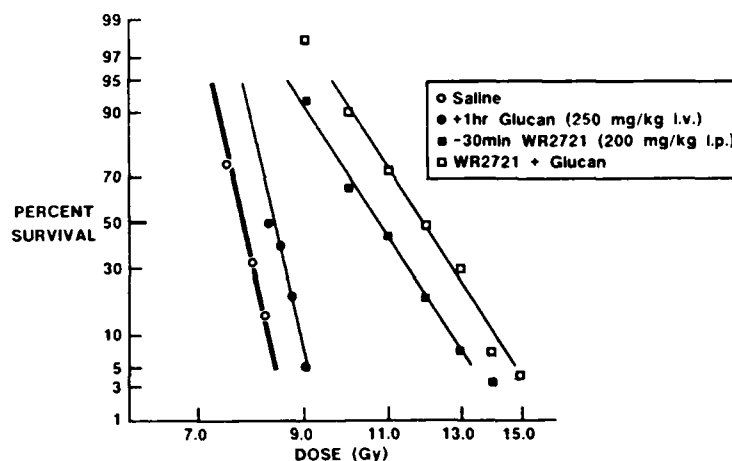
FIG. 1. Effects of WR-2721. glucan. or both agents on survival in irradiated mice. C3H/HeN mice were injected with saline. WR-2721 (200 mg/kg ip 30 min prior to irradiation). glucan (250 mg/kg iv 1 h after irradiation). or both agents. and survival was monitored for 30 days following exposure to 7-16 Gy of ^{60}Co radiation. Percentage survival at 30 days was probit-plotted against radiation dose and used to determine lethal dose values and dose reduction factors. Points representing 100 and 0% survival are not represented. Based on LD$_{50\,10}$ values: Glucan versus saline. $P < 0.001$; WR-2721 versus saline. $P < 0.001$; WR-2721 versus glucan. $P < 0.001$; WR-2721 + glucan versus saline. $P < 0.001$; WR-2721 + glucan versus WR-2721. $P < 0.001$.

sized. combined treatment enhanced survival significantly more than either WR-2721 or glucan treatment alone. The LD$_{5/30}$. LD$_{50/30}$. and LD$_{95/30}$ values for combination-treated mice were 9.60 [9.19. 9.92] Gy. 11.92 [11.70. 12.14] Gy. and 14.80 [14.30. 15.46] Gy. respectively. and resulted in DRFs of 1.33. 1.52. and 1.74. Like WR-2721 treatment. the combined treatment was more effective at the higher radiation doses. Compared to WR-2721-treated mice. combined WR-2721 and glucan treatment produced a DRF of 1.11 at all LD values. Because the LD$_{50/30}$ DRFs of glucan-treated mice compared with saline-treated mice (1.08) and the LD$_{50/30}$ DRF of WR-2721- and glucan-treated mice compared with WR-2721-treated mice (1.11) were nearly equal. glucan appeared to operate independently of WR-2721 in increasing survival.

Effects of WR-2721. Glucan. or Both Agents on Hemopoiesis in Irradiated Mice

E-CFU studies. E-CFU in saline-treated mice ranged from 0.50 ± 0.19 in mice exposed to 8 Gy to 0 in mice exposed to 11 and 12 Gy (Fig. 2). WR-2721 treatment significantly increased E-CFU at all radiation doses. ranging from >40.00 (confluent colony formation) at 8 Gy to 0.74 ± 0.20 at 12 Gy. Postirradiation glucan treatment also increased E-CFU in mice exposed to 8. 9. or 10 Gy (6.00 ± 0.90. 1.20 ± 0.31. and 0.95 ± 0.24. respectively). However. in mice exposed to 11 and 12 Gy. glucan had very little effect: this suggests that glucan is mechanistically dependent on the presence of stem cells. Combined treatment with WR-2721 and glucan resulted in
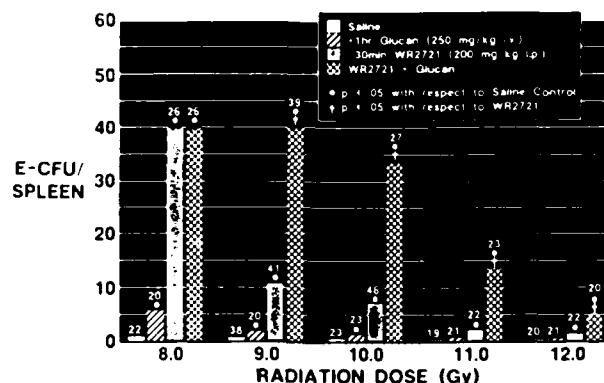
FIG. 2. Effects of WR-2721, glucan, or both agents on endogenous spleen colony formation in irradiated mice. C3H/HeN mice were injected with saline. WR-2721, glucan, or both agents as described for Fig. 1. Endogenously arising hemopoietic colony-forming units in the spleen (E-CFU) were counted 12 days after exposure to ⁶⁰Co radiation doses ranging from 8 to 12 Gy. Number of mice evaluated in each treatment group is indicated above bars. Confluent colony formation is indicated by bars with jagged tops.

E-CFU numbers greater than those observed in WR-2721-treated mice. E-CFU in these mice ranged from >40.00 (confluent colony formation) for mice exposed to 8 and 9 Gy, to 4.85 ± 0.53 for mice exposed to 12 Gy. Further analysis of the effects on E-CFU of combined treatment with WR-2721 and glucan was carried out as follows: Dose-response curves were constructed using data from the current studies and previous data accumulated in our laboratory from saline- and glucan-treated mice exposed to 5.5–8.0 Gy (Fig. 3). These curves allowed the determination of DRFs for
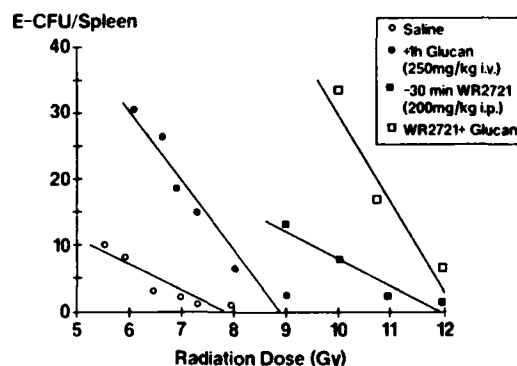
FIG. 3. E-CFU versus radiation dose survival curves. C3H/HeN mice were injected with saline. WR-2721, glucan, or both agents as described for Fig. 1. E-CFU were counted 12 days after exposure to ⁶⁰Co radiation doses ranging from 5.5 to 12.0 Gy. E-CFU data for each radiation dose were plotted and used to construct survival curves. Treatment effects were compared at the levels of 5 and 10 E-CFU/spleen. Glucan versus saline, $P < 0.001$; WR-2721 versus saline, $P < 0.001$; WR-2721 versus glucan, $P < 0.001$ (5 E-CFU/spleen) and $P < 0.01$ (10 E-CFU/spleen); WR-2721 + glucan versus saline, $P < 0.001$; WR-2721 + glucan versus WR-2721, $P < 0.01$ (5 E-CFU/spleen) and $P < 0.001$ (10 E-CFU/spleen).
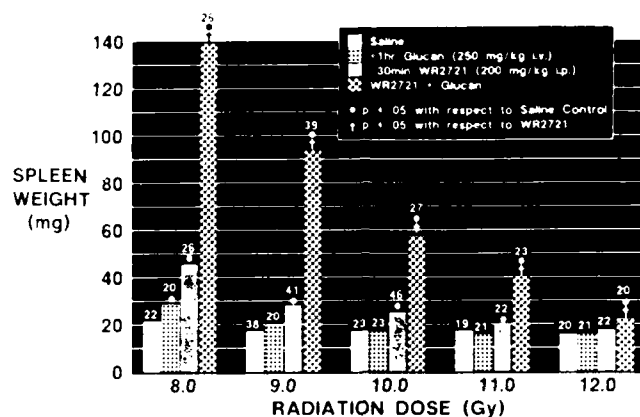
FIG. 4. Effects of WR-2721, glucan, or both agents on splenic weight in irradiated mice. C3H/HeN mice were injected with saline, WR-2721, glucan, or both agents as described for Fig. 1 and irradiated as described for Fig. 2. Data represent the weights of spleens from which E-CFU data illustrated in Fig. 2 were obtained. Number of mice evaluated in each treatment group is indicated above bars.

E-CFU responses obtained in mice treated with glucan, WR-2721, or both agents. For example, the calculated radiation doses which resulted in an average of 10 E-CFU per spleen were 5.16, 7.89, 9.00, and 11.50 Gy for mice treated with saline, glucan, WR-2721, and both agents, respectively. The DRFs resulting from these values were 1.53 for glucan, 1.74 for WR-2721, and 2.22 for the combined treatment with glucan and WR-2721. The change in splenic weights of mice after the various treatments (Fig. 4) showed a pattern similar to that observed for E-CFU (Fig. 2). In addition, at the 8- and 9-Gy radiation doses, where it was difficult to analyze E-CFU data because of confluent colony formation, distinct differences between the treatment groups were clearly evident based on spleen weight.

Bone marrow and splenic cellularity and GM-CFC studies. Hemopoietic recovery in mice treated with WR-2721, glucan, or both agents was evaluated further by examining cellularity and recovery of GM-CFC in the bone marrow and spleens of irradiated mice. In these studies, mice were exposed to 9 Gy ^{60}Co (an $LD_{100/30}$ for saline-treated mice and an approximate $LD_{95/30}$, $LD_{10/30}$, and $LD_{0/30}$ for glucan-, WR-2721-, and combination-treated mice, respectively). Four, 7, 11, 13, and 18 days later, femoral and splenic cellularity and GM-CFC content were assayed.

Relative to normal (nonirradiated) mice, bone marrow cellularity in saline-treated mice was reduced to ~6% at Day 4 postirradiation and recovered to only ~18% by Day 13 (Fig. 5). On Days 4, 7, and 11 postexposure, mice that received only glucan exhibited reduced bone marrow cellularities similar to those observed in saline-treated mice. However, compared to the ~18% recovery observed in saline-treated mice at Day 13 postirradiation, glucan-treated mice exhibited a ~38% recovery. In contrast to mice receiving only glucan, mice treated with only WR-2721 exhibited increased bone marrow cellularity at all times assayed. On Day 4 postexposure, ~33% of normal bone marrow cellularity was evident; this increased to ~71% by Day 18 postirradiation. Bone marrow cellularity in mice treated with both WR-2721
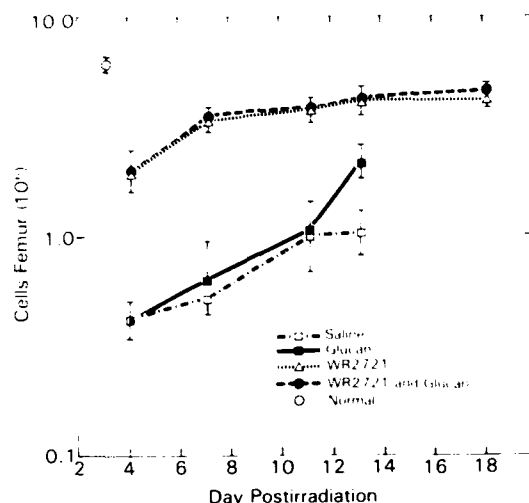
Fig. 5. Effects of WR-2721, glucan, or both agents on bone marrow cellularity in irradiated mice. C3H/HeN mice were injected with saline, WR-2721, glucan, or both agents as described for Fig. 1 and exposed to a 9-Gy dose of ^{60}Co radiation on Day 0. Very few saline- and glucan-treated mice survived until Day 18 postirradiation. Because of this, sufficient data could not be obtained at this time point for these treatment groups. Glucan values are significantly greater than saline values on Day 13 ($P < 0.05$). WR-2721 values are significantly greater than saline values on Day 4 ($P < 0.001$), Day 7 ($P < 0.001$), Day 11 ($P < 0.01$), and Day 13 ($P < 0.01$). WR-2721 + glucan values are significantly greater than saline values on Day 4 ($P < 0.001$), Day 7 ($P < 0.001$), Day 11 ($P < 0.01$), and Day 13 ($P < 0.01$).

and glucan was not significantly different from that observed in mice treated only with WR-2721.

Qualitatively, spleen cell recovery was similar to bone marrow recovery in mice treated with glucan or WR-2721 alone (i.e., compared to saline values, glucan had very little effect, while there was significantly increased cellularity in the WR-2721-treated mice; Fig. 6). However, in contrast to the bone marrow response, mice treated with both WR-2721 and glucan exhibited a splenic cell recovery greater than that of mice treated with WR-2721 alone. This response was most significant at Days 7, 11, and 13 postirradiation.

In saline-treated and in glucan-treated mice, bone marrow GM-CFC content decreased to less than 1% normal by Day 4 postirradiation (Fig. 7). Recovery beyond 1% normal was not observed even at Day 13. However, at all times postirradiation, glucan-treated mice exhibited more GM-CFC per femur than did saline-treated mice. WR-2721 treatment alone also increased GM-CFC content in comparison to saline-treated mice. In this instance, GM-CFC content was much greater than that observed in glucan-treated mice, ranging from ~1% normal at Day 4 postexposure to ~23% at Day 18. The combination of WR-2721 and glucan increased GM-CFC per femur even further, ranging from ~2% normal at Day 4 postexposure to ~73% at Day 18.

Spleen-derived GM-CFC was not detected in either saline- or glucan-treated mice at any postirradiation time assayed. In contrast, mice treated with only WR-2721 exhibited splenic GM-CFC on Day 11 postexposure (<1% normal); by Day 18, GM-
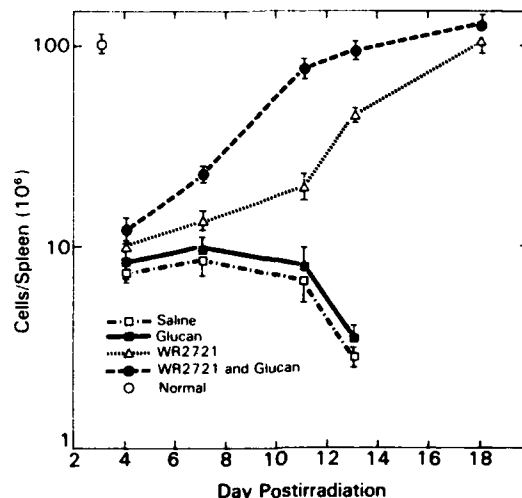
FIG. 6. Effects of WR-2721, glucan, or both agents on splenic cellularity in irradiated mice. C3H/HeN mice were injected with saline, WR-2721, glucan, or both agents as described for Fig. 1 and exposed to a 9-Gy dose of ^{60}Co radiation on Day 0. Very few saline- and glucan-treated mice survived until Day 18 postexposure. Because of this, sufficient data could not be obtained at this time point for these treatment groups. WR-2721 values are significantly greater than saline values on Day 11 ($P < 0.02$) and Day 13 ($P < 0.001$). WR-2721 + glucan values are significantly greater than saline values on Day 4 ($P < 0.03$), Day 7 ($P < 0.008$), Day 11 ($P < 0.001$), and Day 13 ($P < 0.001$). WR-2721 + glucan values are significantly greater than WR-2721 values on Day 7 ($P < 0.02$), Day 11 ($P < 0.002$), and Day 13 ($P < 0.004$).

CFC numbers in these mice had recovered to normal values (Fig. 8). Mice treated with both WR-2721 and glucan exhibited GM-CFC as early as Day 7 postexposure (<1% normal); by Day 18, splenic GM-CFC in these mice had increased to ~326% normal.

DISCUSSION

In general, defense against radiation exposure depends on physical means such as avoidance and shielding (3). However, for activities such as decontamination of fall-out areas, clean-up of radiation accidents, or polar spaceflight, protection by such physical means may be inadequate and/or impractical. In these instances, drugs which can protect against or enhance recovery from radiation injury would be bene-ficial. In addition, agents that are not toxic and do not induce side effects would be desirable for situations in which continued mental and physical performance could be required.

When administered prior to radiation exposure, the thiol compound WR-2721 is a potent radioprotector that prevents radiation-induced lethality via mechanisms such as free-radical scavenging, hydrogen atom donation, and hypoxia (4, 5). This agent, reported to produce DRFs of 2–3, would be extremely beneficial in emergency situations were it not that WR-2721 doses which effect good protection approach toxicity levels and are behaviorally debilitating (7, 8). Using a low and relatively non-
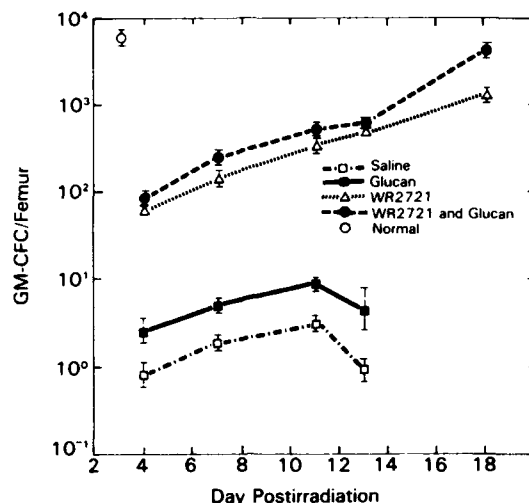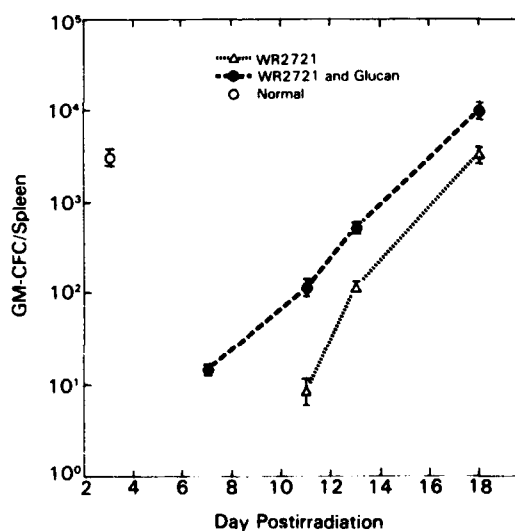
FIG. 7. Effects of WR-2721, glucan, or both agents on bone marrow GM-CFC numbers in irradiated mice. C3H/HeN mice were injected with saline, WR-2721, glucan, or both agents as described for Fig. 1 and exposed to a 9-Gy dose of ^{60}Co radiation on Day 0. Very few saline- and glucan-treated mice survived until Day 18 postexposure. Because of this, sufficient data could not be obtained at this time point for these treatment groups. Glucan values are significantly greater than saline values on Day 7 ($P < 0.04$), Day 11 ($P < 0.02$), and Day 13 ($P < 0.04$). WR-2721 values are significantly greater than saline values on Day 4 ($P < 0.001$), Day 7 ($P < 0.001$), Day 11 ($P < 0.001$), and Day 13 ($P < 0.001$). WR-2721 + glucan values are significantly greater than saline values on Day 4 ($P < 0.001$), Day 7 ($P < 0.001$), Day 11 ($P < 0.001$), and Day 13 ($P < 0.001$). WR-2721 + glucan values are significantly greater than WR-2721 values on Day 7 ($P < 0.04$) and Day 18 ($P < 0.005$).

FIG. 8. Effects of WR-2721, glucan, or both agents on splenic GM-CFC numbers in irradiated mice. C3H/HeN mice were injected with saline, WR-2721, glucan, or both agents as described for Fig. 1 and exposed to a 9-Gy dose of ^{60}Co radiation on Day 0. No GM-CFC were detected in saline- or glucan-treated mice at any time point. WR-2721 + glucan values are significantly greater than WR-2721 values on Day 11 ($P < 0.002$), Day 13 ($P < 0.001$), and Day 18 ($P < 0.009$).

toxic dose of WR-2721, we observed an $LD_{50/30}$ DRF of 1.37 when this agent was administered ~30 min prior to irradiation (Fig. 1). Interestingly, administration of the immunomodulator glucan ~1 h after irradiation also resulted in increased survival. However, glucan's effect was not as dramatic as that of WR-2721 and produced an $LD_{50/30}$ DRF of only 1.08 (Fig. 1). Further, data presented in this study clearly indicate that tolerable doses of WR-2721 and glucan can be used in combination to obtain better survival than with either agent alone. The combination of WR-2721 and glucan resulted in an $LD_{50/30}$ DRF of 1.52.

Glucan's "radioprotective" effect depends in part on its ability to accelerate the regeneration of hemopoietic stem cell populations (13, 22). Thus it was not surprising that, following radiation doses that eradicated all or most hemopoietic stem cells, glucan treatment alone was ineffective at enhancing survival (Figs. 1–3). On the other hand, because of WR-2721's protective chemical mechanisms (4, 5), this agent alone was capable of reducing radiation-induced hemopoietic cell death (Figs. 2, 3, 7). In mice receiving both agents, it appeared that both WR-2721-mediated and glucan-mediated mechanisms contributed to accelerated hemopoietic reconstitution. Both the E-CFU (Figs. 2, 3) and GM-CFC (Figs. 7, 8) data presented here suggest that the accelerated repopulation observed in mice treated with both agents occurred because the population of stem cells upon which glucan could act was larger. In other words, the more stem cells that survived the radiation insult as a consequence of the protective effects of WR-2721, the faster hemopoietic repopulation occurred because more cells were present to respond to glucan's stimulatory effects. This suggestion can also be supported by the fact that if GM-CFC population doubling times are calculated from data presented in Fig. 7, they are 5.93, 3.74, 3.20, and 2.65 days for mice treated with saline, glucan, WR-2721, or both agents, respectively.

These studies have clearly established a potential role for the postirradiation use of immunomodulators in combination with traditional thiol radioprotectors. Specifically, they have demonstrated at least additive radioprotective effects when WR-2721 is used prior to irradiation and glucan is used after irradiation. Such combinations appear to depend on the sequential thiol-mediated cell protection and immunomodulator-mediated hemopoietic stimulation. They also make it possible to reduce WR-2721 dosages while maintaining the ability to obtain relatively good DRFs. The possibility of further enhancing the effectiveness of this combination by the addition of radioprotective agents that act via still different mechanisms is now being explored.

REFERENCES

1   I. R. SWEENEY, A Survey of Compounds from the Antiradiation Drug Development Program of the U.S. Army Medical Research and Development Command Walter Reed Research Institute, Washington, DC, 1979.

2   J. M. YUHAS and J. B. STORER, Chemoprotection against three modes of radiation death in the mouse. Int. J. Radiat. Biol. 15, 233–237 (1969).

3   L. GIAMBARRESI and A. JACOBS, Radioprotectants. In Military Radiobiology (J. J. Conklin and R. I. Walker, Eds.), pp. 265–401. Academic Press, New York, 1987.

4   J. F. WARD, Chemical aspects of DNA radioprotection. In Radioprotectors and Anticarcinogens (O. F. Nygaard and M. G. Simic, Eds.), pp. 73–85. Academic Press, New York, 1983.

5   T. ALPER, Cellular Radiobiology Cambridge Univ. Press, London, 1979.

6   D. E. DAVIDSON, M. M. GRENAN and T. R. SWEENEY, Biological characteristics of some improved radioprotectors. In Radiation Sensitizers (L. W. Brady, Ed.), pp. 309–320. Masson, New York, 1979.

7   J. M. YUHAS, Biological factors affecting the radioprotective efficiency of S-2-[3-aminopropylamino] ethylphosphorothioic acid (WR-2721). LD$_{50,30}$ doses. Radiat. Res. 44, 621–628 (1970).

8   M. R. LANDAUER, H. D. DAVIS, J. A. DOMINITZ, and J. F. WEISS, Dose and time relationship of the radioprotector WR-2721 on locomotor activity in mice. Pharmacol. Biochem. Behav. 27, 573–576 (1987).

9   E. J. AINSWORTH, From endotoxins to newer immunomodulators: Survival promoting effects of microbial polysaccharide complexes in irradiated animals. Pharmacol. Ther., in press.

10 M. L. PATCHEN, Immunomodulators and hemopoiesis. Surv. Immunol. Res. 2, 237–242 (1983).

11 M. L. PATCHEN and T. J. MACVITTIE, Stimulated hemopoiesis and enhanced survival following glucan treatment in sublethally and lethally irradiated mice. Int. J. Immunopharmacol. 7, 923–932 (1985).

12 M. L. PATCHEN and T. J. MACVITTIE, Comparative effects of soluble and particulate glucans on survival in irradiated mice. J. Biol. Response Modif. 5, 45–60 (1986).

13 M. L. PATCHEN, M. M. D'ALESANDRO, I. BROOK, W. F. BLAKELY, and T. J. MACVITTIE, Glucan: Mechanisms involved in its radioprotective effect. J. Leukocyte Biol. 42, 95–105 (1987).

14 J. R. MAISIN, A. KONDI-TAMBA, and G. MATTELIN, Polysaccharides induce radioprotection of murine hemopoietic stem cells and increase the LD$_{50,30}$. Radiat. Res. 105, 276–281 (1986).

15 M. L. PATCHEN and T. J. MACVITTIE, Use of glucan to enhance hemopoietic recovery after exposure to cobalt-60 irradiation. Adv. Exp. Med. Biol. 155, 267–272 (1982).

16 M. L. PATCHEN, T. J. MACVITTIE, and L. M. WATHEN, Effects of pre- and postirradiation glucan treatment on pluripotent stem cells, granulocyte, macrophage, and erythroid progenitor cells, and on hemopoietic stromal cells. Experientia 40, 1240–1244 (1984).

17 N. R. DILUZIO, D. L. WILLIAMS, R. B. MCNAMEE, B. F. EDWARDS, and A. KILAHAMA, Comparative tumor-inhibitory and antibacterial activity of a soluble and particulate glucan. Int. J. Cancer 24, 773–779 (1979).

18 J. SCHULZ, P. R. ALMOND, J. R. CUNNINGHAM, J. G. HOLT, R. LOEVINGER, N. SUNTHARALINGAM, K. A. WRIGHT, R. NATH, and D. LEMPERT, A protocol for the determination of absorbed dose from high energy photon and electron beams. Med. Phys. 10, 741–771 (1983).

19 D. J. FINNEY, Probit Analysis. Cambridge Univ. Press, London, 1971.

20 D. J. FINNEY, Statistical Methods in Biological Assays. Macmillan Co., New York, 1978.

21 J. E. TILL and E. A. MCCULLOCH, Early repair processes in marrow cells irradiated and proliferating in vivo. Radiat. Res. 18, 96–105 (1963).

22 M. L. PATCHEN and T. J. MACVITTIE, Hemopoietic effects of intravenous soluble glucan administration. J. Immunopharmacol. 8, 407–425 (1986).

23 T. R. BRADLEY and D. METCALF, The growth of mouse bone marrow cells in vitro. Aust. J. Exp. Biol. Med. Sci. 44, 287–300 (1966).

24 D. H. PLUZNIK and L. SACHS, The cloning of normal mast cells in tissue culture. J. Cell Physiol. 66, 319–324 (1965).

Attenuation and Cross-Attenuation in Taste Aversion Learning in the Rat: Studies With Ionizing Radiation, Lithium Chloride and Ethanol

BERNARD M. RABIN,*†[1] WALTER A. HUNT* AND JACK LEE*

*Behavioral Sciences Department, Armed Forces Radiobiology Research Institute
Bethesda, MD 20814-5145
and †Department of Psychology, University of Maryland Baltimore County
Baltimore, MD 21228

RABIN, B. M., W. A. HUNT AND J. LEE. *Attenuation and cross-attenuation in taste aversion learning in the rat: Studies with ionizing radiation, lithium chloride and ethanol.* PHARMACOL BIOCHEM BEHAV 31(4) 909–918, 1988.— The preexposure paradigm was utilized to evaluate the similarity of ionizing radiation, lithium chloride and ethanol as unconditioned stimuli for the acquisition of a conditioned taste aversion. Three unpaired preexposures to lithium chloride (3.0 mEq/kg, IP) blocked the acquisition of a taste aversion when a novel sucrose solution was paired with either the injection of the same dose of lithium chloride or exposure to ionizing radiation (100 rad). Similar pretreatment with radiation blocked the acquisition of a radiation-induced aversion, but had no effect on taste aversions produced by lithium chloride (3.0 or 1.5 mEq/kg). Preexposure to ethanol (4 g/kg, PO) disrupted the acquisition of an ethanol-induced taste aversion, but not radiation- or lithium chloride-induced aversions. In contrast, preexposure to either radiation or lithium chloride attenuated an ethanol-induced taste aversion in intact rats, but not in rats with lesions of the area postrema. The results are discussed in terms of relationships between these three unconditioned stimuli and in terms of implications of these results for understanding the nature of the proximal unconditioned stimulus in taste aversion learning.

Conditioned taste aversion   Attenuation   Cross-attenuation   Ionizing radiation   Lithium chloride
Ethanol   Area postrema

A conditioned taste aversion (CTA) is produced when ingestion of a novel tasting solution is paired with a novel unconditioned stimulus (UCS), such that the organism will avoid ingestion of that solution at a subsequent presentation. This avoidance behavior can be produced by pairing a novel saccharin or sucrose solution with a wide variety of stimuli, including treatment with lithium chloride (LiCl), ethanol, or exposure to ionizing radiation (13,33).

Rabin and Hunt (25) have proposed that exposure to ionizing radiation or injection of LiCl causes the release of the same endogenous humoral factor which mediates the acquisition of a CTA following treatment with these stimuli. However, the support for this hypothesis is based, for the most part, on the indirect evidence provided by the observation that lesions of the area postrema (AP) disrupt the acquisition of both LiCl- and radiation-induced taste aversions (19, 24, 27, 30).

A more direct test of this hypothesis may be provided by

pairing different toxins in a UCS preexposure paradigm. In this design, the subject is exposed to a UCS before it is paired with the conditioned stimulus. When this UCS is later paired with ingestion of a novel solution, a CTA does not develop (3, 5, 7). While the mechanisms underlying the UCS preexposure effect vary depending upon the nature of the drug UCS (2, 4, 6, 7, 10), the previous experience with the drug-induced effects disrupts the CTA learning. The attenuation of the CTA may be due to the development of physiological tolerance, as with morphine (8, 9, 34), or to the associative effects of prior experience with the UCS, as with LiCl (2–6, 10). While tolerance produces a broad change in the sensitivity of the central nervous system resulting in a reduced capacity to respond to a variety of stimuli, preexposure that does not cause tolerance has a more limited effect because it is restricted to learned generalization gradients. The more similar the effects of the unconditioned stimuli, the greater the generalization and the greater the preexposure

---

effect. such that the greatest disruption of CTA learning by preexposure would be expected from the use of the same UCS in both the conditioning and test phases of the experiment.

In addition to single-drug effects. the preexposure paradigm can also be utilized to assess the similarity of different unconditioned stimuli [e.g.. (1.22)]. If preexposure to one UCS disrupts the acquisition of a CTA to treatment with a second UCS. the clear implication is that the effects of treatment with the preexposure UCS have generalized to the conditioning UCS. This suggests that the two different stimuli must be similar in some way in order for the experience with one UCS to affect the novelty of the second UCS. Therefore. if taste aversions produced by radiation and LiCl. both of which are dependent upon the integrity of the AP. result from the action of a common endogenous factor. then it should be possible to disrupt the acquisition of a CTA produced by one UCS by preexposure to the other UCS. Conversely. since the acquisition of a CTA following treatment with ethanol does not depend upon the integrity of the AP (16) and may. therefore. involve different mechanisms. preexposure to one UCS should not affect the capcity of the other UCS to produce a CTA. These experiments were designed to evaluate these hypotheses.

GENERAL METHOD

Subjects

The subjects were male Sprague-Dawley-derived rats weighing 300-400 g at the start of the experiment. Rats were maintained in an AAALAC-accredited facility. Animal holding rooms were maintained at 21 ± 1 C with 50 ± 10% relative humidity. The rats were maintained on a 12-hr light:dark cycle. Food and water were continually available. except as required by the experimental protocol.

Procedure

The general procedure was to place the subjects on a 23.5-hr water deprivation schedule during which water was available for 30 min during the early light part of the diurnal cycle. During the preexposure phase. the rats were treated with one UCS or with a control treatment immediately following the drinking period on days 2. 5 and 8. On the conditioning day (day 10). they were presented with two calibrated drinking tubes. one containing tap water and the other containing a 10% sucrose solution. Immediately following the 30-min drinking period. the rats were treated with either the UCS that they received during the preexposure phase. with a second UCS. or with a control treatment. On the test day (day 12). all rats were again given a choice between the tap water and sucrose solution.

Data Analysis

For all experiments. the relative intake of water and sucrose solution was transformed into preference score: sucrose intake divided by total fluid intake. A preference score less than 0.50 indicates a greater intake of water than sucrose and. therefore. an aversion to the normally preferred sucrose solution. For statistical analyses. the arcsin transformation was used to normalize the distribution of preference scores. and initial data analyses were done with mixed analyses of variance. Where necessary. comparisons between relevant groups were made using planned comparisons with the Scheffe test to correct for familywise Type I error (18).
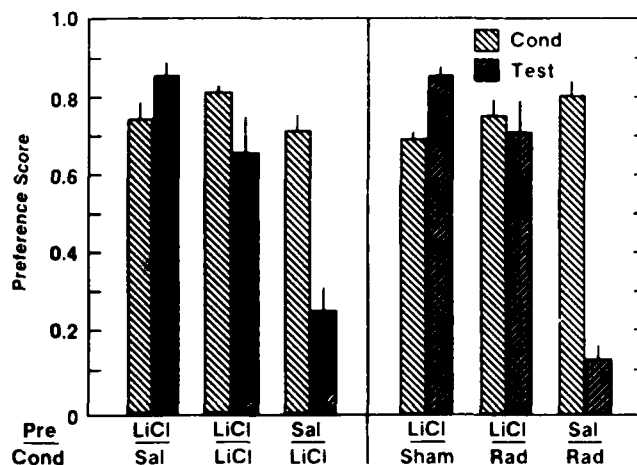

FIG. 1. Effects of pretreatment with lithium chloride (LiCl) or saline (Sal) on LiCl or radiation-induced (Rad) conditioned taste aversions. or sham-irradiated (Sham) rats. Pre: Preexposure UCS; Cond: Conditioning Day UCS. Error bars indicate the standard error of the mean.

EXPERIMENT 1

The first set of experiments was designed to evaluate the hypothesis that a similar factor mediates the acquisition of both radiation- and LiCl-induced taste aversions. but not ethanol-induced aversions. by determining whether or not preexposure to one UCS would disrupt the acquisition of a CTA following treatment with the other UCS.

Method

The subjects were 252 male rats divided into 24 groups of 9–13 rats each. Each UCS served as both preexposure and conditioning day treatment.

For irradiation. the rats were placed in ventilated plastic restraining boxes and carried to a ⁶⁰Co source. The radiation UCS for both preexposure and conditioning consisted of 100 rad at a dose rate of 40 rad/min. Dosimetry was accomplished using thermoluminescent detectors (LiF TLD 100s) and a 3.3-ml Victoreen chamber. The sham-irradiated rats were placed in plastic boxes and carried to the source. but not exposed. Two doses of LiCl were used. For the preexposure phase. all rats were given 3.0 mEq/kg. IP. On the conditioning day. rats were given either 3.0 or 1.5 mEq/kg. IP. The control animals were given equivalent volume injections of isotonic saline. Ethanol (4 g/kg) was administered intragastrically with an infant feeding tube in both preexposure and conditioning phases of the experiment. Control rats were intubated with an equivalent volume of water.

Results

Repeated treatment with radiation or LiCl produced no major effects on either conditioning day water or sucrose intake in comparison to the control treatments. Preexposure to LiCl disrupted the acquisition of a CTA to both LiCl and ionizing radiation (Fig. 1). For the LiCl-induced aversion. the analysis with planned comparisons showed that there were no differences in sucrose preference between the group preexposed to LiCl and given saline on the conditioning day
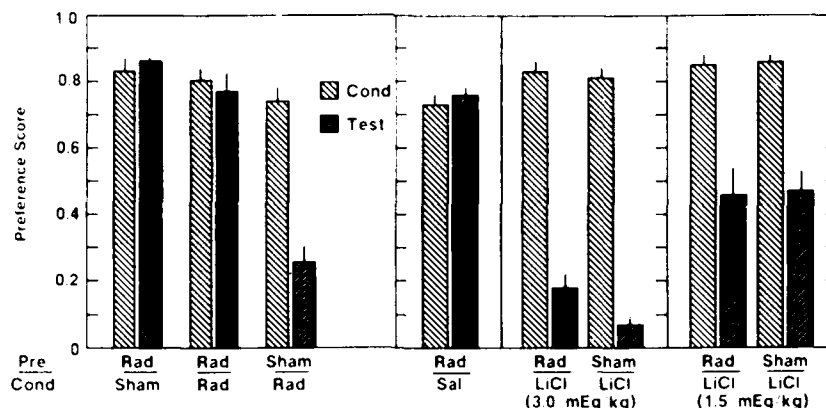
FIG. 2. Effects of preexposure to radiation on the acquisition of radiation- and LiCl-induced taste aversions. LiCl-induced aversions were produced by injection of either 3.0 mEq/kg or 1.5 mEq/kg, as indicated. Abbreviations as in Fig. 1.
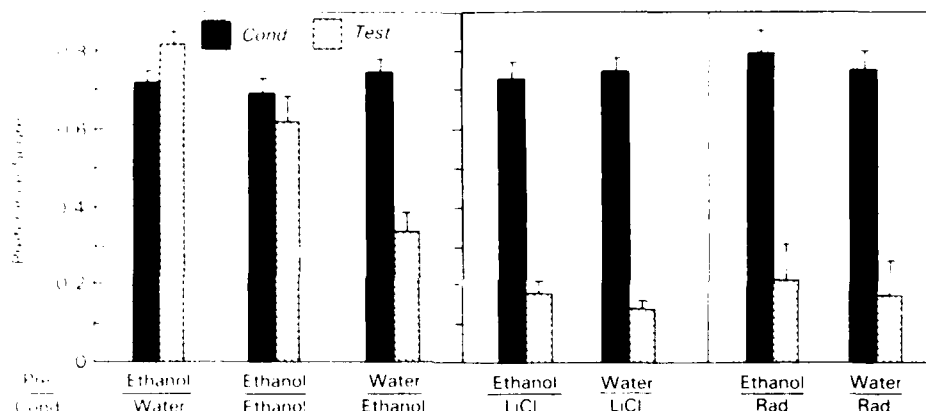

FIG. 3. Effect of preexposure to ethanol (4 g/kg, PO) on the acquisition of a CTA produced by intubation of ethanol or by injection of LiCl (3.0 mEq/kg) or exposure to ionizing radiation (100 R). Abbreviations as in Fig. 1.

and the group preexposed to LiCl and given LiCl on the conditioning day, $F(1,27) = 7.45$, $p < 0.05$. Both LiCl preexposure groups differed significantly from the group given saline during the preexposure phase and LiCl on the conditioning day, $F(1,27) = 42.31$, $p < 0.01$.

For the radiation-induced CTA following preexposure to LiCl, the planned comparisons indicated that the sucrose preference of the two groups given LiCl during the preexposure phase did not differ significantly from each other, $F(1,27) = 4.33$, $p < 0.05$. Both of these groups differed significantly from the group given saline injections during the preexposure phase and exposed to radiation on the conditioning day, $F(1,27) = 150.06$, $p < 0.001$.

As shown in the first panel of Fig. 2, preexposure to ionizing radiation prevented the acquisition of a radiation-induced CTA. Planned comparisons showed that the two radiation preexposure groups did not differ significantly from each other, $F(1,30) = 1.25$, $p < 0.05$, in test day sucrose preference even though one group was exposed to radiation on the conditioning day while the other group was given a sham exposure. Both of these groups did differ from the group that was

subjected to sham irradiation procedures during the preexposure phase of the experiment and irradiated on the conditioning day, $F(1,30) = 11.64$, $p < 0.01$.

In contrast, preexposure to radiation had no effect on a CTA produced by treatment with either 3.0 or 1.5 mEq/kg LiCl (Fig. 2). Analysis of the data using a three-way analysis of variance with one repeated factor showed that the main effects for the dose, $F(1,40) = 34.14$, $p < 0.001$, and for day, $F(1,40) = 280.99$, $p < 0.001$, were significant. However, the observation that neither the main effect for treatment between the radiation- and sham-preexposed groups, $F(1,40) = 1.14$, $p < 0.05$, nor the dose by treatment, $F(1,40) = 1.80$, $p < 0.05$, nor day by treatment, $F(1,40) = 0.69$, $p < 0.05$, interactions were significant would indicate that there were no differences in sucrose preferences between the radiation- and sham-preexposed groups at either dose level.

Preexposing the organism to ethanol (4 g/kg, PO) blocks the acquisition of a CTA following intubation with the same dose of ethanol (Fig. 3). The analysis with planned comparisons showed that the group preexposed to ethanol and given ethanol on the conditioning day did not show a significant

test day decrease in sucrose preference. F(1,24)=0.03, p -0.10. In contrast, the controls given water intubation during the preexposure phase did show a significant decrease in sucrose prefe..nce on the test day. F(1,24)=26.04, p<0.01.

Preexposing rats to ethanol had no effect on the acquisition of either a LiCl- or radiation-induced CTA (Fig. 3). For the LiCl-induced CTA, the analysis of variance showed that the main effect for treatment for the comparison between the ethanol- or water-treated rats was not significant. F(1,20) 0.20, p -0.10, while the main effect for the comparison between conditioning and test day was highly significant. F(1,20) 306.74, p 0.001. The treatment by day interaction was not significant. F(1,22)=0.58, p -0.10, indicating that the rats developed an LiCl-induced aversion to the sucrose regardless of whether they received ethanol or water during the preexposure phase of the experiment.

Similar results were obtained with the analysis of the radiation-induced CTA. Neither the main effect for treatment. F(1,16) 0.28, p -0.10, nor the treatment by day interaction. F(1,16) 0.005, p 1.00, was significant. The main effect for day was significant. F(1,16) 57.79, p -0.001, indicating that preexposure to ethanol does not attenuate the development of a CTA when the rats are subsequently exposed to radiation on the conditioning day.

In contrast, pretreatment with LiCl blocks the acquisition of an ethanol-induced CTA (Fig. 4). The analysis using planned comparisons showed that there were no significant differences between the animals pretreated with LiCl and given ethanol on the conditioning day and those given water on the conditioning day. F(1,28) 2.02, p -0.05. However, the test day sucrose preference of these groups of animals did differ significantly from the preference of the animals pretreated with saline and given ethanol on the conditioning day. F(1,28)-32.30, p< 0.01.

Discussion

These results only partially support the original hypothesis that radiation and LiCl utilize a common humoral factor to produce CTA learning. The observation of asymmetrical preexposure effects between LiCl and radiation suggests that these two stimuli do have some effects in common. However, the failure of radiation preexposure to attenuate a LiCl-induced CTA would indicate that preexposure to ionizing radiation did not produce effects sufficiently similar to those produced by LiCl to attenuate a CTA in response to treatment with LiCl on the conditioning day. This failure to attenuate an LiCl-induced CTA cannot be due to a general inability of the radiation UCS to produce a preexposure effect because preexposure did attenuate a radiation-induced CTA. Also, because attenuation of the LiCl-induced CTA was seen with neither the high nor the low dose of LiCl, it would not seem likely that the failure to observe a cross-attenuation between the radiation preexposure and LiCl could be due to inappropriate doses of either UCS.

The results with ethanol agree with previous research showing that preexposure to ethanol will block the acquisition of an ethanol-induced CTA (6). They are also consistent with the hypothesis that different mechanisms are involved
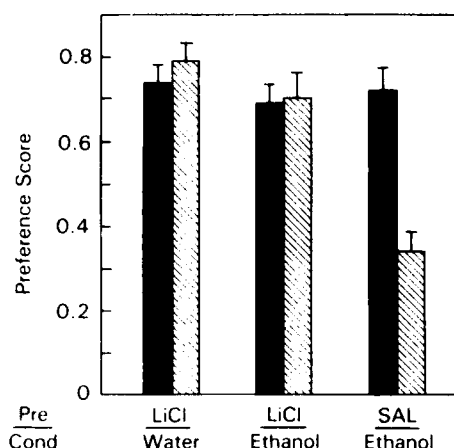

FIG. 4. Effects of preexposure to LiCl (3.0 mEq/kg) on the acquisition of ethanol-induced CTA. Abbreviations as in Fig. 1. Black bars: Cond; hatched bars: Test.

in CTA learning with these different stimuli, so that exposure to radiation or LiCl on the conditioning day may be perceived as a novel UCS resulting in the acquisition of a CTA, despite the prior exposure to ethanol. Because there is the possibility that the failure of ethanol preexposure to attenuate a LiCl-induced CTA is dose-dependent, some additional animals were run using 1.5 mEq LiCl as the conditioning day UCS. At this dose, there was also no effect of ethanol preexposure on the LiCl-induced aversion.

These results apparently differ from those of Cannon et al. (6) who reported that preexposure to ethanol could block a LiCl-induced CTA. However, they did not verify that their procedure of 4 consecutive daily intubations of 5 g/kg ethanol did not produce tolerance to ethanol. In contrast to the present procedures which have been shown not to produce tolerance, their procedure is very similar to a procedure which has been shown to produce ethanol tolerance as measured by sleep times (15). Ethanol tolerance, unlike simple preexposure to ethanol, does produce an attenuation of both radiation- and LiCl-induced taste aversions [(15); Rabin and Hunt, unpublished observations].

In contrast to the effects of ethanol preexposure on a LiCl-induced CTA, the observation that preexposing rats to LiCl will block the acquisition of an ethanol-induced CTA is in agreement with the results reported by Cannon et al. (6), and therefore not consistent with the present hypothesis. This asymmetrical cross-attenuation between LiCl preexposure and ethanol-induced CTA learning may derive from the fact that LiCl, which crosses the blood-brain barrier (21), does have central effects similar enough to those produced by ethanol to result in the attenuation of the ethanol-induced CTA following pretreatment with LiCl.

EXPERIMENT 2

Although lesions of the AP will disrupt the acquisition of a LiCl-induced CTA (27,30), if it is the central actions of LiCl that are responsible for the attenuation of an ethanol-induced CTA by preexposure to LiCl, then destruction of the AP should have no effects on the cross-attenuation of the ethanol-induced CTA because LiCl should still be expected to cross the blood-brain barrier even in the absence of the AP. The present experiment was designed to evaluate the role of the AP in the LiCl-induced attenuation of an ethanol-induced CTA by preexposing rats with AP lesions to LiCl.

Method

The subjects were 21 rats with lesions of the AP. The behavioral methods were identical to those detailed above, except that only two conditions were run: LiCl and saline pretreatment groups. Both groups received ethanol on the conditioning day.

The surgical procedures have been detailed in previous reports (27–29). Briefly, all rats were anesthetized with sodium pentobarbital (35 mg/kg, IP). The AP was exposed and thermal lesions were made using a cautery probe under direct visual control. After surgery, the rats were given an injection of bicillin (60,000 units) and allowed to recover in their home cages for a period of 2–4 weeks before beginning behavioral testing.

At the conclusion of the testing, all rats were anesthetized with sodium pentobarbital (50 mg) and perfused intracardially with isotonic saline followed by 10% formalin saline. Sections were cut through the brainstem at the level of the AP at 50 μm and stained with thionin. Representative sections from an intact rat and one with AP lesions are presented in Fig. 5. Examination of the histological material indicated that for the most part the lesions were restricted to the AP, although they did occasionally affect the dorsal parts of the nucleus of the solitary tract.

Results

Pretreating rats with AP lesions with LiCl did not affect conditioning day fluid intake relative to rats that were given saline injections. In rats with AP lesions, preexposure to LiCl does not attenuate the acquisition of an ethanol-induced CTA (Fig. 6). The analysis of variance showed that neither the main effect for treatment, $F(1,19) = 0.01$, $p > 0.10$, nor the treatment by day interaction, $F(1,19) = 0.02$, $p > 0.10$, was significant. The main effect for day, however, $F(1,19) = 38.41$, $p < 0.001$, was significant, indicating that both the LiCl- and saline-preexposed rats showed identical aversions following conditioning day intubation with ethanol regardless of the nature of the preexposure treatment.

Discussion

These results do not support the hypothesis that the cross-attenuation of an ethanol-induced CTA by preexposure to LiCl in intact rats is due to the central actions of LiCl. Rather, the failure to observe a cross-attenuation in rats with lesions of the AP suggests that the AP is somehow involved in this effect. Because AP lesions do not disrupt the acquisition of an ethanol-induced CTA (16), the nature of the AP involvement in the cross-attenuation of an ethanol-induced CTA by LiCl is not certain. It may be that the effects of treatment with specific toxins on AP neurons is a sufficient condition for the cross-attenuation of a CTA produced by a
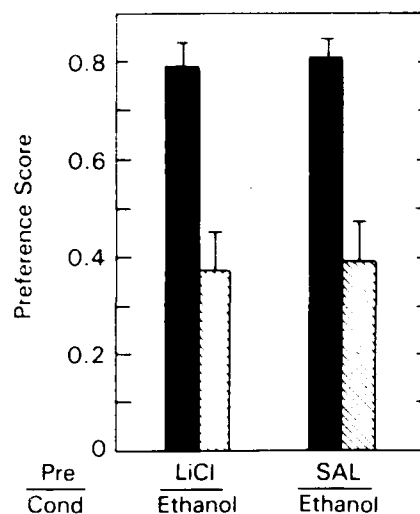

FIG. 6. Effects of preexposure to LiCl on the acquisition of an ethanol-induced CTA in rats with lesions of the area postrema. Abbreviations as in Fig. 1. Black bars: Cond; hatched bars: Test.

UCS that does not require the mediation of the AP for the original learning.

EXPERIMENT 3

If, as suggested above, the action of specific toxins on AP neurons is sufficient for the attenuation of an ethanol-induced CTA by LiCl, then preexposure to radiation, which also involves the AP, should result in a similar attenuation of an ethanol-induced CTA in intact rats, but not in rats with lesions of the AP. The present experiment was designed to evaluate this hypothesis.

Method

The first phase of the experiment utilized 18 intact rats divided into two groups of 9 rats each. The second phase of the experiment utilized 19 rats, all of which had histologically verified lesions of the AP and which were divided into two groups of 10 and 9 rats. The surgical and histological procedures were identical to those detailed above. In each phase, the first group of rats was given three preexposures to ionizing radiation (100 rad) while the second group was given sham exposures. On the conditioning day, all rats were treated with ethanol (4 g/kg, PO) immediately following sucrose ingestion.

Results

For the intact rats, preexposure to ionizing radiation resulted in the attenuation of an ethanol-induced CTA compared to the sham preexposed rats (Fig. 7). The analysis of variance indicated that the main effect for day, $F(1,16) = 13.16$, $p < 0.01$, and the preexposure by day interaction, $F(1,16) = 11.62$, $p < 0.01$, were both significant. Although the main effect for preexposure condition did not achieve significance, $F(1,16) = 1.39$, $p > 0.10$, the significant interaction would indicate that the test day sucrose preference of the rats preexposed to radiation was different than the preference of the groups given the sham preexposures.
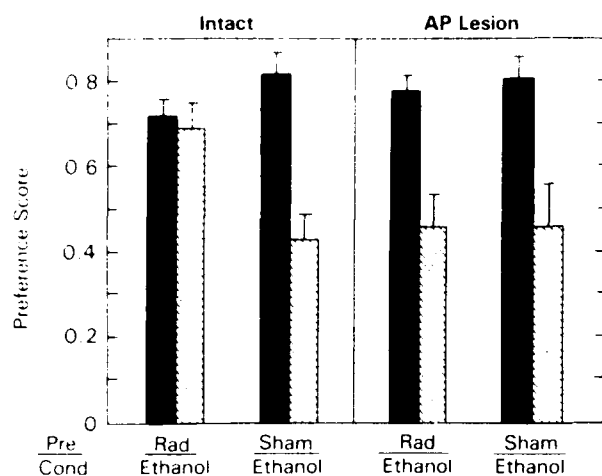
Intact   AP Lesion

FIG. 7. Effects of preexposure to ionizing radiation on the acquisition of an ethanol-induced CTA in intact rats and in rats with lesions of the area postrema. Abbreviations as in Fig. 1. Black bars: Cond; hatched bars: Test.

In contrast, preexposing rats with lesions of the AP to radiation had no effect on an ethanol-induced CTA (Fig. 7). The analysis of variance showed that neither the main effect for preexposure, $F(1,17)$ 0.17, p 0.10, nor the preexposure by day interaction, $F(1,17)$ 0.10, p 0.10, were significant. Only the main effect for day, $F(1,17) = 24.80$, p 0.001, was significant, indicating that equivalent reductions in test day sucrose preference were observed in both the radiation- and sham-preexposed rats with lesions of the AP.

Discussion

The observation that preexposure to ionizing radiation disrupts the acquisition of an ethanol-induced aversion in intact rats, but not in rats with lesions of the AP, is concordant with the hypothesis that activation of the AP by a UCS may be a sufficient condition for the UCS preexposure effect even though the conditioning day UCS itself does not require the mediation of the AP for CTA learning to occur.

GENERAL DISCUSSION

The initial experiments were designed to test two hypotheses about the nature of the proximal UCS in taste aversion learning and the relationships between ionizing radiation, LiCl and ethanol as unconditioned stimuli for CTA learning. First, that because radiation and LiCl may utilize a common mediator, preexposure to one UCS should block the acquisition of a CTA following treatment with the other UCS. Second, that ethanol, which does not require the mediation of the AP, may involve different mechanisms for CTA learning and, therefore, that preexposure to one UCS would not disrupt the acquisition of a CTA following treatment with another UCS. The results of the experiments, which show asymmetrical preexposure effects between radiation and LiCl and between ethanol and both radiation and LiCl, provide only partial support for these hypotheses.

The results of the first series of experiments, which showed that preexposure to LiCl blocks the acquisition of

a radiation-induced CTA, would be consistent with the hypothesis that the stimulus effects produced by treatment with LiCl encompass those produced by exposure to radiation. The attenuation of a LiCl-induced CTA by preexposure to LiCl seems to be primarily an associative phenomenon because changing the environmental conditions between the two phases of the experiment disrupts the UCS preexposure effect (4,10). As such, the cross-attenuation between LiCl and radiation would seem to require generalization from the effects of the pretreatment UCS to those of the conditioning UCS. The greater the perceived similarity of the UCS effects by the organism across the two phases of the experiment, the greater the degree of cross-attenuation. Because the degree of LiCl attenuation of a radiation-induced CTA was nearly identical to the degree of LiCl attenuation of a LiCl-induced CTA, the stimulus effects of treatment with LiCl must be very similar to those of treatment with ionizing radiation. Otherwise, such strong stimulus generalization would not occur and, consequently, cross-attenuation would not occur.

Conversely, the failure to observe cross-attenuation of a LiCl-induced CTA by preexposure to radiation would suggest that the stimulus effects which result from exposing an organism to ionizing radiation are not similar enough to those produced by LiCl for generalization and cross-attenuation to occur. It may be that treating an organism with LiCl, which crosses the blood-brain barrier (21), produces a series of changes in neural functioning which are not produced by exposure to ionizing radiation at the dose levels used in the present experiment (28). Thus, for example, injection of LiCl has been reported to produce changes in neurohypophyseal functioning (23), in phospholipid metabolism (17), and in dopamine and serotonin receptor activity in the brain (20,35). Although these changes in neural functioning following treatment with LiCl do not constitute a sufficient condition for CTA learning (32), they form a part of the stimulus configuration when peripheral LiCl is used as a UCS for CTA learning. The failure of radiation to reproduce the complete constellation of stimulus events associated with LiCl treatment would mean that there is a weaker generalization gradient when radiation is used as the preexposure UCS and, consequently, preexposure to radiation does not produce cross-attenuation of a LiCl-induced CTA because LiCl is perceived as a novel discriminative UCS on the conditioning day.

Similar factors may be involved in the asymmetrical relationship between ethanol and radiation and LiCl. Preexposure to ethanol does not produce cross-attenuation of a radiation- or LiCl-induced CTA because ethanol, as a UCS for taste aversion learning, does not require the mediation of the AP (16). As a result, the pattern of neural activity produced by pretreatment with ethanol may not be similar enough to that produced by LiCl or radiation, particularly since it might not result in similar effects on the AP. Conversely, it is possible that anatomical connections of the AP are sufficiently broad that the stimulus pattern resulting from stimulation of the AP by pretreatment with a radiation or LiCl UCS will encompass the stimulus pattern produced by treatment with ethanol leading to the generalization from one UCS to the others and, therefore, to the cross-attenuation of an ethanol-induced CTA by preexposure to LiCl or radiation.

Similarly, an intact AP is necessary for preexposure to LiCl or radiation to produce an attenuation of an ethanol-induced CTA because the AP is necessary for CTA learning when either of these stimuli is used as the UCS (19, 24, 27, 30). It is only when the AP is intact that a pattern of neural
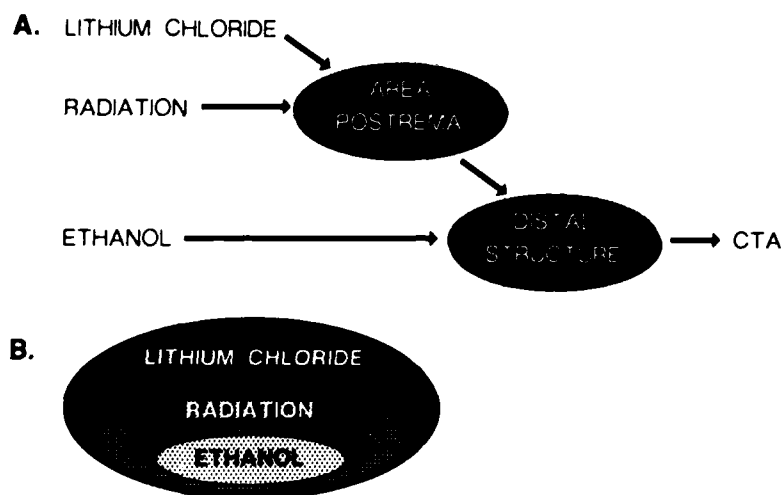
FIG. 8. (A) Diagrammatic representation of the neural pathways associated with the response of the organism to the UCS leading to the acquisition of a CTA following exposure to ionizing radiation or treatment with LiCl or ethanol. (B) Schematic illustration of the range of the stimulus configuration produced by exposure to ionizing radiation or by treatment with LiCl or ethanol. Each labelled oval represents the stimulus complex associated with the UCS. Preexposure to a UCS having a greater range of effects will disrupt the acquisition of a CTA produced by a UCS having a smaller range of stimulus effects. See text for details.

activity relevant to CTA learning with these stimuli can be initiated. In the absence of the AP, this pattern of neural activity is not produced by preexposure and, therefore, there is no generalization related to CTA learning from the preexposure stimuli to the conditioning day UCS. As a result, preexposure to radiation or LiCl cannot lead to the cross-attenuation of an ethanol-induced CTA in rats with lesions of the AP.

The proposed role of the AP in the UCS preexposure effect between radiation, LiCl and ethanol is shown schematically in Fig. 8A. Treatment with either ionizing radiation or LiCl produces changes in the activity of the AP which, in turn, affects the activity of some distal orain structure leading to the acquisition of a CTA (29). Although presently available data do not allow the specification of this intermediate structure, anatomical studies have shown that the AP sends projections to both the nucleus of the solitary tract and the parabrachial nuclei (31,36). Ethanol, which does not require the mediation of the AP for CTA learning, may affect this distal structure directly. Preexposure to LiCl or radiation produces an attenuation of an ethanol-induced CTA only when the AP is intact because treatment with these stimuli can affect the activity of this distal structure only through the mediation of the AP. In contrast, ethanol, which may affect this distal structure directly, cannot produce an attenuation of a radiation- or LiCl-induced CTA because the ethanol pretreatment does not affect the activity of the AP.

With regard to the determination of the proximal UCS in CTA learning, a number of different effects of treatment have been proposed. Because most stimuli that will lead to CTA learning also make the organism sick, Garcia (13) has proposed that the experience of a UCS-induced gastrointestinal illness is the proximal UCS for the acquisition of a CTA. In contrast, Gamzu (11,12) and Hunt and Amit (14), noting that a CTA will develop with nontoxic stimuli such as

amphetamine that do not produce overt signs of illness, have suggested that any stimulus that produces a novel pattern of neural activity will also produce a CTA. Rabin and Rabin (26) obtained a CTA in anesthetized rats treated with LiCl or exposed to ionizing radiation. Since these rats could not have experienced a UCS-induced illness under the anesthesia, they suggested that any stimulus that excited the neural pathways associated with illness would lead to the acquisition of a CTA, independently of any possible experiential factor.

The present observation of an asymmetrical UCS preexposure effect between LiCl and ionizing radiation would be most consistent with the hypothesis that the proximal UCS for CTA learning involves activation of the neural pathways associated with illness (26). If an experienced gastrointestinal illness itself were the proximal UCS, then preexposure to the radiation-induced "illness" should have attenuated the CTA response to the LiCl-induced "illness" just as preexposure to the LiCl-induced "illness" attenuated the CTA response to the radiation-induced "illness." While it is possible that the cross-attenuation between radiation preexposure and LiCl might be dose-dependent, then cross-attenuation between radiation and LiCl should have been obtained when the conditioning day dose of LiCl was reduced if dose were a significant factor. The failure to observe such an effect (Fig. 2) does not support this possibility.

Rather, as discussed above and illustrated in Fig. 8B, the observation of asymmetrical preexposure effects would seem to derive from the total pattern of neural activity resulting from treatment with a specific UCS. Where the pattern of neural activity produced by the preexposure UCS fully encompasses the pattern of such activity produced by the conditioning day UCS, either because the same stimuli are used in both phases of the experiment or because the preexposure UCS produces all the neural stimulus effects of the condi-

tioning day UCS, then attenuation of the CTA will result. Since both LiCl and irradiation produce a CTA using an AP-dependent peripheral mediator, preexposure to LiCl attenuates a radiation-induced CTA. However, because LiCl apparently has effects in addition to those produced by the low dose of radiation, preexposure to radiation does not attenuate a LiCl-induced aversion. Similarly, preexposure to ethanol does not attenuate either a radiation- or LiCl-induced CTA because the ethanol-induced CTA, unlike one produced by radiation or LiCl, is independent of the AP and may not, therefore, produce an appropriate pattern of neural activity which involves the AP. Conversely, both LiCl and radiation may attenuate an ethanol-induced CTA, in rats with an intact AP, because the pattern of neural activity induced by these stimuli completely mimics the pattern of neural activity produced by intubation of ethanol.

In summary, preexposure to ionizing radiation or LiCl attenuates the CTA produced by conditioning day treatment with the same UCS and an asymmetrical cross-attenuation following treatment with the other UCS; such that LiCl attenuates a radiation-induced CTA, but radiation does not attenuate a LiCl-induced aversion. Because the UCS preexposure paradigm, in contrast to a tolerance paradigm, is based upon a generalization gradient from the preexposure UCS to the conditioning UCS, these results are consistent with the hypothesis that, as stimuli for CTA learning, both

radiation and LiCl have common components, although they are not identical stimuli. Both LiCl and ionizing radiation attenuate an ethanol-induced CTA in intact rats, but not in rats with lesions of the AP. In contrast, preexposure to ethanol, which does not require the integrity of the AP for CTA learning, does not attenuate either radiation- or LiCl-induced taste aversions. These observations are consistent with the hypothesis that the critical stimulus for the acquisition of a CTA is the generation of a particular pattern of activity, perhaps related to the neural circuits associated with illness, in the central nervous system.

REFERENCES

1. Aragon, C. M. G.; Abibtol, M.; Amit, Z. Acetaldehyde may mediate reinforcement and aversion by ethanol. An examination using a conditioned taste-aversion paradigm. Neuropharmacology 25:79–83; 1986.
2. Batson, J. D.; Best, P. J. Drug preexposure effects in flavor-aversion learning: Associative interference by conditioned environmental stimuli. J. Exp. Psychol. [Anim. Behav. Proc.] 5:273–283; 1979.
3. Braveman, N. S. Formation of taste aversions in rats following prior exposure to sickness. Learn. Motiv. 6:512–534; 1975.
4. Braveman, N. S. The role of blocking and compensatory conditioning in the treatment preexposure effect. Psychopharmacology (Berlin) 61:177–189; 1979.
5. Cain, N. W.; Baenninger, R. Habituation to illness: Effects of prior experience with US on the formation of learned taste aversions in rats. Anim. Learn Behav. 5:359–364; 1977.
6. Cannon, D. S.; Baker, T. B.; Berman, R. F. Taste aversion disruption by drug pretreatment: Dissociative and drug-specific effects. Pharmacol. Biochem. Behav. 6:93–100; 1977.
7. Cannon, D. S.; Berman, R. F.; Baker, T. B.; Atkinson, C. A. Effect of preconditioning unconditioned stimulus experience to learned taste aversions. J. Exp. Psychol. [Anim. Behav. Proc.] 104:270–284; 1975.
8. Cappell, H.; Le Blanc, A. E. Parametric investigations of the effects of prior exposure to amphetamine and morphine on conditioned gustatory aversion. Psychopharmacology (Berlin) 51:265–271; 1977.
9. Cappell, H.; Poulos, C. X. Associative factors in drug pretreatment effects on gustatory conditioning: Cross-drug effects. Psychopharmacology (Berlin) 64:209–213; 1979.
10. Dacanay, R. J.; Riley, A. T. The UCS preexposure effect in taste aversion learning: Tolerance and blocking are drug specific. Anim. Learn. Behav. 10:91–96; 1982.
11. Gamzu, E. The multifaceted nature of taste-aversion-inducing agents: Is there a single common factor? In: Barker, L. M.; Best, M. R.; Domjam, M., eds. Learning mechanisms in food selection. Waco, TX: Baylor University Press; 1977:477–509.

12. Gamzu, E.; Vincent, G.; Boff, E. A pharmacological perspective of drugs used in establishing conditioned food aversions. Ann. NY Acad. Sci. 443:231–249; 1985.
13. Garcia, J.; Lasiter, P. A.; Bermudez-Ratoni, F.; Deems, D. A. A general theory of aversion learning. Ann. NY Acad. Sci. 443:8–21; 1985.
14. Hunt, T.; Amit, Z. Conditioned taste aversions induced by self-administered drugs: Paradox revisited. Neurosci. Biobehav. Rev. 11:107–130; 1987.
15. Hunt, W. A.; Rabin, B. M. Attenuation of a radiation-induced conditioned taste aversion after the development of ethanol tolerance. Life Sci. 43:59–66; 1988.
16. Hunt, W. A.; Rabin, B. M.; Lee, J. Ethanol-induced taste aversions: Lack of involvement of acetaldehyde and the area postrema. Alcohol 4:169–173; 1987.
17. Joseph, N. E.; Renshaw, P. F.; Leigh, J. S., Jr. Systemic lithium administration alters rat cerebral cortex phospholipids. Biol. Psychiatry 22:540–544; 1987.
18. Keppel, G. Design and analysis: A researcher's handbook. Englewood Cliffs, NJ: Prentice-Hall; 1973.
19. Ladowski, R. L.; Ossenkopp, K.-P. Conditioned taste aversions and changes in motor activity in lithium treated rats: Mediating role of the area postrema. Neuropharmacology 25:71–77; 1986.
20. McIntyre, I. M.; Kuhn, C.; Demitriou, S.; Flick, F. R.; Stanley, M. Modulating role of lithium on dopamine turnover, prolactin release, and behavioral supersensitivity following haloperidol and reserpine. Psychopharmacology (Berlin) 81:150–154; 1983.
21. Nelson, S. C.; Herman, M. M.; Bensch, K. G.; Barchas, J. D. Localization and quantitation of lithium in rat tissue following intraperitoneal injections of lithium chloride. II. Brain. J. Pharmacol. Exp. Ther. 212:11–15; 1980.
22. Ng Cheong Ton, J. M.; Amit, Z. Symmetrical effect of preexposure between alcohol and morphine on conditioned taste aversion. Life Sci. 33:665–670; 1983.

23. O'Connor, E. F.; Cheng, S. W. T.; North, W. T. Effects of intraperitoneal injection of lithium chloride on neurohypophyseal activity: Implications for behavioral studies. Physiol. Behav. 40:91–95; 1987.

24. Ossenkopp, K.-P. Taste aversions conditioned with gamma radiation: Attenuation by area postrema lesions in rats. Behav. Brain Res. 7:295–305; 1983.

25. Rabin, B. M.; Hunt, W. A. Mechanisms of radiation-induced conditioned taste aversion learning. Neurosci. Biobehav. Rev. 10:55–65; 1986.

26. Rabin, B. M.; Rabin, J. S. Acquisition of radiation- and lithium chloride-induced conditioned taste aversions in anesthetized rats. Anim. Learn. Behav. 12:439–441; 1984.

27. Rabin, B. M.; Hunt, W. A.; Lee, J. Acquisition of radiation and drug-induced conditioned taste aversions following area postrema lesions in the rat. Radiat. Res. 93:388–394; 1983.

28. Rabin, B. M.; Hunt, W. A.; Lee, J. Effects of dose and of partial body ionizing radiation on taste aversion learning in rats with lesions of the area postrema. Physiol. Behav. 32:119–122; 1984.

29. Rabin, B. M.; Hunt, W. A.; Lee, J. Recall of a previously acquired conditioned taste aversion in rats following lesions of the area postrema. Physiol. Behav. 32:503–506; 1984.

30. Ritter, S.; McGlone, J. L.; Kelly, K. W. Absence of lithium-induced taste aversion after area postrema lesions. Brain Res. 201:501–506; 1980.

31. Shapiro, R. E.; Miselis, R. R. The central neural connections of the area postrema of the rat. J. Comp. Neurol. 234:344–364; 1985.

32. Smith, D. F. Central and peripheral effects of lithium on conditioned taste aversions in rats. Psychopharmacology (Berlin) 68:315–317; 1980.

33. Smith, J. C. Radiation: Its detection and its effects on taste preferences. In: Stellar, E.; Sprague, J. M., eds. Progress in physiological psychology. vol. 4. New York: Academic Press; 1971:53–117.

34. Stewart, J.; Eikelboom, R. Pre-exposure to morphine and the attenuation of conditioned taste aversion in rats. Pharmacol. Biochem. Behav. 9:639–645; 1978.

35. Tanimoto, K.; Maeda, K.; Terada, T. Inhibitory effect of lithium on neuroleptic and serotonin receptors in rat brain. Brain Res. 265:148–151; 1983.

36. van der Kooy, D.; Koda, L. Y. Organization of the projections of a circumventricular organ: The area postrema in the rat. J. Comp. Neurol. 219:328–338; 1983.

A Low-Energy x-Ray Irradiator for Electrophysiological Studies

D. A. SCHAUER,* G. H. ZEMAN and T. C. PELLMAR

Armed Forces Radiobiology Research Institute, Bethesda, MD 20814 5145, U.S.A.

A 50 kVp molybdenum target filter x-ray tube has been installed inside a lead-shielded Faraday cage. High-dose rates of up to 1.54 Gy min⁻¹ (17.4 keV weighted average photons) have been used to conduct local *in vitro* irradiations of the hippocampal region of guinea pig brains. Electrophysiological recordings of subtle changes in neuronal activity indicate this system is suitable for this application.

Introduction

High dose rate acute whole-body exposures have been the main focus of radiobiology research conducted at the Armed Forces Radiobiology Research Institute (AFRRI) for many years. Extensive quantitative studies have been conducted analyzing behavioral effects, radiation induced syndromes and combined injury phenomena. The sources of radiation used in these studies are the AFRRI TRIGA Pulsed Reactor, cobalt-60 whole-body facility and the 50 MeV LINAC.

Selective irradiation of specific organs has become an area of investigation with emphasis on mechanistic effects. Specifically, cellular and tissue studies have been initiated using the above mentioned sources. For example, Tolliver and Pellmar (Tolliver and Pellmar, 1987) initiated a study to evaluate radiation damage to brain neurophysiology. Slices from the hippocampal region of guinea pig brains were remotely irradiated *in vitro*, and subsequently examined for neuronal damage by means of electrophysiological recording of neuronal activity. The remoteness of the irradiation source in relation to the recording chamber presented some inherent limitations with this type of analysis:

—The analysis of a large number of samples was required and only large changes could be observed, as electrophysiological responses varied greatly even within the same animal.

—It was not possible to observe early transient neuronal effects, because data collection could only begin approximately 30 min post-irradiation.

In spite of the above limitations Tolliver and Pellmar (1987) documented statistically significant impairment in the function of the neural tissue at doses as low as 50 Gy at a dose rate of 20 Gy min⁻¹. While this was a significant advance showing direct damage to neural tissue, it was desirable to study the effects of lower doses of radiation at earlier time points. To accomplish this it was necessary to increase the sensitivity of the experimental system by actually conducting tissue irradiations within the electrophysiology recording chamber. If this were possible, then each brain slice preparation could act as its own control as the stimulating/recording electrodes remained in place before, during and after the irradiation. This would eliminate the limitations listed above and allow more subtle neuronal changes to be examined and quantified. To this end, a small x-ray unit was set-up for operation in a Faraday cage enclosing the electrophysiology recording apparatus.
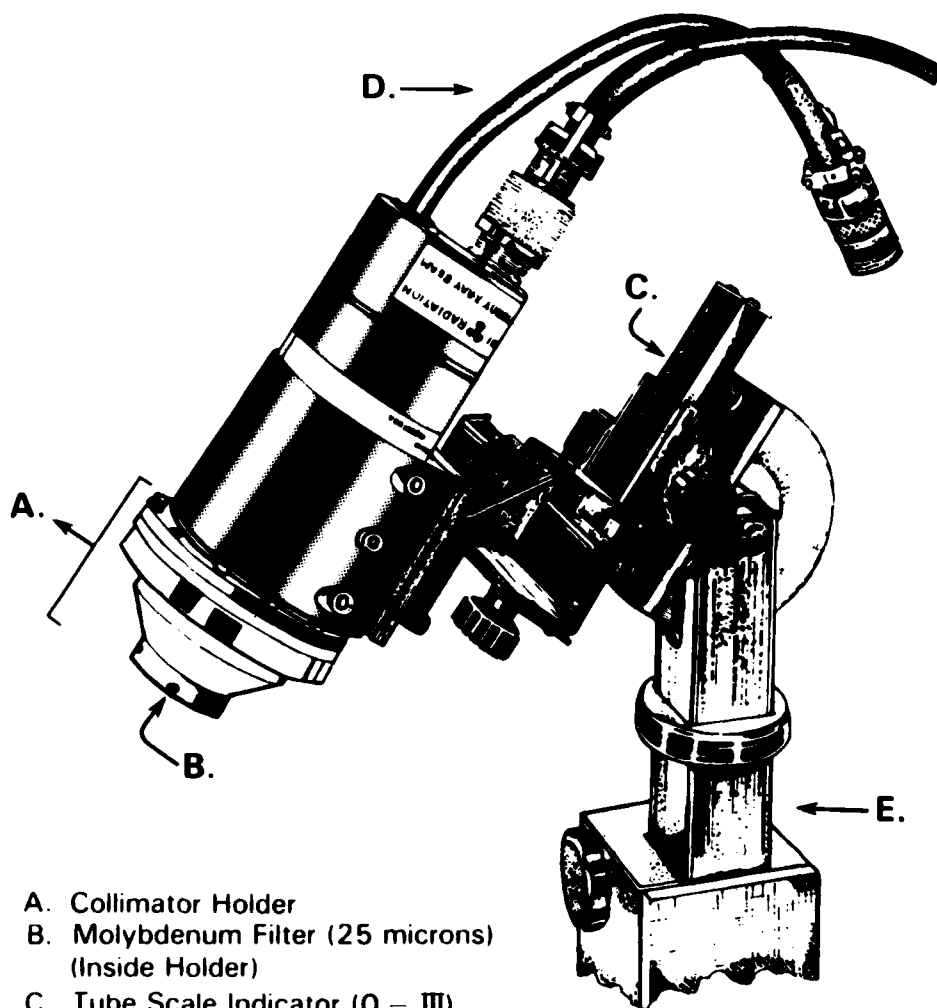
Radiation Source

The source of radiation was a Kevex (K5010T) 50 kVp/1 mA x-ray tube manufactured by Kevex x-ray Tube Division, Scotts Valley, Calif. (Kevex, 1983). The key components of the system were the x-ray head, x-ray tube with added molybdenum filter, collimators, x-ray tube holder, x-ray source control unit and cables. See Figs 1 and 2 for schematics of the above components. A detailed description of the various components follows:

x-Ray head

The hermetically sealed and completely radiation shielded x-ray head housed the x-ray tube and high

A. Collimator Holder
B. Molybdenum Filter (25 microns)
   (Inside Holder)
C. Tube Scale Indicator (0 — III)
D. High and Low Voltage Connectors
E. Mounting Post

Stainless Steel Collimators
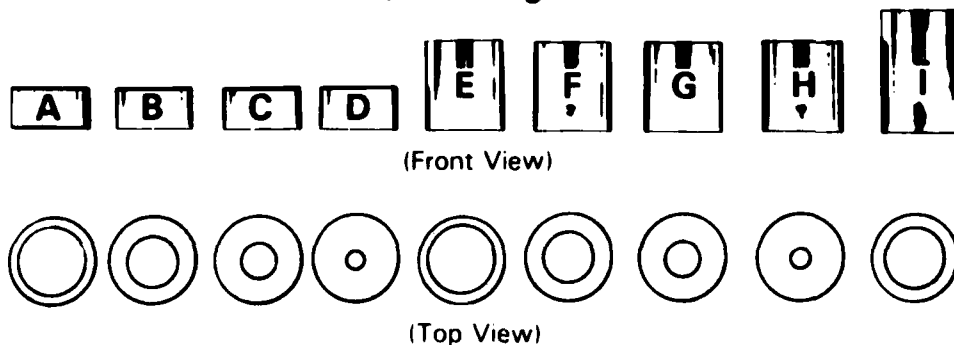
(A Through I)

(Front View)

(Top View)

Fig. 1. Kevex 50 kVp/1 mA x-ray tube with added molybdenum filter, tube holder/precision positioning stand and stainless steel collimators. The tube is approximately 20 cm in length and 7 cm in diameter and the dimensions of the collimators are as follows: A-D, 15 mm in length, 20-25 mm i.d. respectively; E-H, 30 mm in length, 20-25 mm i.d. respectively; I, 40 mm in length, 20 mm i.d.
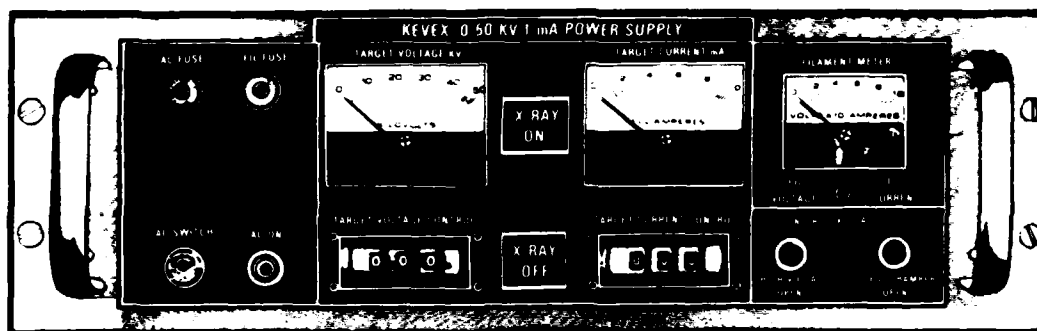
Fig. 2. Standard 50 kVp 1 mA power supply.

voltage and low voltage connectors. For high voltage insulation and efficient heat conduction the head was filled with a liquid dielectric. Additionally, a gas bubble was provided to accommodate differential expansion in materials due to heating.

x-Ray tube

The x-ray tube consisted of a cathode, beam current and electron focal spot control grids, and molybdenum transmission target. The oxide coated, thermionic cathode was an indirectly heated electron emitter that was controlled by an electrostatic field produced by the grid potential. The first double grid, which was closest to the cathode controlled electron beam emission; the second, single grid located between the first grid and the target, controlled the electron beam spot size. The focal spot grid operated independently from the beam emission grid and could be used to vary spot size from 0.5 to 4 mm in diameter. The transmission target yielded x-rays emitted in the direction of the longitudinal axis of the x-ray head. These x-rays were further filtered with a 25 μm thick molybdenum filter which was added external to the end of the tube adjacent to the 127 μm thick beryllium transmission window. This Mo–Mo configuration should yield a quasi-monoenergetic x-ray spectrum consisting primarily of the approximately 17.4 keV K_z x-rays of Mo (NCRP 85, 1986) (see Table 1).

Collimators

The tube head was modified with an external adapter to hold various collimators (see Fig. 1) of three different lengths and three different inner diameters.

x-Ray tube holder

The tube holder was locally designed and fabricated to allow variation of the tube positioning in both the horizontal and vertical axes. By utilizing the positioning indicators as illustrated in Fig. 1 the distance between the tube and the specimen could be varied to control the dose rate to the sample. This design

also afforded extremely accurate reproducibility in positioning the unit from run-to-run.

x-Ray source control unit

The 115 Vac, 60 Hz control unit consisted of a filament grid bias and beam current control, focal spot size control, and high voltage power supplies along with the control circuitry necessary to provide the settings/limits of operation (Fig. 2). The kV was selectable over the range 00.0–49.9 in steps of 00.1 kV and the mA was selectable over the range 0.00–0.99 in steps of 0.01 mA.

Cables

The power supply and tube were interfaced by separate high voltage and multiconductor low

Table 1. Physical aspects of the molybdenum target and filter

K Series	Photon energy (keV)
K_z1	17.478
K_z2	17.373
$K_\beta1$	19.607
$K_\beta2$	19.964
K_{ab}	20.002

Wtd avg: $K_z = 17.443$ keV; $K_\beta = 19.663$ keV

L series	Photon energy (keV)
LIII	
L_{z1}	2.015
$l_{z}2$	2.518
L_z1	2.293
LIII$_{ab}$	2.523
LII	
$L_\beta1$	2.395
L l	2.623
LII$_{ab}$	2.627
LI	
LI$_{ab}$	2.884

With the 25 μm Mo filter the predominant radiation should be the K_z1 series (relative intensity of 100) which results from the transition of LIII to the K shell. The K_z2 series or the LII to K shell occurs with a relative intensity of approximately 50. The K_β series, which are MIII & MII to K are of higher energies than K_z, however the relative intensity is only about 25. Accordingly, the weighted averages listed above best describe the energy spectrum anticipated for this tube configuration, with K_z most prevalent.

Kevex Brain Cell Irradiator
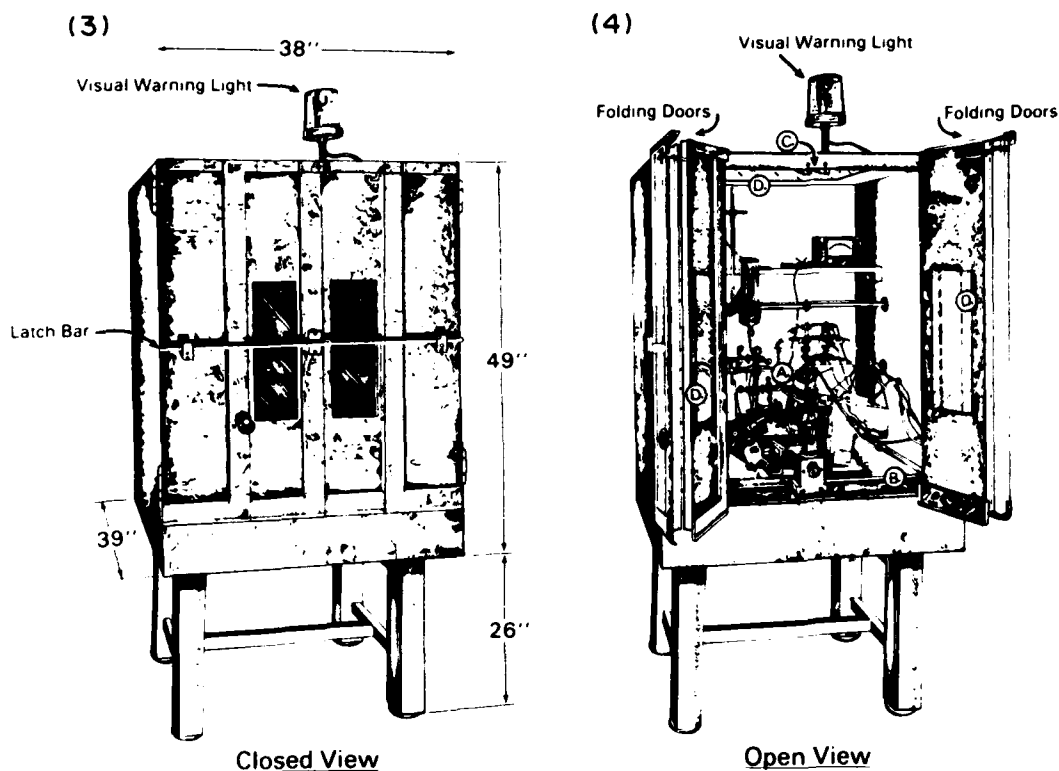
(3)

Closed View

(4)

Open View

A Kevex 50 kVp/1 mA X-Ray Unit
B Base of Interior - 4" Marble (Primary Barrier) *Rests on Air Cushion
C Interlocks
D Clear Pb-plastic

*The Entire Unit is Shielded With Lead Walls (1mm Thick) (Secondary Barrier)

Fig. 3. Closed view of the lead-shielded Faraday cage.
Fig. 4. Open view of the Faraday cage with the x-ray tube in place.

voltage cables. The cables which were approximately 2.3 meters in length allowed for remote operation of the unit.

Irradiation System

In order to meet the unique requirements for this local *in vitro* irradiator, a system was designed in which the irradiation could be conducted inside a Faraday cage enclosing the electrophysiology recording chamber (see Figs 3 and 4). The purpose of a Faraday cage was to block out any external electromagnetic interference to allow accurate measurement of the low level electrophysiological potentials. For these experiments, the standard copper mesh Faraday cage was replaced by a lead-lined box. The design and fabrication of the box had to meet radiation safety and operational constraints.

The entire cage was shielded in accordance with the National Council on Radiation Protection and Measurements Report No. 49, *Structural Shielding*

Design and Evaluation for Medical Use of X-Rays and Gamma Rays of Energies up to 10 MeV (NCRP 49, 1976). The criteria for the shielding design included a highly conservative assumption that the workload for the Kevex x-ray tube could be as high as to include continuous operations with the beam for up to 10 h per day, 6 days per week, at maximum voltage (50 kVp) and tube current (1 mA), i.e. $W = 3600$ mA·min/week, and that occupancy by members of the general public would be possible at any location within 0.4 m from the tube while it operated within the shield. On the basis of these assumptions, the required shielding thicknesses derived from NCRP 49 were 0.75 mm Pb or 7.5 cm concrete for the primary (direct beam) barrier, and 0.60 mm Pb or 5.5 cm concrete for secondary (leakage/scatter) barriers.

The installed shielding of 1 mm Pb in the walls of the lead-lined box, and 0.8 mm Pb-equivalent plastic in the window and top of the box met the above criteria. Likewise the 10-cm thick marble (density of 2.47–2.86 g cm⁻³) table top was even more massive

than the concrete (density 2.35 g cm⁻³) thickness required for a primary barrier, so no additional shielding was required on the table top.

Note that the x-ray shielding parameters covered in NCRP Report 49 applied to tungsten target x-ray tubes. This leads to some overestimation of the shielding requirements for a molybdenum target x-ray tube due to the fact that the bremmstrahlung x-ray spectrum has reduced output intensity from the lower atomic number target. The highly intense low energy (17–19 keV) characteristic x-rays from Mo do not effect the shield design because these are preferentially absorbed in the initial layers of the shield compared to the more energetic (20–50 keV) and penetrating bremsstrahlung portion of the x-ray spectrum.

The clear-Pb plastic of lead equivalence equal to 0.8 mm (Nuclear Associates, Carle Place, N.Y.) used in the window was included to allow the investigator to view the sample during irradiation. The ability to see inside of the box during the irradiation proved beneficial in aligning the field. Additionally, to allow ample light into the array a section of the top of the box was made of the clear-Pb plastic.

An interlock system was designed and installed according to the recommendations of NCRP 88, with the benefit of the interlock jack on the back of the power supply (NCRP 88, 1986). The system consisted of an interface box between the power supply and x-ray tube that must first be turned on to supply power to the system. Additionally, whenever the switch was ON a red visual warning light was illuminated. Microswitches were also installed on both doors such that the doors required positive pressure (i.e. both doors secured with the cross bar as illustrated in Fig. 3) before power could be supplied to the unit. The design of this system was "fail-safe", in that if the interlock was in any way violated the production of all radiation ceased immediately. Lastly, when the interlock was tripped, the system required manual resetting to prevent a sudden surge of power to the x-ray tube.

NCRP Report No. 88 also recommends a visual warning light as a caution to other personnel in the laboratory that an irradiation is in progress. Such a light was installed in conjunction with the interlock system. The light was ON whenever power was provided to the unit.

(L20 and L50) to span the x-ray energy range encountered in these experiments. The difference of 2.4% between the two calibration factors indicated the chamber response varies only slightly over a wide spectrum of low energies. The chamber was operated at ±300 V bias and all data represent the average of readings made at opposite polarities, which differed by no more than 0.5%.

Radiographic film

The x-ray film used in these tests was Kodak X-Omat V film (for therapy verification) in paper packs. Exposure of the film was conducted at 5 cm from the end of the collimator holder with the tube positioned at the normal operating angle (35 from vertical). Collimators A 1 and the open beam were analyzed at a 25 kV 0.2 mA setting for a 30 s exposure. The open beam density was studied using density scans in the horizontal and vertical axes in order to quantify the consistency of the field and hence the exposure rate.

Beam diameter gauge

A fluorescent screen beam diameter gauge (Nuclear Associates Model No. 07-604) was used in the positioning of the chamber for measurements taken inside of the array. The room and cage were darkened and the fluorescent screen was placed in the array at the location of the tissue. The tube was then powered-up and the beam location and size were viewed through the front panel. This provided vital information for the angle of the irradiation and the positioning of the chamber for dosimetry. Accordingly, the sample holder was modified to allow the chamber to be situated in the exact center of the beam where radiograph studies indicated the exposure rate was constant. Furthermore, the center of the chamber coincided with the tissue location during normal irradiations and the top of the chamber was at the same height as the sample. The beam diameter gauge data was confirmed with the radiograph results and this will be further addressed in the Results section. The characterization of the beam using the above techniques allowed for determination of dose rates at various points. Once this information was determined the chamber was removed and the irradiations were performed for calculated periods of time until the desired doses were delivered.

Dosimetry Procedures

Ionization chamber

A Capintec parallel-plate ionization chamber (Model No. PS-033) was used to determine the exposure rate from the tube. The sensitive volume of the detector was 0.5 cm³ and the aluminized Mylar window was 0.5 mg cm⁻² thick. The diameter of the sensitive area of the detector was 16 mm. The detector and electrometer were calibrated at the National Bureau of Standards for two beam codes

Dosimetry Calculations

Electrical charge from the parallel-plate ionization chamber was collected using a Keithley 616 electrometer set in the charge (10⁻⁹C) mode, which was in turn interfaced with a Hewlett Packard (HP) Data Acquisition unit and a HP-85 computer. The exposure (X) in roentgens (R) was calculated from the average of 10 sequential readings taken over 10 s intervals (M) at both polarities with the chamber

irradiated free-in-air with no build-up as follows:

$$\text{Exposure } (X) = M \cdot N_x \cdot K_q \cdot K_{tp}$$

where N_x was the NBS exposure calibration factor for the chamber in the L50 field, K_q was the electrometer correction factor and K_{tp} was the temperature (T) and pressure (P) correction factor given by,

$$K_{tp} = \frac{273.2 + T(\text{C})}{295.2} x \frac{760}{P(\text{mmHg})}.$$

The dose (D_m) was calculated as follows:

$$D_m = X \cdot f_{med}$$

where

$$f_{med} = 0.873 \left[\frac{\mu_{ah}}{\rho} \right]_{air}^{med}$$

for various materials in (cGy R^{-1}).

For approximately 17.4 keV photons in water $f_{med} = 0.889$ (Johns and Cunningham, 1983).

The tissue slices being studied in the electrophysiology recording chamber were perfused by an aqueous solution to maintain tissue viability during the course of the experiments. A dose attenuation factor was applied to account for the thin layer of water covering the sample. On the average the tissue was under 0.5 mm of water, so the dose to the tissue (D_{mt}) was calculated by,

$$D_{mt} = D_m \cdot I/I_0$$

where I/I_0 is the correction factor for the attenuation of the primary beam by the 0.5 mm of water. Using μ/ρ (Table 2) for approximately 17.4 keV photons in water the attenuation correction was 0.943. During normal perfusion of the tissue sample, it was estimated that the amount of water on top of the sample could vary by as much as ± 0.2 mm. This variance would cause the above attenuation correction factor to vary by $\pm 2.2\%$.
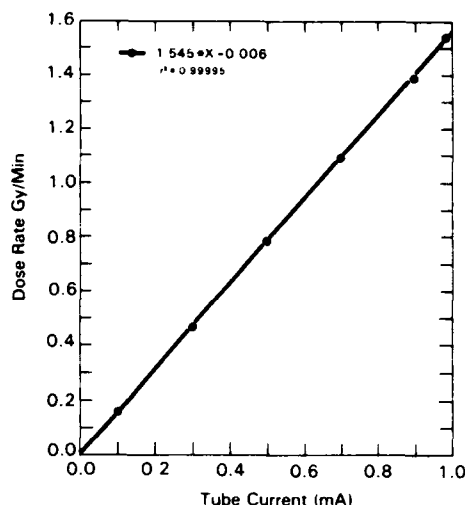

Fig. 5. Graph of dose rate vs current (mA) with a constant potential of 49 kV.

Results

Dose rate vs current

With a constant potential difference setting of 49 kV and the tube positioned at 10.7 cm from the anode to the detector (i.e. Tube Scale Indicator 0) dose rate data was collected for 0.1, 0.3, 0.5, 0.7, 0.9 and 0.99 mA. The increase in radiation output was linear with the increase in current and Fig. 5 is a plot of the data acquired. With this inherent linear characteristic the dose rate from the tube can be changed by varying the current without having to reposition the tube.

Dose rate vs potential difference

With a constant current setting dose rate data was collected for 10, 20, 30, 40, 45 and 49 kV. The data plotted in Fig. 6 show a curvilinear response for
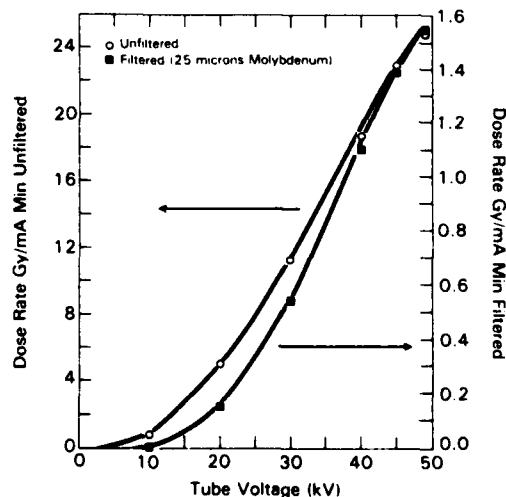
Table 2. Table of mass attenuation coefficients for photon energies 10-50 keV (μ/ρ)

Energy (keV)	Medium			
	Lucite	Water	Brain*	Soft tissue*
10	2.273	5.223	5.338	4.783
15	1.077	1.639	1.687	1.523
17.4†	0.835	1.244	1.280	1.161
20	0.562	0.796	0.819	0.750
30	0.301	0.372	0.379	0.358
40	0.234	0.267	0.270	0.261
50	0.207	0.226	0.228	0.222
				Units: cm² g⁻¹

*ICRP.
†Values based on interpolation.
Source: (Hubbell, 1982)

Fig. 6. Graph of dose rate vs potential difference (kV) with a constant current normalized to 1 mA for the filtered and unfiltered tube.
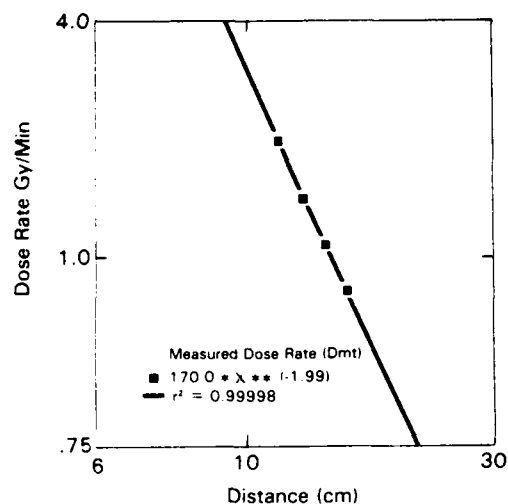
Fig. 7 Graph of dose rate vs distance (focus surface distance). The slope of the line −1.99 vs the expected −2.0 confirms the expected inverse square behavior of the x-ray output. See Table 3 for details.

Fig. 8. Half-value layer measurements for the filtered and unfiltered tube.

both the filtered (25 μm of molybdenum) and the unfiltered configurations. The effect of the 25 μm Mo filter was to reduce the measured dose rate by a factor of 16 at 49 kV to 33 at 20 kV, and to accentuate the curvature of the output curve. In routine use the unit was set up to operate at a fixed 49 kV.

Dose rate vs distance

Dose rate measured at varying distances from the four tube scale indicators were compared to confirm the expected inverse square behavior of the x-radiation. See Fig. 7 for the plotting of the above data. Table 3 provides a listing of the results obtained.

Radiation quality

Half-value layer (HVL) and homogeneity coefficient are frequently used in describing the quality of an x-ray beam. The HVL is the thickness of a material that reduces the exposure rate of the beam to one-half (ICRU 17, 1970). The homogeneity coefficient is the quotient of the thickness of the attenuator required to reduce the exposure rate to one-half, divided by the thickness of attenuator required to further reduce
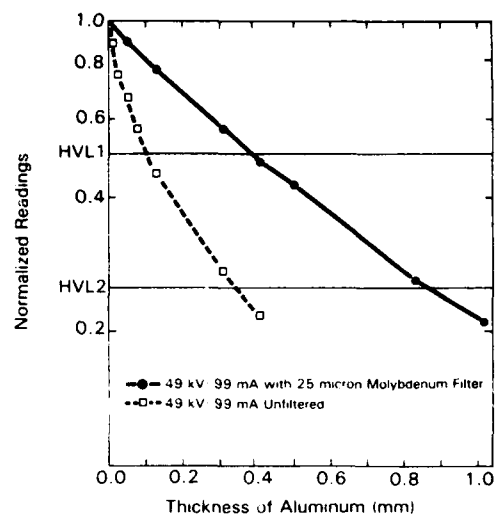
the exposure rate from one-half to one-fourth. The material used in the 10–120 kV range is usually aluminum (density = 2.7 × 10³ kg m⁻³) and a chemical purity of >99.8% (Hendee, 1984). To minimize the number of scattered photons which are detected, narrow-beam geometry or "good geometry" was used. All measurements were made at a distance of approximately 0.5 m focus–surface–distance (FSD) with the Al attenuators placed halfway. The tube setting was 49 kV/0.99 mA and the 25 μm molybdenum filter was positioned at the end of the tube.

As plotted in Fig. 8 the first and second HVL for the unfiltered beam were 0.1 and 0.24 mm, for a homogeneity coefficient of 0.42. For the 25 μm Mo filtered beam the first HVL was equal to 0.40 mm Al and second HVL was equal to 0.46 mm Al; the homogeneity coefficient for the beam was therefore 0.87. Thus for the filtered beam the HVL (0.41 mm Al) agrees within 3% with the calculated value (0.40 mm Al) for 17.4 keV photons. This close agreement demonstrates the quasi-monoenergetic nature of the Mo filtered x-ray beam.

Beam uniformity and penumbra

As indicated in the *Dosimetry Procedures* section radiographs of the nine collimated beams and the open beam were taken and analyzed. Table 4 summar-

Table 3 Radiation dose rates

Tube scale indicator	TDD*	FSD+	Gy min
0	5.0 cm	10.7 cm	1.54
I	6.0 cm	11.7 cm	1.28
II	7.0 cm	12.7 cm	1.10
III	8.0 cm	13.7 cm	0.94

*TDD This is the tube detector distance which is measured from the end of the tube to the surface of the detector. The tube scale indicator is marked to allow easy and accurate variation in the TDD

+FSD This is the focus-to-surface distance. The FSD is the sum of the TDD plus 5.7 cm, which is the distance from the end of the tube collimator to the molybdenum target. The 5.7 cm distance was provided by the tube manufacturer

Table 4 Collimated field sizes

Collimator	Diameter (mm)	
	Horizontal	Vertical
A	25	27
B	21	23
C	13	15
D	05	06
E	24	26
F	18	20
G	11	13
H	05	06
I	22	24
Open	26	27

izes the results of the beam diameter measurements for the horizontal and vertical axes with an FSD = 10.7 cm.

The diameter in the vertical axis was in all cases greater than that in the horizontal axis, due to the requirement of irradiating at a 35 angle. Due to constraints imposed by the electrophysiology apparatus it was necessary to angle the tube at 35. Since the irradiation must be conducted at an angle the beam is ellipsoidal.

Preliminary density scans of the film showed that the optical density in the center of the beams varied less than 5% between the various collimators. Also each beam profile appeared to be of uniform density with no artifacts other than a surrounding penumbra region. From these results it was concluded that the dose rate was approximately the same for all collimators, so that the output data for the OPEN beam applied to all other beam sizes. This finding was particularly important because of the relatively large diameter (16 mm) of the ionization chamber used to measure dose rates. Further analysis of the OPEN beam was conducted using the Drexel Image Processing Center Brain software package (see Figs 9 and 10).

In the horizontal direction the penumbra region was 8-mm wide on either side of the main beam (i.e. the 26 mm region listed above). During dose measurements it was crucial to keep the ionization chamber out of this region. The vertical analysis provided integral information in the area of tissue positioning.

Another effect of angling the tube is that the beam intensity varied according to inverse square. Quantification of the density of the film in the 27-mm vertical region indicated an optical density of 0.59

in the center of the beam. Due to inverse square the density closest to the tube was 0.61 and farthest from the beam was 0.56. The difference in output relative to the center of the beam, which the doses in Table 3 are quoted at, could vary from 3 to 5%.

Depth dose

Depth dose measurements were done by positioning sheets of lucite on top of the Capintec chamber. The referenced mass attenuation coefficient for lucite $(0.835 \text{ cm}^2 \text{ g}^{-1})$ (Hubbell, 1982) for approximately 17.4 keV photons was in close agreement with the experimental measurements (see Fig. 11).

Discussion

This system provides a unique irradiation capability with built-in flexibility allowing the investigator to observe even the most subtle changes. Furthermore, the quantitative study of radiobiological damage on the cellular level is greatly facilitated. The following are some additional advantages of this system:

The entire unit is in the laboratory under the control of the user. Irradiations can be performed whenever the biological system is ready.

—Simultaneous irradiation and observation of the sample both visually and by microelectrodes.

Variable dose rate.

The tube is easily removed with highly reproducible dose rates after repositioning.

—Various collimators are provided to give selected beam diameters.

- The Mo–Mo target filter system gives an excellent compromise between high dose rate and acceptable penetration ability of the beam. The x-ray energy spectrum is quasi-monoenergetic with well defined radiation quality.

The x-ray tube is extremely small and operates at low power with no external cooling system. It is also capable of versatile positioning in a complicated experimental apparatus.

During tube operation no electrical interference was noted on electrophysiology recordings.

This unit is a prototype and with such a system come many learning experiences. Some recommendations for future improvements are:

Encase the lead sheets in plywood to avoid possible sagging problems

Install a shutter to eliminate the radiation dose delivered during the brief 1 min warm-up time. For high dose irradiations (>6 Gy) the warm-up dose was negligible (<1%) compared to the total dose delivered. However, for low dose irradiations special accounting may be necessary for the dose delivered during the brief warm-up period

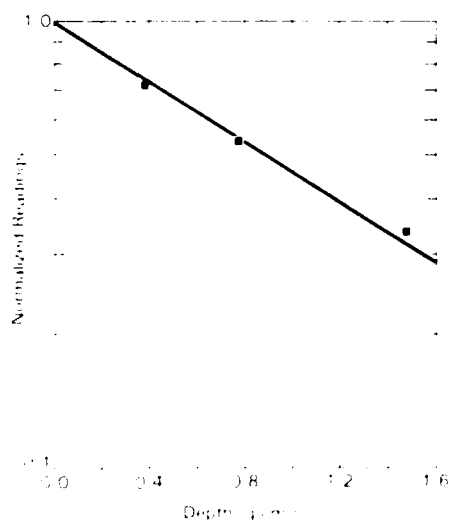Improve the alignment and positioning mechanism to give more versatile beam location

Fig. 11 Depth dose through lucite. The slope of the line is 0.77 cm² g which agrees with the referenced mass attenuation coefficient for 17.4 keV photons in lucite to within 5% (see Table 2). The referenced value includes coherent scattering and it is believed this accounts for much of the disparity
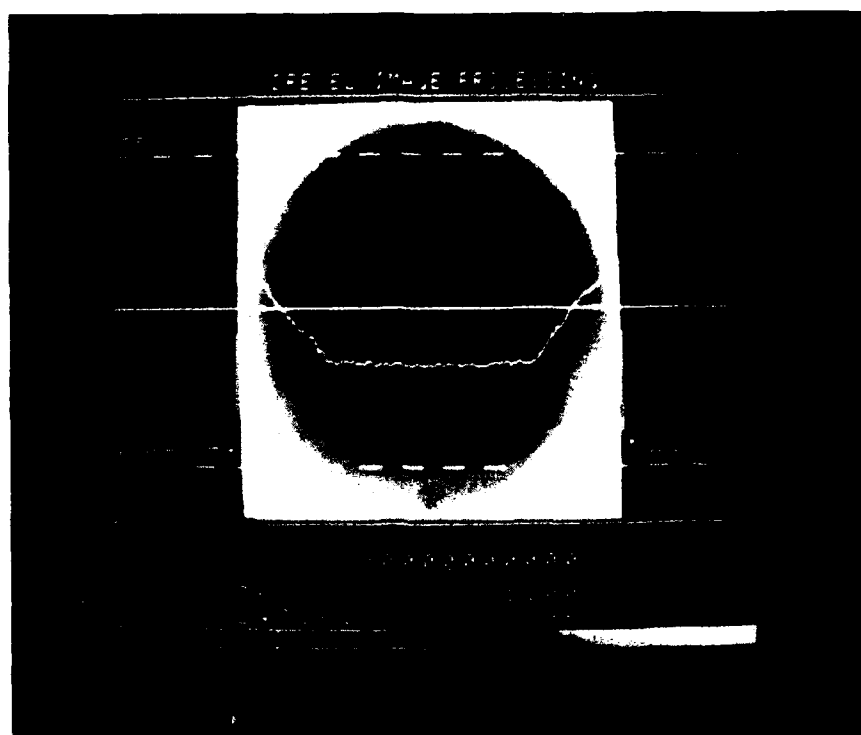
Fig. 9. Beam uniformity and penumbra analysis in the horizontal axis. Note: the optical density is constant across the field.
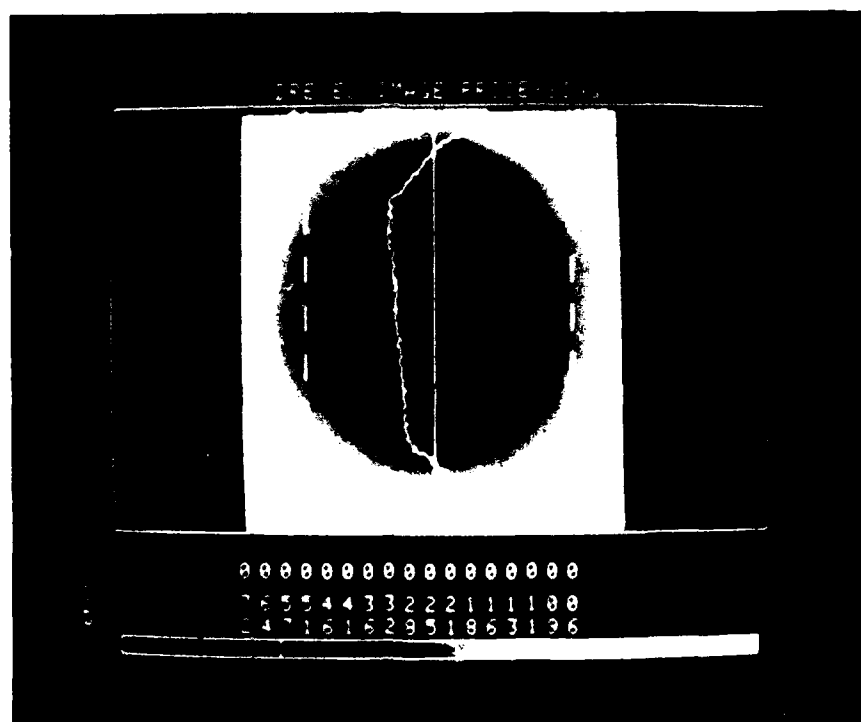

Fig. 10. Beam uniformity and penumbra analysis in the vertical axis. Due to the 35° angle of the x-ray tube during irradiation the optical density is greater close to the tube and less as the distance increases, relative to the center of the beam. The dose rate across the useful area of the beam varies by approximately ± 5%.

Have the capability to deliver dose rates as high as 20 Gy min

From a dosimetry perspective, in dealing with a narrow beam it would be advantageous to acquire a smaller diameter parallel-plate ionization chamber.

A rugged and submersible beam intensity monitor is needed for active in-beam dosimetry, such as a small (< 1 mm³) plastic scintillation detector.

The x-ray apparatus described in this report is presently being used to conduct local *in vitro* irradiations of the hippocampal region from guinea pig brains. Preliminary quantification of the electrophysiological response indicates the x-ray apparatus is suitable for this application

References

AFRRI Instruction 3020.6b. (20 August 1979) *Radiological Safety Instruction* RSI-530 Radiation producing machines: Bethesda, Md

Hendee W. R. (1984) *Medical Radiation Physics*, 2nd edn. Year Book Medical Publishers Inc., Chicago.

Hubbell J. H. (1982) Photon mass attenuation and energy-absorption coefficients from 1 keV to 20 MeV. *Int. J. Appl. Radiat. Isot.* **33**, 1269

Johns H. E. and Cunningham J. R. (1983) *Physics of Radiology*. Charles C. Thomas, Springfield, Ill.

Mammography: A Users Guide (1 March 1986) Report No. 85. National Council on Radiation Protection and Measurements, Bethesda, Md

Operation and Maintenance Manual (K5010 & K5020) (21 April 1983) Kevex X-ray tube division, Scotts Valley, Calif.

Radiation Alarms and Access Control Systems. (30 December 1986) Report No. 88. National Council on Radiation Protection and Measurements, Bethesda, Md.

Radiation Dosimetry: X-Rays Generated at Potentials of 5 to 150 kV (15 June 1970) Report No. 17. International Commission on Radiation Units and Measurements, Washington, D.C.

Structural Shielding Design and Evaluation for Medical Use of X-Rays and Gamma Rays of Energies of up to 10 MeV (15 September 1976) Report No. 49. National Council on Radiation Protection and Measurements, Washington, D.C.

Tolliver J. M. and Pellmar T. C. (1987) Ionizing radiation alters neuronal excitability in hippocampal slices of the guinea pig. *Radiat. Res.* **112**, 555.
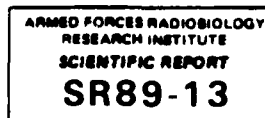
THERMOSPRAY LIQUID CHROMATOGRAPHY MASS SPECTROMETRY OF THIOL RADIOPROTECTIVE AGENTS: CHARACTERISTIC SPECTRA

Thomas L. Walden Jr*, James Buchner†, Vincent Pizzitola† and
William F. Blakely*

*Radiation Biochemistry and †Radiation Sciences Department, Armed Forces Radiobiology Research Institute, Bethesda, Maryland 20814-5145, U.S.A.

†Extrel Corporation, P.O. Box 11512, Pittsburgh, Pennsylvania, 15238, U.S.A.

1. INTRODUCTION

Ethiofos (S-2(3-aminopropylamino)ethylphosphorothioic acid or WR-2721) is currently being evaluated in clinical radiotherapy trials (Kligerman *et al.*, 1980) because of its potential for enhancing the efficacy of radiotherapy (Kligerman *et al.*, 1980; Yuhas and Storer, 1969). For proper drug usage and pharmacological studies, it is necessary to assess the stability of the aminothiol and the presence of impurities or decomposition products. In addition, monitoring the plasma levels of WR-2721 and its metabolites should improve the therapeutic usefulness of WR-2721. Several high-performance liquid chromatography (HPLC) methodologies have been developed that are applicable for routine analysis of aminothiols and endogenous cellular thiols (Newton *et al.*, 1981; Swynnerton *et al.*, 1984). One of these methodologies, electrochemical detection, permits the simultaneous detection of the free thiol and the disulfides (Swynnerton *et al.*, 1984).

Mass spectrometry (MS) is a sensitive technique that can confirm purity and provide useful structural information. Using a thermospray interface, samples can be introduced into the mass spectrometer from a liquid chromatograph (LC) (Vestal, 1984). The interface thermally nebulizes the eluant into a high-pressure region of the mass spectrometer where a variety of soft ionization techniques may be used to ionize the analyte molecules. We have investigated the feasibility of LC coupled to MS-detection for the analysis of thiol-containing radioprotective agents, including glutathione, WR-2721, and WR-1065, the dephosphorylated sulfhydryl form of WR-2721, which has been shown to be its active radioprotective metabolite (Calabro-Jones *et al.*, 1983).

2. METHODS

The LC–MS system was an Extrel EL Mass Spectrometer (Model 400-2) coupled to a Varian 8500 syringe pump by a Vestec Thermospray interface. The HPLC solvent consisted of 0.1 M ammonium acetate at a flow rate of 2 ml/min. The thiol compounds to be analyzed were resuspended in the mobile phase buffer to a concentration of 1 µg/µl and injected either directly into the solvent stream bypassing the HPLC column (Zorbax C-8 column, 4.5 × 150 mm) or through the column before entering the thermospray interface and the mass spectrometer. The thermospray probe temperature was optimized at 225°C, and samples were analyzed using the filament-on mode. The vapor temperature was approximately 277°C. Ion spectra were obtained by scanning from 100 to 800 daltons, and the data were collected for either positive or negative ion mass spectra. The mass ranges for scanning, as well as preliminary assignment of fragment ions, were based on the expected fragment pattern and nominal molecular weights of the compounds examined.
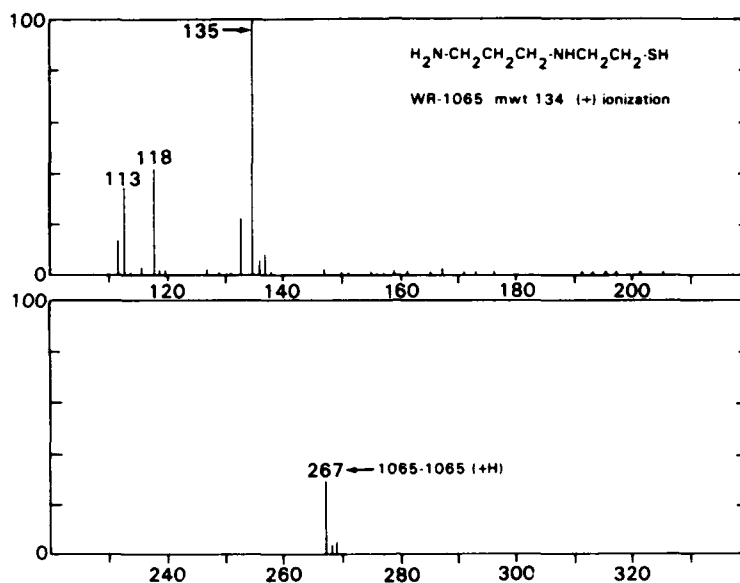
FIG. 1. WR-1065 spectra from LC–MS analyses. WR-1065 was analyzed by positive ionization techniques.
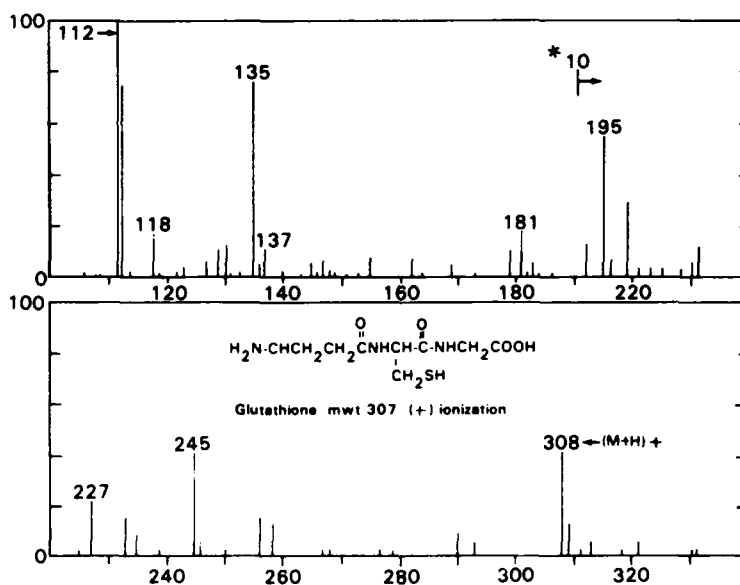

FIG. 2 Glutathione spectra from LC–MS analyses. Glutathione was analyzed using positive ionization.

3. RESULTS AND DISCUSSION

Glutathione, WR-2721, and WR-1065 were analyzed by positive chemical ionization. The positive spectra for WR-2721 and WR-1065 were indistinguishable, and only the spectrum for WR-1065 is shown (Fig. 1). The major ion occurring in the spectra of both WR-2721 and WR-1065 is at m/z 135, in agreement with an ion produced by the protonated mass of the WR-1065 mercaptan (M + 1). A peak observed at m/z 267 is in agreement with the protonated mass of the disulfide of WR-1065. Other major peaks were observed at m/z 112 and 118. WR-2721 has a molecular weight of 214, although no M + 1 ion was observed at m/z 215. Interestingly, the spectra for glutathione (Fig. 2) also contained an m/z ion peak at 135. Other peaks were

observed at m z 112 and 118 as well as a small molecular ion at 308 (M + 1). Final identification of the chemical structures represented by the major ions will require either MS—MS analyses or the analysis of standards of probable fragments.

Preliminary experiments show that this technique can be coupled with HPLC separation to detect these thiol compounds in the extracts of plasma from mice injected with WR-2721 (data not shown). The detection response appears to be linear with the concentration of the compound, and preliminary estimates of the low sensitivity limits are near 10 pg. In addition, recent experiments (not shown) indicate that the mass spectra of WR-2721 and WR-1065 obtained with negative ionization may produce unique ions that help to distinguish the two compounds. The chromatography separation is being further refined to allow negative ionization-thermospray LC—MS analysis of both the parent compounds and their metabolites from biological samples.

Thermospray—MS appears to provide a reliable method for confirmation of thiol radioprotective agents without prior derivatization. Structural information and elemental composition about unknown thiol compounds could be obtained readily using the soft ionization MS analysis. As described here, the detection of thiols using HPLC separation and MS detection represents a novel methodology for the detection of thiols. Accurate HPLC retention times would be coupled with compound detection using selective ion monitoring of the major characteristic ion fragments. LC—MS is an exquisitely sensitive technique for detection of WR-2721 and WR-1065, with estimates for the lower limit of sensitivity in the pg range. Comparable detection limits for electrochemical methodologies for thiols (McGovern et al., 1984) and for detection of fluorescent monobromobimane derivatives of thiols (Newton et al., 1981) are in the low ng range.

REFERENCES

CALABRO-JONES. P. M., FAHEY, R. C., SMOLLR, G. D. and WARD, J. F. (1983) Alkaline phosphatase promotes radioprotection and accumulation of WR-1065 in V79-171 cells incubated in medium containing WR-2721. Int. J. Radiat. Biol. 47: 23–27.

KLIGERMAN. M. M., SHAW. M. T., SLAVIK. M. and YUHAS, J. M. (1980) Phase I clinical studies with WR-2721. Cancer Clin. Trials 3: 217–221.

McGOVERN. E. P., SWYNNERTON. N. F., STEELE, P. D. and MANGOLD. D. J. (1984) HPLC assay for 2-(3-amino-propylaminoethanethiol (WR-1065) in plasma. Int. J. Radiat. Oncol. Biol. Phys. 10: 1517–1520.

NEWTON. G. L., DORIAN. R. and FAHEY. R. C. (1981) Analysis of biological thiols: Derivatization with mono-bromobimane and separation by reverse-phase high-performance liquid chromatography Anal. Biochem. 114: 383–387.

SWYNNERTON. N. F., McGOVERN. E. P., NINO, J. A. and MANGOLD. D. J. (1984) An improved HPLC assay for S-2(3-aminopropylaminoethylphosphorothioate (WR-2721) in plasma. Int. J. Radiat. Oncol. Biol. Phys. 10: 1521–1524.

VESTAL. M. L. (1984) High performance liquid chromatography—mass spectrometry. Science 226: 275–281.

YUHAS. J. M. and STORER. J. B. (1969) Differential chemoprotection of normal and malignant tissues. J. Natl. Cancer Inst. 42: 331–335.

RADIOPROTECTION BY LEUKOTRIENES: IS THERE A RECEPTOR MECHANISM?

THOMAS L. WALDEN JR* and JOHN F. KALINICH

Radiation Biochemistry Department, Armed Forces Radiobiology Research Institute, Bethesda, Maryland 20184-5145, U.S.A.

1. PROPERTIES OF LEUKOTRIENES

Leukotrienes are a class of biological mediators derived from arachidonic acid through the lipoxygenase pathway (Fig. 1). Early studies showed that lipophilic factors capable of constricting smooth muscle and inducing anaphylaxis were produced in the guinea pig in response to cobra venom (Feldberg and Kellaway, 1938). These observations were followed up by a number of investigators, and the factors became collectively referred to as the slow-reacting substances of anaphylaxis (SRS-A), although their exact chemical compositions and structures remained undetermined (Brocklehurst, 1962). In the late 1970s and early 1980s, the pathway for synthesis of leukotrienes as well as their structures were elucidated (Samuelsson *et al.*, 1980), and those compounds previously studied as SRS-A were shown to be identical to the recently discovered leukotrienes (Bach *et al.*, 1980). Leukotrienes have pathological roles in inflammation and anaphylaxis (Samuelsson *et al.*, 1980; reviewed in Bach, 1983, and Sirosis, 1985), act as vasoactive agents, as chemotactic factors for neutrophils (Bray *et al.*, 1981), and are more potent constrictors of smooth muscle than histamine (Drazen *et al.*, 1980).
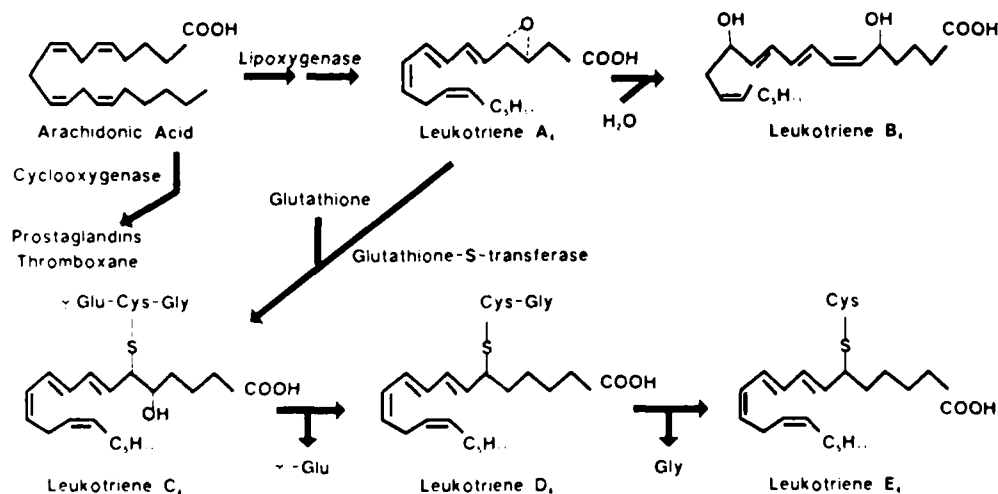
FIG 1 Leukotriene synthesis The lipoxygenase pathway for the formation of leukotrienes from arachidonic acid is illustrated Lipoxygenase metabolizes arachidonic acid to 5-hydroperoxy eicosatetraenoic acid (not shown), which serves as a substrate for 5-hydroxy eicosatetraenoic acid and for leukotriene A4 Other lipoxygenases specific for different sites of action on arachidonic acid exist, such as the 12-lipoxygenase However, the initial synthesis of the biologically derived leukotrienes begins with the 5-lipoxygenase

*Author to whom correspondence should be addressed

Leukotriene A_4 (LTA$_4$, Fig. 1), an epoxide intermediate in the leukotriene pathway, is synthesized from arachidonic acid by a two-step process involving lipoxygenase (Radmark *et al.*, 1980). Leukotrienes are characterized by three conjugated double bonds (triene), and the '4' subscript refers to the number of double bonds in the parent arachidonic acid substrate. Leukotrienes have been synthesized from eicosatrienoic acid (three double bonds) and eicosapentaenoic acid (five double bonds) (Ford-Hutchinson, 1986). LTA$_4$ serves as the precursor for the synthesis of the peptidoleukotrienes C_4, D_4 and E_4, and also LTB$_4$, a nonpeptide leukotriene containing two hydroxyl groups. LTB$_4$ is one of the most potent chemotactic factors for neutrophils (Bray *et al.*, 1981).

Leukotriene C_4, (5S,6R)-5-hydroxy-6-S-glutathionyl-7,9-*trans*-11,14-*cis*-eicosatetraenoic acid, is formed by the action of glutathione-S-transferase in combining glutathione to LTA$_4$ through a thiol−ether linkage. Leukotriene D_4 (LTD$_4$) is formed from LTC$_4$ by removal of gamma-glutamic acid. Removal of glycine from LTD$_4$ forms LTE$_4$, leaving cysteine attached to the 20-carbon backbone. LTE$_4$ is inactivated by acetylation at the N-position of cysteine (Orning *et al.*, 1986).

2. LEUKOTRIENES AND RADIOPROTECTION

The lipoxygenase metabolites of arachidonic acid have not been as extensively characterized in terms of their cytoprotective and radioprotective properties as have the cyclooxygenase metabolites (prostaglandins, thromboxane, and prostacyclin). Research on the radioprotective properties of leukotrienes is limited by the expense and availability of pure compounds, and very little research has been done in this area thus far. Preliminary studies are presented here with the goal of discussing the current understanding of this problem and to introduce future research directions.

2.1. INDUCTION OF RADIOPROTECTION IN CULTURED CELLS

We recently observed that treatment with LTC$_4$ 2 hr before 10 Gy ^{60}Co gamma irradiation induces a decrease in the radiosensitivity of V79A03 Chinese hamster lung fibroblasts *in vitro* (Walden *et al.*, 1986). The optimum radioprotective dose of LTC$_4$ is 2.5 μM, and the protection is not attributable to radical scavenging by the glutathione portion of the molecule. Studies were performed with cells harvested by trypsinization and replated 16 hr before irradiation. The cellular reproductive survival was quantitated 7 days later on the basis of colony formation. The LTC$_4$ pretreated group contained two to three times more surviving colonies than the control irradiation groups (Walden *et al.*, 1986).

2.2. RADIOPROTECTION OF HEMATOPOIETIC STEM CELLS IN MICE

Radioprotection was induced by LTC$_4$ rather than as a direct result of its presence during irradiation. This was determined by monitoring the metabolism of LTC$_4$ by the tissue culture medium alone and in the presence of V79A03 cells. At the time of irradiation, only 33% of the LTC$_4$ was present, with the remainder converted to LTD$_4$ and LTE$_4$ (Walden *et al.*, 1986). The latter two leukotrienes were not as effective radioprotective agents as LTC$_4$.

Leukotrienes have also been shown to provide radioprotection to the hematopoietic stem cells of mice *in vivo* and *in vitro* (Walden *et al.*, 1988). Mice received a pretreatment of 10 μg LTC$_4$/mouse subcutaneously in the nape of the neck before ^{60}Co gamma irradiation. LTC$_4$ was found to be radioprotective for endogenous spleen colonies (E-CFU), exogenous spleen colonies (CFU-S), and granulocyte-macrophage progenitor cells (GM-CFC) in mice. The optimal time for administration is 15 min before irradiation, with 20% of the optimal protection still present 60 min postirradiation. The dose reduction factors were 1.5 for CFU-S protection and 2.0 for

GM-CFC protection (Walden et al., 1988). LTB$_4$, LTD$_4$, and LTE$_4$ provided equal protection but were not as effective as LTC$_4$. In addition, a 1 hr pretreatment with LTC$_4$ will protect the intestinal crypt cells of mice from radiation damage (Hanson, 1987).

3. EVIDENCE FOR A RECEPTOR MECHANISM IN LEUKOTRIENE RADIOPROTECTION

The underlying mechanism(s) for the leukotriene-induced radioprotection remains undetermined. Many of the biological responses to leukotrienes are thought to be mediated by specific receptors (Fleisch et al., 1984), and evidence for the association of a specific LTC$_4$ binding site on the V79A03 cell with LTC$_4$-induced radioprotection has been obtained. Radiation survival experiments with V79A03 Chinese hamster fibroblasts were conducted by modifying methods previously described (Walden et al., 1986). Briefly, V79A03 cells were grown in MEM medium supplemented with Earle's salts in HEPES, 2 mM L-glutamine, and antibiotics. Cells were maintained in a humidified atmosphere of 5% CO$_2$ in air, in an incubator at 37°C. The previously described method was modified by harvesting the cells with 0.02% EDTA, 6 hr before irradiation. Leukotriene C$_4$ (2.5 μM) was added to the medium of treated cells 2 hr before irradiation. Irradiated cells received X-irradiation at a rate of 1.69 Gy/min. Reproductive survival was assayed by colony formation seven days postirradiation. The number of colonies was corrected for plating efficiency and multiplicity, and the surviving fraction was determined.

Specific binding of [^{3}H]LTC$_4$ by V79A03 cells was determined as previously described (Walden, Marr, Watts and Fitz, submitted for publication). Binding assays contained 1 × 10^6 cells and 20 fmol [^{3}H]LTC$_4$ (DuPont, Boston, Massachusetts) in 50 μl of Hank's buffered saline (Gibco, Grand Island, New York) per tube. Assays were incubated for 15 min on ice, and the nonspecific binding was determined in parallel assay tubes containing 200 ng of unlabeled LTC$_4$. Assays were performed in quadruplicate, and standard errors of the means were determined.

3.1. LTC$_4$ RECEPTOR ACTIVITY AND RADIOPROTECTION

In an attempt to reduce the preparation time for the cellular radioprotection experiments, the protocol was modified from a 16 hr preplating to 4 hr before irradiation, without changing the 2 hr LTC$_4$ pretreatment. These experiments did not exhibit any indication of LTC$_4$-induced radioprotection and failed to verify previously reproducible results (data not shown). An examination of this problem led to the identification of specific binding sites on this cell line for LTC$_4$ (Walden, Marr, Watts and Fitz, submitted for publication; Table 1). The binding characteristics of the [^{3}H]LTC$_4$ specific binding sites on V79A03 cells have also recently been described (Walden, Marr, Watts and Fitz, submitted for publication). The binding was specific for LTC$_4$, and LTD$_4$ and LTE$_4$ did not compete. In an equivalent number of V79A03 cells

TABLE 1. *Binding of [^{3}H]leukotriene C$_4$ to V79A03 Cells*

LTC$_4$ binding to cells harvested by 0.02% EDTA phosphate-buffered saline	
Percent total [^{3}H]LTC$_4$ binding	40.2 ± 1.3 (S.E.M., N = 4)
Percent nonspecific binding	10.0 ± 1.6
Percent specific binding	30.2 ± 1.3
Percent specific LTC$_4$ binding to cells harvested by trypsinization (0.02% trypsin in phosphate-buffered saline)	0.4 of labeled material

TABLE 2. *Survival fraction following 10 Gy irradiation in the presence or absence of 2.5 µM leukotriene C_4*

Experiment no	Control ($\pm$ S.E.M.)	LTC_4 ($\pm$ S.E.M.)
1	0.0430 ($\pm$ 0.0170)	0.0950 ($\pm$ 0.0200)
2	0.0300 ($\pm$ 0.0011)	0.0919 ($\pm$ 0.0025)
3	0.0310 ($\pm$ 0.0010)	0.0640 ($\pm$ 0.0020)
4	0.0460 ($\pm$ 0.0015)	0.0881 ($\pm$ 0.0026)
5	0.0288 ($\pm$ 0.0016)	0.0909 ($\pm$ 0.0015)

$N = 24$

harvested by trypsinization. LTC_4 binding was reduced from the 30% observed for EDTA-harvested cells, to 0.4% (Table 1). This indicated the possibility that LTC_4 might require interaction with a protein component on the cell membrane to induce radioprotection.

Consequently, we resumed cellular radioprotection studies using cells harvested by EDTA rather than by trypsinization, and the cells were replated 4—6 hr prior to irradiation, as described above. LTC_4 (2.5 µM) was added to the culture medium 2 hr prior to receiving 10 Gy of ^{60}Co gamma irradiation. Radioprotection by LTC_4 was observed and consistently repeated in five subsequent experiments (Table 2). The ability of LTC_4 to induce radioprotection in the cells harvested using EDTA but not those harvested at similar times by trypsinization implies the importance of an intact binding site (receptor?).

4. AREAS OF FUTURE RESEARCH

Two future areas of research hold promise for leukotriene-induced radioprotection: (a) investigation of the mechanism(s) involved and (b) investigation of the receptor/protection relationship. There appear to be at least two mechanisms for radioprotection, one at the cellular level, based on specific receptors, and the second at the systemic level. This is supported by studies on radioprotection to cells in culture and by whole-animal survival studies. Radioprotection by LTC_4 and specific LTC_4 binding sites has been demonstrated in the V79A03 Chinese hamster fibroblasts *in vitro* (Walden et al., 1986; Walden, Marr, Watts and Fitz, submitted for publication).

Many leukotriene-induced activites are thought to be mediated by specific receptors (Fleisch et al., 1984), and in some instances they may also induce the synthesis of other eicosanoids (Welton et al., 1983). The role of a receptor in leukotriene-induced radioprotection holds promise for development of specific radiotherapy protocols for those patients whose tumors do not possess LTC_4 receptors. Because there are both cellular level (receptor) and systemic bases for protection, those tumor cells that do not possess LTC_4 receptors should not be protected to the same degree as normal tissues possessing the receptors. Specific receptors for LTC_4 have been identified in a number of tissue homogenates, including lung (Hogaboom et al., 1983; Cheng et al., 1985), brain (Cheng et al., 1985), smooth muscle (Clark et al., 1984), and endothelial cells (Muller et al., 1987). The role of specific receptors in radioprotection and their possible significance to radiotherapy was re-enforced in studies of isoproterenol protection of cells in culture (Chirkov and Sobolev, 1985). Isoproterenol radioprotection is thought to be β-adrenergic-receptor mediated, resulting in an elevation of cyclic AMP. Cells that do not possess β-adrenergic receptors are not protected by isoproterenol (Chirkov and Sobolev, 1985). Not all tumor cell lines possess LTC_4 specific binding sites (Balapure et al., 1987). In the event that the tumor cell possesses a specific receptor for LTD_4 or LTE_4, there remains the possibility that the use of LTC_4 or an appropriate analog in radiotherapy may protect the tumor through conversion of LTC_4 to LTD_4 or to LTE_4. However, these two leukotrienes are much less effective than LTC_4 both in cells *in vitro* (Walden et al., 1986) and in mouse hematopoietic cells *in vivo* (Walden et al., 1988).

Conversely, is a tumor with the capacity to produce leukotrienes more resistant to therapy? Tumor production of prostaglandins has been well studied, but few reports exist regarding the

ability of tumors to produce leukotrienes. The rat basophilic leukemia cell is known to produce leukotrienes, and much of the pathway for leukotriene synthesis was determined in this cell line (Orning et al., 1980). Rat mastocytoma cells also produce leukotrienes (Bach et al., 1980).

16.16-Dimethyl prostaglandin ($DiPGE_2$) is an effective radioprotector of mouse intestinal crypt cells (Hanson and Ainsworth, 1985) and hematopoietic stem cells (Hanson and Ainsworth, 1985; Walden et al., 1987), and also for whole-animal survival (Walden et al., 1987). However, radioprotective doses suppress locomotor activity (Landauer et al., 1987) and induce diarrhea (Walden et al., 1987). The ataxia induced in mice by $DiPGE_2$ is dose-dependent and requires up to 30 hr for recovery to control levels (Landauer et al., 1987). Unlike $DiPGE_2$, radio-protective doses of LTC_4 do not cause diarrhea, but do temporarily suppress locomoter activity (Walden, unpublished). Experiments to quantitate the behavioral effects of the leukotrienes are planned. Aside from the temporary suppression of behavior, there are no visible side effects from administration of sublethal doses of LTC_4. Death usually occurs within 30 min following the administration of a lethal dose to mice.

LTC_4 is one of the more effective biological mediators in terms of radioprotection, and is one of the more effective radioprotectors. Its exogenous administration in radioprotective doses to mice is limited by toxicity and short biological half-life. In terms of radioprotection, a single injection of $5 - 10$ μg/mouse is effective for less than 1 hr (Walden et al., 1988). A time-release process may extend the duration of the radioprotection. Since LTC_4 is a mediator of inflammation (Sirosis, 1985; Bach, 1983), questions concerning its prolonged use need to be addressed. It may be more feasible to develop analogs of LTC_4 that retain its radioprotective properties without some of the more potent biological effects. More work is necessary to delineate possible roles of LTC_4 in radiotherapy and develop analogs for radioprotection.
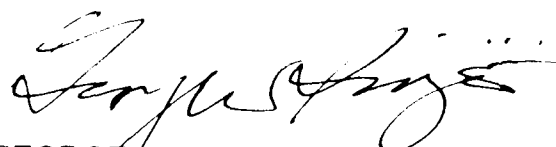
REFERENCES

Bach, M. K. (1983) The Leukotrienes: Their Structure, Actions, and Role in Diseases. UpJohn, Kalamazoo, Michigan.

Bach, M. K., Brashler, J. R., Hammerstrom, S. and Samuelsson, B. (1980) Identification of a component of rat mononuclear cell SRS as leukotriene D_4. Biochem. Biophys. Res. Commun. 93: 1121–1126.

Balapure, A., Watt, D. and Fitz, T. (1987) Specific binding sites for leukotriene C_4 (LTC) in diverse cells and bacteria. Fed. Proc. 46: 874.

Bray, M. A., Ford-Hutchinson, A.W. and Smith, M. J. H. (1981) Leukotriene B_4: Biosynthesis and biological activities. In: SRS-A and Leukotrienes, pp. 253–270. Piper, P. J. (ed.) Research Studies Press, Chichester.

Brocklehurst, W. E. (1962) Slow-reacting substance and related compounds. Prog. Allergy 6: 539–558.

Cheng, J. B., Lang, D., Bewtra, A. and Townley, R. G. (1985) Tissue distribution and functional correlation of [³H]leukotriene C_4 and [³H]leukotriene D_4 binding sites in guinea pig uterus and lung preparation. J. Pharmacol. Exp. Ther. 232: 80–87.

Chirkov, Y. Y. and Sobolev, A. S. (1985) Selective effect of isoproterenol on cell radiosensitivity determined by adrenoreceptor expression. Med. Radiol. (U.S.S.R.) 30: 55–58.

Clark, M. A., Cook, M., Mong, S., Hogaboom, G. K., Shorr, R., Stadel, J. and Crooke, S. T. (1984) Leukotriene C_4 ([³H]LTC₄) binding to membranes isolated from a hamster smooth muscle cell line (DDT_1MF_2). Life Sci. 35: 441–448.

Drazen, J. M., Austen, K. F., Lewis, R. A., Clark, D. A., Goto, G., Marfat,A. and Corey, E. J. (1980) Comparative airway and vascular activities of leukotrienes C-1 and D in vivo and in vitro. Proc. Natl. Acad. Sci. U.S.A. 77: 4354–4380.

Feldberg, W. and Kellaway, C. H. (1938) Liberation of histamine and formation of lysocithin-like substances by cobra venom. J. Physiol. (Lond.) 94: 187–226.

Fleisch, J. H., Rinkema, L. E. and Marshall, W. S. (1984) Commentary: Pharmacological receptors for the leukotrienes. Biochem. Pharmacol. 33: 3919–3922.

Ford-Hutchinson, A. W. (1986) Alternative fatty acids and the production and action of leukotriene B. Transplant. Proc. 18: 33–36.

Hanson, W. R. (1987) Radiation protection by exogenous arachidonic acid and several metabolites. In: Prostaglandins and Lipid Metabolism in Radiation Injury, pp. 233–243. Walden, T. L. and Hughes, H. N. (eds) Plenum Press, New York.

Hanson, W. R. and Ainsworth, E. J. (1985) 16,16-Dimethyl prostaglandin E_2 induces radioprotection in murine intestinal and hematopoietic stem cells. *Radiat. Res.* **103:** 196–203.

Hogaboom, G. K., Mong, S., Wu, H.-L. and Crooke, S. T. (1983) Peptidoleukotrienes: distinct receptors for leukotriene C_4 and D_4 in the guinea pig lung. *Biochem. Biophys. Res. Commun.* **116:** 1136–1143.

Landauer, M. R., Walden, T. L. Jr, Davis, H. D. and Dominitz, J. A. (1987) Alterations in locomotor activity induced by radioprotective doses of 16,16-dimethyl prostaglandin E_2. In: *Prostaglandins and Lipid Metabolism in Radiation Injury*, pp. 245–251. Walden, T. L. and Hughes, H. N. (eds) Plenum Press, New York.

Muller, A., Ghiglieri-Bertez, C., Modat, G. and Bonne, C. (1987) Specific binding of leukotriene C_4 to endothelial cell membranes. *Prostaglandins, Leukotrienes Med.* **26:** 233–240.

Orning, L., Hammarstrom, S. and Samuelsson, B. (1980) Leukotriene D: A slow reacting substance from rat basophilic leukemia cells. *Proc. Natl. Acad. Sci. U.S.A.* **77:** 2014–2017.

Orning, L., Norin, E., Gustafsson, B. and Hammarstrom, S. (1986) In vivo metabolism of leukotriene C_4 in germ-free and conventional rats. Fecal excretion on N-acetylleukotriene E_4. *J. Biol. Chem.* **261:** 766–771.

Radmark, O., Malmsten, C., Samuelsson, B., Goto, G., Marfat, A. and Corey, E. J. (1980) Leukotriene A: Isolation from human polymorphonuclear leukocytes. *J. Biol. Chem.* **255:** 11828–11831.

Samuelsson, B., Borgeat, P., Hammarstrom, S. and Murphy, R. C. (1980) Leukotrienes: A new group of biologically active compounds. *Adv. Prostaglandin Thromboxane Leukotriene Res.* **6:** 1–18.

Sirois, P. (1985) Pharmacology of the leukotrienes. *Adv. Lipid Res.* **21:** 79–101.

Walden, T. L. Jr, Holahan, E. V. and Catravas, G. N. (1986) Development of a model system to study leukotriene-induced modification of radiation sensitivity in mammalian cells. *Prog. Lipid Res.* **25:** 587–590.

Walden, T. L. Jr, Patchen, M. L. and Snyder, S. L. (1987) 16,16-Dimethyl prostaglandin E_2 increases survival in mice following irradiation. *Radiat. Res.* **109:** 540–549.

Walden, T. L. Jr, Patchen, M. L. and MacVittie, T. J. (1988) Leukotriene-induced radioprotection of hematopoietic stem cells in mice. *Radiat. Res.* **113:** 388–395.

Welton, A. F., O'Donnell, M., Anderson, W., Crowley, H., Medford, A., Simko, B. and Yaremko, B. (1983) The role of cyclooxygenase products in some of the biological effects of chemically synthesized leukotrienes (LTB$_4$, LTC$_4$, LTD$_4$, and LTE$_4$). *Adv. Prostaglandin Thromboxane Leukotriene Res.* **12:** 145–152.

REVIEWED AND APPROVED

GARY H. ZEMAN
CDR, MSC, USN
Head, Military Requirements and
  Applications Department

GEORGE W. IRVING, III
Col, USAF, BSC
Director

AFRRI

TECHNICAL REPORT

A low-energy x-ray irradiator for electrophysiological studies

D. A. Schauer

G. H. Zeman

T. C. Pellmar

AFRRI TR88-2

CONTENTS

INTRODUCTION

High-dose-rate, acute, whole-body exposures have been the main focus of radiobiology research conducted at the Armed Forces Radiobiology Research Institute (AFRRI) for many years. Extensive quantitative studies analyzing behavioral effects, radiation induced syndromes, and combined injury phenomena have been conducted. The sources of radiation used in these studies are the AFRRI TRIGA Mark-F pulsing nuclear reactor, cobalt-60 whole-body facility, and 50-MeV linear accelerator.

Selective irradiation of specific organs has become an area of investigation with emphasis on mechanistic effects. Specifically, cellular and tissue studies have been initiated using the above-mentioned sources. For example, Tolliver and Pellmar (1) initiated a study to evaluate radiation damage to brain neurophysiology. Slices from the hippocampus of guinea pig brains were remotely irradiated in vitro and subsequently examined for neuronal damage by means of electrophysiological recording of neuronal activity. The remoteness of the radiation source in relation to the recording chamber presented some inherent limitations in this type of analysis:
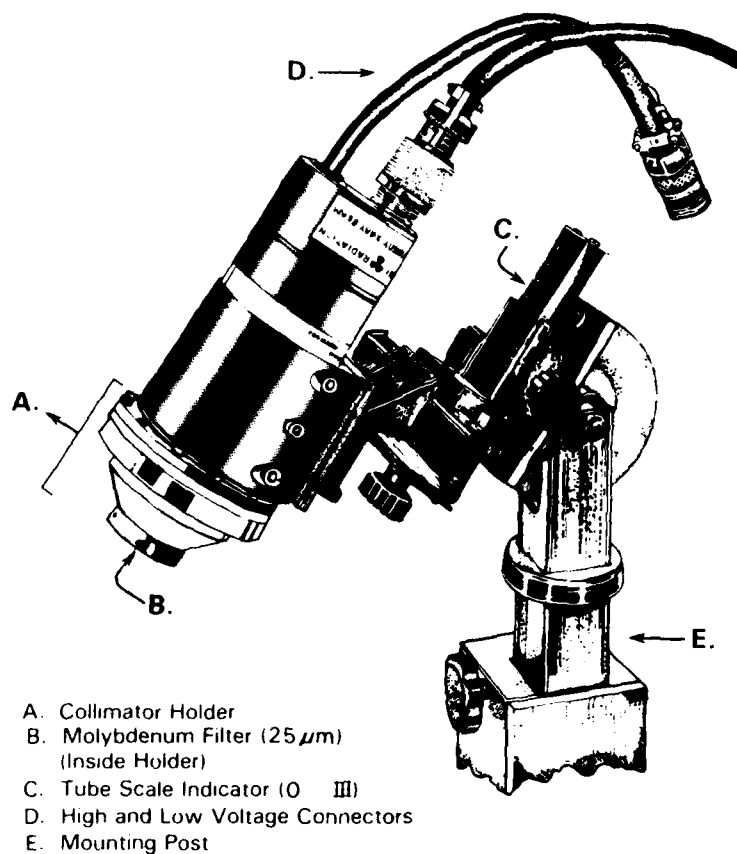
• The analysis of a large number of samples was required, and only large changes could be observed, since electrophysiological responses vary greatly even within the same animal.

• It was not possible to observe early transient neuronal effects because data could only be collected approximately 30 minutes postirradiation.

Despite the above limitations, Tolliver and Pellmar (1) documented statistically significant impairment in the function of the neural tissue at doses as low as 50 Gy with a dose rate of 20 Gy/min. While this research showing direct damage to neural tissue was a significant advance, it was desirable to study the effects of lower doses of radiation at earlier times. To accomplish this end, it was necessary to increase the experimental system's sensitivity by actually conducting tissue irradiations within the electrophysiology recording chamber. If this were possible, each brain slice preparation could act as its own control as the stimulating/recording electrodes remained in place before, during, and after the irradiation. This type of study would eliminate the limitations listed above and allow more subtle neuronal changes to be examined and quantified. A small x-ray unit was therefore set up to operate in a Faraday cage enclosing the electrophysiology recording apparatus.

RADIATION SOURCE

The source of radiation is a Kevex (K5010T) 50-kVp, 1-mA x-ray tube manufactured by Kevex X-ray Tube Division, Scotts Valley, CA (2). The system's key components are an x-ray head, x-ray tube with added molybdenum (Mo) filter, collimators, x-ray tube holder, x-ray source control

unit, and cables. (See figures 1 and 2 for schematics of the above components.) A detailed description of the various components follows.

A. Collimator Holder
B. Molybdenum Filter (25 μm)
   (Inside Holder)
C. Tube Scale Indicator (0   III)
D. High and Low Voltage Connectors
E. Mounting Post

Stainless Steel Collimators

(Front View)

(Top View)

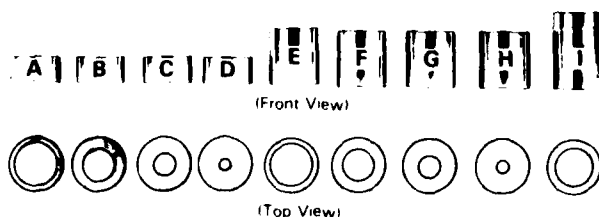Figure 1. Kevex 50 kVp/1 mA x-ray tube with added Mo filter, tube holder/ precision positioning stand, and stainless steel collimators. Tube is approximately 20 cm in length and 7 cm in diameter. Dimensions of the collimators are as follows: A-D, 15 mm in length, 20-5 mm inner diameter, respectively; E-H, 30 mm in length, 20-5 mm inner diameter, respectively; and I, 40 mm in length, 20 mm inner diameter.

4
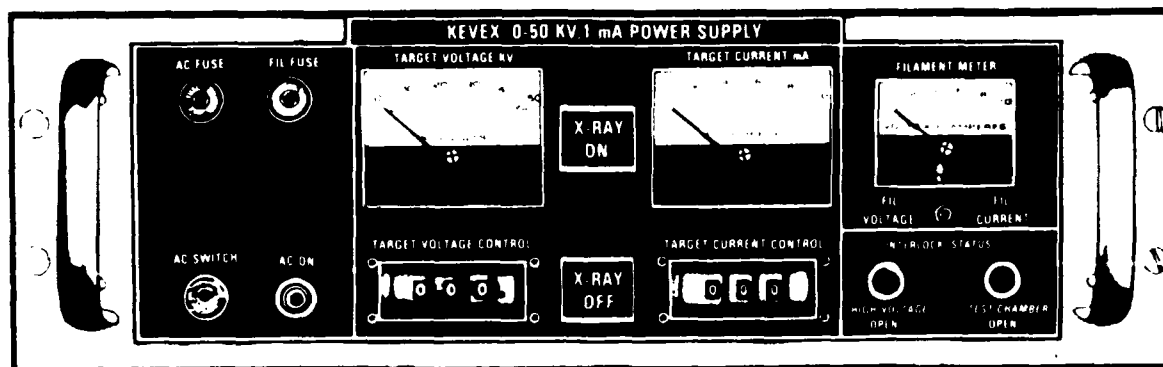
Figure 2. Standard 50 kVp and 1 mA power source.

X-RAY HEAD

The hermetically sealed and completely radiation-shielded x-ray head houses the x-ray tube and high- and low-voltage connectors. For high-voltage insulation and efficient heat conduction, the head is filled with a liquid dielectric. Additionally, a gas bubble is provided to accommodate differential expansion in materials due to heating.

X-RAY TUBE

The x-ray tube consists of a cathode, beam current and electron focal spot control grids, and an Mo transmission target. The oxide-coated, thermionic cathode is an indirectly heated electron emitter controlled by an electrostatic field produced by the grid potential. The first double grid, closest to the cathode, controls the electron beam emission; the second single grid, between the first grid and the target, controls the electron beam spot size. The focal spot grid operates independently from the beam emission grid and can be used to vary spot size from 0.5 to 4 mm in diameter. The transmission target yields x rays emitted in the direction of the longitudinal axis of the x-ray head. These x rays are further filtered with a 25-μm-thick Mo filter, added externally to the end of the tube adjacent to the 127-μm-thick beryllium transmission window. This Mo-Mo configuration should yield a quasi-monoenergetic x-ray spectrum consisting primarily of the approximately 17.4 keV K α x rays of Mo (3) (see table 1).

5

Table 1. Physical Aspects of the Molybdenum Target and Filter

K Series	Photon Energy (keV)	L Series		Photon Energy (keV)
K α 1	17.478	LIII	L ℓ	2.015
K α 2	17.373		L β 2	2.518
K β 1	19.607		L α 1	2.293
K β 2	19.964		LIII ab	2.523
K ab	20.002	LII	L β 1	2.395
			L γ 1	2.623
			LII ab	2.627
		LI	LI ab	2.884

With the 25-μm Mo filter, the predominant radiation should be the K α 1 series (relative intensity of 100) that results from the transition of L III to the K shell.   The K α 2 series or the L II to K shell occurs with a relative intensity of approximately 50.   The K β series, which is M III and M II to K, is of higher energy than K α; however, the relative intensity is only about 25.   Accordingly, the weighted averages (K α = 17.443 keV, K β = 19.663 keV) best describe the energy spectrum anticipated for this tube configuration, with K α most prevalent.

COLLIMATORS

The tube head is modified with an external adapter to hold various collimators (see figure 1) of three different lengths and three different inner diameters.

X-RAY TUBE HOLDER

The tube holder was locally designed and fabricated to allow variation of the tube positioning in the horizontal and vertical axes.   By using the positioning indicators as illustrated in figure 1, the distance between the tube and the specimen could be varied to control the dose rate to the sample.   This design also affords extremely accurate reproducibility in positioning the unit from run to run.

X-RAY SOURCE CONTROL UNIT

The 115 Vac, 60 Hz control unit consists of a filament grid bias and beam current control, focal spot size control, and high-voltage power supplies along with the control circuitry necessary to provide the settings/limits of operation (figure 2). The kV can be selected in the range 00.0 to 49.9 in steps of 00.1 kV, and the mA in the range 0.00 to 0.99 in steps of 0.01 mA.

CABLES

The power supply and tube are interfaced by separate high-voltage and multiconductor low-voltage cables. The cables, which are approximately 2.3 meters long, allow for remote operation of the unit.

IRRADIATION SYSTEM

To meet the unique requirements for this local in vitro irradiator, a system was designed in which the irradiation could be conducted inside a Faraday cage enclosing the electrophysiology recording chamber (see figures 3a,b). The purpose of the Faraday cage was to block out any external electromagnetic interference and allow accurate measurement of the low-level electrophysiological potentials. For these experiments, a lead-lined box replaced the standard copper mesh Faraday cage. The box's design and fabrication had to meet radiation safety and operational constraints.

The entire cage was shielded in accordance with the National Council on Radiation Protection and Measurements (NCRP) Report No. 49, "Structural Shielding Design and Evaluation for Medical Use of X-rays and Gamma Rays of Energies up to 10 MeV" (4). The criteria for the shielding design included a highly conservative assumption that the workload for the KEVEX x-ray tube could be as high as to include continuous operations with the beam for up to 10 hours per day, 6 days per week, at maximum voltage (50 kVp) and tube current (1 mA), i.e., W = 3600 mA•min/week, and that occupancy by members of the general public would be possible at any location within 0.4 meter from the tube while it operated within the shield. On the basis of these assumptions, the required shielding thicknesses derived from appendix C, table 8, of NCRP Report No. 49 were 0.75 mm lead (Pb) or 7.5 cm concrete for the primary (direct beam) barrier, and 0.60 mm Pb or 5.5 cm concrete for secondary (leakage/scatter) barriers.

The installed shielding of 1 mm Pb in the walls of the box and the 0.8 mm Pb-equivalent plastic in the window and top of the box met the above criteria. Likewise, the 10-cm-thick marble (density of 2.47-2.86 g/cm^3) table top was even more massive than the concrete (density 2.35 g/cm^3) thickness required for a primary barrier, so no additional shielding was required on the table top.

(a)

38"

Visual Warning Light

Pb Bar

49"

39"

26"

Closed View

(b)

Visual Warning Light

Folding Doors

Folding Doors

Open View

A Kevex 50 kVp 1 mA X Ray Unit
B Base of Interior 4" Marble (Primary Barrier) *Rests on Air Cushion
C Interlocks
D Clear Pb plastic

*The Entire Unit is Shielded With Lead Walls (1mm Thick) (Secondary Barrier)
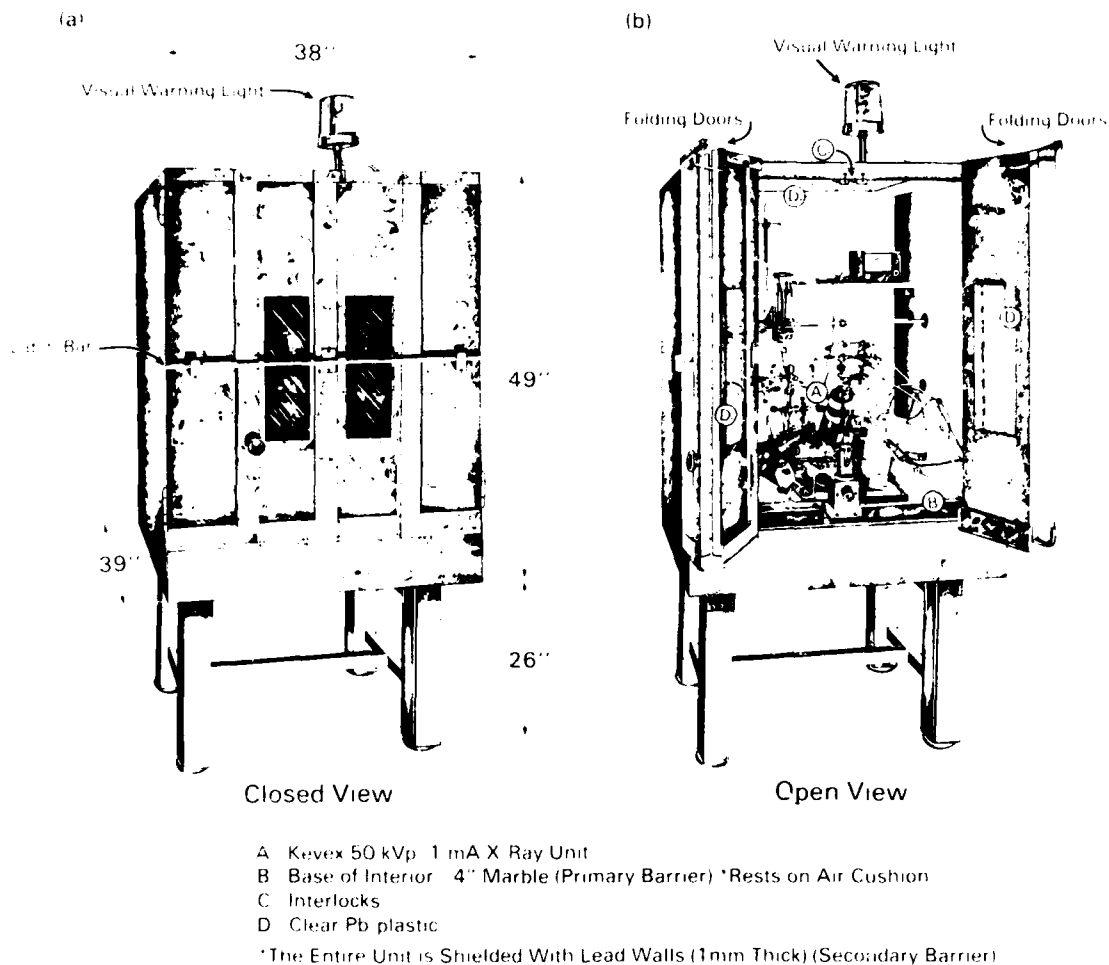
Figure 3. Lead-shielded Faraday cage: (a) closed view; (b) open view with
x-ray tube in place.

Note that the x-ray shielding parameters covered in NCRP Report No. 49
apply to tungsten target x-ray tubes (4). This fact leads to some
overestimation of the shielding requirements for an Mo target x-ray tube
because the bremsstrahlung x-ray spectrum has reduced output intensity from
the lower atomic number target. The highly intense low-energy (17-19 keV)
characteristic x rays from Mo do not affect the shield design because they are
preferentially absorbed in the initial layers of the shield, compared to the
more energetic (20-50 keV) and penetrating bremsstrahlung portion of the x-
ray spectrum.

The 0.8 mm Pb-equivalent plastic (Nuclear Associates, Carle Place, NY) used in the window was included to allow the investigator to view the sample during irradiation. The ability to see inside the box during irradiation proved beneficial in aligning the field. To allow ample light into the array, a section of the top of the box was also made of the Pb-equivalent plastic.

Interlock recommendations for an x-ray apparatus are described in NCRP Report No. 88, "Radiation Alarms and Access Control Systems" (5): "Areas containing radiation-producing equipment or sources that could produce potential doses in the high-to-extreme categories should have interlocks as an integral part of their access control system."

An interlock system was designed and installed with the benefit of the interlock jack on the back of the power supply. The system consisted of an interface box between the power supply and the x-ray tube that first had to be turned on to supply power to the system. Additionally, whenever the switch was ON, a red warning light was illuminated. Microswitches were also installed on both doors so that the doors required positive pressure (i.e., both doors secured with a latch bar, as illustrated in figure 3a) before power could be supplied to the unit. The design of this system was "fail-safe" in that if the interlock was violated in any way, all radiation production ceased immediately. Last, when the interlock was tripped, the system required manual resetting to prevent a sudden surge of power to the x-ray tube.

NCRP Report No. 88 (5) also recommends a warning light as a caution to other personnel in the lab that radiation is in progress. Such a light was installed in conjunction with the interlock system. The light is ON whenever power is provided to the unit.

DOSIMETRY PROCEDURES

IONIZATION CHAMBER

A Capintec parallel-plate ionization chamber (Model No. PS-033) was used to determine the exposure rate from the tube. The sensitive volume of the detector was 0.5 cm^3, and the aluminized mylar window was 0.5 mg/cm^2 thick. The diameter of the detector's sensitive area was 16 mm. The detector and electrometer were calibrated at the National Bureau of Standards for two beam codes (L20 and L50) to span the x-ray energy range encountered in these experiments. (See appendix A.) The difference of 2.4 percent between the two calibration factors indicates that the chamber response varies only slightly over a wide spectrum of low energies. The chamber was operated at ±300 volts bias, and all data represent average readings made at opposite polarities, which differed by no more than 0.5 percent.

9

RADIOGRAPHIC FILM

The x-ray film used in these tests was Kodak X-Omat V film (for therapy verification) in paper packs. The film was exposed at 5 cm from the end of the collimator holder with the tube positioned at the normal operating angle (35° from vertical). Collimators A-I and the open beam were analyzed at a 25 kV and 0.2 mA setting for a 30-second exposure. The open beam density was studied using density scans in the horizontal and vertical axes to quantify the field's consistency and, hence, the exposure rate.

BEAM DIAMETER GAUGE

A fluorescent screen beam diameter gauge (Nuclear Associates Model No. 07-604) was used to position the chamber for measurements taken inside the array. The room and cage were darkened, and the fluorescent screen was placed in the array at the tissue's location. The tube was then powered up, and the beam location and size were viewed through the front panel. This observation provided vital information for the radiation's angle and the chamber's positioning for dosimetry. Accordingly, the sample holder was modified to allow the chamber to be situated in the exact center of the beam where radiograph studies indicated that the exposure rate was constant. Furthermore, the chamber's center coincided with the tissue location during normal radiations, and the top of the chamber was at the same height as the sample. The beam diameter gauge data were confirmed with the radiograph results (addressed further in the Results section). The characterization of the beam using the above techniques allowed for determination of dose rates at various points. Once this information was determined, the chamber was removed and the irradiations were performed for calculated periods of time until the desired doses were delivered.

DOSIMETRY CALCULATIONS

Electrical charge from the parallel-plate ionization chamber was collected using a Keithley 616 electrometer set in the charge (10^{-9} C) mode, which was in turn interfaced with a Hewlett-Packard (HP) data acquisition unit and an HP-85 computer. The exposure (X) in roentgens (R) was calculated from the average of 10 sequential readings taken over 10-second intervals (M) at both polarities with the chamber irradiated free-in-air with no buildup as follows:

$$X = M \bullet N_x \bullet K_q \bullet K_{tp}$$

where N_x was the NBS exposure calibration factor for the chamber in the L50 field (see appendix A), K_q was the electrometer correction factor (see appendix A), and K_{tp} was the temperature (T) and pressure (P) correction factor given by

10

$$K_{tp} = \frac{273.2 + T \ (^{O}C)}{295.2} \cdot \frac{760}{P \ (mm \ Hg)} .$$

The dose (D_m) was calculated as follows:

$$D_m = X \cdot f_{med}$$

where

$$f_{med} = 0.873 \left[\frac{\mu_{ab}}{\rho} \right]^{med}_{air} \quad \text{for various materials in cGy/R.}$$

For approximately 17.4 keV photons in water, $f_{med} = 0.889$ (6).

An aqueous solution perfused the tissue slices being studied in the electrophysiology recording chamber to maintain tissue viability during the experiments. A dose attenuation factor was applied to account for the thin layer of water covering the sample. On an average, the tissue was under 0.5 mm of water, so the dose to the tissue (D_{mt}) was calculated as follows:

$$D_{mt} = D_m \cdot I/I_o$$

where I/I_o is the correction factor for the attenuation of the primary beam by 0.5 mm of water. Using μ/ρ for approximately 17.4 keV photons in water, the attenuation correction was 0.943 (see table 2). During normal perfusion of the tissue sample, it was estimated that the amount of water on top of the sample could vary by as much as ±0.2 mm. This variance would cause the above attenuation correction factor to vary by ±2.2 percent.

RESULTS

DOSE RATE VERSUS CURRENT

With a constant potential difference setting of 49 kV and the tube positioned at 10.7 cm from the anode to the detector (i.e., Tube Scale Indicator 0), dose rate data were collected for 0.1 mA, 0.3 mA, 0.5 mA, 0.7 mA, 0.9 mA, and 0.99 mA. The increase in radiation output was linear with the increase in current, and figure 4 is a plot of the data acquired. With this inherent linear characteristic, the dose rate from the tube can be changed by varying the current without having to reposition the tube.

Table 2. Table of Mass Attenuation Coefficients (μ/ρ) for Photon Energies 10 keV to 50 keV

Energy (keV)	Medium			
	Lucite	Water	Brain*	Soft Tissue*
10	2.273	5.223	5.338	4.783
15	1.077	1.639	1.687	1.523
17.4 $^+$	0.835	1.244	1.280	1.161
20	0.562	0.796	0.819	0.750
30	0.301	0.372	0.379	0.358
40	0.234	0.267	0.270	0.261
50	0.207	0.226	0.228	0.222

Units: cm^2/g

*As defined by the International Commission on Radiological Protection (ICRP)
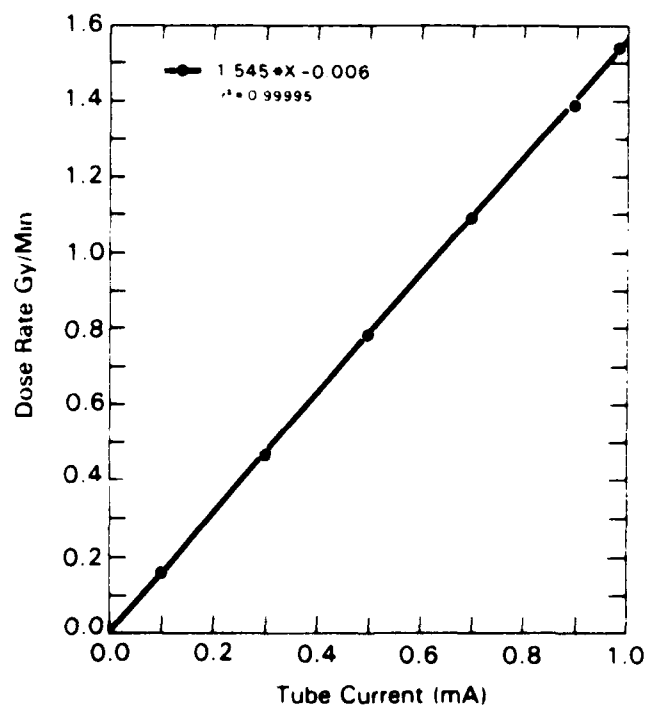
$^+$Values based on interpolation

Figure 4. Dose rate vs. current (mA) with a constant potential of 49 kV.

DOSE RATE VERSUS POTENTIAL DIFFERENCE

With a constant current setting dose rate, data were collected for 10 kV, 20 kV, 30 kV, 40 kV, 45 kV, and 49 kV. The data plotted in figure 5 show a curvilinear response for the filtered (25 μm Mo) and the unfiltered configurations. The effect of the 25-μm Mo filter was to reduce the measured dose rate by a factor of 16 at 49 kV to 33 at 20 kV, and to accentuate the curvature of the output curve. In routine use, the unit was set up to operate at a fixed 49 kV.

DOSE RATE VERSUS DISTANCE

Dose rates measured at varying distances from the four tube scale indicators were compared to confirm the expected inverse square behavior of the x radiation. See figure 6 for the plotting of the above data. Table 3 lists the results obtained.

RADIATION QUALITY

Half-value layer (HVL) and homogeneity coefficient are frequently used to describe the quality of an x-ray beam. HVL is the thickness of a material that reduces the exposure rate of the beam to one-half (7). The homogeneity coefficient is the quotient of the thickness of attenuator required to reduce the exposure rate to one-half divided by the thickness of attenuator required to further reduce the exposure rate from one-half to one-fourth. The material used in the 10- to 120-kV range is usually aluminum (Al) (density = 2.70 • 10^3 kg/m^3) and a chemical purity of >99.8 percent (8). To minimize the number of scattered photons that are detected, narrow-beam geometry or "good geometry" was used. All measurements were made at a distance of approximately 0.5 m focus-to-surface distance with the Al attenuators placed halfway. The tube setting was 49 kV and 0.99 mA, and the 25-μm Mo filter was positioned at the end of the tube.

As plotted in figure 7, the first and second HVL's for the unfiltered beam were 0.1 mm and 0.24 mm, for a homogeneity coefficient of 0.42. For the 25-μm Mo-filtered beam, the first HVL was equal to 0.40 mm Al, and the second HVL was equal to 0.46 mm Al; the homogeneity coefficient for the beam was therefore 0.87. Thus, for the filtered beam, the HVL (0.41 mm Al) agrees within 3 percent with the calculated HVL (0.40 mm Al) for 17.4 keV photons. This close agreement demonstrates the quasi-monoenergetic nature of the Mo-filtered x-ray beam.
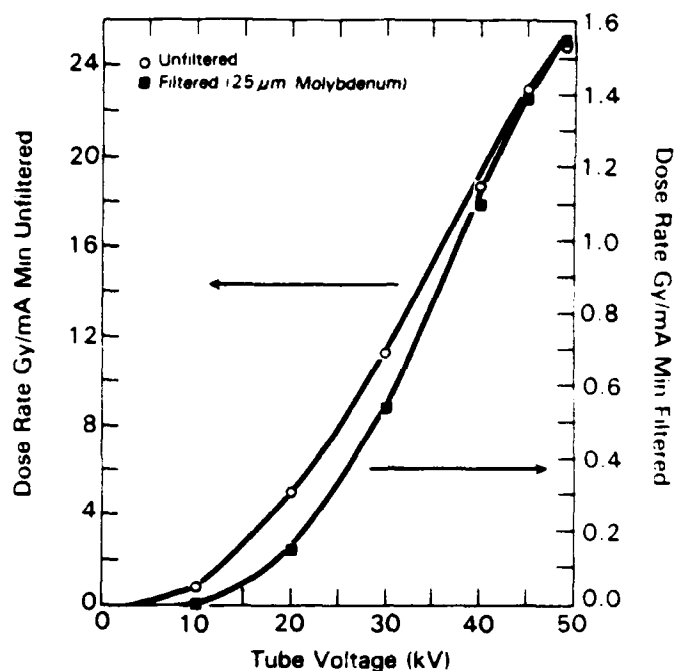
Figure 5. Dose rate vs. potential difference (kV) with a constant current
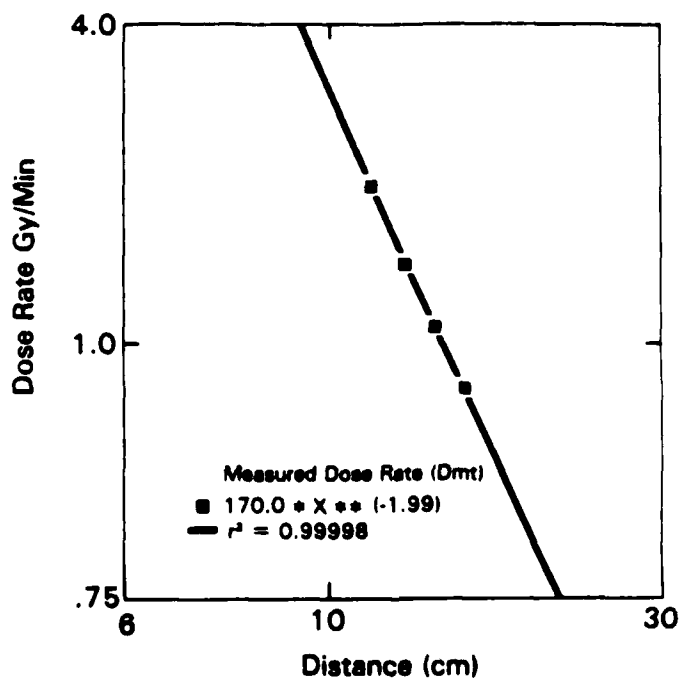normalized to 1 mA for filtered and unfiltered tubes.

Figure 6. Dose rate vs. distance (focus-to-surface distance). Slope of the
line, -1.99 vs. expected -2.0, confirms expected inverse square behavior of
x-ray output. See table 3 for details.

Table 3. Radiation Dose Rates

Tube Scale Indicator	TDD* (cm)	FSD† (cm)	Gy/min
0	5.0	10.7	1.54
I	6.0	11.7	1.28
II	7.0	12.7	1.10
III	8.0	13.7	0.94

*TDD: tube-detector distance, which is measured from the end of the tube to the surface of the detector. The tube scale indicator is marked to allow easy and accurate variation in the TDD.

†FSD: focus-to-surface distance, which is the sum of the TDD plus 5.7 cm (the distance from the end of the tube collimator to the Mo target). The 5.7-cm distance was provided by the tube manufacturer.
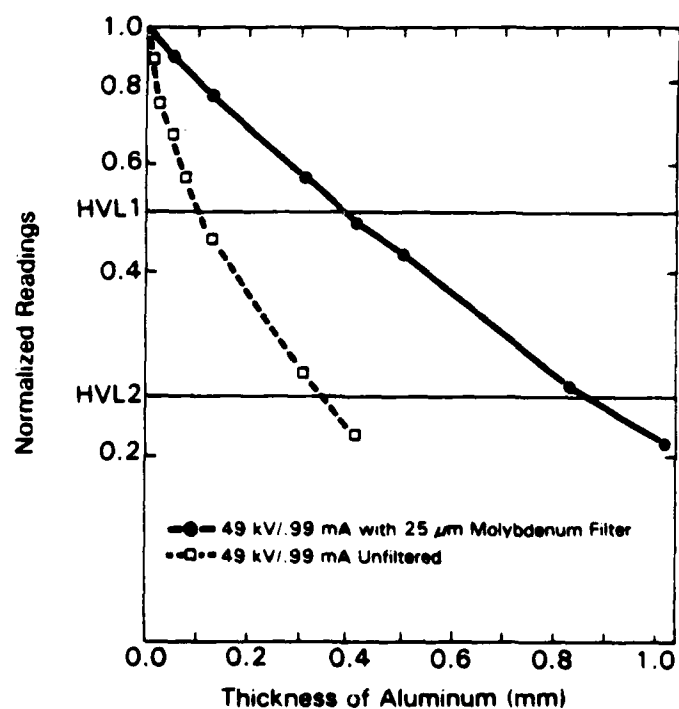

Figure 7. Half-value layer measurements for filtered and unfiltered tubes.

BEAM UNIFORMITY AND PENUMBRA

As indicated in the Dosimetry Procedures section, radiographs of the nine collimated beams and the open beam were taken and analyzed. Table 4 summarizes the results of the beam diameter measurements for the horizontal and vertical axes with a focus-to-surface distance of 10.7 cm.

The diameter in the vertical axis was in all cases greater than that in the horizontal axis because of the requirement of radiating at a 35° angle. Because of constraints imposed by the electrophysiology apparatus, it was necessary to angle the tube at 35°. Since the radiation must be conducted at an angle, the beam is ellipsoidal.

Table 4. Collimated Field Sizes

	Diameter (mm)	
Collimator	Horizontal	Vertical
A	25	27
B	21	23
C	13	15
D	05	06
E	24	26
F	18	20
G	11	13
H	05	06
I	22	24
OPEN	26	27

Preliminary density scans of the film showed that the optical density in the center of the beams varied less than 5 percent between the various collimators. Also, each beam profile appeared to be of uniform density with no artifacts other than a surrounding penumbra region. From these results it was concluded that the dose rate was approximately the same for all collimators, so that the output data for the OPEN beam applied to all other beam sizes. This finding was particularly important because of the relatively large diameter (16 mm) of the ionization chamber used to measure dose rates. Further analysis of the OPEN beam was conducted using the Drexel Image Processing Center Brain software package (see figures 8 and 9).

In the horizontal direction, the penumbra region was 8 mm wide on both sides of the main beam (i.e., the 26-mm region). During dose measurements, it was crucial to keep the ionization chamber out of this region. The vertical analysis provided integral information in the area of tissue positioning.

Another effect of angling the tube is that the beam intensity varied according to inverse square. Quantification of the film's density in the 27-mm vertical region indicated an optical density of 0.59 in the center of the beam. Due to inverse square, the density closest to the tube was 0.61; the density farthest from the tube was 0.56. The difference in output relative to the center of the beam, at which the doses in table 3 are quoted, could vary from 3 to 5 percent.
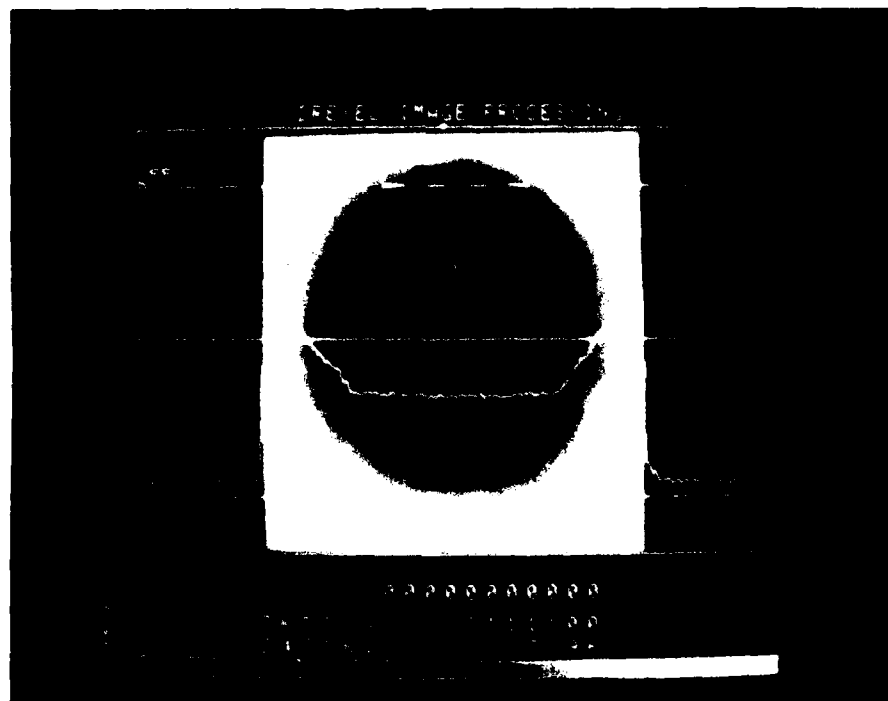
Figure 8. Beam uniformity and penumbra analysis in the horizontal axis. Optical density is constant across the field.

Figure 9. Beam uniformity and penumbra analysis in the vertical axis. Because of the 35° angle of the x-ray tube during radiation, optical density is greater close to the tube and less as distance increases, relative to the center of the beam. Dose rates across the useful area of the beam vary from 3 to 5 percent.

DEPTH DOSE

Depth-dose measurements were done by positioning sheets of lucite on top of the Capintec chamber. The referenced mass attenuation coefficient for lucite (0.835 cm^2/g) (9) for approximately 17.4 keV photons was in close agreement with the experimental measurements (figure 10).

Figure 10. Depth dose through lucite. Slope of the line is -0.77 cm^2/gm, which agrees with referenced mass attenuation coefficient for 17.4 keV photons in lucite to within 8 percent (see table 2). Referenced value includes coherent scattering, which, it is believed, accounts for much of the disparity.
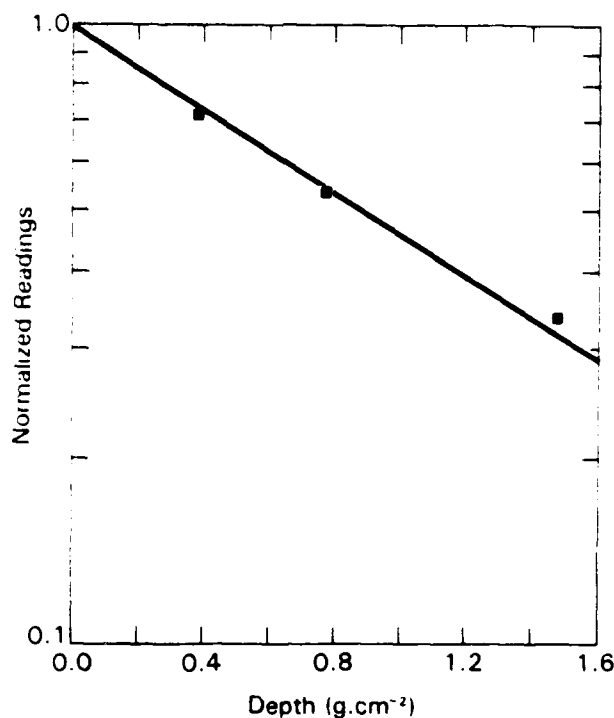
RADIATION SAFETY SURVEY

A comprehensive radiation safety survey was conducted to evaluate the primary and secondary protective barriers for the primary beam and leakage/scatter (10). A multistep survey process was conducted and included the following:

- Film studies around the tube head verified its shielding integrity.

- Lead sheets and lead overlaps were examined visually at all edges and joints.

- A qualitative shield survey was conducted with ^{99m}Tc (technetium) and a pancake Geiger-Müller (GM) counter.

- A quantitative shield survey was conducted with x rays at maximum kV and mA in the actual scatter geometry, using a GM tube to find hotspots and an ionization chamber to measure mR/hr.

The maximum radiation leakage of <0.5 mR/hr quoted by the x-ray tube manufacturer (appendix B) was confirmed using a Victoreen 471 survey meter in contact with the tube while operating at maximum power. Additionally, film studies were conducted around the tube, and results were negative for pinhole leakage.

Visual examination of all lead sheets/overlaps before operation each day was imperative. Because of the malleable characteristic of lead, the joints and edges can bend, and streaming could occur. The Standard Operating Procedures (appendix C) emphasize the need to visually inspect the entire cage as part of the routine start-up procedure.

For the qualitative survey, an unshielded vial containing 4 mCi of ^{99m}Tc was positioned in the lead box, and a sensitive GM survey meter was used to locate any hotspots. During the initial survey, readings of up to 5 mR/hr were noted at the edges and joints. Accordingly, the cage was modified to ensure that no readings above background were obtained outside the lead box.

Last, the quantitative survey was conducted with the tube settings at maximum kV and mA. The Victoreen 471 survey meter was used with particular attention given to the joints and edges. The modifications mentioned above were sufficient as no readings above 0.05 mR/hr were noted.

DISCUSSION

This system provides a unique radiation capability with built-in flexibility that allows the investigator to observe even the most subtle changes. Further, the quantitative study of radiobiological damage on the cellular level is much easier. The following are some additional advantages of the system:

• The entire unit is in the lab, under the user's control. Radiations can be performed whenever the biological system is ready.

• Simultaneous radiation and observation of the sample, both visually and by microelectrodes.

• Variable dose rates.

• The tube is easily removed with highly reproducible dose rates after repositioning.

• Various collimators are provided to give selected beam diameters.

• The Mo-Mo target/filter system gives an excellent compromise between high-dose rate and acceptable penetration ability of the beam. The x-ray energy spectrum is quasi-monoenergetic with well-defined radiation quality.

- The x-ray tube is extremely small and operates at low power with no external cooling system. The x-ray tube is also capable of versatile positioning in a complicated experimental apparatus.

- During tube operation, no electrical interference is noted on electrophysiology recordings.

This unit is a prototype, and with such a system come many learning experiences. Some recommendations for future improvements are as follows:

- Encase the lead sheets in plywood to avoid possible sagging problems.

- Install a shutter to eliminate the radiation dose delivered during the brief, 1-minute warm-up time (see appendix C). For high-dose radiations (>6 Gy), the warm-up dose is negligible (<1 percent) compared to the total dose delivered. However, for low-dose radiations, special accounting may be necessary for the dose delivered during the brief warm-up period.

- Improve the alignment and positioning mechanism to give more versatile beam location.

- Develop the capability to deliver dose rates as high as 20 Gy/min.

- Acquire a smaller diameter parallel-plate ionization chamber, which, from a dosimetry perspective, would be advantageous in dealing with a narrow beam.

- Install a rugged and submersible beam intensity monitor for active in-beam dosimetry, such as a small (<1 mm^3) plastic scintillation detector.

The x-ray apparatus described in this report is currently being used to conduct local in vitro radiations of the hippocampal region of guinea pig brains. Preliminary quantification of the electrophysiological response indicates the apparatus is suitable for this application.

ACKNOWLEDGMENTS

REFERENCES

1. Tolliver, J. M., and Pellmar, T. C. Ionizing radiation alters neuronal excitability in hippocampal slices of the guinea pig. _Radiation Research_ 112: 555-563, 1988.

2. Operation and Maintenance Manual (K5010 and K5020). Kevex X-ray Tube Division, Scotts Valley, CA, 1983.

3. Marshall, M., Peaple, L. H. J., Ardran, G. M., and Crooks, H. E. A comparison of X-ray spectra and outputs from molybdenum and tungsten targets. _British Journal of Radiology_ 48: 31-39, 1975.

4. Structural Shielding Design and Evaluation for Medical Use of X rays and Gamma Rays of Energies up to 10 MeV. NCRP Report No. 49. National Council on Radiation Protection and Measurements, Washington, DC, 1976.

5. Radiation Alarms and Access Control Systems. NCRP Report No. 88. National Council on Radiation Protection and Measurements, Bethesda, MD, 1986.

6. Johns, H. E., and Cunningham, J. R. _Physics of Radiology_. Charles C. Thomas, Springfield, IL, 1983.

7. Radiation dosimetry: X-rays Generated at Potentials of 5 to 150 kV. ICRU Report No. 17. International Commission on Radiation Units and Measurements, Washington, DC, 1970.

8. Hendee, W. R. _Medical Radiation Physics_, 2d ed. Year Book Medical Publishers, Inc., Chicago, 1984.

9. Hubbell, J. H. Photon mass attenuation and energy-absorption coefficients from 1 keV to 20 MeV. _International Journal of Applied Radiation and Isotopes_ 33: 1269-1290, 1982.

10. Radiological Safety Instruction (RSI) 530: Radiation-Producing Machines. Armed Forces Radiobiology Research Institute, Bethesda, MD, 20 August 1979.

APPENDIX A. NBS CALIBRATION REPORTS

DG 8454 85
TFN G45095
1985 OCT 30

U. S. DEPARTMENT OF COMMERCE

NATIONAL BUREAU OF STANDARDS

GAITHERSBURG, MD 20899

REPORT OF CALIBRATION

CAPINTEC CHAMBER

MODEL PS-033   SERIAL NUMBER CII.334495

MANUFACTURED BY CAPINTEC INSTRUMENT CO.
            MONTVALE, NJ 07645

SUBMITTED BY ARMED FORCES RADIOBIOLOGY RESEARCH INSTITUTE
            BETHESDA, MD 20814-5145

RECEIVED AT NBS ON 1985 SEP 23

THE CALIBRATION FACTORS GIVEN IN THIS REPORT ARE QUOTIENTS OF THE
X- OR GAMMA-RAY EXPOSURE AND THE CHARGE GENERATED BY THAT RADIATION
IN THE IONIZATION CHAMBER. CHARGE WAS MEASURED FOR BOTH POLARITIES OF
THE STATED POTENTIAL AND THE AVERAGE VALUE WAS USED IN COMPUTING THE
CALIBRATION FACTOR. LEAKAGE CORRECTIONS WERE APPLIED IF NECESSARY.
IF THE CHAMBER WAS OPEN TO THE ATMOSPHERE THE MEASUREMENTS WERE
NORMALIZED TO ONE STANDARD ATMOSPHERE AND 22 DEGREES CELSIUS. USE OF
THE CHAMBER AT OTHER PRESSURES AND TEMPERATURES REQUIRES NORMALIZATION
OF THE ION CURRENTS TO THESE REFERENCE CONDITIONS. THE NORMALIZING
FACTOR F IS COMPUTED FROM THE FOLLOWING EXPRESSION:

$$F = (273.15 + T)/(295.15\ H)$$

WHERE T IS THE TEMPERATURE IN DEGREES CELSIUS, AND
        H IS THE PRESSURE EXPRESSED AS A FRACTION OF A STANDARD
ATMOSPHERE. (1 STANDARD ATMOSPHERE = 101.325 KILOPASCALS = 1013.25
MILLIBARS = 760 MILLIMETERS OF MERCURY)
        THE EXPOSURE RATE AT THE CALIBRATION POSITION WAS MEASURED BY A
FREE-AIR IONIZATION CHAMBER FOR X RADIATION, AND BY GRAPHITE CAVITY
IONIZATION CHAMBERS FOR COBALT-60 AND CESIUM-137 GAMMA RADIATION.
THE GAMMA-RAY EXPOSURE RATES WERE CORRECTED TO THE DATE OF CALIBRATION,
FROM PREVIOUSLY MEASURED VALUES, BY DECAY CORRECTIONS BASED ON
HALF-LIVES OF 5.27 AND 30.0 YEARS, FOR COBALT-60 AND CESIUM-137
RESPECTIVELY.

THE UNCERTAINTY OF THE EXPOSURE-RATE MEASUREMENTS IS BELIEVED TO
BE WITHIN ONE PERCENT AND THE ION CURRENT MEASUREMENTS ARE BELIEVED
TO BE ACCURATE TO WITHIN A FEW TENTHS OF ONE PERCENT.
THE CALIBRATION FACTOR IS GIVEN TO FOUR DIGITS TO PREVENT
ROUNDING ERRORS UP TO 0.5 PERCENT WHEN THE FIRST DIGIT IS UNITY.
INFORMATION ON TECHNICAL ASPECTS OF THIS REPORT MAY BE OBTAINED
FROM J. T. WEAVER OR P. J. LAMPERTI. RADIATION PHYSICS C210.
NATIONAL BUREAU OF STANDARDS. GAITHERSBURG. MD 20899. (301) 921-2361.

REPORT REVIEWED BY

REPORT APPROVED BY R. LOEVINGER

FOR THE DIRECTOR
BY

RANDALL S. CASWELL
CHIEF. IONIZING RADIATION DIVISION
CENTER FOR RADIATION RESEARCH
NATIONAL MEASUREMENT LABORATORY

DG 8454 85
1985 OCT 30

NATIONAL BUREAU OF STANDARDS REPORT OF CALIBRATION

ARMED FORCES RADIOBIOLOGY RESEARCH INSTITUTE
BETHESDA. MD 20814-5145

CAPINTEC CHAMBER
MODEL PS-033   SERIAL NUMBER CII.334495
OPEN TO THE ATMOSPHERE WHEN TESTED
WALL POTENTIAL WAS - AND - 300 VOLTS WITH RESPECT TO INNER ELECTRODE

BEAM CODE	HALF-VALUE LAYER AL (MM)	CU (MM)	CALIBRATION FACTOR 22 DEG C AND 1 ATM	DIST (M)	BEAM SIZE (MM)	EXP RATE (R·S)
L20	.07		6.349E+09 R/C	.50	C 43	1.2E+00
L50	.75		6.502E+09 R/C	.50	C 43	2.6E-01
M300	21.90	5.3	*6.723E+09 R/C	.78	C 26	6.0E-02
CO-60		14.9	*6.970E+09 R/C	1.46	S 63	4.2E-01

DURING CALIBRATION THE CAVITY WAS POSITIONED IN THE CENTER OF THE BEAM
WITH THE STEM PERPENDICULAR TO THE BEAM DIRECTION. THE WINDOW
FACED THE SOURCE OF RADIATION.

3.E-15 AMPERES WAS THE LEAKAGE CURRENT MEASURED BEFORE CALIBRATION.

.998 WAS THE RATIO OF THE AVERAGE FOR BOTH POLARITIES OF THE
CURRENTS MEASURED AT FULL COLLECTION POTENTIAL. TO THE AVERAGE FOR
HALF COLLECTION POTENTIAL FOR A CURRENT OF 7.5E-12 AMPERES. A DETAILED
SATURATION STUDY WAS NOT CARRIED OUT AND NO CORRECTION FOR LACK OF
SATURATION WAS APPLIED TO THE DATA.

1.2% WAS THE LARGEST DIFFERENCE BETWEEN THE CURRENTS MEASURED FOR FULL
POSITIVE AND NEGATIVE COLLECTION POTENTIALS. THIS OCCURRED FOR THE
BEAM QUALITY M300.

* THE CHAMBER WALL THICKNESS WAS INCREASED FOR THIS BEAM QUALITY BY
ADDITION OF THE SHELL SUPPLIED WITH THE CHAMBER.

NOTE: THE REFERENCE PLANE FOR THIS CHAMBER WAS THE FRONT SURFACE OF THE
PLASTIC BODY FOR BEAM CODES L20 AND L50. AND THE FRONT SURFACE OF THE
EQUILIBRIUM SHELL FOR BEAM CODES M300 AND CO-60.

CHECKED BY *P. Lampert*

27

TFN G44975
DB 819:151
1985 SEP 06

<div align="center">

U. S. DEPARTMENT OF COMMERCE
NATIONAL BUREAU OF STANDARDS
GAITHERSBURG, MD 20899

REPORT OF TEST

</div>

Keithley Electrometer   Electrometer Serial Number 163317
Model 616
Manufactured by Keithley Instrument Company
            Cleveland, OH 44137

Submitted by Armed Forces Radiobiology Research Institute
            Bethesda, MD 20814

Received at NBS on 1985 AUG 09

The referenced electrometer has been tested for use with the ionization chamber
covered by Report of Calibration DG 8425/85. The system was tested for the
following combination of switch positions:

Switch	Position
Function	10^{-9} C
Mode	Fast
Sensitivity	Auto
Bias	N/A
Input	N/A
Background	N/A

When the electrometer charge measurements were corrected by K_Q, where

$$K_Q = 0.986$$

measurements with the system using Beam Code Co-60 were found to be consistent
with the calibration factor in DG 8425/85. K_Q was determined by injecting a
known charge into the electrometer input and observing the corresponding change
in the charge reading. The value of the injected charge is believed to have an
uncertainty of less than 0.1%.

The exposure in air at the reference point of the ionization chamber, with the chamber replaced by air, is given by

$$X = K_Q \, F \, Q \, N = 0.986 \, F \, Q \, N$$

where
    N is the chamber calibration factor in terms of exposure per unit charge, for stated conditions of calibration;
    Q is the change in charge on the electrometer system as indicated by the digital panel-meter readings, using the tested combination of switch positions; and
    F is a factor that normalizes the measurements to the temperature and pressure reference conditions for N. F is defined in Report of Calibration DG 8425/85.

Information on technical aspects of this report may be obtained from P. J. Lamperti, Radiation Physics C210, National Bureau of Standards, Gaithersburg, MD 20899, (301) 921-2361.

Measurements supervised by P. J. Lamperti

Report approved by R. Loevinger

For the Director
by

Randall S. Caswell
Chief, Ionizing Radiation Division
Center for Radiation Research
National Measurement Laboratory

APPENDIX B.   TUBE SPECIFICATIONS

FINAL TEST DATA SHEET
FOR
X-RAY PRODUCTS

MODEL K __5010 Tmo__ S/N __3183__

TARGET MATERIAL __Moly__

TEST CONDITIONS:

TARGET VOLTAGE   __50__   KILOVOLTS DC

TARGET CURRENT   __1.0__   MILLIAMPERES DC

FILAMENT VOLTAGE   __6.3__   VOLTS RMS (REF)

AMBIENT TEMPERATURE   22 +/- 2 DEGREES CENTIGRADE

WARM-UP PERIOD   30 MINUTES MINIMUM

TESTED WITH: K __5010 P/S__ S/N __1500__

    TEST STAND A - SI(LI) DET.   (X TEST STAND B - SCINT. DET.

LONGTERM X-RAY OUTPUT STABILITY:

    BETTER THAN __.08__ % COEFFICIENT OF VARIATION

    IN ANY 4-HOUR PERIOD OVER 24 HOURS

MAXIMUM RADIATION LEAKAGE: __<.5__ mR/hr

                                        at 1 inch from the surface of housing

MAXIMUM LEAKAGE CURRENT: __N/A__ uA at __N/A__

                                        (with no current programmed)

TESTED BY __Paul Praijfs__   DATE __4/21/83__

Q. C. INSPECTION _____   DATE APR 2 1 1983

33

APPENDIX C. STANDARD OPERATING PROCEDURES

(Kevex X-ray Unit Model No. K5010T, Serial No. 3183)

The following are the Standard Operating Procedures for the Kevex X-ray Unit being used by the Physiology Department for brain cell irradiations. No deviation from these procedures is authorized unless first approved by the officer in charge, the Radionuclide and X-Ray Safety Committee, or the Safety and Health Department. The procedures emphasize radiation safety and tube preservation, with radiation safety receiving the higher priority.

1. Visual Inspection Safety. Before any irradiations, the operator shall conduct a thorough visual inspection of the following:

    a. Faraday cage. Examine the top and bottom of the cage, all door corners, the front junction, and all edges to ensure that all lead shielding is intact.

    b. All interlocking mechanisms (addressed in paragraph 3d).

    c. Visual warning light.

    d. Control panel.

2. Log Book. In accordance with RSI 530, paragraphs 7b and c, the unit operator log shall be readily available and used for every operation of the unit. An entry must be made for each run, except that one entry may be used for a series of identical runs if the number is clearly specified in the log. Log entries shall include the following:

    a. All machine settings (time, kVp, collimation, mA).

    b. Operator's name.

    c. Description of use and special conditions.

    d. Date and time.

3. Warm-up Procedure for the X-Ray Tube. While preparing the array for radiation, warm up the tube using the following procedure:

    a. Ensure that the front doors are properly closed and secured with the latch-bar.

    b. Ensure that the switch on the grey box is in the ON position and the warning light is activated.

c. Insert the operation key in the control panel and turn it ON to provide AC power to the control panel.

d. With the tube settings at 0 kV/0 mA and the red x-ray light illuminated on the control panel, trip the interlock to ensure that the unit shuts down. Unit shutdown will include the following:

(1) Red light on top goes OFF.

(2) Red x-ray ON light on the control panel goes OFF.

(3) Green x-ray OFF light illuminates.

NOTE. IF THIS DOES NOT OCCUR, CEASE ALL OPERATIONS AND CONTACT THE SAFETY AND HEALTH DEPARTMENT IMMEDIATELY.

e. Ensure that the following steps are adhered to when increasing voltage and current (daily when in use):

Step	kV/mA	Time (min)
1	0/0	Interlock check (paragraph d above)
2	10.0/.10	1
3	20.0/.10	1
4	30.0/.30	1
5	35.0/.30	20
6	40.0/.50	2
7	45.0/.70	2
8	49.0/.99	2

f. When increasing kV/mA, increase the kV first, then the mA. When decreasing the settings, decrease the mA first, then the kV.

g. When increasing kV, be alert to any arcing (an audible "ticking" sound produced in the tube or the power supply). If more than one or two arcs are observed, back the voltage down to the previous voltage and rerun for the designated time. After the time has elapsed, step the voltage back up, and continue the procedure.

NOTE: Tube should never be switched into operation with kV settings greater than one-half their maximum values.

4. <u>Tissue Electrode Positioning</u>. When the warm-up procedure is completed and the array is ready for radiation, the unit may be shut down. At this point, the cage may be opened and the tube temporarily removed to allow ample room for array/electrode positioning. Upon completion, the tube should be repositioned in accordance with the dosimetric parameters determined by the Operational Dosimetry Division.

5. <u>Brain Cell Radiation Exposures</u>. Repeat procedures in paragraphs 3a-c. Because the tube should NEVER be switched into operation with kV settings greater than one-half their maximum values, ensure that the following steps are adhered to:

<u>Step</u>	<u>kV/mA</u>	<u>Time (min)</u>
1	25.0/.10	1
2	49.0/.99	until desired dose is delivered

This procedure will involve a slight rise time with the cells in place, but at high doses it will be an extremely small percentage of the total dose delivered.

6. <u>Shut Down</u>. The operator shall ensure that at the end of the radiation exposure all equipment as well as the operator key is properly secured.

7. <u>Musts</u>

   a. The operator must remain in the room at all times when the key is in the power supply.

   b. The key must be kept in the control of a qualified operator and may <u>not</u> be left in the power supply.

   c. The operator shall wear proper personnel dosimetry as required by RSI 530.

8. <u>Posting of the Area</u>. The area shall be posted in accordance with RSI 530, paragraph 7d.

9. <u>Access to the Area</u>. Access to the area is not restricted while the unit is in operation.